Fate and Remediation of Biomass Gasification Gas Contaminants

by

Nourredine Abdoulmoumine

A dissertation submitted to the Biosystems Engineering Faculty of
Auburn University
in partial fulfillment of the
requirements for the Degree of
Doctor of Philosophy

Auburn, Alabama
August 2, 2014

Keywords: Biomass, pine, gasification, gas cleanup, syngas contaminants

Approved by

Sushil Adhikari, Chair, Associate Professor of Biosystems Engineering
Steven Taylor, Professor of Biosystems Engineering
Mario Eden, Professor of Chemical Engineering
Christopher Roberts, Professor of Chemical Engineering

Abstract

The development of alternative and renewable energy and fuels is at the forefront of research because of the forecasted depletion of crude oil reserves and the growing concern of irreversible environmental damage caused by the greenhouse gases. As lignocellulosic biomass is a renewable feedstock, its conversion to energy and fuels is particularly very attractive as it has the potential to replace fossil fuels derived liquid fuels, chemicals and energy while recycling carbon dioxide (CO_2) into plant material by photosynthesis.

Lignocellulosic biomass conversion can be achieved thermally by pyrolysis, gasification or combustion and biologically by fermentation. Biomass gasification is well suited among other thermochemical technologies due to its higher efficiency and the plethora of applications that could increase efficiency as well as synthesize value-added by-products. Energy and fuel production from biomass is well adapted to southern states in the United States due to abundant biomass resources. Of the woody biomass feedstocks, pine is the most likely feedstock for large-scale production as it accounts for 83 % of tree species in the aforementioned states. Therefore, this dissertation project focuses on pine gasification with an emphasis on the fate of syngas contaminants. In addition, means of remediating these contaminants were also explored.

In Chapter 3, the effects of equivalence ratios (0.15, 0.25 and 0.35 at 934°C) and temperature (790, 934 and 1078°C at 0.25 equivalence ratio) on primary gases and contaminants were investigated. It was observed that carbon monoxide (CO) and hydrogen (H_2) increased while carbon dioxide (CO_2) and methane (CH_4) decreased from 790 to 1078°C. Opposite trends were

observed for equivalence ratio (ER). Based on overall contaminant weight, tar was highest at all temperatures (7.81, 8.24 and 8.93 g/kg dry biomass) and ERs (13.08, 8.24 and 2.51 g/kg dry biomass). Ammonia (NH_3) varied from 1.63 to 1.00 g/kg dry biomass between 790 and 1078°C and 1.76 to 1.47 g/kg dry biomass between 0.15 to 0.35 ERs. Hydrogen sulfide (H_2S) ranged between 0.13 and 0.17 g/kg dry biomass from 790 to 1078°C and 0.15 to 0.18 g/kg dry biomass from 0.15 to 0.35 ER. Finally, hydrogen chloride (HCl) yields ranged from 13.63 mg/kg dry biomass to below detection limit and 11.51 to 0.28 mg/kg dry biomass over the range of temperature and ER, respectively. For primary gases, the major finding was that the endothermic Boudouard and water gas reactions play a key role in controlling CO and H_2 in the product gas as temperature is increased. As oxygen supply (*i.e.* ER) increases, char and homogeneous oxidation reactions largely explain increasing trends of fully oxidized major species in the producer gas (CO_2 and water (H_2O)) while CO and H_2 decreased. While higher temperatures are known to promote hydrocarbon cracking, it also leads to secondary and tertiary tar formation. It was observed that increasing oxygen availability to induce tar oxidation is more effective than increasing temperature to reduce tar content. NH_3 and HCl both decrease as temperature increased, the first due to its thermal decomposition to nitrogen (N_2) and H_2 and the latter due to speciation to metal chloride. Increasing oxygen supply did not significantly affect H_2S and NH_3 because of oxygen consumption by major species. HCl significantly decreased likely because of reactions with biomass trace metals released as biomass is decomposed.

Chapter 4 looks at air gasification of pine from a performance angle by carrying out mass and energy balances as well as energy analysis at 790, 934 and 1078˚C and 0.15, 0.25 and 0.35 ERs. Mass balance closures ranged from 94.73 to 96.72 % and from 89.82 to 96.93 % as temperature and ER increased. Over the same range of temperature and ER, carbon closures ranged from 80.77 to 92.29 % and from 79.09 and 87.13 %. Carbon conversion efficiencies increased from 72.26 to 84.32 % and 72.26 to 84.66 % as temperature and ER increased. The carbon flow analysis showed that the char product streams retained 10.26 to 6.94 % and 8.82 to 2.13 % of the total carbon feed to the gasifier as temperature and ER increases, respectively. The carbon content in the liquid condensate was minimal compared to the carbon in other product streams and accounted for less than 0.1 % of the carbon input to the gasifier at all conditions.

The cold and hot gas efficiencies increase from 56.12 to 67.45 % and from 67.51 to 83.83 % as temperature is increased and in contrast decreased from 63.85 to 52.84 % and from 78.06 to 73.00 as equivalence ratio increase. The air equivalent heating value of producer gas increased from 4.93 to 5.73 MJ/m^3 with increasing temperature and decreased from 7.11 to 3.28 MJ/m^3 with increasing ER.

Chapters 5 and 6 investigate contaminant removal using solid sorbents and catalysts in a fixed bed reactor. Chapter 5 deals H_2S removal on vanadium oxide (V_2O_5) and zinc oxide (ZnO) and SrO supported sorbents. Five sorbents (V_2O_5, 5 wt % ZnO/V_2O_5, 10 wt % ZnO/V_2O_5 and 10 wt % ZnO-10 wt % SrO/ V_2O_5) were investigated for H_2S removal. In the absence of syngas constituents (CO, CO, CH_4, H_2) V_2O_5 was an effective H_2S sorbent in temperature ranges of

interest in cold and warm gas cleanup. At 50˚C, H_2S was removed below detection limit by V_2O_5 for more than 5 days at 1500 ml/g h WHSV. As temperature increased and gas space velocity was increased to 12,000 ml/h g, the breakthrough time increased to 36, 95 and 140 min at 50, 150 and 250˚C, respectively for V_2O_5. Bulk V_2O_5 was less effective in H_2S removal when syngas constituents were introduced along with H_2S due to competitive chemisorption of other syngas constituents as H_2S adsorption was not observed. However, subsequent ZnO and SrO impregnation to produce 10wt % ZnO/V_2O_5 and 10wt % ZnO-10wt % SrO/V_2O_5 improved the performance and increased the breakthrough time from 0 to 20 min in the presence of syngas constituents. This sorbent formula outperformed ZnO, commonly considered one of the best H_2S sorbent, at the same temperature. In the presence of syngas, the breakthrough times were shorter than when inert gas (argon) alone was used. The following order was observed for sorbents: V_2O_5 < ZnO < 10wt % ZnO/V_2O_5 < 10wt % ZnO-10wt % SrO/V_2O_5. XRD characterization of spent V_2O_5 sorbent interestingly revealed that adsorption rather than sulfidation is the mode of H_2S removal. This mechanism of removal can be potentially advantageous for sorbent regeneration as H_2S is merely adsorbed on the sorbent. The major findings of this chapter are: 1) on bulk V_2O_5, the mode of sulfur removal appears to be by chemisorption rather than by sulfidation to metal sulfide and 2) competitive adsorption of syngas constituents hinder H_2S removal on V_2O_5 and other V_2O_5 based sorbents and 3) supported catalyst of V_2O_5 are effective in H_2S removal at warm gas cleanup temperature range (< 300˚C).

In Chapter 6, the catalytic removal of naphthalene, as model tar compound, on strontium oxide (SrO) was investigated from 300 to 900˚C. Naphthalene concentration was reduced from 6628.47 to 6392.70, 4787.97, 1562.43 and 43.68 mg/m^3 at 300, 500, 700 and 900°C, respectively corresponding to 3.56, 27.77, 76.43 and 99.34 % conversion at the same temperature in the presence of syngas. It was observed that in the presence of syngas, SrO was more active in naphthalene decomposition suggesting the occurrence of dry reforming. When helium was used as a carrier gas, the concentration of naphthalene was reduced from 6628.47 to 6512.29, 5383.03 and 3677.51 mg/m^3 at 500, 700 and 900°C corresponding to 1.75, 18.79 and 44.52 % conversion. The activation energies were 45.24 kJ/mol when syngas was used as a carrier gas and 61.23 kJ/mol when helium was used. At higher temperature, SrO was equally as active as nickel based catalysts tested in this study. The major findings in this chapter are: 1) the presence of syngas constituents improve the catalyst activity by enhancing dry reforming, 2) 700 to 900˚C is required to achieve conversions higher than 80 % and 3) SrO is as effective as nickel based or other basic mineral catalysts that regarding as the best tar removal catalysts at 900˚C with 99.34 % conversion.

Acknowledgments

In June 2010, at the annual international meeting of the American Society of Biological and Agricultural Engineers (ASABE), I met Dr. Steven Taylor and Dr. Sushil Adhikari. Little did I know that as far as meetings go, this one would forever impact my graduate studies and set me on a challenging and equally rewarding educational course. In the pursuit of my graduate degree at Auburn University I have found many successes due to all the people that have invested in me as much as I was willing to invest in my studies. Therefore, I gladly show my appreciation and gratitude.

First and foremost, I would like to express my sincere gratitude to my advisor, Dr. Sushil Adhikari, for his infinite support, patience, advice and guidance throughout my work. His unwavering high standards and above par example are qualities I strive to emulate as I continue to grow as a researcher and scientist. I am particularly thankful for his adaptive management style and his willingness to allow me to explore as much as my scientific curiosity desired.

I would also like to thank Dr. Taylor who first referred me to my advisor at the career fair at the annual ASABE meeting. His speedy response to my interest and his enthusiasm has greatly influenced my decision to join the biosystems engineering department.

Additionally, I would like to thank all my committee members, Drs. Steven Taylor, Christopher Roberts and Mario Eden. Their encouragements, insightful comments, questions and discussions have truly made our meetings jovial and rich in educational possibilities.

In my daily work, I have been blessed with a group of great teammates and fellow graduate students who have provided me with technical and moral support on those days when nothing seems to work, a different prospective when I hit the wall, plenty of laughter in the lab and good memories that I will forever cherish.

My final acknowledgements go to my family and friends. I owe my deepest gratitude to my friends Chenell, Chaibou, Ofei, Badra, Junia, Avanti, Shyam, Rachel, Chris, the Lushingtons, the Friedmans and all the Abdoulmoumines, in whatever corner of the world you might reside. To my family, my sisters, Chamsiya, O'Shea, Angel and brothers Farouk, Madjid and Malik, you are simply the best. I know that you know (as we say among Abdoulmoumines) that I appreciate all the support you have provided me not only during my undergraduate and graduate studies but through my lifetime. To my parents, **Hadjio Yayé Abdoulmoumine** and **Abdoulmoumine Housseini,** words are not sufficient to describe my gratitude to you. You have been the pillars in my life and a constant source of support, wisdom and prayers. Thank you for dreaming for me long before I ever could. Finally, I dedicate this work to my grandmother, **Maïmouna Amadou**, may she rest in peace, from the small city of Dosso in Niger, who is flourishing in the big world through her sons and daughters.

Table of Contents

Abstract ii
Chapter 1 Introduction 1
1.1 Introduction 1
1.2 Research Problem 4
1.4 Research Proposal and Objectives 6
1.5 Organization of the Dissertation 9
References 11
Chapter 2 Literature Review 16
2.1 Introduction 16
2.2 Fundamentals of Biomass Gasification 17
2.2.1 Gasification Primary Gas Constituents 19
2.2.2 Gasification Contaminants 21
2.2.2.1 Tar 21
2.2.2.2 Nitrogenous Contaminants 27
2.2.2.3 Sulfurous Contaminants 27
2.2.2.4 Hydrogen Halide Contaminants 28
2.2.2.5 Trace Metal Contaminants 28
2.3 Biomass Feedstocks for Gasification 28
2.4 Effect of Operating Conditions on Primary Gases and Gasification Performance Indicators 30
2.4.1 Temperature 30
2.4.2 Gasifying Agent 31
2.5 Gasifiers and their Implications on Product Gas 33
2.5.1 Entrained-Flow Gasifier 34
2.5.2 Bubbling and Circulating Fluidized-Bed Gasifier 36

2.5.3 Moving-Bed Gasifier 38
2.6 Effect of Feedstock and Operating Conditions on Contaminants 40
2.6.1 Tar Contaminants 40
2.6.1.2 Effect of Feedstock Type on Tar 40
2.6.1.3 Effect Operating Conditions on Tar 41
2.6.2 Nitrogenous Contaminants 43
2.6.2.1 Effect of Feedstock on Nitrogenous Contaminants 43
2.6.2.2 Effect of Operating Conditions on Nitrogenous Contaminants 44
2.6.3 Sulfurous Contaminants 46
2.6.3.1 Effect of Feedstock on Sulfurous Contaminants 46
2.6.3.2 Effect of Operating Conditions on Sulfur Contaminants 47
2.6.4 Hydrogen Halide Contaminants 48
2.6.4.1 Effect of Feedstock on Hydrogen Halides 48
2.6.4.2 Effect of Operating Conditions on Hydrogen Halide Contaminants 49
2.6.5 Trace Metals Contaminants 49
2.6.5.1 Effect of Feedstock on Trace Metals 49
2.6.5.2 Effect of Operating Conditions on Trace Metals 50
2.7 Gas Cleanup 51
2.7.1 Cold Gas Cleanup 51
2.7.1.1 Tar 51
2.7.1.2 Nitrogenous Contaminants 53
2.7.1.3 Sulfurous Contaminants 54
2.7.1.4 Hydrogen Halide Contaminants 56
2.7.1.5 Trace Metals 57
2.7.2 Hot Gas Cleanup 57
2.7.2.1 Catalysts for Tar Removal 59
2.7.2.2 Catalysts for Ammonia Removal 67

2.7.2.3 Sorbents for Sulfur Removal 75
2.7.2.4 Sorbents for Hydrogen Halides Removal 81
2.7.2.5 Trace Metals Removal 83
2.7.3 Barriers to Biomass Gasification Commercialization 83
2.7.3.1 Technical Barriers 84
2.7.3.1.1 Biomass Logistics 84
2.7.3.1.2 Product Gas Contaminants 86
2.7.3.1.3 Pilot and Large Scale Demonstration 87
2.7.3.2 Economic Barriers 88
2.7.3.3 Policy Barrier 89
2.8 Applications of Gasification Syngas 89
2.8.1 Power Generation 90
2.8.2 Liquid Fuel 91
2.9 Conclusions 93
References 96
Chapter 3 Effect of Temperature and Equivalence Ratio on Primary Gases and Contaminants in an Atmospheric Air Blown Bench-Scale Fluidized Bed Gasifier 116
Abstract 116
3.1 Introduction 117
3.2 Materials and Methods 119
3.2.1 Material Characterization 119
3.2.1.1 Gasification Experimental Setup 119
3.2.1.1.1 Product sampling and analysis 120
3.2.1.1.1 Tar sampling and analysis 121
3.2.1.2 Experimental Design and Statistical Analysis 122
3.3 Results and Discussion 122
3.3.1 Biomass Characterization 122

3.3.2 Syngas Composition Profiles 123
3.3.3 Effect of Temperature and ER on Product Distribution 124
3.3.4 Effect of Gasification Temperature and ER on Primary Gas Constituents 127
3.3.5 Effect of Temperature and ER on Syngas Contaminants 131
3.3.5.1 Tar 132
3.3.5.2 Nitrogen Contaminants: NH_3 and HCN 136
3.3.5.3 Sulfur Contaminants: H_2S 139
3.3.5.4 Hydrogen Halides: HCl 140
3.4 Conclusions 143
References 144
Chapter 4 Effects of Temperature and Equivalence Ratio on Mass Balance and Energy Analysis in Pine Air Gasification 147
Abstract 147
4.1 Introduction 148
4.2 Materials and Methods 148
4.2.1 Experimental Setup and Product Sampling 148
4.2.2 Material Characterization 150
4.2.3 Mass Balance and Energy Analysis 151
4.2.3.1 Mass and Carbon Balance 151
4.2.3.2 Carbon Conversion Efficiency 153
4.2.3.3 Energy Analysis 153
4.2.3.4 Cold and Hot Gas Efficiencies and Volumetric Gas Heating Value 154
4.3 Results and Discussion 155
4.3.1 Effect of Temperature and Equivalence Ratio on Products 155
4.3.2 Effect of Temperature and Equivalence Ratio on Mass and Carbon Balance 158
4.3.3 Effect of Temperature and Equivalence Ratio on Energy Analysis 163
4.4 Conclusions 167

Nomenclature 169
References 171
Chapter 5 Vanadium Oxide Based Sorbents for Hydrogen Sulfide Adsorption 173
Abstract 173
5.1 Introduction 174
5.2 Materials and Methods 175
5.2.1 Catalyst Synthesis and Characterization 175
5.2.2 Experimental Setup and Sorption Experiments 178
5.3 Results and Discussion 181
5.3.1 Sorbent Characterization 181
5.3.1.1 Elemental Composition 181
5.3.1.2 Sorbent Surface Area 183
5.3.1.3 X-ray Diffraction Analysis 184
5.3.3 H_2S Sorption 186
5.3.3.1 H_2S Sorption in the Absence of Syngas Constituents 188
5.3.3.2 H_2S Sorption in the Presence of Syngas Constituents 189
5.3.4 Spent Sorbent Characterization 192
5.4 Conclusions 193
References 194
Chapter 6 Naphthalene Removal as Tar Model Compound on Strontium Oxide 196
Abstract 196
6.1 Introduction 197
6.2 Materials and Methods 198
6.2.1 Experimental Setup 198
6.2.2 Catalyst Characterization 199
6.2.3 Naphthalene Sampling and Analysis 200
6.2.3 Kinetic of Naphthalene Reforming in Syngas 201

6.3 Results and Discussion 202
6.3.1 Effect of Temperature on Naphthalene Removal 202
6.3.2 Catalyst Characterization 205
6.3.3 Kinetics of Naphthalene Removal on Strontium Oxide 207
6.4 Conclusions 207
References 209
Chapter 7 Recommendations 212
7.1 Biomass Gasification 212
7.1.1 Fluidized Bed Gasifier: Lessons Learned and Suggestions 212
7.1.1.1 Operating Procedure 212
7.1.1.2 Design Modification 215
7.1.2 Biomass Contaminants Studies in Fluidized Bed Gasifier 215
7.1.3 Biomass Contaminants Formation and Evolution Studies 216
7.2 Gas Cleanup Studies 216
Appendix A1 220
Tar Compounds in Syngas 220
Appendix A2 225
One-way Analysis of Variance of the Effect of Temperature on Product Distribution 225
One-way Analysis of Variance of the Effect of Equivalence ratio on Product Distribution 225
One-way Analysis of Variance of the Effect of Temperature on Primary Gases 226
One-way Analysis of Variance of the Effect of Equivalence Ratio on Primary Gases 227
One-way Analysis of Variance of the Effect of Temperature on Contaminants 229
One-way Analysis of Variance of the Effect of Equivalence Ratio on Contaminants 230
Appendix A3 231
Sample Mass and Carbon Balance Calculations 232
Sample Energy Analysis and Gas Heating Value Calculations 235

List of Tables

Table 1.1. Upper limits of undesirable compounds in gasification syngas 5
Table 2.1. Effect of gasifying agents on concentration of primary gases and contaminants in fluidized bed gasifiers 20
Table 2.2. Properties of selected feedstocks and coal with potential usage in gasification..... 29
Table 2.3. Ranges of syngas primary gases and contaminants for air gasification of biomass 33
Table 2.4. Primary gas composition from biomass feedstocks in entrained flow gasifiers..... 36
Table 2.5. Metals in various feedstocks in biomass gasification..... 50
Table 2.6. Comparison of wet scrubbing technologies for tar removal..... 52
Table 2.7. Absorption efficiencies of tar components by different liquid scrubbing solvents 52
Table 2.8. Conventional methods for sulfur removal from gasification syngas. 55
Table 2.9. Summary of catalytic tar reforming studies..... 61
Table 2.10. Summary of catalytic ammonia decomposition studies 69
Table 2.11. Catalytic desulfurization studies of syngas sulfur (mostly H_2S) contaminants..... 76
Table 2.12. Chemical and fuel synthesis process conditions..... 92
Table 3.1. Pine physical and chemical properties..... 123
Table 3.2. Effect of temperature on primary gas composition at ER = 0.25 127
Table 3.3. Effect of equivalence ratio on primary gas composition at 934°C 127
Table 3.4. Comparison of primary gas concentrations with study under similar conditions..... 131
Table 3.5. Effect of temperature on contaminants at ER = 0.25..... 131
Table 3.6. Effect of equivalence ratio on contaminants at 934°C 132
Table 3.7. Tar yield of GC detectable compounds at three different temperatures (ER = 0.25) 133
Table 3.8. Tar yield of GC detectable compounds at three different equivalence ratio (934˚C) 134
Table 3.9. Effects of temperature and ER on fuel-bound nitrogen conversion to NH_3 and HCN 136

Table 3.10. Comparison of NH_3 syngas concentration for feedstock with different nitrogen content during air gasification 138
Table 3.11. Effects of temperature and ER on fuel-bound sulfur conversion to H_2S..... 139
Table 4.1. Effect of temperature on char and liquid condensate product streams at 0.25 ER 156
Table 4.2. Effect of equivalence ratio on char and liquid condensate product streams at 934°C156
Table 4.3. Properties of char collected at different temperatures at ER = 0.25 157
Table 4.4. Properties of char collected at different equivalence ratios at 934°C..... 157
Table 5.1. Composition of gas mixtures tested in H_2S removal 179
Table 5.2. Elemental composition of catalysts by SEM-EDS 184
Table 5.3. Physical properties of sulfidation catalysts..... 184
Table A1.1. List of primary, secondary and tertiary tar compounds.....220
Table A2.1. Effect of temperature on char product yield one-way analysis of variance.....225
Table A2.2. Effect of temperature on condensate product yield one-way analysis of variance..225
Table A2.3. Effect of temperature on syngas product yield one-way analysis of variance.....225
Table A2.4. Effect of equivalence ratio on char yield one-way analysis of variance.....225
Table A2.5 Effect of equivalence ratio on condensate product yield one-way analysis of variance 226
Table A2.6. Effect of equivalence ratio on gas product yield one-way analysis of variance.....226
Table A2.7. Effect of temperature on CO one-way analysis of variance.....226
Table A2.8. Effect of temperature on CO_2 one-way analysis of variance.....226
Table A2.9 Effect of temperature on CH_4 one-way analysis of variance.....226
Table A2.10. Effect of temperature on H_2 one-way analysis of variance.....227
Table A2.11. Effect of temperature on C_2H_2 one-way analysis of variance.....227
Table A2.12. Effect of temperature on C_2H_4 one-way analysis of variance.....227
Table A2.13. Effect of equivalence ratio on CO one-way analysis of variance.....227
Table A2.14. Effect of equivalence ratio on CO_2 one-way analysis of variance.....227
Table A2.15. Effect of equivalence ratio on CH_4 one-way analysis of variance..... 228

Table A2.16. Effect of equivalence ratio on H_2 one-way analysis of variance 228
Table A2.17. Effect of equivalence ratio on C_2H_2 one-way analysis of variance 228
Table A2.18. Effect of equivalence ratio on C_2H_2 one-way analysis of variance 228
Table A2.19. Effect of temperature on H_2S one-way analysis of variance 228
Table A2.20. Effect of temperature on NH_3 one-way analysis of variance..... 229
Table A2.21. Effect of temperature on HCN one-way analysis of variance 229
Table A2.22. Effect of temperature on HCl one-way analysis of variance 229
Table A2.23. Effect of equivalence ratio on H_2S one-way analysis of variance..... 229
Table A2.24. Effect of equivalence ratio on NH_3 one-way analysis of variance 230
Table A2.25. Effect of equivalence ratio on HCN one-way analysis of variance..... 230
Table A2.26. Effect of equivalence ratio on HCl one-way analysis of variance..... 230
Table A3.1. Higher heating value and Shomate heat capacity coefficients for gas components 231
Table A3.2. Densities of primary gas constituents at 25°C and 1 atm 231

List of Figures

Figure 2.1. Cyclic reuse of CO_2 during biomass gasification 16
Figure 2.2. Oxygen supply relative to stoichiometric requirement for full combustion in thermochemical conversion technologies 17
Figure 2.3. Biomass particle decomposition and product evolution during gasification 18
Figure 2.4. Lumped model of biomass decomposition in pyrolysis 22
Figure 2.5. Proposed reaction schemes of tertiary tar formation 23
Figure 2.6. Tentative explanation of (a) O-acetyl-4-O-methylglucurono-xylan and (b) O-acetylxylan and 4-O-methylglucuronic as hemicelluloses model compounds. 25
Figure 2.7. Mechanism for the formation of primary, secondary, and tertiary tars. 26
Figure 2.8. Effect of gasification temperature on primary gases 30
Figure 2.9. Effect of equivalence ratio on primary gas components in air gasification. 32
Figure 2.10. Effect of S/B on primary gas composition in fluidized bed gasification. 32
Figure 2.11. Top-fed entrained flow gasifier solid-gas flow pattern and temperature profile 35
Figure 2.12. Side-fed entrained flow gasifier solid-gas flow pattern and temperature profile 35
Figure 2.13. Bubbling fluidized bed and circulating fluidized bed gasifiers 37
Figure 2.14. Moving bed gasifiers. Counter-current or updraft gasifier (left) and co-current or downdraft gasifier (right) 39
Figure 2.15. The distribution of the four tar classes as a function of temperature. 41
Figure 2.16. Impact of ER and S/B on tar concentration in producer for fluidized bed gasifiers. 42
Figure 2.17. Effect of fuel bound nitrogen on ammonia concentration in syngas at gasification temperature at 800°C and ER = 0.25. 43
Figure 2.18. Impact of temperature on NH_3 in air gasification. ER = 0.25. 44
Figure 2.19. Effect of temperature and ER on fuel bound nitrogen conversion to NH_3. Reproduced from tabulated data 45
Figure 2.20. Effect of fuel bound sulfur on H_2S concentration in syngas. 46

Figure 2.21. Effect of fuel Cl on Cl concentration in syngas. Feedstocks are banagrass and bagass gasified at 800°C and equivalence ratio from 0.26 to 0.33 48
Figure 2.22. Diagram of common sulfur removal solvents employed in conventional acid gas removal (AGR). 55
Figure 2.23. Elements in the periodic table used as catalyst, catalyst promoter, catalyst support or sorbents in gas cleanup. References for promoters and supports 58
Figure 2.24. Potential application of syngas from biomass gasification upon adequate gas cleanup 90
Figure 3.1. Representation of the overall gasification product distribution 117
Figure 3.2. Schematic of bench-scale fluidized bed gasification set-up. 120
Figure 3.3. Primary gas composition profile at 790, 934 and 1078^{o}C for ER = 0.25 123
Figure 3.4. Primary gas composition profile at ER of 0.15, 0.25 and 0.35 at 934^{o}C 124
Figure 3.5. Effect of (a) temperature (790, 934 and 1078^{o}C at ER = 0.25) and (b) ER (0.15, 0.25 and 0.35 at 934°C) on gasification product distribution.. 125
Figure 3.6. Effect of gasification temperature (790, 934 and 1078°C at ER = 0.25) on (a) concentration and (b) yield of primary gases in pine gasification 129
Figure 3.7. Effect of ER (0.15, 0.25 and 0.35 at 934°C) on (a) concentration and (b) yield of primary gases in pine gasification. 130
Figure 3.8. Effect of (a) temperature (790, 934 and 1078^{o}C at ER = 0.25) and (b) ER (0.15, 0.25 and 0.35 at 934°C) on gravimetric tar yield 132
Figure 3.9. Effect of (a) temperature (790, 934 and 1078°C at ER = 0.25) and (b) ER (0.15, 0.25 and 0.35 at 934°C) on tar yield determined gravimetrically and by GC analysis. 135
Figure 3.10. Effect of (a) temperature (790, 934 and 1078^{o}C at ER = 0.25) and (b) ER (0.15, 0.25 and 0.35 at 934°C) on the concentration and yield of NH_3 137
Figure 3.11. Effect of (a) temperature (790, 934 and 1078^{o}C at ER = 0.25) and (b) ER (0.15, 0.25 and 0.35 at 934°C) on the concentration and yield of HCN 138

Figure 3.12. Effect of (a) temperature (790, 934 and 1078°C at ER= 0.25) and (b) ER (0.15, 0.25 and 0.35 at 934°C) on concentration and yield of H_2S 140
Figure 3.13. Effect of (a) temperature (790, 934 and 1078°C at ER = 0.25) and (b) ER (0.15, 0.25 and 0.35 at 934°C) on concentration and yield of HCl 142
Figure 4.1. Material balance input and output streams 149
Figure 4.2. Carbon conversion efficiency in this study compared with several reports in woody biomass air gasification in bubbling fluidized bed reactors. 159
Figure 4.3. Effect of temperature on carbon distribution in product streams 160
Figure 4.4. Effect of equivalence ratio on carbon distribution in product streams 161
Figure 4.5. Process mass, carbon and energy balance diagram at 934°C and 0.25 ER 162
Figure 4.6. Effect of temperature on energy flow illustrated by Shankey diagrams. 163
Figure 4.7. Effect of equivalence ratio on energy flow illustrated by Shankey diagrams. 164
Figure 4.8. Effect of temperature on cold and hot gas efficiencies and heating value of producer gas 165
Figure 4.9. Effect of equivalence ratio on cold, hot gas efficiencies and gas heating value 166
Figure 4.10. Cold gas efficiency in this study compared with several reports in woody biomass air gasification in fluidized bed reactors. 167
Figure 5.1. Synthesis flow diagram of ZnO supported V_2O_5 sorbents and SEM images at 10000 magnification 177
Figure 5.2. Synthesis flow diagram of SrO and ZnO supported V_2O_5 sorbents and SEM images at 10000 magnification 177
Figure 5.3. Schematic of fixed bed experimental setup for H_2S removal 179
Figure 5.4. External mass transfer elucidation assessment. 180
Figure 5.5. Internal mass transfer assessment. 181
Figure 5.6. SEM images of V2O5, ZnO and SrO at 10,000 magnification 182
Figure 5.7. SEM images of 5 wt% ZnO/V_2O_5, 10 wt% ZnO/V_2O_5 and 10 wt% ZnO-10 wt% SrO/ V_2O_5 at 10,000 magnification 183

Figure 5.8. XRD diffraction pattern of V_2O_5 185
Figure 5.9. XRD pattern for fresh ZnO and ZnO supported V_2O_5 sorbents 185
Figure 5.10 Particle sizes for V_2O_5 used for internal mass transfer limitation investigation 186
Figure 5.11. External mass transfer limitation for V_2O_5 at 250°C. 187
Figure 5.12. Internal mass transfer limitation for V_2O_5 at 250°C 187
Figure 5.13. Effect of temperature on H_2S removal on ZnO and V_2O_5 at temperature ranging from 50˚C to 500˚C 189
Figure 5.14 Effect of temperature on H_2S removal in the presence of syngas constituents for V_2O_5, ZnO and ZnO supported on V_2O_5 at 250^{o}C and WHSV = 12,000 ml/h g 191
Figure 5.15. XRD patterns of spent V_2O_5 from H_2S removal from syngas 192
Figure 6.1. Distribution of producer gas contaminants per unit biomass 197
Figure 6.2. Experimental setup. 199
Figure 6.3. Determination of gas phase naphthalene concentration from naphthalene concentration from scrubbing solvent 201
Figure 6.4. Effect of temperature on naphthalene conversion profiles without (a.) and with (b.) syngas 203
Figure 6.5. Effect of temperature on naphthalene steady state concentration under different carrier gas 204
Figure 6.6. Comparison of SrO with a commercial Ni-based catalyst 205
Figure 6.7. Scanning electron microscopic image of SrO 205
Figure 6.8. Coke formation on spent SrO 206
Figure 6.9. Activation energy plot of naphthalene on SrO 207
Figure 7.1. Proposed systematic approach to H_2S removal studies 217
Figure A3.1. Process mass and energy balance diagram at 790˚C and 0.25 ER 238
Figure A3.2. Process mass and energy balance diagram at 1078˚C and 0.25 ER 239
Figure A3.3. Process mass and energy balance diagram at 934˚C and 0.15 240
Figure A3.4. Process mass and energy balance diagram at 934˚C and 0.35 ER 241

Chapter 1
Introduction

1.1 Introduction

Energy is an essential commodity that is required by any industrialized nation. In recent years, there has been in a significant push in policies by many countries to migrate from fossil and non-renewable fuels to alternatives biofuels.[1] In the United States, this push is dictated primarily by the need to reduce the dependence on foreign oil. In addition to national security, domestic renewable energy production has the advantage of satisfying several environmental and economical issues: reduction of greenhouse gas emissions and creation of jobs. Consequently, research and development in alternative fuels has attracted great attention.[2] Conversion of woody biomass to alternative and renewable fuels is particularly appealing as it has the potential to replace petroleum derived transportation fuels while simultaneously producing electricity and chemicals in a carbon dioxide (CO_2) neutral fashion if carried out sustainably.[3] Two platforms are currently promoted for the conversion of woody biomass to energy: biochemical and thermochemical.

The biochemical platform primarily utilizes biological agents to convert biomass into chemicals and fuels. The conversion of corn to bioethanol is a perfect example of this conversion platform. In 2008, 9.6 billion gallons of ethanol were used as vehicle fuel in the United States.[4] This number is projected to rise to 11.2 billion gallons or 7.5% of the gasoline consumption in the United States by 2012.[5] While ethanol is not the only output of a biochemical platform, it is

nonetheless one of the most important economically. Currently, ethanol produced through the biochemical platform is predominantly derived from corn.[4] However, the utilization of corn as a feedstock for ethanol production has its own limitations: with increase in fuel prices results in higher feedstock prices. One potential consequence of this tendency is the risk of diverting farmland, otherwise used for food production, or food crops for biofuel production. Furthermore, several life cycle assessment studies have questioned the greenhouse gas and other environmental benefits of producing bioethanol from corn.[6, 7] Due to all these disadvantages, governmental agencies and research organizations have shifted their attention to next generation feedstocks like agricultural and forest lignocellulosic residues [4], for which the biochemical conversion technology is not as mature as it is for starches and sugars like corn or sugarcane.[8]

The thermochemical conversion platform thermolytically converts biomass into gaseous or liquid intermediate chemicals that can be upgraded to transportation fuels or commodity chemicals. This platform is more efficient than the biochemical counterpart because of its ability to convert all components in a relatively short reaction time.[9] It promotes the use of thermal energy with or without other chemical agents, such as catalyst or solvent, for the conversion of biomass into ready to use fuels and other products that can serve as feedstocks for downstream chemical processes.[10] Three thermochemical conversion technologies have been used in biomass conversion: combustion, pyrolysis and gasification.

Combustion has been used for more than a hundred years for waste management and energy production and presently accounts for more than 97% of all bioenergy production.[9] For biomass, combustion is the conversion in excess oxygen to CO_2 and H_2O accompanied by heat release. The combustion hot gas has been used for direct heating and steam production for electricity generation.[11] While biomass combustion is widely used worldwide for waste management and/or

energy production, its main shortcoming is its limited downstream applications which is largely limited to heat and power.

Pyrolysis, at the opposite end of the spectrum, is the conversion of organic macromolecules into smaller molecules in the absence of oxygen at temperatures ranging from 400^{o}C to 650^{o}C.[10, 12] Biomass pyrolysis yields liquid, gas and solid products, the proportion of which varies depending on the temperature and heat transfer rate, residence time, type of downstream catalytic operation and reactor configuration among others. The main benefit of pyrolysis is the production of a liquid crude oil that is storable, transportable, and can potentially be processed or co-processed in existing petrochemical infrastructures in a fashion much similar to petroleum crude to generate transportation fuels and chemicals. However, the chemical composition of this liquid oil has made the technical and economical feasibility of this scenario improbable in the near future.

In between pyrolysis and combustion, gasification is the partial combustion of biomass to produce gaseous and solid fuels. The gas produced in gasification is referred to as producer gas or loosely as syngas.[13-15] Biomass gasification syngas has numerous applications. Syngas can be used for heat and power production through internal combustion engines, gas or steam turbines combined with heat recovery for improved efficiency and revenue. Power production is also feasible with fuel cells. In addition, once cleaned and conditioned, producer gas can be used as chemical feed in liquid transportation synthesis through various catalytic routes and processes such as the Fischer-Tropsch (FT) process or methanol synthesis with subsequent upgrading to gasoline. However, for all applications, the concentrations of contaminants in the product gas must adhere to strict limits in order to avoid complications. The term contaminant refers to particulates, condensable organic compounds collectively named tars, nitrogenous inorganic

compounds like ammonia (NH_3) and hydrogen cyanide (HCN), sulfur containing inorganic compounds like hydrogen sulfide (H_2S), carbonyl sulfide (COS) and, carbon disulfide (CS_2), hydrogen halides such as hydrogen chloride (HCl) and hydrogen fluoride (HF) and finally trace metals like sodium (Na) and potassium (K). These contaminants pose technical and operational issues ranging from equipment corrosion and fouling, environmental pollution and catalyst deactivation. The process of reducing the concentration of these impurities is referred to as gas cleanup and can be done through physical or catalytic means. For several decades, syngas cleanup has been a highly active research area due to the potential impact it could have on the economic viability of the overall gasification process.[16]

1.2 Research Problem

Biomass gasification gas cleanup is essential if the product gas is to serve as a feedstock for chemical and energy production. In addition to the desirable compounds, gasification syngas contains impurities such tars, NH_3, H_2S, halides and trace metals that must be removed to avoid damage to downstream equipment and meet environmental requirements. Before burning in a gas turbine for electricity and heat production, gasification syngas stream requires almost complete removal of alkali metals to protect blades from erosion and corrosion [17]. In addition to alkali metals, tar must be eliminated to prevent condensation issues in conduits, coolers and filters as well as catalyst deactivation by coking. Similarly, the concentration of NH_3 and other nitrogenous impurities must be minimized in the syngas because they are considered as precursors to NOx, the emissions of which are strictly regulated. The removal of H_2S and other sulfurous contaminants is crucial to avoid equipment corrosion, catalyst deactivation as well as to comply with emission regulations. Finally, hydrogen halides are very important to minimize degradation on equipment such as filters, turbine blades[18], heat exchanger surfaces[18], to prevent

catalyst deactivation particularly by chlorine and to meet often stringent downstream application requirements. In particular, fuel cell applications have very stringent limits due to the susceptibility of electrolytes and electrodes degradation by halide ions. Table 1.1 summarizes the tolerable concentration limits for various contaminants in common applications where gasification product gas will be used.

Table 1.1. Upper limits of undesirable compounds in gasification syngas

Applications	**Limitation**						**Ref**
	Tars (mg/Nm^3)	HCl (ppm)	H_2S (ppm)	NH_3 (ppm)	Alkali (ppm)	CO (ppm)	
ICE	10-500						[19]
	10						[20]
	30						[15]
DFIGT	0.5-5	<0.5[15]	< 1[15]		0.02-2[15]		[21, 22, 15]
SOFC	29†	<0.1[23]	1[24]	5000 [24]			[25, 26, 24]
PEMFC	3†					10[24]	[27, 24]
MCFC		<0.1[23]	0.5[24]	10000[24]			[24, 28]
PAFC		4[24]	50[24]	2000[24]		10000[24]	[24]
FT	< 0.1†	0.01	0.01	0.02	0.01		[29]
Methanol	< 1†	0.01	0.5	10			[30]

DFIGT means Direct-Fired, Industrial Gas Turbines, ICE means internal combustion engine, SOFC means solid oxide fuel cell, PEMFC means proton exchange membrane fuel cell, PAFC means phosphoric acid fuel cell, † values were converted from ppm to mg/Nm^3 assuming an average tar molecular weight equal to that of benzene

Gas cleanup challenges arise from the complex, highly feedstock and process dependent variability of contaminant concentrations. Historically, gas cleanup in coal gasification applications has relied on conventional and proven technologies. While these technologies can effectively reduce the concentrations of contaminants to very low levels, they result in loss in efficiency. Moreover, lignocellulosic biomass generates different concentration levels of contaminants when compared to coal due to the inherent differences in physical and chemical

properties. At present, comprehensive investigations of contaminants produced during the gasification of lignocellulosic biomass at various operating conditions is sparingly available, with the bulk of studies focused on tar thus causing a knowledge gap. Spotty coverage of contaminant cleanup, stability and cost of catalysts, pilot scale testing and poor understanding of reactor engineering have hindered transition from research to large scale applications.[19]

1.4 Research Proposal and Objectives

It has been suggested that warm or hot gas cleanup and conditioning could potentially reduce the cost of biomass gasification by 15 to 25% while improving the overall efficiency.[31] In addition to the cost reduction, biomass gasification product gas could be use for a host of applications making gas cleanup critical for the future economic viability of the thermochemical platform. Consequently, understanding the impact of operating condition on second generation lignocellulosic feedstock and developing effective and cost competitive catalytic gas cleanup systems is of the utmost priority.

It is proposed in this project to carry out a comprehensive investigation of the impact of crucial gasification control parameters on all major contaminants and to explore hot gas removal approaches using catalysts and sorbents. Specifically, the following research objectives are targeted:

Objective 1. To elucidate the effect of temperature and equivalence ratio on primary gases and contaminants.

Goal: The goal of this objective is to understand the effect of primary measures (temperature and equivalence ratio) on primary gases and contaminants for pine, the most abundant woody biomass species in southern states.

Rationale: In recent years, various studies investigated the effect of temperature[3, 5-9], ER[3, 5-7, 9] and S/B[3, 5-8] on primary gas products in fluidized bed gasifiers. In addition, few studies have explored the effect of these conditions on few contaminants.[3, 8-11] However, of these studies, only few investigated the effect of gasification conditions on primary gases and major contaminants over a wide range of temperature and equivalence ratio. Consequently, there is a limited understanding of the effect of gasification conditions, like temperature and ER, on major contaminants over a wide range of conditions in biomass gasification. The rationale behind this objective is to carry out an in-depth investigation of gasification gas products at different conditions for pine as a benchmark for similar woody biomass feedstock.

Objective 2. To understand the effect of temperature and equivalence ratio on process performance assessed by mass and energy balance.

Goal: The goal of this objective is to clarify the effect of temperature and equivalence ratio on gasification performance indicators by carrying out detailed mass and energy balances.

Rationale: Detailed mass and energy balance assessment is crucial for process development and model validation. As with contaminants, comprehensive experimental studies of process performance are limited to few studies, especially for pine.[32-35] For example, the distribution of carbon, energy and other parameters such as trace metals and contaminants is sparingly available. This objective complements Objective 1 and provides additional benchmark data for pine.

Objective 3. To investigate H_2S removal by vanadium pentoxide (V_2O_5) based sorbents.

Goal: The goal of this objective is to investigate the removal of H_2S at concentrations typically observed in woody biomass derived producer gas using V_2O_5 based sorbents and to develop an explanatory theory for the mode of removal.

Rationale: The bulk of H_2S removal studies have focused on H_2S concentrations typically observed in coal derived producer gas. However, H_2S concentration in biomass derived product gas is significantly different. While in coal derived product gas, it is typical to observe 1 or 2 vol % of H_2S, in biomass derived gas product, its concentration is typically around 100 ppmv or less. Furthermore, most coal gas based studies define the outlet breakthrough concentration, the outlet concentration at or below which the sorbent is deemed effective, at 100 ppmv or even higher. The rationale of this objective is to investigate the effectiveness of V_2O_5 based sorbent for typical concentrations observed for biomass product gas.

Based on thermodynamic calculations, it has previously been established that Ca, Sr, Ba, V, Mo, W, Mn, Fe, Co, Cu and Zn would produce sorbents with high sulfur adsorption capacity in their oxide form.[36] Of all these elements, Zn, Cu and Fe based catalysts have been the most studied for sulfur removal. Based on a literature survey, oxides of Sr and V have not received considerable attention as sorbents for H_2S removal and were therefore selected for an exploratory study in this project.

Objective 4. To investigate strontium oxide (SrO) for tar removal using naphthalene as a model compound.

Goal: The goal of this objective is to investigate the potential of SrO as a basic catalyst for naphthalene removal over a range of temperatures of interest in hot gas cleanup.

Rationale: Tar in biomass derived producer gas has been identified as one of the major technical hurdles to the commercial adoption of biomass gasification for large-scale applications.[37] Tar removal can be achieved by catalytic cracking and steam or dry reforming. Tar cracking can be achieved with strong acidic catalysts like silica-alumina and zeolites. However on strong acidic catalysts, tar cracking results in significant coke formation. On the other hand, basic catalysts are among the most effective in tar decomposition.[38] In recent years, there has been a plethora of tar removal studies that employed basic mineral catalysts such as dolomite[39-41], olivine[42-46] and limonite[43] or nickel based catalysts[39, 40, 46-52]. The basic mineral catalysts are mixed oxides of alkaline earth metals such as Ca and Mg. While Ca and Mg based catalysts have been extensively used for tar removal, oxides of strontium (Sr) in the same group have received virtually no attention. Since basicity is important for tar removal, it is expected that these catalysts will be well suited for tar elimination.

1.5 Organization of the Dissertation

The notation adopted in this dissertation distinguished between mathematical equations and chemical reactions. Mathematical equations are included in parentheses whereas chemical reactions are included in brackets. Both mathematical equations and chemical reactions are prefixed with the chapter number, a dot and the equation or reaction number in order descending order of appearance in the chapter. An illustration of this notation is shown below for the law of conservation of mass by eq. 1.1 (in-text citation) and the oxidation reaction of carbon and oxygen to carbon dioxide [1.1] (in-text citation):

$$\sum m^{in} = \sum m^{out} \qquad (1.1)$$

$$C + O_2 \rightarrow CO_2 \qquad [1.1]$$

The American Society of Chemistry (ACS) style guide was used in the text as well for the bibliographies. Organizationally, this dissertation is divided into seven chapters. Chapter 1 presents a brief introduction of biomass gasification and a discussion of the research problems tackled in this project. It also outlines the research proposal and objectives as well as the rationale behind the specific objectives. In Chapter 2, a comprehensive literature review is presented and the impact of operating conditions such reactor and feedstock types, temperature and extent of oxygen supply on gasification products are summarized. This chapter also includes reviews of cold and hot gas cleanup technologies and a discussion of applications and barriers to biomass commercialization. Chapter 3 summarizes the effect of temperature and equivalence ratio (ER) on primary gas composition as well as on contaminants during air gasification of pine in a bench-scale fluidized bed gasifier. It elucidates the expected trends for all major gaseous species as well as all major contaminants over a wide range of temperature and equivalence ratio. Chapter 4 looks at air gasification of pine from a performance angle by carrying out mass and energy balances at various temperatures and equivalence ratios. It establishes mass and energy flows for the main products streams in laboratory as well as large scale units. Chapters 5 and 6 investigate contaminant removal using solid sorbents and catalysts in a fixed bed reactor. Chapter 5 deals with H_2S removal on V_2O_5 based sorbents while Chapter 6 studied the catalytic removal of naphthalene, a tar model compound, on SrO as well as on commercial nickel based catalysts. This chapter also includes a kinetic study. Finally, Chapter 7 presents recommendations for future projects.

References

(1) Dufey, A. *Biofuels production, trade and sustainable development: emerging issues*. IIED: London, UK, 2006.

(2) Escobar, J. C.; Lora, E. S.; Venturini, O. J.; Yáñez, E. E.; Castillo, E. F.;Almazan, O. Biofuels: Environment, technology and food security. *Renew. Sust. Energ. Rev.* 2008, 13, 1275-1287.

(3) Vasudevan, P.; Sharma, S.;Kumar, A. Liquid fuel from biomass: An overview. *J. Sci. Ind. Res.* 2005, 64, 822-831.

(4) Mu, D.; Seager, T.; Rao, P.;Zhao, F. Comparative Life Cycle Assessment of Lignocellulosic Ethanol Production: Biochemical Versus Thermochemical Conversion. *J. Environ. Manage.* 2010, 46, 565-578.

(5) EIA. Biofuels in the U.S. transportation sector. In Annual energy outlook 2007. In Administration, E. I., Ed. Washington, DC, 2007.

(6) Crutzen, P.; Mosier, A.; Smith, K.;Winiwarter, W. N_2O release from agro-biofuel production negates global warming reduction by replacing fossil fuels. *Atmos. Chem. Phys. Discuss.* 2007, 7, 11191-11205.

(7) Searchinger, T.; Heimlich, R.; Houghton, R. A.; Dong, F.; Elobeid, A.; Fabiosa, J.; Tokgoz, S.; Hayes, D.;Yu, T.-H. Use of U.S. Croplands for Biofuels Increases Greenhouse Gases Through Emissions from Land-Use Change. *Science* 2008, 319, 1238-1240.

(8) Demirbas, A. Progress and recent trends in biofuels. *Prog. Energy Combust. Sci.* 2007, 33, 1-18.

(9) Zhang, L.; Xu, C.;Champagne, P. Overview of recent advances in thermo-chemical conversion of biomass. *Energy Convers. Manage.* 2010, 51, 969-982.

(10) Moens, L. Chapter 9 Renewable feedstocks. In *Sustainability Science and Engineering*, Abraham, M. A., Ed. Elsevier: 2006; Vol. Volume 1, pp 177-199.

(11) Van Loo, S.;Koppejan, J. *The handbook of biomass combustion and co-firing*. Earthscan/James & James: 2008.

(12) Agblevor, F.; Beis, S.; Mante, O.;Abdoulmoumine, N. Fractional Catalytic Pyrolysis of Hybrid Poplar Wood. *Ind. Eng. Chem. Res.* 2010, 49, 3533-3538.

(13) Breault, R. Gasification Processes Old and New: A Basic Review of the Major Technologies. *Energies* 2010, 3, 216-240.

(14) Bridgwater, A. Catalysis in thermal biomass conversion. *Appl. Catal., A* 1994, 116, 5-47.

(15) Bridgwater, A. The technical and economic feasibility of biomass gasification for power generation. *Fuel* 1995, 74, 631-653.

(16) Corella, J.; Orio, A.;Toledo, J. Biomass gasification with air in a fluidized bed: Exhaustive tar elimination with commercial steam reforming catalysts. *Energy Fuels* 1999, 13, 702-709.

(17) Hepola, J. Sulfur transformations in catalytic hot gas cleaning of gasification gas. Dissertation, Helsinki University of Technology, Espoo, 2000.

(18) Ohtsuka, Y.; Tsubouchi, N.; Kikuchi, T.;Hashimoto, H. Recent progress in Japan on hot gas cleanup of hydrogen chloride, hydrogen sulfide and ammonia in coal-derived fuel gas. *Powder Technol.* 2009, 190, 340-347.

(19) Xu, C.; Donald, J.; Byambajav, E.;Ohtsuka, Y. Recent advances in catalysts for hot-gas removal of tar and NH3 from biomass gasification. *Fuel* 2010, 89, 1784-1795.

(20) Bui, T.; Loof, R.;Bhattacharya, S. C. Multi-stage reactor for thermal gasification of wood. *Energy* 1994, 19, 397-404.

(21) Milne, T.; Abatzoglou, N.; Evans, R.; Kemestrie, I.;Laboratory, N. R. E. Biomass gasifier" tars": their nature, formation, and conversion. In National Renewable Energy Laboratory Golden, CO: 1998.

(22) Hasler, P.;Nussbaumer, T. Gas cleaning for IC engine applications from fixed bed biomass gasification. *Biomass Bioenergy* 1999, 16, 385-395.

(23) Jansen, D.; van der Laag, P.; Oudhuis, A.;Ribberink, J. Prospects for advanced coal-fuelled fuel cell power plants. *J. Power Sources* 1994, 49, 151-165.

(24) Brown, R. C.; Smeenk, J.;Norton, G. *Development of analytical techniques and scrubbing options for contaminants in gasifier streams intended for use in fuel cells*; Center for Sustainable Environmental Technologies at Iowa State University: Ames, IA, 2001.

(25) Norheim, A.; Wærnhus, I.; Broström, M.; Hustad, J. E.;Vik, A. Experimental Studies on the Influence of H_2S on Solid Oxide Fuel Cell Performance at 800 °C. *Energy Fuels* 2007, 21, 1098-1101.

(26) Aravind, P. V.; Ouweltjes, J. P.; Woudstra, N.;Rietveld, G. Impact of Biomass-Derived Contaminants on SOFCs with Ni/Gadolinia-Doped Ceria Anodes. *Electrochem. Solid-State Lett.* 2008, 11, B24-B28.

(27) Sardesai, P.; Seames, W.; Dronen, L.;Kozliak, E. Exploring the gas-phase anaerobic bioremoval of H2S for coal gasification fuel cell feed streams. *Fuel Process. Technol.* 2006, 87, 319-324.

(28) Hirschenhofer, J. H.; Stauffer, D. B.; Engleman, R. R.;Klett, M. G. *Fuel Cell: A Handbook*. 4th ed.; Parsons Corporation: Reading, PA, 1998.

(29) Tijmensen, M. J. A.; Faaij, A. P. C.; Hamelinck, C. N.;van Hardeveld, M. R. M. Exploration of the possibilities for production of Fischer Tropsch liquids and power via biomass gasification. *Biomass Bioenergy* 2002, 23, 129-152.

(30) Spath, P. L.;Dayton, D. C. *Preliminary Screening — Technical and Economic Assessment of Synthesis Gas to Fuels and Chemicals with Emphasis on the Potential for Biomass-Derived Syngas*; NREL/TP-510-34929; National Renewable Energy Laboratory: Golden, CO, December 2003, 2003.

(31) Craig, K. Thermochemical Platform Overview. In *2nd Meeting of the USDA Multistate Research Committee on the Science and Engineering for a Biobased Industry and Economy*, USDA Multistate Research Committee on the Science and Engineering for a Biobased Industry and Economy: Washington, D.C., November 7, 2003.

(32) Rao, M.; Singh, S.; Sodha, M.; Dubey, A.;Shyam, M. Stoichiometric, mass, energy and exergy balance analysis of countercurrent fixed-bed gasification of post-consumer residues. *Biomass Bioenergy* 2004, 27, 155-171.

(33) Chern, S.; Walawender, W. P.;Fan, L. Mass and energy balance analyses of a downdraft gasifier. *Biomass* 1989, 18, 127-151.

(34) Zainal, Z.; Rifau, A.; Quadir, G.;Seetharamu, K. Experimental investigation of a downdraft biomass gasifier. *Biomass Bioenergy* 2002, 23, 283-289.

(35) Dogru, M.; Midilli, A.;Howarth, C. R. Gasification of sewage sludge using a throated downdraft gasifier and uncertainty analysis. *Fuel Process. Technol.* 2002, 75, 55-82.

(36) Westmoreland, P. R.;Harrison, D. P. Evaluation of candidate solids for high-temperature desulfurization of low-Btu gases. *Environ. Sci. Technol.* 1976, 10, 659-661.

(37) Pfeifer, C.; Puchner, B.;Hofbauer, H. Comparison of dual fluidized bed steam gasification of biomass with and without selective transport of CO_2. *Chem. Eng. Sci.* 2009, 64, 5073-5083.

(38) Brown, R. C.;Stevens, C. *Thermochemical Processing of Biomass: Conversion Into Fuels, Chemicals and Power*. Wiley: 2011; Vol. 11.

(39) Simell, P.; Kurkela, E.; Ståhlberg, P.;Hepola, J. Catalytic hot gas cleaning of gasification gas. *Catal. Today* 1996, 27, 55-62.

(40) Sun, Y.; Jiang, J.; Kantarelis, E.; Xu, J.; Li, L.; Zhao, S.;Yang, W. Development of a bimetallic dolomite based tar cracking catalyst. *Catal. Commun.* 2012, 20, 36-40.

(41) Cao, Y.; Wang, Y.; Riley, J. T.;Pan, W.-P. A novel biomass air gasification process for producing tar-free higher heating value fuel gas. *Fuel Process. Technol.* 2006, 87, 343-353.

(42) Devi, L. Catalytic Removal of Biomass Tars; Olivine as Prospective in-Bed Catalyst for Fluidized-Bed Biomass Gasifiers,. PhD thesis, Technical University of Eindhoven, Eindhoven, The Netherlands, 2005.

(43) Hurley, S.; Xu, C.; Preto, F.; Shao, Y.; Li, H.; Wang, J.;Tourigny, G. Catalytic gasification of woody biomass in an air-blown fluidized-bed reactor using Canadian limonite iron ore as the bed material. *Fuel* 2012, 91, 170-176.

(44) Kuhn, J.; Zhao, Z.; Felix, L.; Slimane, R.; Choi, C.;Ozkan, U. Olivine catalysts for methane-and tar-steam reforming. *Appl. Catal., B* 2008, 81, 14-26.

(45) Link, S.; Arvelakis, S.; Paist, A.; Martin, A.; Liliedahl, T.;Sjöström, K. Atmospheric fluidized bed gasification of untreated and leached olive residue, and co-gasification of olive residue, reed, pine pellets and Douglas fir wood chips. *Appl. Energy* 2012, 94, 89-97.

(46) Ferella, F.; Stoehr, J.; Michelis, I. D.;Hornung, A. Zirconia and alumina based catalysts for steam reforming of naphthalene. *Fuel* 2013, 105, 614-629.

(47) D'Orazio, A.; Di Carlo, A.; Dionisi, N.; Dell'Era, A.;Orecchini, F. Toluene steam reforming properties of CaO based synthetic sorbents for biomass gasification process. *Int. J. Hydrogen Energy* 2013, 38, 13282-13292.

(48) Dou, B.; Gao, J.; Sha, X.;Baek, S. W. Catalytic cracking of tar component from high-temperature fuel gas. *Appl. Therm. Eng.* 2003, 23, 2229-2239.

(49) Guan, G.; Chen, G.; Kasai, Y.; Lim, E. W. C.; Hao, X.; Kaewpanha, M.; Abuliti, A.; Fushimi, C.;Tsutsumi, A. Catalytic steam reforming of biomass tar over iron- or nickel-based catalyst supported on calcined scallop shell. *Appl. Catal., B* 2012, 115–116, 159-168.

(50) Kaewpanha, M.; Guan, G.; Hao, X.; Wang, Z.; Kasai, Y.; Kakuta, S.; Kusakabe, K.;Abudula, A. Steam reforming of tar derived from the steam pyrolysis of biomass over metal catalyst supported on zeolite. *J. Taiwan Inst. Chem. Eng.* 2013, 44, 1022-1026.

(51) Michel, R.; Łamacz, A.; Krzton, A.; Djéga-Mariadassou, G.; Burg, P.; Courson, C.;Gruber, R. Steam reforming of α-methylnaphthalene as a model tar compound over olivine and olivine supported nickel. *Fuel* 2013, 109, 653-660.

(52) Wang, T.; Chang, J.; Lv, P.;Zhu, J. Novel catalyst for cracking of biomass tar. *Energy Fuels* 2005, 19, 22-27.

Chapter 2
Literature Review

2.1 Introduction

In recent years, there has been a growing renewed interest in utilizing renewable feedstocks in energy, fuel and chemical production. Production of fuels from renewable feedstocks is a critical research area today because of the forecasted depletion of crude oil reserves and the growing concern of irreversible environmental damage caused by greenhouse gases.[1, 2] Economically, the conversion of woody biomass to biofuel, bio-based chemicals and bioenergy is particularly attractive as it has the potential to replace petroleum derived liquid fuels while simultaneously producing power, heat and chemicals and promoting rural economies.[2, 3] At present, two platforms are promoted for the conversion of biomass to energy: biochemical and thermochemical platforms.

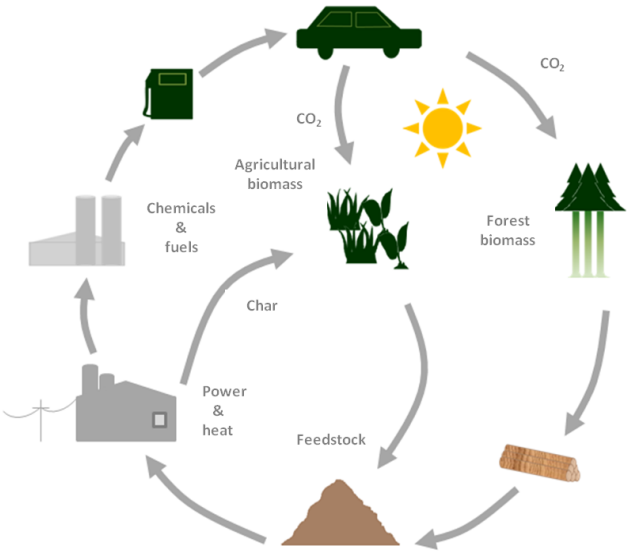

Figure 2.1. Cyclic reuse of CO_2 during biomass gasification[4]

The latter of these two platforms is the concern of this review. In the thermochemical conversion scheme, in addition to the economical benefit, there is the added advantage of potentially reduced greenhouse gas emissions, particularly CO_2, which can be recycled back into plant materials through photosynthesis as shown in Figure 2.1. The thermochemical platform promotes the use of thermal energy with or without other chemical agents for the conversion of biomass. Its goal is to convert biomass into power and heat and/or ready to use or "drop-in" fuels and other intermediate products that can be used as feedstocks for other downstream chemical processes.[5] Four main thermochemical conversion technologies commonly considered for biomass conversion are pyrolysis, gasification, hydrothermal liquefaction and combustion. This present literature only covers one of the thermochemical technologies, gasification, as it is the relevant technology to this work.

2.2 Fundamentals of Biomass Gasification

Gasification occurs in the presence of a sub-stoichiometric amount of oxygen, relative to that required for full combustion, at high temperatures, typically between 650^{o}C and 1500^{o}C.[5, 6] In the continuum of thermochemical conversion technologies with regards to oxygen supply, gasification lies in between pyrolysis and combustion as illustrated in Figure 2.2.

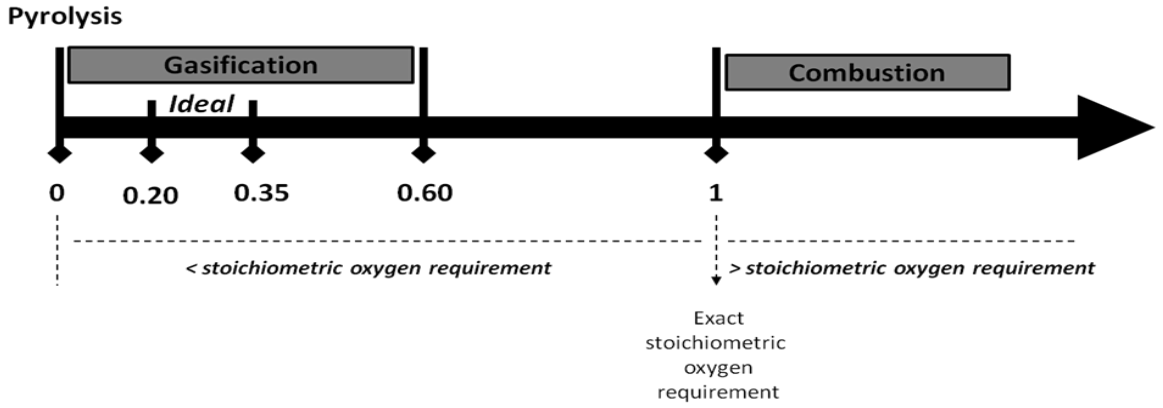

Figure 2.2. Oxygen supply relative to stoichiometric requirement for full combustion in thermochemical conversion technologies

Globally, biomass gasification yields gaseous and solid products. The gaseous product is referred to as producer gas or commonly as syngas in the open literature, and biochar or char. The major constituents in producer gas are carbon monoxide (CO), carbon dioxide (CO_2), hydrogen (H_2), methane (CH_4), non-condensable hydrocarbons (C_1-C_4), water (H_2O). Fundamentally, biomass gasification takes place according to three major steps as illustrated in Figure 2.3: biomass drying or step I, biomass devolatilization or step II, char reactions or step III and finally gas phase (or homogenous) reaction or step IV.

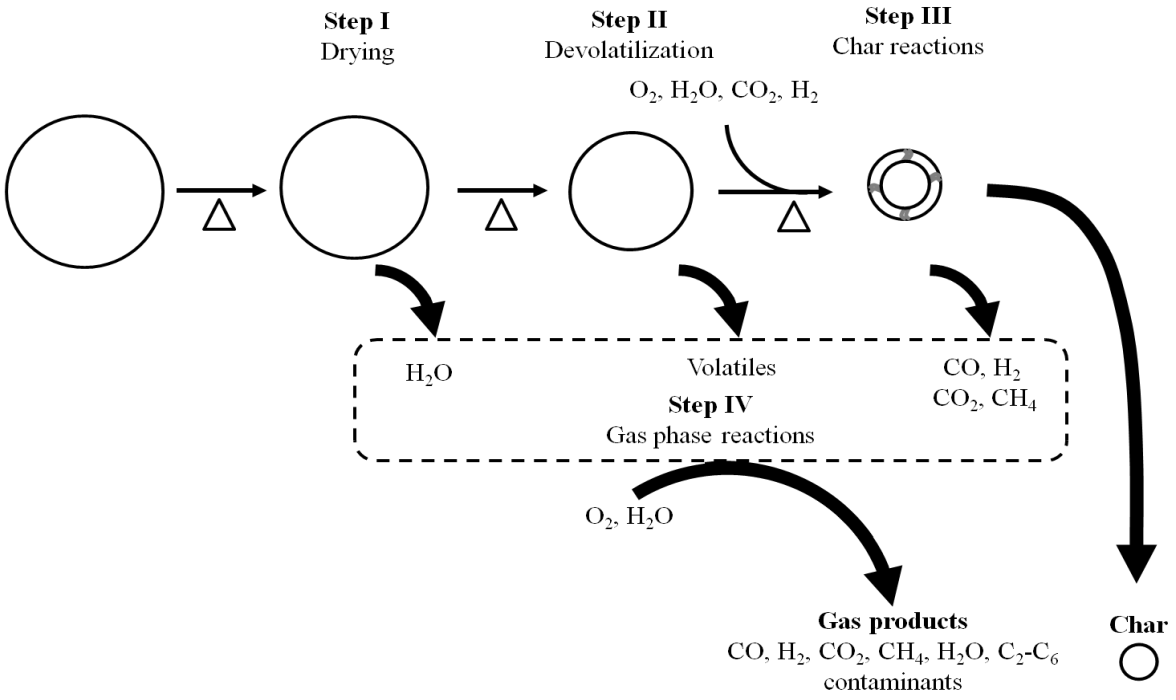

Figure 2.3. Biomass particle decomposition and product evolution during gasification

Various media can be used as a source of oxygen in gasification including air, air/steam or O_2/steam and steam. As such, the oxygen supply media are denoted as oxidizing or gasifying media or agents. The extent of gasifying agent supplied is measured by the equivalence ratio

(ER) for air and steam to biomass ratio (S/B) for steam. When air is used as gasifying agent, considerable amount of nitrogen could appear in the producer gas thus diluting the concentration of other components. The product distribution as well as the composition of the syngas depends on several parameters including the operating conditions, feedstock and gasifier design.[6]

2.2.1 Gasification Primary Gas Constituents

Gasification operating conditions like temperature and gasifying agents are the primary factors that determine primary gas composition and gasification performance indicators (heating value, gas yield, carbon conversion, cold gas efficiency). However, prior to looking at the impact of these operating parameters, it is useful to look at key gasification reactions as they are helpful in making sense of trends that might emerge. These reactions are listed below as oxidation or combustion reactions and reduction reactions.

Oxidation reactions

	$C + O_2 \rightarrow CO_2$	ΔH_{298K} = -394 kJ/mol	[2.1]
	$C + 0.5O_2 \rightarrow CO_2$	ΔH_{298K} = -111 kJ/mol	[2.2]
	$CO + 0.5O_2 \rightarrow CO_2$	ΔH_{298K} = -284 kJ/mol	[2.3]
	$H_2 + 0.5O_2 \rightarrow H_2O$	ΔH_{298K} = -242 kJ/mol	[2.4]

Reduction reactions

Water-gas	$C + H_2O \leftrightarrow CO + H_2$	ΔH_{298K} = +131 kJ/mol	[2.5]
Boudouard	$C + CO_2 \leftrightarrow 2CO$	ΔH_{298K} = +172 kJ/mol	[2.6]
Shift (water-gas shift)	$CO + H_2O \leftrightarrow CO_2 + H_2$	ΔH_{298K} = -41 kJ/mol	[2.7]
Hydro gasification	$C + 2H_2 \leftrightarrow CH_4$	ΔH_{298K} = -75 kJ/mol	[2.8]
Methanation	$CO + 3H_2 \leftrightarrow CH_4 + H_2O$	ΔH_{298K} = -206 kJ/mol	[2.9]

Oxidation reactions are those reactions through which char and gases can be further oxidized into CO_2 or H_2O to give off heat used to drive other gasification reactions.[7] Reduction reactions, on the other hand, lead to the formation of more primary gases through a combination of cracking, steam reforming, oxidation and shift reactions. Table 2.1 summarizes gas composition for different gasifying agents and operating temperatures for fluidized bed gasifiers.

Table 2.1. Effect of gasifying agents on concentration of primary gases and contaminants in fluidized bed gasifiers

Gasifying agent	***Air***[(a)8-13]	***Air/steam***[(b),(d)14-16]	***Steam***[(c)13, 17-20]
Fuel properties, wt % dry ash free			
C	48.45-53.00	50.81-52.67	49.85-52.18
H	5.55-7.91	5.57-6.26	5.68-6.08
O	37.60-44.50	40.56-42.89	38.81-45.69
N	0.1-3.39	0.11-0.51	0.13-2.70
S	0-0.62	0.02-0.23	0.06-0.24
Cl	0.02-0.09	n/a	n/a
Ash	0.4-23.53	0.2-22.53	5.83-7.18
Volatile matter	71.33-83.5	78.86-83.47	80.03-85.38
Process conditions			
ER	0.19-0.66	0.07-0.79	0
S/B	0	0-1.22	1.71-2
Temperature, ˚C	701-890	663-901	800-800
Pressure, bar	1-1.19	1-2.5	n/a
Primary gases, vol %			
CO	5.08-22	7.1-28.5	10.4-28.02
H_2	3-29	7.8-38.38	40.66-60.6
CO_2	11.29-45	9.2-45	5.8-25.20
CH_4	1.2-8	1.8-8.2	7.81-30.2
C_xH_y	0.67-3.2	2-3.2	0.6-3.66
N_2	43.25-72.99	0-63.60	

n/a means not available, [(a),(b),(c)]Range of typical syngas constituents for 101 individual runs at various ER, S/B and temperature for woody (68), herbaceous (2), agricultural residues (3), biomass coal blends (25) and other biomass wastes (3) gasified in fluidized bed gasifiers (BFBG or CFBG). [(d)]O_2/steam data was also included in this category.

2.2.2 Gasification Contaminants

2.2.2.1 Tar

Tar is a complex group of organic compounds that evolves during gasification and condenses in transfer lines, conduits and other equipment downstream of the gasifier. Tars have been defined by a panel of experts of EU/IEA/US-DOE in 1998 as all gasification organic compounds with molecular weight greater than benzene.[21] Relative to other contaminants, tar is the most abundant per unit weight of biomass gasified.[22] Its concentration in syngas depends on the feedstock, process conditions and the type of gasifier. Tar must be removed to prevent condensation issues in conduits, coolers and filters. It is consequently regarded as the biggest technical hindrance to the commercial deployment of biomass gasification.[23, 24]

Tar compounds are classified into four groups listed below:

1. ***Primary tar***: cellulose and hemicellulose derived products like levoglucosan, hydroxyl-acetaldehyde, and furfurals and lignin derived methoxyphenols
2. ***Secondary tar***: phenolics and olefins
3. ***Alkyl tertiary tar***: methyl derivative of aromatics (methyl acenaphthylene, methylnaphthalene, toluene, indene etc)
4. ***Condensed tertiary tar***: polyaromatic hydrocarbons (benzene, naphthalene, acenaphthylene, anthracene/phenanthrene, pyrene)

Milne and coworkers[23] has listed 173 primary, secondary and tertiary tar compounds reported in various studies. This list is presented in Table A1.1 in Appendix A1. It is also common to group tar compounds into classes depending on characteristics of their chemical structures and properties. The five tar classes are listed and described below[25]:

1. ***Class 1***: This class contains very heavy hydrocarbon compounds with 7 or more rings. The compounds are usually not GC detectable.

2. ***Class 2***: This class encompasses a group of heterocyclic hydrocarbons with heteroatoms. These compounds are highly water soluble. Example of these compounds is phenol, cresol, and pyridine.

3. ***Class 3***: This class represents light aromatic compounds that do not readily condense on surfaces. They also have poor solubility in water. Examples of such compounds are toluene, styrene and xylene.

4. ***Class 4***: A class of light polyaromatic of 2 and/or 3 ring compounds. Unlike Class 3 compounds, these compounds readily condense at intermediate temperatures. Naphthalene, phenanthrene and anthracene are class 4 compounds.

5. ***Class 5***: This class covers heavy polyaromatic 4-6-ring compounds that condense even at high temperatures and low concentrations. Examples of these compounds are fluoranthene, pyrene, etc.

It is understood that biomass tar compounds are remnants of volatile compounds of the biomass pyrolysis or devolatization step discussed earlier in section 2.2. The nature and composition of primary, secondary and tertiary tar compounds varies depending on the biomass constituents (i.e lignin, cellulose and hemicelluloses). Therefore, most fundamental tar formation studies have been carried out in pyrolysis mode. In these studies, the decomposition of biomass constituents is represented by lumped models, the simple form of which is illustrated below in Figure 2.4. While the effect of temperature and gasifier types on tar groups is well understood, there is limited detailed information on the mechanism of formation and evolution of tar compounds by group or class.

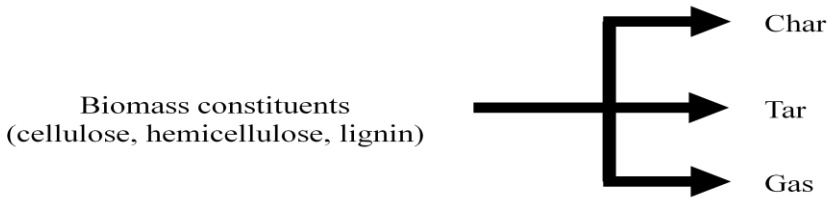

Figure 2.4. Lumped model of biomass decomposition in pyrolysis

2.2.2.1.1 Lignin pyrolysis and tar formation

During primary pyrolysis (< 50 s), lignin produces char (60 wt %), primary tar (30 wt %) and gaseous products.[26] Lignin primary tar compounds are largely guaiacol, syringol and their derivatives.[26 27]

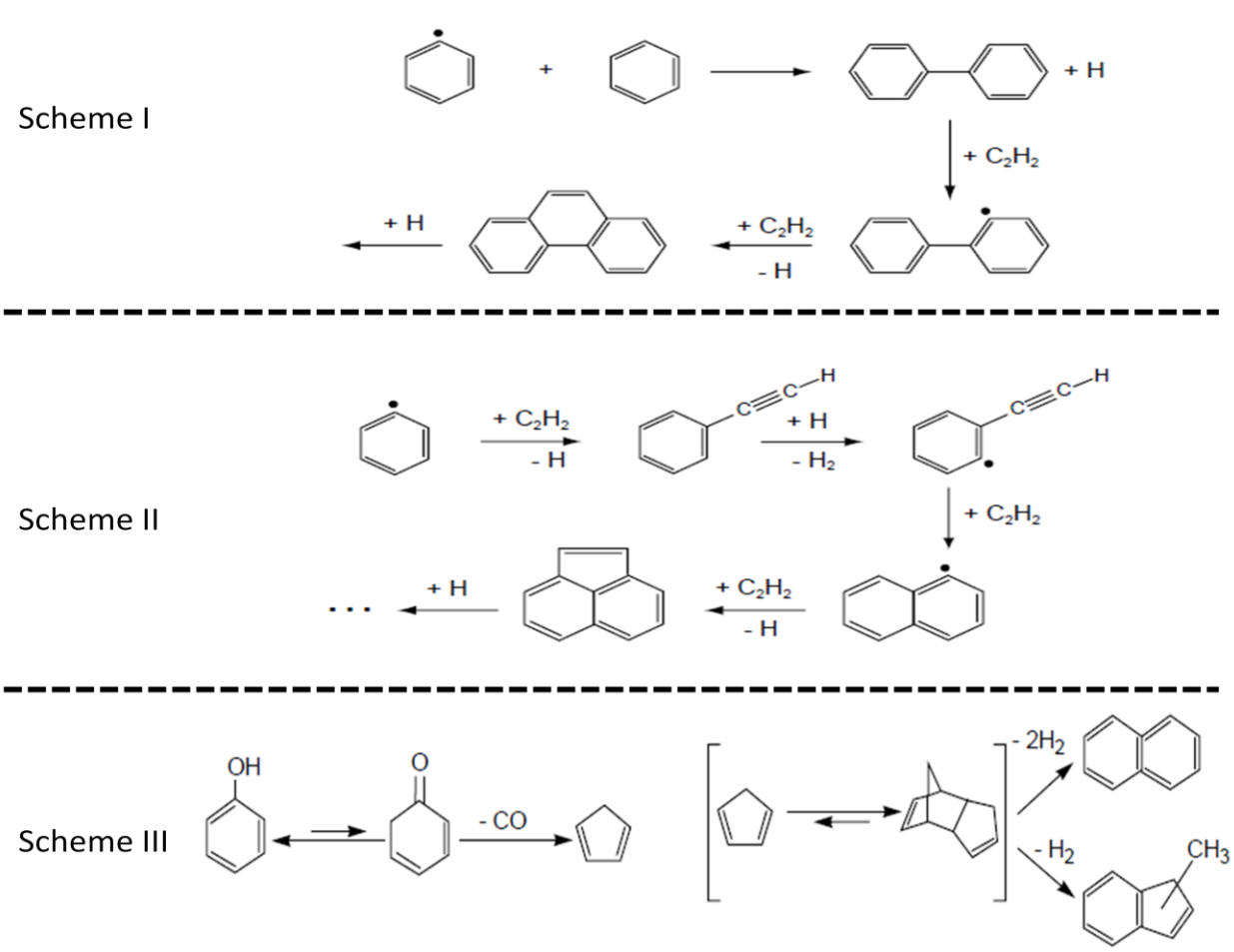

Figure 2.5. Proposed reaction schemes of tertiary tar formation

The primary tar compounds thus produced undergo secondary reactions to produce catechols and pyrogallols, cresols and xylenols, phenol, polyaromatic hydrocarbons, coke and gases.[27] Primary and secondary tar compounds can further react to produce polyaromatic tertiary tar compounds through three potential tar growth mechanisms shown in Figure 2.5 and are: *scheme I*) direct combination of aromatic rings[28], *scheme II*) chain propagation by H_2 abstraction and C_2H_2

addition[28] and *scheme III*) chain reaction of primary tar guaiacol precursors that involves CO abstraction, cyclopentadiene radical formation and chain elongation by addition[29, 30].

2.2.2.1.2 Cellulose pyrolysis and tar formation

During primary pyrolysis, cellulose is first decomposed into primary tar compounds (39.4 wt %) followed by gaseous products (~ 43.0 wt %) and char product (17.7 wt %).[26] The primary tar compounds are predominantly levoglucosan, furan derivatives (furfural, 5-hydromethyl furfural), smaller aldehyde, ketone and carboxylic molecules (glycolaldehyde, hydroxyacetone, formic acid and acetic acid). As time is increased and primary tar vapors undergo secondary reactions, levoglucosan and furan derivatives are significantly reduced by secondary reactions as primary tar yield decrease from 39.4 wt % to 8.6 wt % while gas yield increases.[26] Nonetheless, a fraction of levoglucosan and furan derivatives still remain during secondary pyrolysis. Evans and Milne[31] demonstrated that primary tar carbohydrates can be converted to secondary tar olefins and aromatics even though a specific mechanism has not been established. It is therefore likely that residual levoglucosan and furan derivatives can be converted to olefins and secondary aromatics. These secondary tar compounds can then react according to the reaction schemes discussed in the previous section to produce tertiary tar compounds.

2.2.2.1.3 Hemicellulose pyrolysis and tar formation

Cellulose and hemicelluloses are suggested as the main source for primary tar compounds. Pyrolysis products of hemicelluloses are carboxylic acids such as acetic acid and formic acid, alcohols such as methanol, carbohydrate derivatives such as furfural and 1,4 anhydro-D-xylopyranose.[30, 31] Acetic acid formation occurs mainly through elimination reactions of the *O*-acetyl groups while furfural and 1,4 anhydro-D- xylopyranose are derived from xylan units.[31, 32]

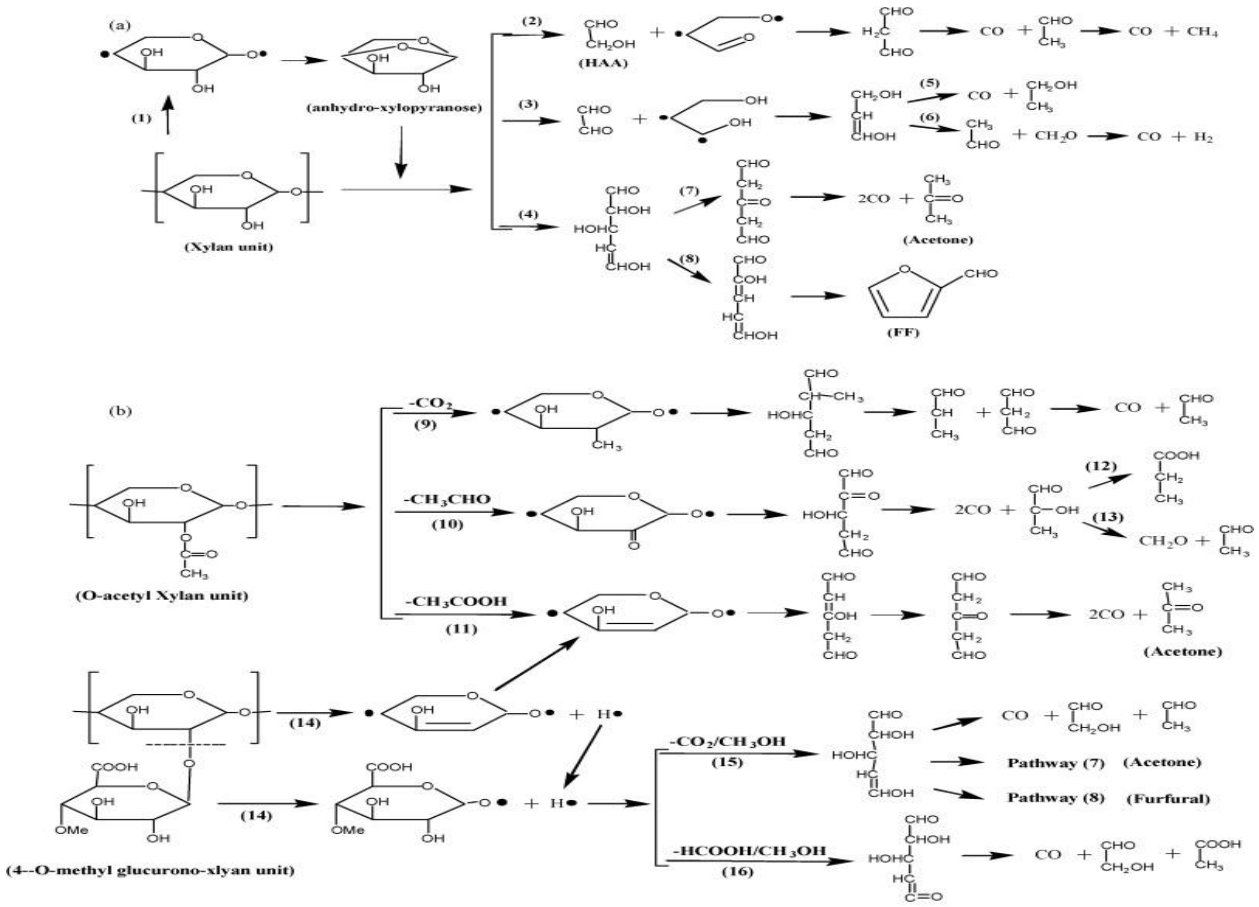

Figure 2.6. Tentative explanation of (a) O-acetyl-4-O-methylglucurono-xylan and (b) O-acetylxylan and 4-O-methylglucuronic as hemicelluloses model compounds.[32] FF = furfural, HAA = 2-hydroacetaldehyde

2.2.2.1.4 Biomass gasification and tar formation

Evans and Milne[31] first proposed a pathway for tar formation from biomass pyrolysis. The pathway shows intermediate groups of tar compounds but does not however clearly elucidate the mechanism of formation. More recently, Palma proposed a concerted mechanism for the formation of primary, secondary and tertiary tar compounds based on the most favorable reactions thermodynamically as illustrated in Figure 2.7.[33] The author used lignin as the basis for tar model and later compared the performance of the model with experimental biomass gasification experiments.

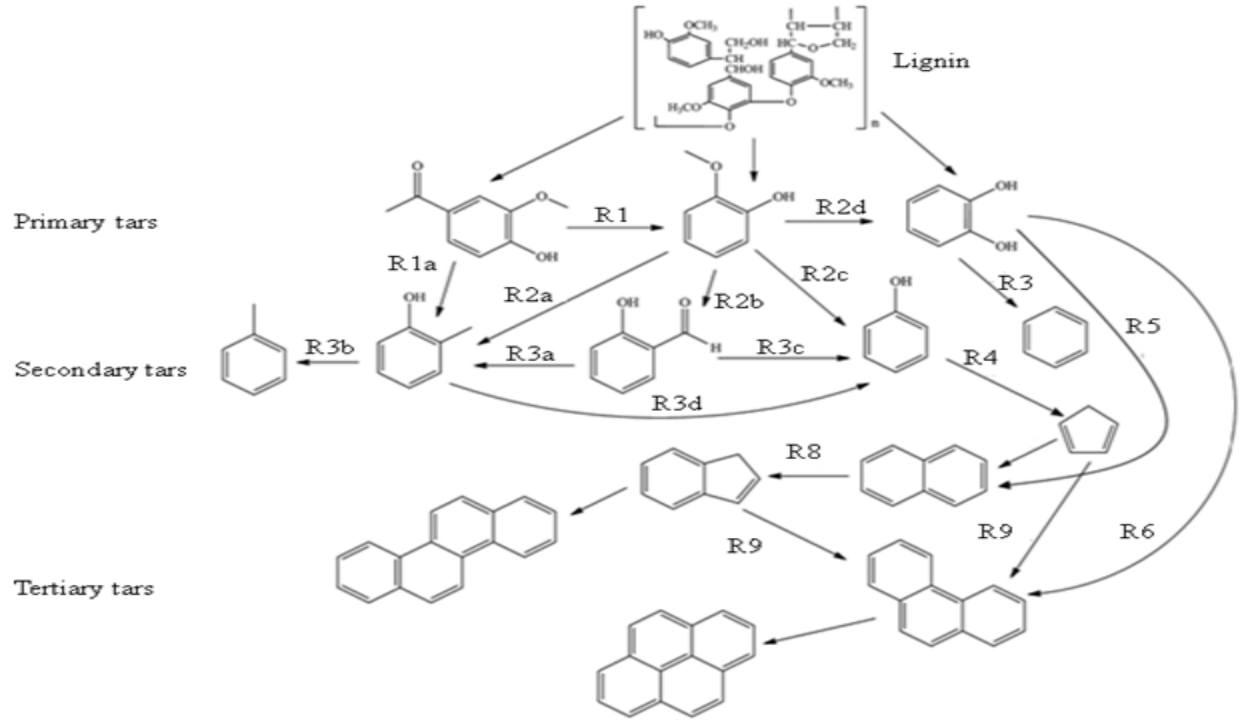

Figure 2.7. Mechanism for the formation of primary, secondary, and tertiary tars.[33]

The kinetic model derived from this mechanism was used to predict tar formation in fluidized bed gasification experiments. At various conditions, the model over predicted the concentration of tar in the product gas. The author suggested that this deviation is due to the omission of combustion reactions for which no kinetic information was available.

2.2.2.2 Nitrogenous Contaminants

Nitrogen in biomass is converted to ammonia (NH_3), hydrogen cyanide (HCN) and oxides of nitrogen (NO, NO_2, N_2O and other NO_x).[34] However, among all nitrogenous species in biomass gasification producer gas, ammonia is the most abundant with widely varying concentrations typically between 350 and 18,000 ppmv depending on the nitrogen content in the feedstock.[2, 20, 34] NH_3, HCN and NOx compounds account for 63.5, 0.11 and 0.06 wt % of fuel bound nitrogen at 750˚C, respectively.[34] These proportions decrease with increasing temperature to less than 25

wt % for NH_3, 1.50 wt % for HCN and 0.01 wt % for NOx at temperature higher than 950˚C.s[2, 34-36] The primary incentive for ammonia removal is the reduction of NO_x emissions in downstream applications such as burners, gas engines and turbines.[20]

2.2.2.3 Sulfurous Contaminants

Sulfur in the biomass is converted primarily to hydrogen sulfide (H_2S), carbonyl sulfide (COS), carbon disulfide (CS_2) and other minor sulfur containing compounds with H_2S being the most dominant in gasification.[37] Most downstream applications require the removal of sulfur based contaminants to avoid equipment corrosion, catalyst deactivation as well as to comply with emission regulations. Since concentrations as low as one ppmv of sulfur in gas stream can severely deactivate catalysts, producer gas requires extensive cleaning of H_2S and other sulfur based contaminants if it is intended for use in catalytic chemical processes downstream.

2.2.2.4 Hydrogen Halide Contaminants

Halogens, like chlorine in biomass feedstocks, are released as hydrogen halides such as hydrogen chloride (HCl) and their respective salts by binding to metals in biomass such as alkali metals. Among all hydrogen halides, HCl is the most abundant.[38] Hydrogen halide removal is very important to minimize corrosion on equipment such as filters, turbine blades, heat exchanger surfaces and to meet often stringent requirements for downstream application.[2, 38] Fuel cell applications particularly have very stringent requirements for hydrogen halide concentrations due to the susceptibility of electrolytes and electrodes attack by halogen ions.

2.2.2.5 Trace Metal Contaminants

Metals such as Ca, Mg, P, Si, Na, K, Fe, Al, Cu, Mn, Fe, Zn, Mo, As, Cd, Hg and Pb are taken during the plant growth from soil, water and air. These metals are partitioned in char and gas

product during gasification. The gas phase metals are the major source of concern as they must be captured downstream prior to exhausting the gas into the atmosphere. Consequently, they must be removed as they are a source of concern for human health and environmental pollution. In addition, some of these elements can contribute to catalyst deactivation as well as corrosion and fouling of equipment.[39]

2.3 Biomass Feedstocks for Gasification

Main sources of gasification feedstocks can be grossly grouped in four categories with varying physical and chemical characteristics: woody biomass, herbaceous biomass, agricultural residues and coal. A summary of these properties is outlined in Table 2.2. Besides feedstocks from these main categories, other feedstocks, like municipal and industrial wastes have been used employed in gasification. Due to the wide variability in their composition and their low potential for usage at a large scale, these feedstocks are not discussed here.

Table 2.2. Properties of selected feedstocks and coal with potential usage in gasification

	Woody biomass		**Agricultural residue**	**Herbaceous biomass[a]**	**Coal**		
Name	**Pine**[40]	**Poplar**[41]	**Corn stover**[41]	**Switchgrass**[42]	**Daw Mill,U**[43]	**Grundy, IL #4**[41]	**Rosebud MT**[41]
Proximate analysis, wt % dry basis							
VM	80.8	86.1	80.0	76.0	35.6	40.6	39.04
FC	18.5	13.7	13.9	16.0	58.5	45.47	49.08
Ash	0.7	1.2	5.0	8.0	6.5	13.93	9.16
Ultimate analysis, wt % dry basis							
C	50.9	49.4	46.3	44.9	73.8	68.58	68.39
H	6.1	6.0	5.7	5.2	4.9	4.61	4.64
N	0.5	0.2	0.7	0.6	1.3	1.18	0.99
Cl	N/A	0.1	0.1	0.1	N/A	0.12	0.02
O	41.8	43.1	41.2	37.9	12.3	6.79	16.01
S	0.15	0.01	0.26	0.18	1.6	4.76	9.16

MC = moisture content | VM = volatile matter | FC = fixed carbon | N/A = not available

[a] While there are other promising herbaceous bioenergy crops in different regions, switchgrass has been identified as the most viable globally due to its wide adaptability and high yields[44]

As can be expected, these differences will have implications on the gaseous primary products as well as on the major contaminants. While different biomass feedstocks result in different primary gas composition, the effect of feedstock is secondary to the effects of temperature and gasifying agents particularly when the feedstock elemental composition and physical properties are not significantly different. One the other hand, feedstock significantly impacts the concentrations of contaminants. The impact of feedstock will be discussed later in contaminant section.

2.4 Effect of Operating Conditions on Primary Gases and Gasification Performance Indicators

2.4.1 Temperature

Gasification temperature is of the utmost importance in determining the composition of primary gases as it not only affects the reaction rates but also dictates whether or not a reaction is favored based on thermodynamics.

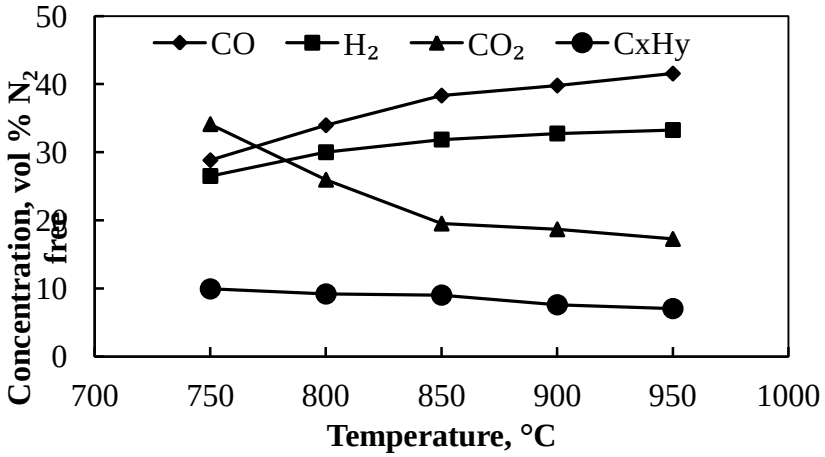

Figure 2.8. Effect of gasification temperature on primary gases[34]

In general, as temperature is increased, CO and H_2 are expected to increase as well.[45] Since the forward direction is favored in endothermic reactions as temperature is increased, it implies that CO and H_2 formation is favored as temperature is increased via the water gas and Boudouard reactions. This expected trend has been illustrated by various authors.[8, 11, 34, 35] The increase in

CO and H_2 comes at the detriment of CO_2[8, 11, 34, 35] based on experimental results and consistent with the expected trend for the Boudouard reaction. CH_4 and light hydrocarbons are not significantly impacted by temperature except at higher temperature (> 1000°C).[11, 35]

Due to the increase in CO and H_2, the heating value of the product gas should increase as temperature is increased beyond 850°C, a decrease was observed.[46] Gas yield, cold gas efficiency and carbon conversion also increase as temperature increases while keeping other parameters (ER and S/B) constant.[46]

2.4.2 Gasifying Agent

When air is used as the sole gasifying agent, it is observed that as ER increases CO and H_2 decrease as CO_2 increases, in contrast with trends observed for temperature.[11, 35] This is due to the promotion of oxidation reactions, which convert CO and H_2 to CO_2 and H_2O, respectively as illustrated Figure 2.9. In turn, this decrease in CO and H_2 results in a decrease in heating value but an increase in gas yield[11] and carbon conversion and a decrease in cold gas efficiency.[47]

If steam is used either as the sole gasifying agent or in combination with oxygen or air, H_2 production is drastically improved resulting in a high heating value.[47] As S/B is increased, H_2 increases while CO_2 decreases conversely as illustrated in Figure 2.10 likely due to the water gas shift reaction. On the other hand, CO and CH_4 are modestly affected. In addition, higher carbon conversion and gas yield are observed, relative to air gasification with heating value, gas yield and carbon conversion decreasing as S/B ratio was increased from 0.6 to 1.8.[46] The decrease in heating value is due to a decrease in CO and CH_4 as well as other light hydrocarbon. One well known drawback of steam as a gasifying agent is the reduction in reaction temperature which is manifested by lower carbon conversion and cold gas efficiency when compared to air gasification.[46, 47]

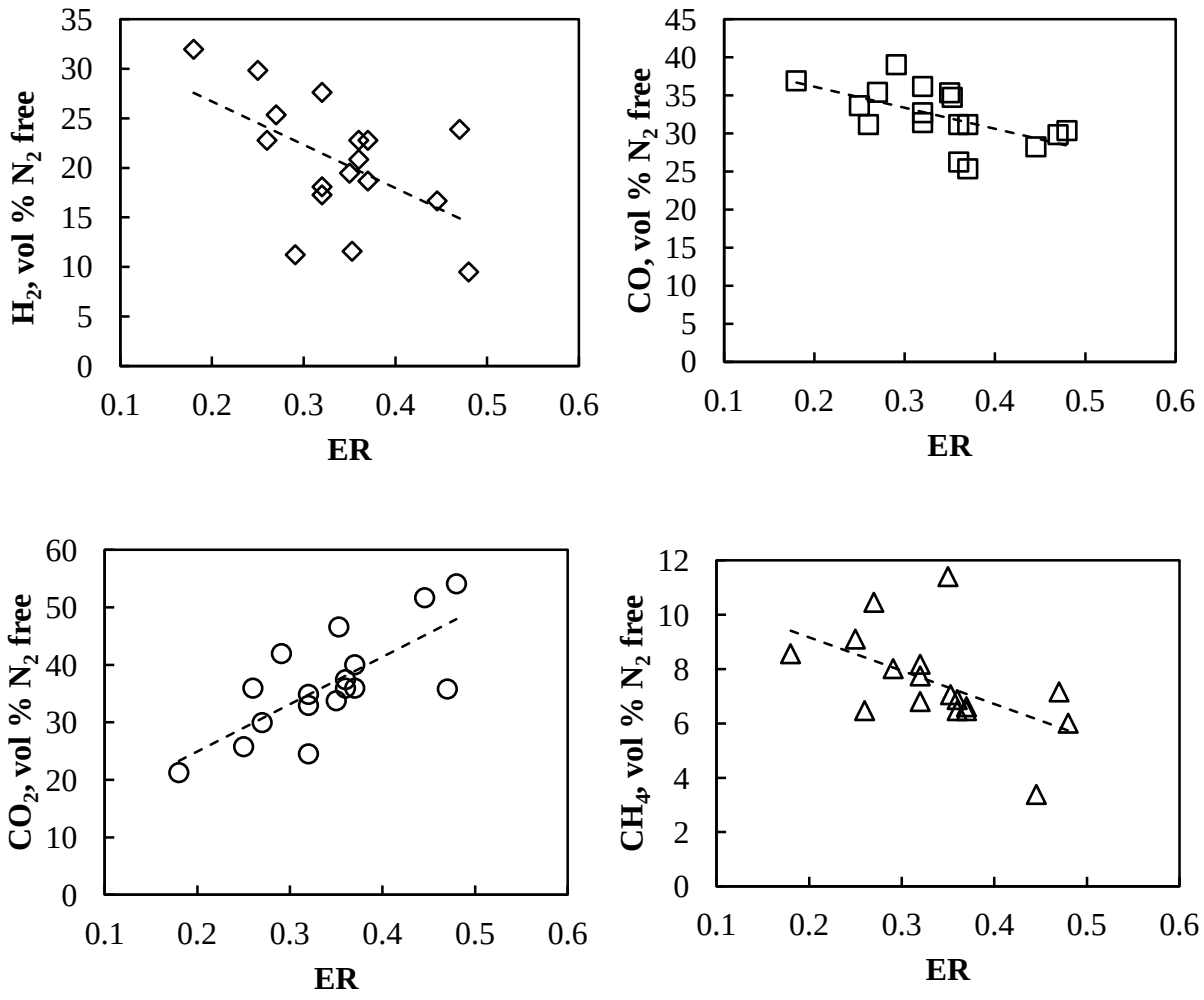

Figure 2.9. Effect of equivalence ratio on primary gas components in air gasification All temperatures used in this dataset are within 800 ±15°C.[9, 11, 13, 18, 35]

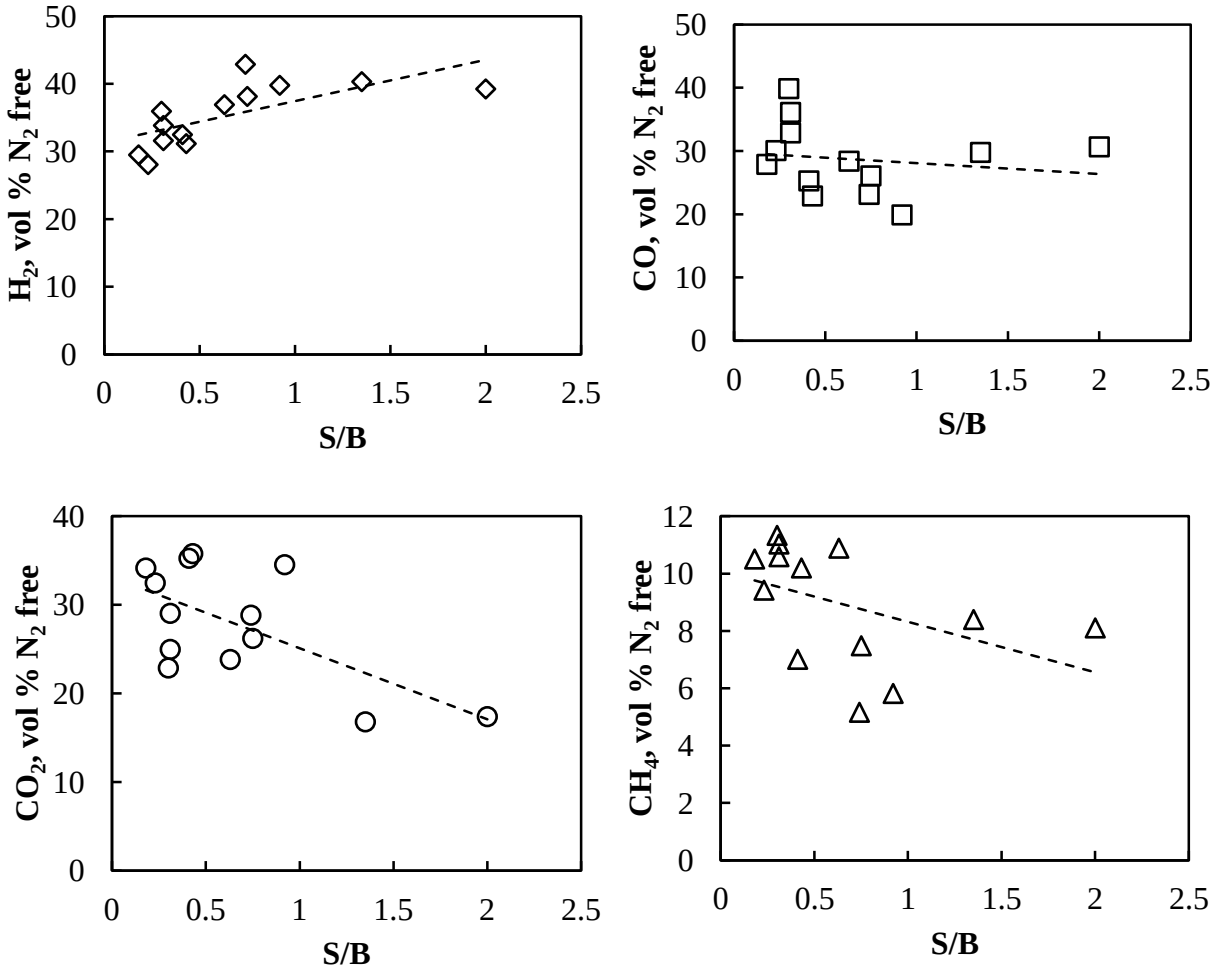

Figure 2.10. Effect of S/B on primary gas composition in fluidized bed gasification. Temperature ranged from 750 to 800°C with a mean of 787°C and equivalence ratio ranged from 0.19 to 0.28 with mean of 0.24[15, 18, 46]

2.5 Gasifiers and their Implications on Product Gas

Gasifiers are classified based on their geometry, flow patterns and process conditions. Three main types of gasifiers exist: (1) entrained-flow gasifier, (2) moving-bed gasifier, and finally (3) fluidized-bed gasifier. Salient characteristics of each gasifier will be discussed in the following sections.

Table 2.3. Ranges of syngas primary gases and contaminants for air gasification of biomass

	Entrained flow[b 48]	***Fluidized bed***		***Downdraft***[d 49]	***Updraft***[50]
		CFB[9, 10]	BFB[11, 12, 51, 52]		
Fuel properties, wt % dry ash free					
C	51.1	48.7-53.0	42.6-52.2	48.4	43.8
H	6.3	5.6-7.9	4.9-5.9	6.0	6.8
O	42.6	37.6-44.5	28.8-44.5	45.3	39.1
N	0.1	0.2-3.4	0.1-1.7	0.2	1.2
S	0.01	0-0.5	0-0.1	0.10	0.05
Cl	0.02	0.02-0.09	0.01-0.64	n/a	n/a
Volatile matter	80.8	75.8-83.5	71.3-82.7	63.4	77.0
Ash[a]	0.40	0.40-17.6	0.4-12.7	3.9	0.83
Process conditions					
ER	0.43-0.50	0.20-0.48	0.26-0.66	0.32-0.37	0.10-0.50
Temperature, °C	1200	701-1042	790-890	800-1000	750-950
Pressure, bar	1.95	1-1.19	1	1	1
Primary gases, vol %					
H_2	19-23	3-17	7-12	16.5	7-18
CO	35-40	8-21	5-18	15.9	8-32
CO_2	17-19	13-17	11-15	15.3	10-22
CH_4	1-2	2-7	2-5	2.1	4-6
N_2	18-26	43-68	45-73	50.2	36-65

CFB stands for circulating fluidized bed, BFB stands for bubbling fluidized bed, n/a means not available, [a] reported as wt % dry basis, [b]oxygen enriched air oxidant ranging from 58 to 63 vol % of O_2, [c]figures valid for woody biomass, [d]figures for primary gases represent average values of wood chips

Table 2.3 summarizes the composition of primary gases and contaminants along with relevant ultimate and proximate data. As the gas phase contaminant concentrations are dependent of the fuel bound concentration of its precursors (N, S and Cl), ultimate and proximate information is necessary in order to provide a reference. Furthermore, since tar concentration is affected primarily by the volatile matter in the fuel and by the catalytic activity of inorganic compounds

in ash, volatile matter and ash content is also summarized in Table 2.3 as well. All the data pertains to air gasification in order to avoid the effect of mixtures of gasifying agents.

2.5.1 Entrained-Flow Gasifier

Entrained- flow gasifiers are characterized by very high temperature operations, typically between 1000 to 1500°C for biomass[53, 54] and 1350 to 1650°C for coal with very fine particle size (< 100 μm) The injection of fuel into a stream of oxygen enriched air and/or steam causes particles to be suspended and well-mixed in the oxidizing gas stream. As a direct result of the high temperature operation, the solid residual exits as molten slag at the bottom of the gasifier. Entrained bed gasifiers are subdivided into top-fed (Figure 2.11) and side-fed (Figure 2.12) based on the side of the entry point of the solid fuel.

In top-fed entrained flow gasifiers, biomass and oxidant are introduced at the top of the reactor and solid and syngas flow co-currently downward. On the other hand, in side-fed entrained flow gasifiers, biomass and oxidizing medium are fed on the side, near the bottom while syngas is removed from the top.

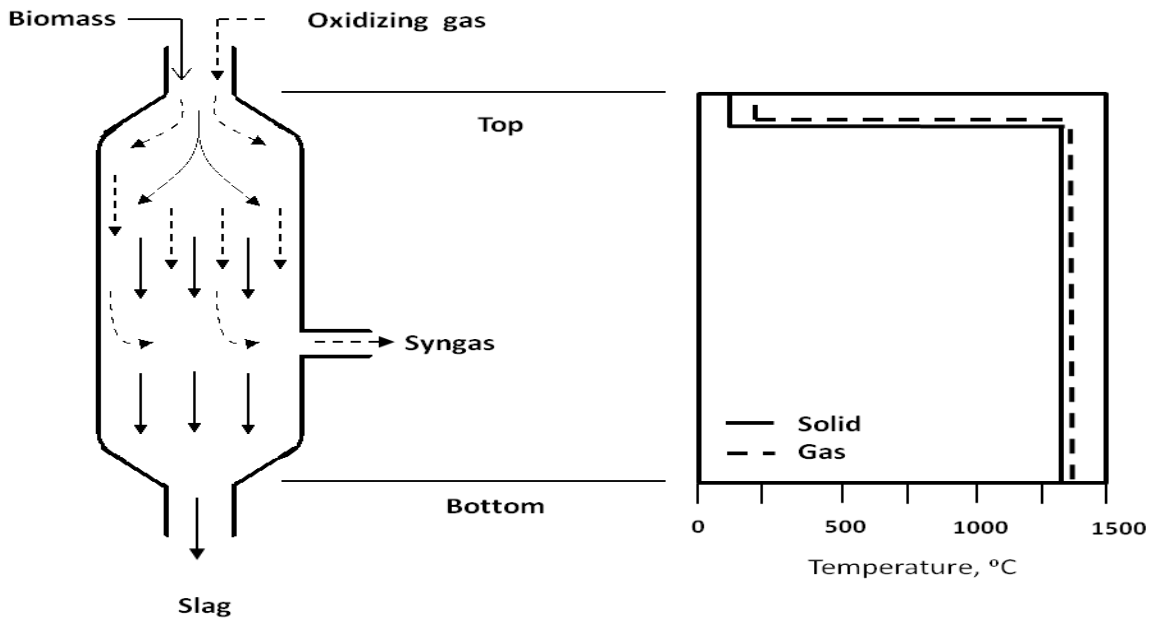

Figure 2.11. Top-fed entrained flow gasifier solid-gas flow pattern and temperature profile [55]

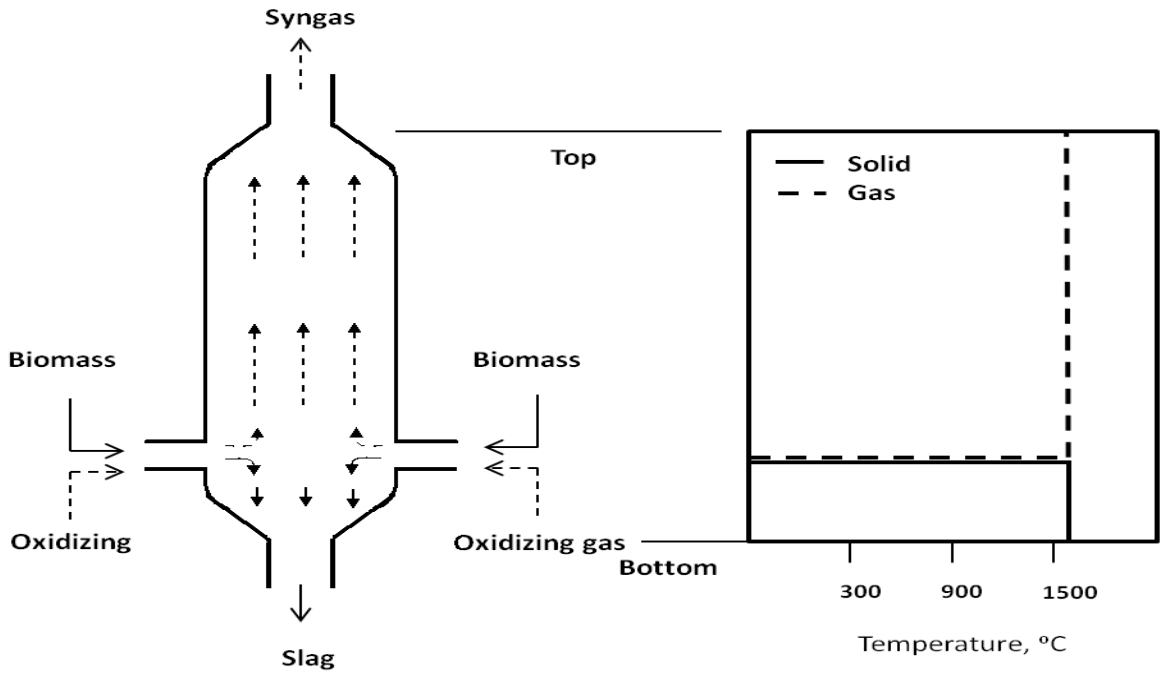

Figure 2.12. Side-fed entrained flow gasifier solid-gas flow pattern and temperature profile [55]

Entrained flow gasifiers have short residence times (3-5s), good mixing, ability to be technically and economically scaled up for pressures up 80 bar [24] and higher temperature. Due these

properties, these gasifiers have a high throughput and carbon conversion efficiency and are consequently well adapted for a variety of very large scale applications (up to 500 MW [24]). A drawback for this system is its higher oxygen requirement and thus yield a lower heating value gas. Several entrained-flow gasifiers have been employed commercially, primarily for coal gasification, and often bare the name of the original parent company or companies that have acquired the parent company. While these systems by design are entrained flow gasification systems, they often deviate from the simplistic classification above.

Table 2.4. Primary gas composition from biomass feedstocks in entrained flow gasifiers

Feedstock	***Sawdust*[54]**	***Sawdust*[54]**	***Rice husk*[54]**	***Rice husk*[54]**	***Woody biomass*[53]**
Oxidizing agent	O_2	O_2	O_2	O_2	O_2
ER	0.29	0.29-0.50	.39	0.29-0.54	n/a
S/B	0	0	0	0	0
Temperature, °C	1000-1400	1300	1000-1400	1300	1200-1500
Pressure, bar	1	1	1	1	20
Primary gases, vol %					
CO	40-50	45-50	45-55	45-50	53
H_2	33-38	37-48	37-48	37.5-47	27
CO_2	10-20	10-20	8-23	7-10	19
CH_4	0-9	1-3	1-8	3-5	0

n/a means not available

2.5.2 Bubbling and Circulating Fluidized-Bed Gasifier

Bubbling (BFB) and circulating (CFB) fluidized bed reactors have been established as major industrial reactors in various processes over the years. However, these reactors have been extensively applied in energy conversion particularly in petroleum refinery, combustion and gasification.

In fluidized-bed gasifiers, feedstock is fluidized along with a bed material like sand or catalysts for removal of gas contaminants with a gasifying medium, which can be air/oxygen, steam or a

combination thereof. Fluidized bed gasifiers are categorized as bubbling fluidized bed (Figure 2.13a) and circulating fluidized bed (Figure 2.13b). By design, the two fluidized bed gasifiers are similar with the exception that bubbling fluidized bed gasifiers operate at lower fluidization velocity. Circulating fluidized bed gasifiers imply that i) particles entrainment is sought and desired and unconverted fuel and bed material are returned back to the reactor and ii) high material flux (10–1000 kg/m^{2}s) and superficial velocity (2–12 m/s)[56] with no clear distinction between dense and dilute material mixing throughout the reactor.

Fluidized bed gasifiers are used for intermediate applications: bubbling fluidized bed gasifiers or BFBG (Figure 2.13.a) are simpler to design and thus preferred in small to medium applications (few kW to 25MW) whereas circulating fluidized bed gasifiers or CFBG (Figure 2.13.b) are emerging as the choice for medium to large scale applications (25MW to 60 MW).[57]

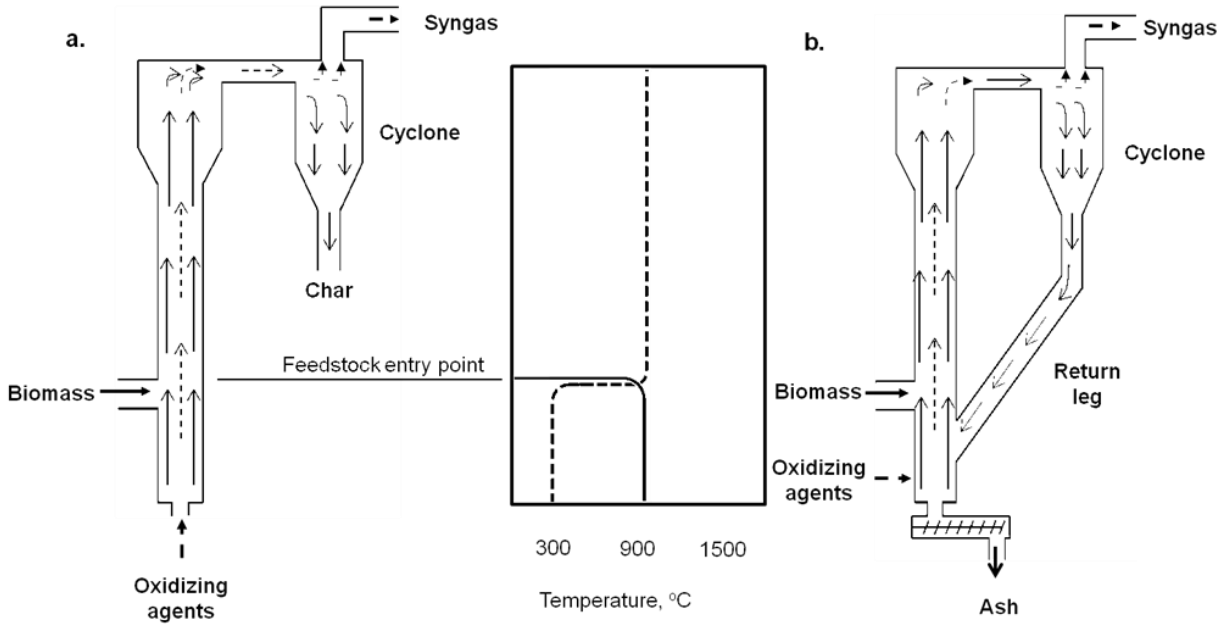

Figure 2.13. Bubbling fluidized bed and circulating fluidized bed gasifiers[58]

2.5.3 Moving-Bed Gasifier

In a moving-bed gasifier, steam and air/oxygen flows through a bed kept fixed by constant addition of fresh solid fuel. Although the bed remains overall constant, there is a slow downward movement of solids as the fuel is decomposed with fuel residence times that can reach 1 hour. There are two main configurations for moving bed based on the fuel and syngas flow patterns. In the first configuration, the solid fuel is fed from the top, while air or oxygen is injected from the bottom as illustrated in the leftmost schematic in Figure 2.14. This is a counter-current or updraft gasifier configuration as the fuel moves downward while the syngas moves in the opposite direction. A counter-current moving-bed gasifier can be divided into four zones (from top to bottom): (i) the drying/preheating zone, (ii) the de-volatilization zone, (iii) the gasification zone, and (iv) the combustion zone. Fuel in the top zone is dried/preheated by hot gas that is flowing from the bottom. It then moves down to the de-volatilization zone, where heat from the hot gas drives volatiles out of coal particles. Gasification occurs in the next zone, and any remaining char is then reacted in the gasification zone. Syngas produced by an updraft moving-bed gasifier has high tar content because the tar released during the de-volatilization process is carried away by the hot gas which is flowing up from gasification zone.

In the second configuration, fuel and syngas move downdraft with syngas and char is removed from the bottom. This is a co-current or downdraft gasifier configuration as shown in the rightmost schematic in Figure 2.14. Unlike for updraft gasifiers, volatiles go through the combustion zone which is oxygen rich relative to other zones and has the highest temperature, prior to exiting. The syngas flow direction has implications on its properties: downdraft yields relatively “cleaner” syngas because it passes through the hottest zone in the reactor resulting in further thermal cracking of tar.

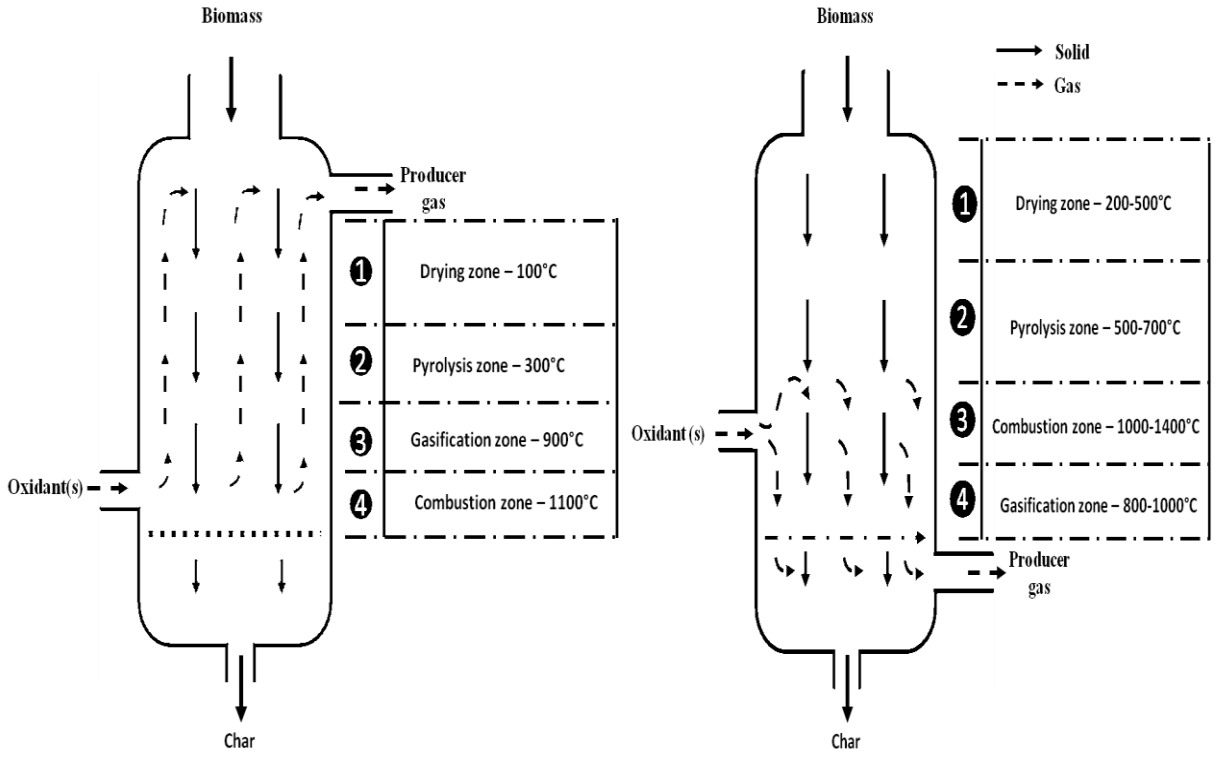

Figure 2.14. Moving bed gasifiers. Counter-current or updraft gasifier (left) and co-current or downdraft gasifier (right)

Moving-bed gasifiers have the advantage of high carbon conversion and high thermal efficiency. However, they have poor radial temperature uniformity, which results in local slagging, bridging, and clinkering problems. In addition, due to the slow movement of the bed, moving bed reactors have a lower throughput. Moving bed gasifiers are suitable for small to medium applications (10 kW-10MW).[57] Furthermore, downdraft gasifiers are preferred for small-scale power generation due to a low amount of tar content in the producer gas.

2.6 Effect of Feedstock and Operating Conditions on Contaminants

2.6.1 Tar Contaminants

2.6.1.2 Effect of Feedstock Type on Tar

In general, during gasification, woody biomass results in overall higher concentration of tar than coal due to its higher volatile matter content[59]. In fact, it appears that tar yield is related to the volatile matter at fixed gasification conditions based coal and pine co-gasification experiments where volatile matter in blends of 77.4, 48.5 and 32.9 wt% dry basis of biomass resulted in tar yields of 6.6, 4.0 and 2.3 g/kg dry fuel, respectively.[60] The chemical classes of tar compounds (primary, secondary and tertiary tar compounds) follow a similar trend in the aforementioned study. Since volatile matter content in herbaceous and agriculture biomasses lies between that of wood biomass and coal, it would be expected that these feedstocks would produce less tar than woody biomass.

Higher ash content, leading to higher catalytic cracking of tar by inorganic elements, has been suggested as possible factor in the reduction of tar yields in gasification of blends of biomass and coal.[60] The role of inorganic constituents in ash on pyrolytic vapors has been observed. It is therefore not appropriate to deduct ash in biomass that would affect tar quantity and composition. In steam gasification of leached olive kernel, it was observed that the reduction in ash content, particularly iron and alkali metals, resulted in higher tar content suggesting that steam reforming of tar is catalytically affected by inorganic elements in biomass ash.[61]

2.6.1.3 Effect Operating Conditions on Tar

2.6.1.3.1 Temperature

Temperature plays a vital role in tar reduction as it induces thermal cracking as well as steam reforming and dry reforming, both endothermic reactions. As such, as temperature increases, tar concentration usually decreases. Indeed, tar concentration was reduced from 19 g/Nm^3 to 3 g/Nm^3 when temperature was increased from 700°C to 800°C.[11]

Temperature also affects the nature of tar compounds. As temperature is increased primary and secondary tar classes decrease while tertiary tar increases as shown in Figure 2.15.

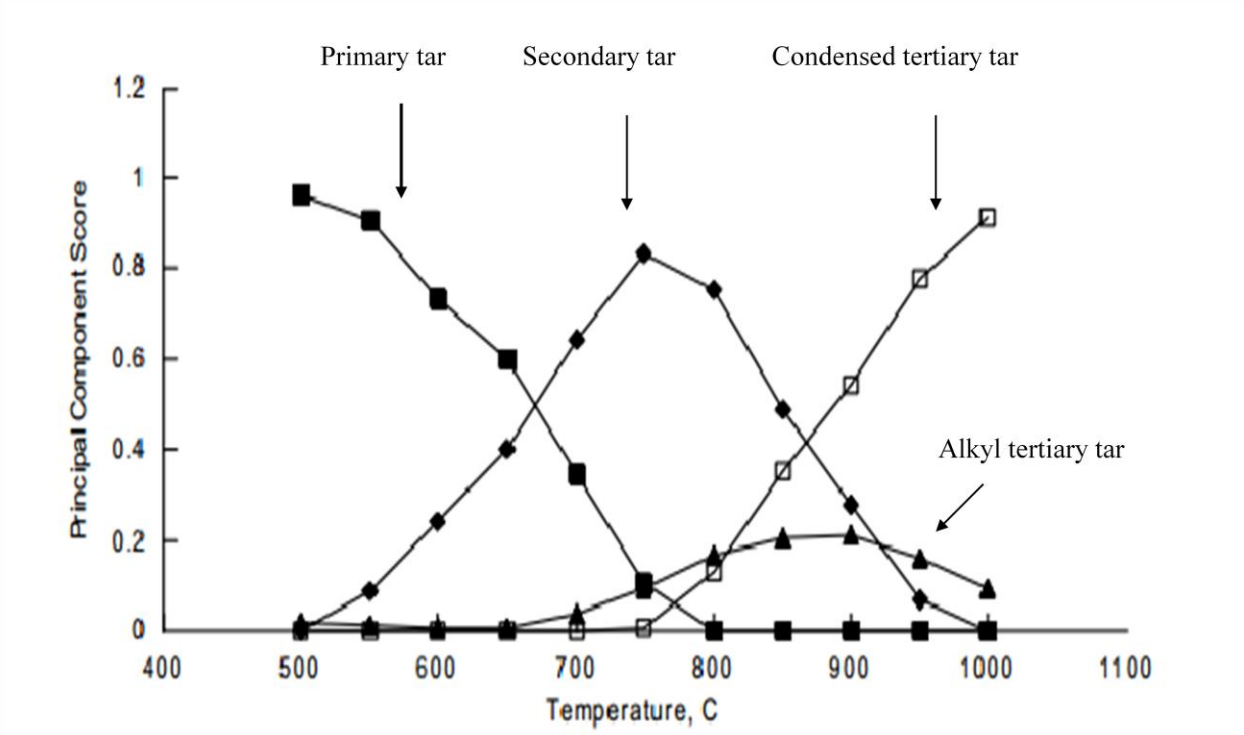

Figure 2.15. The distribution of the four tar classes as a function of temperature. Adapted from Milne *et al.*[62]

2.6.1.3.2 Gasifying Agent

The presence of both air and steam result in tar reduction as illustrated in Figure 2.16. Increasing oxygen availability by way of higher equivalence ratio results in tar reduction due to tar oxidation. In general, an increase in equivalence ratio decreases tar concentration. Everything equal, the tar concentration was decreased from 10 g/Nm^3 to near 2.5 g/Nm^3 by increasing the equivalence ratio from 0.26 to 0.45.[11]

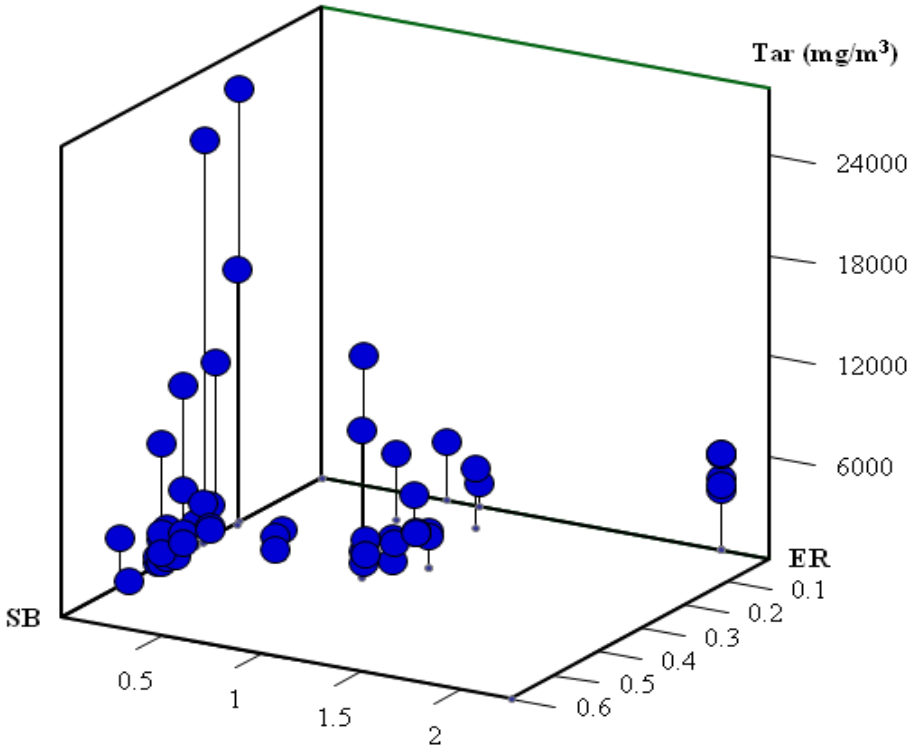

Figure 2.16. Impact of ER and S/B on tar concentration in producer for fluidized bed gasifiers. Mean temperature is 793°C, standard deviation = 50°C, maximum = 901°C and minimum is 645°C [9-11, 13, 15, 17, 20, 63]

At similar equivalence ratio, the addition of steam seems to drastically reduce the tar concentration as evidenced in Figure 2.16, expectedly due to steam reforming of tar compounds.

It appears that steam, as a sole gasifying agent, results in higher tar content than air. Gil *et al.* [64] reported the following for different gasifying agents on tar content: $tar_{steam} > tar_{O2/steam} > tar_{air}$.

2.6.2 Nitrogenous Contaminants

2.6.2.1 Effect of Feedstock on Nitrogenous Contaminants

Since fuel bound nitrogen evolves as nitrogen contaminants, it is expected that different fuel types, with different nitrogen content, would yield varying concentrations of nitrogenous contaminants. Van der Drift and co-workers[65] studied several feedstocks for ammonia formation. Verge grass, with 2.47 wt% nitrogen (dry and ash free basis) yielded an ammonia concentration of 12,500 ppmv. Similarly, Zhou *et al.*[35] reported an ammonia concentration of 18000 ppmv for leucaena with nitrogen content of 2.51 wt % dry basis. However, feedstock samples with lower nitrogen contents yielded lower NH_3 concentrations with a linear correlation between fuel bound nitrogen and syngas ammonia concentration as shown in Figure 2.17. Woody biomass sawdust, with low nitrogen content (0.03 wt % dry basis) resulted in NH_3 concentration between 650 and 300 ppmv at 800˚C and 0.18 to 0.37 ER.

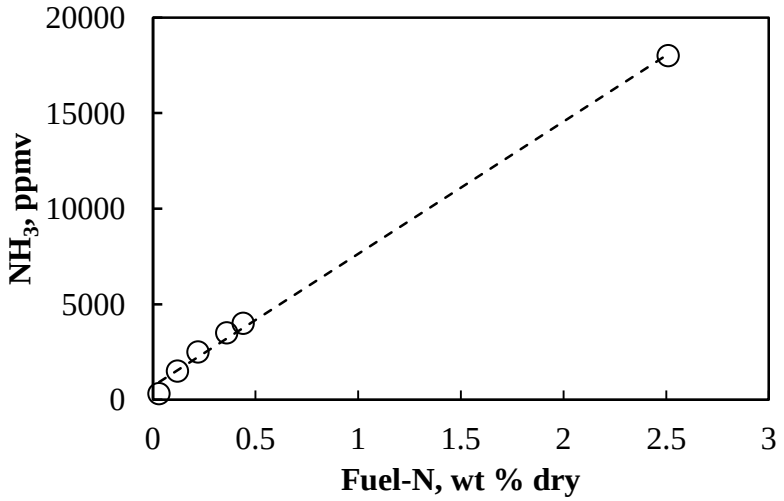

Figure 2.17. Effect of fuel bound nitrogen on ammonia concentration in syngas at gasification temperature at 800˚C and ER = 0.25.[35]

2.6.2.2 Effect of Operating Conditions on Nitrogenous Contaminants

2.6.2.2.1 Temperature

Temperature has the highest impact on NH_3 concentration in producer gas with higher temperatures typically resulting in lower NH_3 concentration. This trend is clearly illustrated in a study conducted by Zhou *et al*.[35] where decreasing trends for NH_3 were observed as temperature increased for several feedstocks as illustrated in Figure 2.18. For example, using sawdust, the concentration of NH_3 decreased by half over temperatures ranging from 700 to 900^{o}C at ER=0.25.[35] The decrease in NH_3 as temperature increases is due to NH_3 decomposition to N_2 and H_2. The fact that N_2 concentration increased as temperature increased in the aforementioned study supports this assumptions. Similar trends are observed for HCN and NO for leucaena and sawdust at the same equivalence ratio aforementioned.[35]

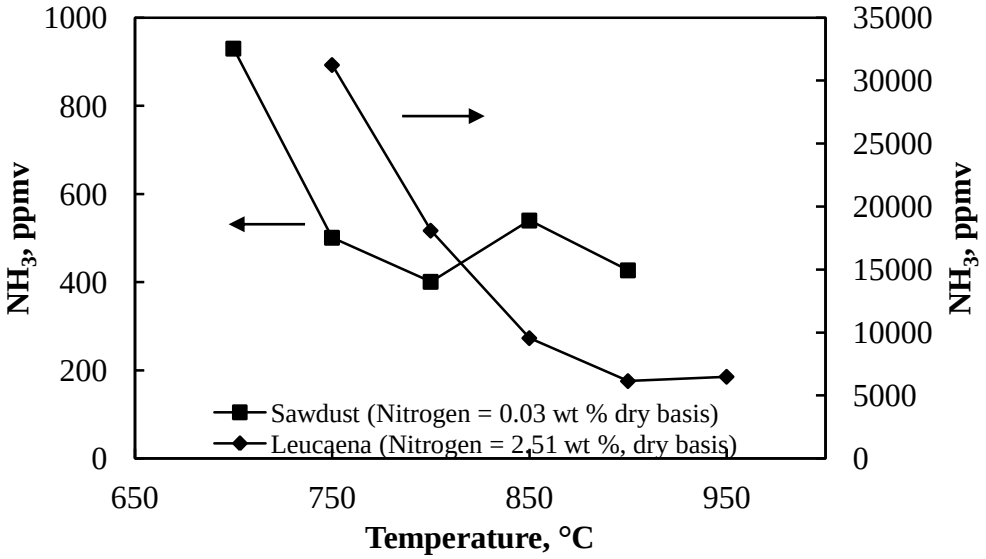

Figure 2.18. Impact of temperature on NH_3 in air gasification. ER = 0.25.[35]

2.6.2.2.2 Gasifying Agent

Besides temperature, ER can also affect the proportion of NH_3, HCN, NO and other nitrogen containing species in syngas. Indeed, it was observed that NH_3, HCN and NO decrease as ER is increased slightly from 0.18 to 0.37 at 800^oC.[35] However, it is evident that temperature, rather than ER, has the most impact in reducing nitrogen contaminants as illustrated in Figure 2.19.

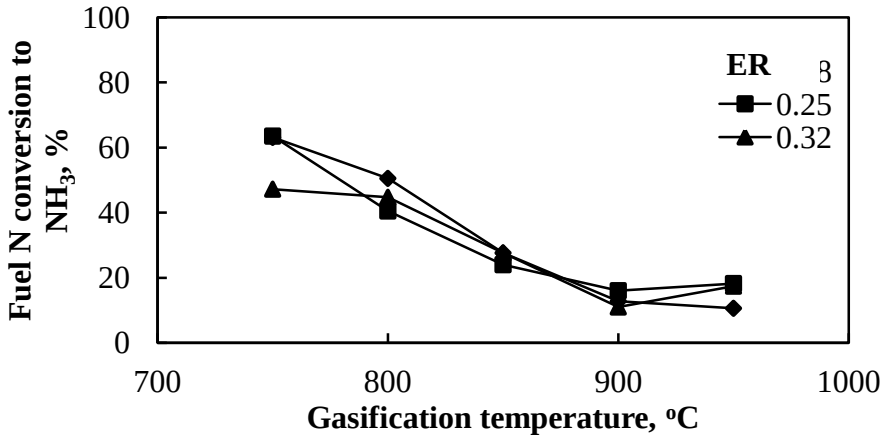

Figure 2.19. Effect of temperature and ER on fuel bound nitrogen conversion to NH_3. Reproduced from tabulated data [35]

Besides temperature and ER, the type of gasifying medium also plays a role in the concentration of NH_3, HCN and other nitrogenous compounds. The presence of steam in gasification enhances the formation of NH_3. A comparison of two fuels with similar nitrogen contents gasified in a circulated fluidized bed reactor with air and steam at similar temperature revealed that NH_3 concentration is doubled when steam is used[10, 66]. Fuel nitrogen conversion to HCN is also affected by gasifying agents. As the use of steam increases the concentration of H_2 in the syngas, it is likely that the increasing reducing environment favors the formation of NH_3.

2.6.3 Sulfurous Contaminants

2.6.3.1 Effect of Feedstock on Sulfurous Contaminants

The concentration of hydrogen sulfide varies depending on the gasification feedstock. Typically, its concentration in producer gas is less than 100 ppmv in most biomass.[67] However, the concentration of H_2S in syngas is dependent on the fuel bound sulfur content as illustrated in Figure 2.20. Sulfur content in coal, agricultural residue, woody and herbaceous biomass is significantly different, the first having the highest concentration. This difference in sulfur content is manifested by different concentrations of sulfurous contaminants in the syngas.

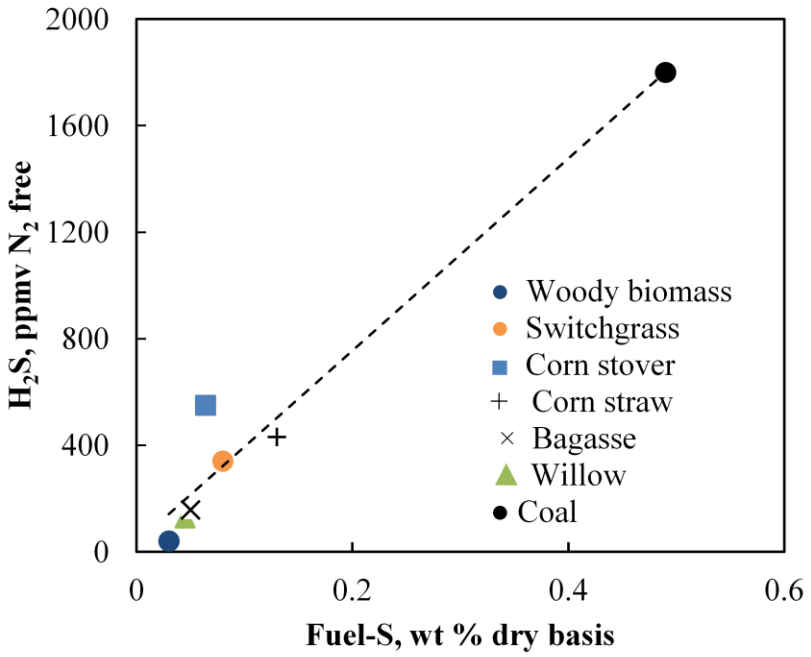

Figure 2.20. Effect of fuel bound sulfur on H_2S concentration in syngas.[10, 52, 68, 69].

Sulfur content in coal, agricultural residue, woody and herbaceous biomass are significantly different. Carpenter *et al.*[52] reported H_2S concentrations of 40, 550 and 380 ppmv for wood, wheat straw and switchgrass with sulfur contents of 0.03, 0.06 and 0.08 wt% on dry basis.

2.6.3.2 Effect of Operating Conditions on Sulfur Contaminants

2.6.3.2.1 Temperature

There are diverging reports of the effect of temperature on H_2S content in syngas. In a study of a mixture of 70% refuse derived fuel and coal (0.62 wt % dry ash free basis sulfur), it was reported that H_2S concentration in syngas increased from 808 to 1081 ppmv from 720 to 850°C but subsequently decreased to 823 ppmv as temperature was further increased to 900°C.[70] However, Carpenter *et al*.[52] reported an increase in H_2S for switchgrass, Vermont wood and wheat grass as temperature was increased from 650 to 875°C.

2.6.3.2.2 Gasifying Agent

Gasifying agent (air, steam, air/steam or O_2/steam) significantly affect the composition of primary gases as discussed earlier. These primary gases, in turn, can be involved in various reactions with H_2S and other sulfur contaminants thus affecting their final concentrations. Several reactions are involved in H_2S and COS formation and conversion during gasification.

$$H_2S + CO_2 \rightarrow COS + H_2O \quad [2.10]$$

$$H_2S + CO \rightarrow COS + H_2 \quad [2.11]$$

$$H_2S + 3/2O_2 \leftrightarrow SO_2 + H_2O \quad [2.12]$$

$$COS + H_2S \leftrightarrow CS_2 + H_2O \quad [2.13]$$

In a study of corn straw gasification in a downdraft gasifier, it was observed that as ER increased from 0.20 to 0.40, H_2S first increased from 473 to 512 ppmv from 0.20 to 0.30 ER and subsequently decreased to 459 ppmv from 0.30 to 0.40 ER.[68] Dias *et al*.[70] also observed that as ER is increased from 0 to 0.40 in a mixture of 70 % refuse derived fuel and coal (0.62 wt % dry ash free basis), H_2S concentration increased from 672 to 1204 ppmv. However, as S/B ratio increased, H_2S concentration decreased according to various studies.[68, 71]

2.6.4 Hydrogen Halide Contaminants

2.6.4.1 Effect of Feedstock on Hydrogen Halides

Hydrogen chloride is present in producer gas at concentrations ranging from few parts per million to 700ppm.[38] Like other contaminants, the concentration of gas phase chlorine increases with increasing concentration of fuel chlorine as shown in Figure 2.21.[72]

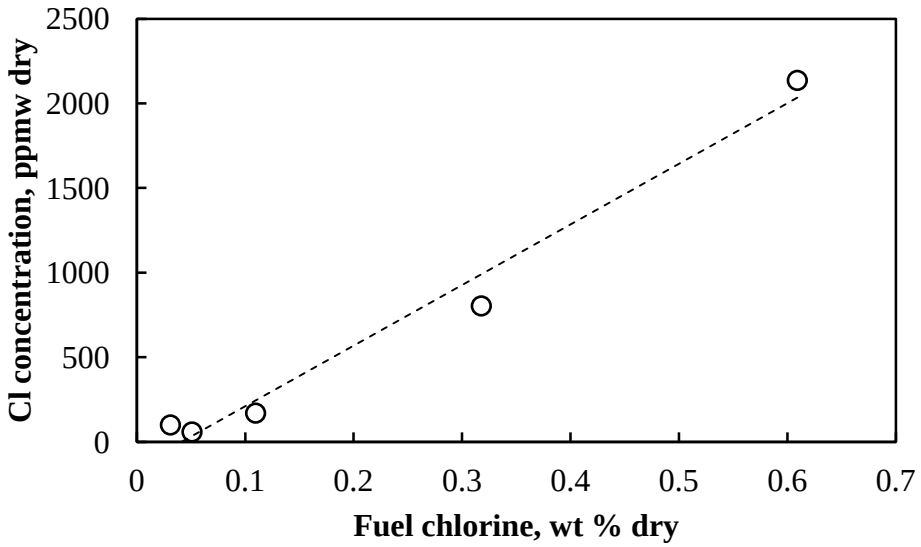

Figure 2.21. Effect of fuel Cl on Cl concentration in syngas. Feedstocks are banagrass and bagass gasified at 800°C and equivalence ratio from 0.26 to 0.33.[72] *Note*: The author does not indicate the form of chlorine in gas phase. Cl concentration might include hydrogen chloride as well as metal chlorides.

2.6.4.2 Effect of Operating Conditions on Hydrogen Halide Contaminants

2.6.4.2.1 Temperature

Temperature impacts hydrogen halides concentration in syngas by enhancing the formation of alkali halides using metals present in ash.[73] While there is little experimental data on the impact of temperature on HCl and other halides, several thermodynamic modeling studies suggested that as temperature is increased, the formation of hydrogen halides decrease while that metal halides increase.[74] At ER of 0.20, it was noticed that HCl concentration decreased from 95 to 65 ppmv as temperature was increased from 720 to 900°C for a mixture of 70 % refuse derived fuel and coal with a weighted average of 0.07 wt % dry ash free basis chloride.[70]

2.6.4.2.2 Gasifying Agent

The impact of gasifying agent on hydrogen halides is not clearly understood at this moment due to the lack of information particularly in air/steam and steam gasification for biomass feedstocks. Of the limited information available on this matter, it appears that as ER is increased from 0 to 0.40, HCl concentration increased from 78 to 85 ppmv at 850°C.[70]

2.6.5 Trace Metals Contaminants

2.6.5.1 Effect of Feedstock on Trace Metals

Trace metals from biomass can vary widely depending on the feedstock (see Table 2.5). During gasification, these metals are distributed in the char, producer gas, bed material as well as other reactor components. In general, herbaceous and biomass residues have higher metals emission than woody biomass in gasification. In a fluidized bed study of wood, straw and miscanthus, it was reported that in general herbaceous feedstock resulted in higher metals emissions than clean wood.[75]

Table 2.5. Metals in various feedstocks in biomass gasification[75]

.	g/kg dry biomass			
	Wood	Waste wood	Miscanthus	Straw
Al	<0.05	0.28	0.48	0.44
Ca	0.77	1.51	3.17	1.21
Fe	0.05	0.56	0.3	0.35
K	0.27	0.36	6.72	15.76
Mg	0.09	0.32	0.72	0.64
Na	<0.05	0.16	0.27	0.22
P	<0.05	0.06	0.48	0.72
Si	0.17	0.94	5.22	30.6
Zn	0.02	0.03	0.14	0.02
Pb	0.01	0.14	0.05	0.02

To a certain extent, the proportion of metal elements in the gas and solid streams (bed material and filtered char) reflect the composition of the feedstock. However, the distribution of elements in the gas phase, bed material and char varies widely. Furthermore, the release of alkali and other metals in the gas phase is not necessarily dependent on its concentration in the biomass.[19] It was observed in a comparative study of wood, straw and miscanthus that wood resulted in the highest content of KOH although it had the lowest fuel potassium.[75] Ca, K, Mg and P appear to be preferentially retained in the bed materials and on char.[19, 72] Of residual minor metals that exit the gasifier, most are concentrated in the filtered char: Ba, Co, Cr, Cu, Mn, Ni, P, Sr, Ti and V are concentrated in char whereas Cd, Mo, Pb and Zn remain mostly in the gas stream.[19]

2.6.5.2 Effect of Operating Conditions on Trace Metals

Alkali and other trace metals are commonly bound to halogen and other inorganic elements in biomass with the formation of alkali halides (NaCl, KCl etc.) increasing as temperature is increased.[74, 76] Porbatzki *et al*.[76] investigated the release of metals in wood and miscanthus during gasification at 800, 900 and 1000°C in a fluidized bed and observed that the release of

potassium decreased as temperature increased for wood but increased as temperature increased for miscanthus. In a thermodynamic modeling of a fluidized bed gasifier, it was reported that Na, K, Fe and Mn are not appreciably released into the gas phase even as gasification temperature is increased to 1000°C.[77] Similar conclusions were drawn by Forment and co-workers[78] where Ba, Mg, K, P and Mn are not released at temperatures lower than 1000°C. On the other hand, Pb, As, Zn, Hg, Sd, Sn and Cd are completely released in the gas phase at 750°C.[77]

2.7 Gas Cleanup

Depending on the exit gas temperature, syngas cleanup can be characterized as cold gas cleanup (< 100˚C) and hot gas cleanup (> 300˚C).[79]

2.7.1 Cold Gas Cleanup

Cold gas cleanup relies predominantly on "wet" processes where contaminants are removed by a liquid absorbent. Due to its proven reliability and high efficiency, cold gas cleanup is commonly considered the conventional approach in syngas cleanup. Cold gas cleanup has two distinguishing characteristics: *i*) it is carried out at low temperature, usually at or below room temperature and *ii*) it requires gas scrubbing through a liquid absorbent. The main disadvantages of cold gas cleanup are the efficiency penalty paid due to syngas cooling and the additional cost incurred to treat or dispose of spent absorbents.

2.7.1.1 Tar

Cold gas tar cleanup is carried out through wet scrubbing in a liquid absorbent. The scrubbing liquid can be as common as water[80, 81], vegetable oil[80] as demonstrated by the OLGA technology developed by ECN and Dahlman, or fatty acid methyl esters[80], an approach demonstrated in Austria at the Güssing Renewable Energy gasification installation.[82] Although water is a cheaper

and readily available absorbent, it is not very effective as a scrubbing solvent when compared to vegetable oil as shown in Table 2.6.

Table 2.6. Comparison of wet scrubbing technologies for tar removal[83]

	% tar removal		
Absorbents	***Water***	***Water and wet ESP***	***Vegetable oil (OLGA)***
Heavy tars	49	99	100
Light tars	62	74	99
Heterocyclic tars	79	79	99
Dew point[a]*, °C*	180	60	10

[a]Dew point here indicates the temperature below which tar in the product gas will condense

The tar removal efficiency is dictated by the solubility of tar compounds in the absorbent. As shown in Table 2.7, the poor removal efficiency of water is due to the poor water solubility of tar compounds as well as its ineffectiveness in removing vapor phase tars in the form of aerosols.[81] In this case, a wet electrostatic precipitator (ESP) or other aerosol filtration devices are required to improve removal efficiency. It has been reported that when water scrubbing and wet electrostatic precipitators are used, the tar concentration can be reduced from 80 to 0.025 g/Nm^3.[83]

Table 2.7. Absorption efficiencies of tar components by different liquid scrubbing solvents.[84]

	% Absorption				
Absorbents	**Water**	**Diesel fuel**	**Biodiesel fuel**	**Vegetable oil**	**Engine oil**
Benzene	24.1	77	86.1	77.6	61.7
Toluene	22.5	63.2	94.7	91.1	82.3
Xylene	22.1	n/a	97.8	96.4	90.7
Styrene	23.5	57.7	98.1	97.1	91.1
Phenol	92.8	n/a	99.9	99.7	97.7
Indene	28.2	97.9	97.2	97.6	88.7
Naphthalene	38.9	97.4	90.3	93.5	76.2

n/a represents values omitted from the primary reference

2.7.1.2 Nitrogenous Contaminants

Cold gas cleanup of nitrogen containing contaminants is commonly achieved through wet scrubbing. Due to the high water solubility of NH_3, the dominant nitrogen based contaminant in syngas, this absorbent is commonly employed for the removal of nitrogen containing contaminants. Absorption in water is enabled by protonation of NH_3 according to the reaction below.

$$NH_3 + H_2O \leftrightarrow NH_4^+ + OH^- \qquad [2.14]$$

In theory, NH_3 protonation to $NH4^+$ can be achieved in various dilute acid solutions. In fact, the EPA's procedure for collecting NH_3 in gas stream from stationary sources such as coal-fired boilers uses 0.1N H_2SO_4 as a scrubbing absorbent (EPA Method CTM-027). However, in practice, dilute acid solutions are not used except for sample collection for analytical quantification. Nonetheless, the solubility of NH_3 in acidic solution is advantageous particularly in acid gas removal where dissolved gases (H_2S and CO_2) enhance co-adsorption of NH_3. Wet scrubbing also presents practical advantages for solvent recovery as absorbent can be regenerated by precipitation as an ammonia salt[83] or by solvent regeneration through temperature swing.[85]

Wet scrubbing of syngas through water can significantly reduced NH_3 concentration with reduction greater than 99% observed when a spray chamber is utilized as a contacting device at room temperature.[85] In fact, even water vapor in syngas can remove more than 90% of NH_3 while condensing during gas cooling.[86]

2.7.1.3 Sulfurous Contaminants

Historically used for coal derived syngas cleanup, cold gas cleanup technologies for H_2S and COS removal employ solvents, the choice of which depends on factors such as gas composition, operating conditions and end-use application intended for cleaned gas. There are two modes of sulfur removal in solvent: chemical reaction or physical absorption. These different mechanisms have led to solvent characterization as "chemical" or "physical" solvents. In the case of chemical solvents, sulfur species form a weak bond with the solvent and are thus stripped from the gas stream. Common chemical solvents are alkanolamines, alkaline salts or aqueous ammonia whereas physical solvents are organic solvents with high affinity for acid gases. Figure 2.22 outlines the most common physical, chemical and hybrid solvents that are employed in acid gas removal.

For integrated gasification combined cycle (IGCC), environmental regulations require syngas sulfur concentration less than 30 ppmv in order to meet stack SO_2 emission limits.[87] In such a case, chemical solvents such as amine-based solvents like DMEA are more suitable due to the relatively high H_2S tolerance in the exit gas stream. For chemical and fuel synthesis, much lower sulfur concentration is required due to severe catalyst poisoning. In this case, physical absorption solvents like Selexol® and Rectisol® are preferred as they can achieve concentrations below 1 ppmv.

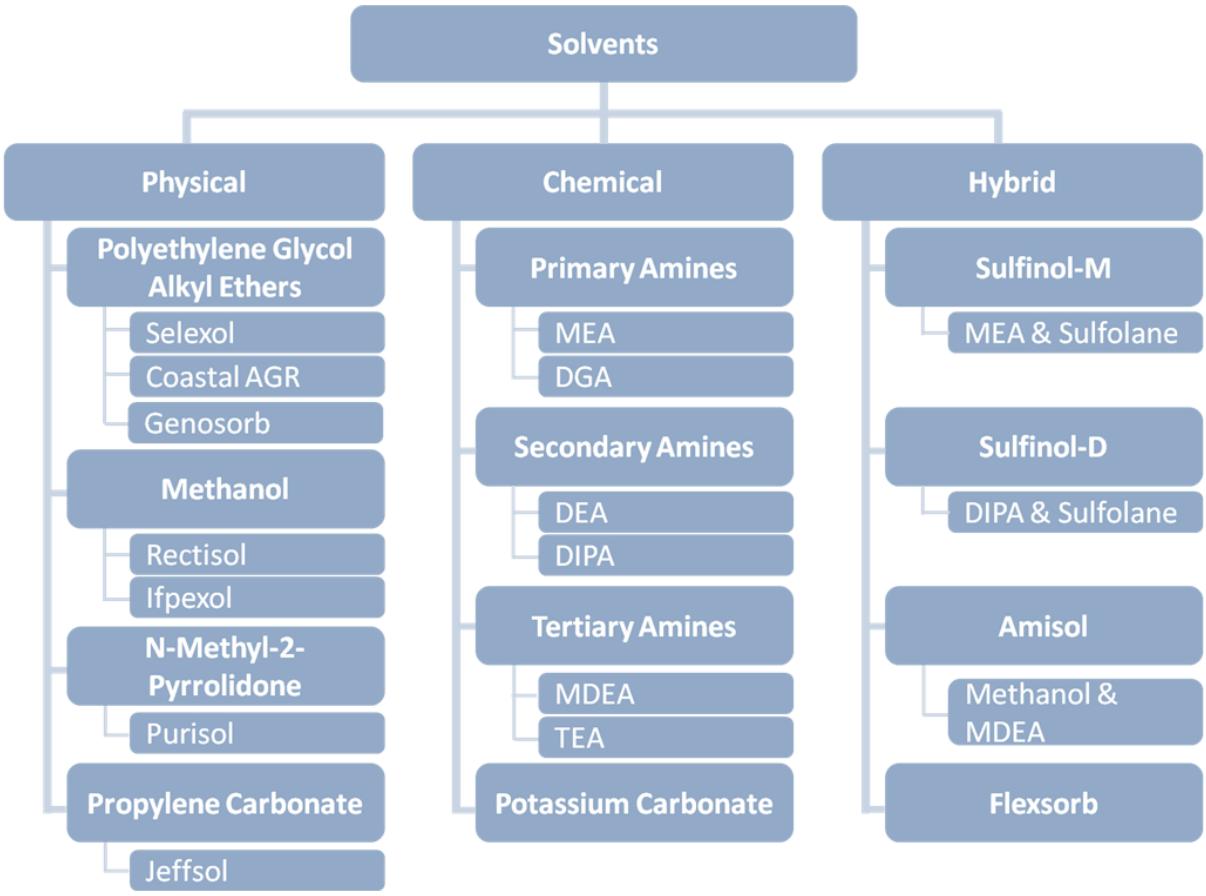

Figure 2.22. Diagram of common sulfur removal solvents employed in conventional acid gas removal (AGR). MEA = methylethanolamine, DGA = diglycolamine, DEA = diethanolamine, DIPA = di-isopropanolamine, MDEA = methyl diethanolamine and TEA = trietahnolamine. Selexol, Coastal AGR, Genosorb, Rectisol, Ifpexol, Purisol, Jeffsol, Sulfonol, Amisol and Flexsorb are commercial names of solvents.[88,89]

Solvent scrubbing has the added advantage of simultaneous co-adsorbing COS and CO_2. Due to the multifunctional attribute of these solvents toward acid gases (H_2S, COS and CO_2), the process is commonly referred to as an Acid Gas Removal process or AGR. Solvents can be regenerated by heat regeneration for chemical solvents and pressure letdown for physical solvents.[88] In addition, the rich sulfur stream recovered from the regenerator can serve as a feed to a Claus sulfur recovery unit to recover elemental sulfur.

Table 2.8. Conventional methods for sulfur removal from gasification syngas.[90]

Solvent	*Mechanism*	*Removal efficiency %*	*Typical process conditions*	*Exit gas quality*
MDEA	Chemical	H_2S: 98-99 CO_2: ≤ 30	T: 30-35°C P: ≤ 2.94 MPa	H_2S: 10-20 ppmv
Selexol®	Physical	H_2S: 99 CO_2: variable	T: 7-4°C P: 6.87 MPa	H_2S: < 30 ppmv
Rectisol®	Physical	H_2S: 99.5-99.9 CO_2: 98.5	T: 35-60°C P: 8.04 MPa	H_2S: < 0.1 ppmv CO_2: down to few ppmv

2.7.1.4 Hydrogen Halide Contaminants

HCl and other hydrogen halides are commonly removed by wet scrubbing usually through a caustic solution or, alternatively, simply water.[91] The use of caustic water, NaOH dissolved in water, is logical as HCl will react with NaOH to produce NaCl which can be precipitated out of solution.

$$HCl + NaOH \rightarrow NaCl + H_2O \quad [2.15]$$

The ability to remove NaCl by precipitation is an added benefit to caustic based wet scrubbing particularly when compared to the alternative water based scrubbing which will require costly ionic exchanger to strip chlorine from the solution.[92] In addition, caustic water can remove other contaminants such as COS[83, 93] as well as CO_2[83] according to the reactions below.

$$H_2S + NaOH \rightarrow NaHS + H_2O \quad [2.16]$$

$$H_2S + 2NaOH \rightarrow Na_2S + 2H_2O \quad [2.17]$$

$$COS + 4NaOH \rightarrow Na_2S + Na_2CO_3 + 2H_2O \quad [2.18]$$

$$COS + 2NaOH \rightarrow Na_2S + H_2CO_3 \quad [2.19]$$

$$CO_2 + 2NaOH \rightarrow Na_2CO_3 + H_2O \quad [2.20]$$

As NaOH reactions with HCl and H_2S are fast, it is possible to significantly reduce the concentrations of these two impurities when caustic water is used as an absorbent. While caustic water is a potential scrubbing solvent, water is still the most common solvent.[91]

2.7.1.5 Trace Metals

Gas cooling induces the condensation of most metals, particularly alkali metals which can be reduced by mild gas cooling below 600°C and subsequent adequate gas filtration.[94, 95] However, this approach only serves as a primary measure as some metals will remain in gas phase and can be removed by wet scrubbing with water.[95] Most trace metals, like alkali metals, are sufficiently soluble in water and can consequently be co-absorbed in water during wet scrubbing of tar and NH_3.

2.7.2 Hot Gas Cleanup

In addition to the conventional techniques described previously, warm and hot gas cleanup approaches are of great interest in contaminant removal from syngas. Warm and hot gas cleanup focuses on contaminant removal from syngas at high temperature (> 300°C).[79] The advantage of hot gas cleanup is that it addresses the loss in efficiency, a downside of cold gas cleanup. Additionally, it reduces the waste streams with the potential of converting some of the contaminants into environmentally benign or even useful products. Over the years, group of catalysts have been tested in hot gas cleanup of syngas. Various elements from the periodic table have demonstrated activity in the removal of one or several contaminants as shown in Figure 2.23.

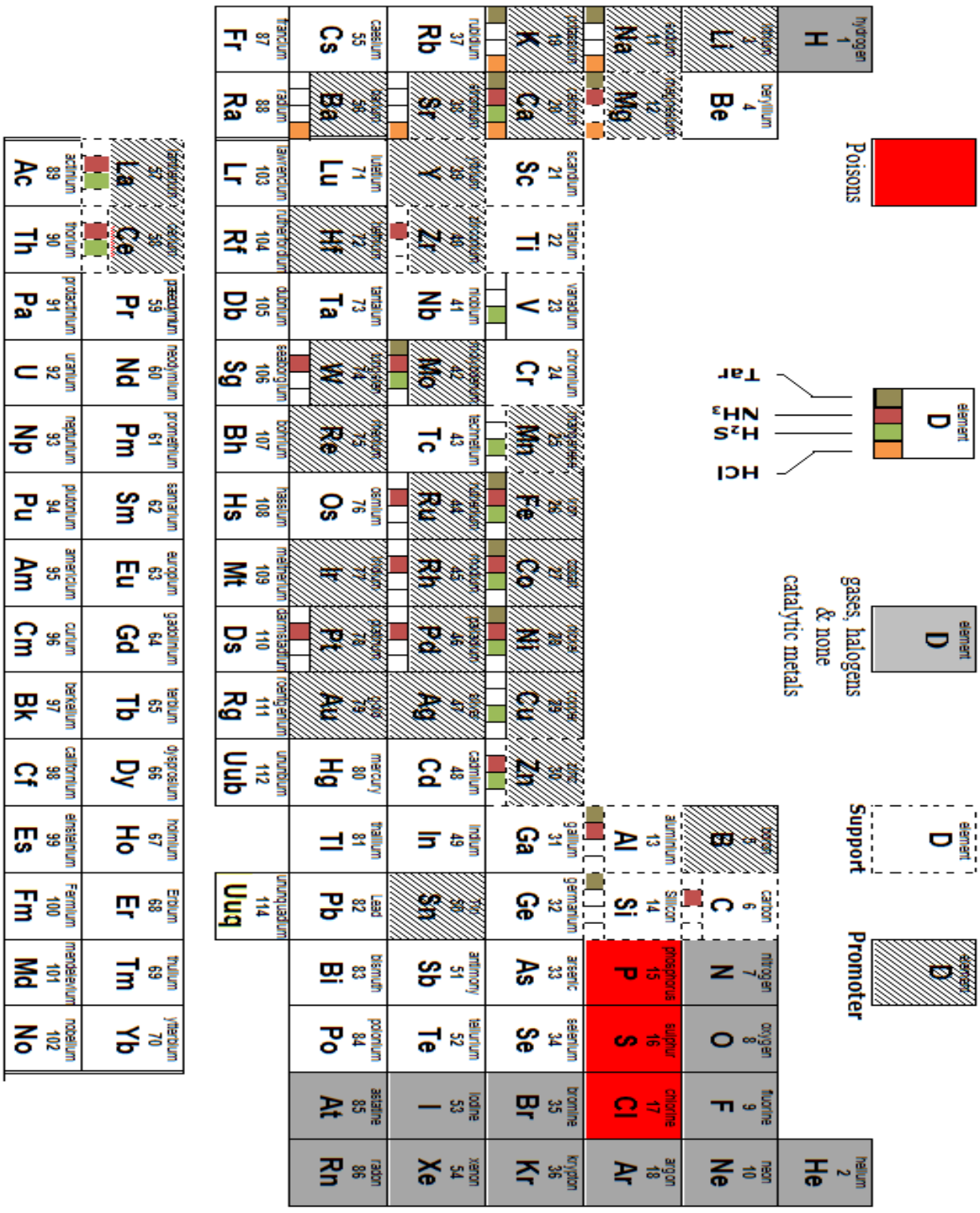

Figure 2.23. Elements in the periodic table used as catalyst, catalyst promoter, catalyst support or sorbents in gas cleanup. References for promoters and supports[96, 97] [97-99] [99] [100] [101] [102] [103] [104]. Catalysts and sorbents compiled from over 20 gas cleanup studies

2.7.2.1 Catalysts for Tar Removal

Tar compounds can be removed by thermal cracking, hydrocracking, steam or dry reforming. Thermal cracking is the conversion of tar to C and H_2 at elevated temperature.

$$C_nH_m \rightarrow nC + \frac{m}{2}H_2 \quad [2.21]$$

Due to the refractory nature of gasification tar[105], extensive tar removal by thermal cracking requires high temperatures (> 1100^{o}C).[106] Tar can be decomposed in the presence of hydrogen through hydrocracking which produces methane as shown below.

$$C_nH_m + \left(\frac{4n-m}{2}\right)H_2 \leftrightarrow nCH_4 \quad [2.22]$$

Tar as well as light hydrocarbons can be converted to carbon monoxide and hydrogen through steam reforming as shown below.

$$C_nH_m + nH_2O \leftrightarrow nCO + \left(n + \frac{m}{2}\right)H_2 \quad [2.23]$$

Due to the high activation energy (250-350 kJ/mol) and its endothermic nature, steam reforming of tars occurs appreciably only above 900^{o}C in the absence of a catalyst.[107] When a suitable catalyst is employed, temperatures ranging between 650 and 900^{o}C are sufficient for high conversion. However, tar steam reforming often suffers from catalyst deactivation through coke although this can be minimized considerably by careful control of the steam to carbon ratio.[108]

Tar compounds could also be reformed in the absence of steam with CO_2 through dry reforming, as shown below.

$$C_nH_m + nCO_2 \rightarrow 2nCO + \frac{m}{2}H_2 \quad [2.24]$$

In practice, several condensable hydrocarbon, oxygenated aromatics and complex polyaromatic hydrocarbons (PAHs) fall within the definition of tar proposed by a panel of experts in 1998.[109] As a direct result of the complex chemical composition of biomass tars, researchers typically employ model compounds in catalytic tar cleanup in order to obtain useful results. While benzene is technically outside the definition of tar, it is commonly quantified tar content in gasification experiments as it is present in high concentrations. Benzene, toluene, phenol, and naphthalene together reflect the majority of tar composition[110,111] and as such are commonly used as model compounds for tar removal studies. However, naphthalene is the most common model compound because it is considered the most stable and recalcitrant in catalytic tar cleanup. Dolomite, olivine, limonite, calcium/magnesium carbonates as well as nickel based catalysts have been widely used in tar removal in bench-scale as well as pilot-scale setup. Table 2.9 summarizes selected catalytic tar reforming studies. Of these catalysts, mineral catalysts (dolomite, olivine), nickel and iron based catalysts have been the most effective at temperatures ranging from 500 to 900°C.

Table 2.9. Summary of catalytic tar reforming studies

Catalysts	*Gas composition, vol %*[a]	*Reaction conditions*	*Conversion*	*Ref*
$Mg_3Ca(CO_3)_4$	Fluidized bed gasification tar: 1400mg/m^3	T: 900, τ: 0.2-0.3s	99	112
$Fe_2O_3/Mg_3Ca(CO_3)_4$	CO: 9.8, CO_2: 14.6, CH_4: 3.6, H_2: 9.8, H_2O: 13.7,		99	
Ni/Al_2O_3	NH_3: 0.41, N_2: balance		100	
Al_2O_3-SiO_2	Updraft gasification tar: 9800 mg/m^3, CO:17.2,	T: 900°C, τ: 0.2-0.3	77	
Fe_2O_3	CO_2: 8.0, CH_4: 1.6, H_2: 13.2, H_2O: 25.9, NH_3:		91	
$Mg_3Ca(CO_3)_4$	0.17, N_2: balance		100	
$Fe_2O_3/Mg_3Ca(CO_3)_4$			100	
Ni/Al_2O_3			100	
Dolomite	Biomass tar from power plant: 5000mg/m^3, CO,	T: 850°C, GHSV: 12,000h^{-1}	~95	81
Fe_2O_3/Dolomite	CO_2, CH_4, H_2 concentration unknown	T: 850°C, GHSV: 12,000h^{-1}	~95	
Ni/dolomite		T: 650°C, GHSV: 12,000h^{-1}	85	
		T: 850°C, GHSV: 12,000h^{-1}	100	
		T: 650°C, GHSV: 12,000h^{-1}	~85	
		T: 700°C, GHSV: 12,000h^{-1}	~90	
		T: 750°C, GHSV: 12,000h^{-1}	~95	
		T: 850°C, GHSV: 12,000h^{-1}	100	
		T: 650°C, GHSV: 12,000h^{-1}	~85	
		T: 850°C, GHSV: 12,000h^{-1}	100	
Dolomite	Biomass tar, CO, CO_2, CH_4, H_2 concentration unknown	T: 760°C, GHSV: 9200h^{-1}	77.8	113
		T: 923°C, GHSV: 10800h-1	96.8	
		T: 830°C, GHSV: 12200 h^{-1}	91.3	
		T:814°C, GHSV: 13700 h^{-1}	94.4	
		T: 805°C, GHSV: 15500 h^{-1}	71.4	
		T: 844°C, GHSV: 9700h^{-1}	91.4	
Y-zeolite	1-Methyl naphthalene 3000 mg/m^3, N_2: 70, H_2:	T: 550°C, GHSV: 30,000h^{-1}	99	114
$NiMo/Al_2O_3$	30		99	
Lime			87	
Al_2O_3			86	

SiO_2			81	
North Carolina olivine	Naphthalene 0.017, H_2: 20.5, CO: 20.5, CO_2: 28, H_2O: 23.5, CH_4: 5.6, Toluene: 0.28, N_2 balance	T: 850°C, GHSV: 2500h^{-1}	77.1	115
		T: 900°C, GHSV: 2500h^{-1}	100	
	Toluene: 0.28, H_2: 20.5, CO: 20.5, CO_2: 28, H_2O: 23.5, CH_4: 5.6, Napthalene: 0.017, N_2 balance	T: 800°C, GHSV: 2500h^{-1}	70.1	
		T: 850°C, GHSV: 2500h^{-1}	88.3	
		T: 900°C, GHSV: 2500h^{-1}	89.4	
Washington olivine	Naphthalene: 0.04, H_2: 16, CO: 8, CO_2: 12, H_2O: 16, CH_4: 4, N_2 balance	T: 850°C, GHSV: 1166h^{-1}	80	
Washington olivine		T: 900°C, GHSV: 1166h^{-1}	97	
North Carolina olivine		T: 800°C, GHSV: 1166h^{-1}	75	
North Carolina olivine		T: 900°C, GHSV: 1166h^{-1}	98	
Australian olivine		T: 800°C, GHSV: 1166h^{-1}	90	
Australian olivine		T: 900°C, GHSV: 1166h^{-1}	100	
Calcined Australian olivine		T: 900°C, GHSV: 1166h^{-1}	92	
Preatreated olivine	Naphthalene: 5000-7000mg/m^3, H_2: 10, CO: 12, CO_2: 12, H_2O: 10, Ar balance	T:900°C, τ: 0.3 s	~70	116
Preatreated olivine	Naphthalene: 5000-7000mg/m^3, Ar balance		~65	
Ni/Olivine	Methylnaphtalene: 0.0509, H_2O: 1, N_2 balance	T: 900°C	~75	117
Ni/CaO–$Ca_{12}Al_{14}O_{33}$	Toluene: Unknown, H_2O, N_2 unknown	T: 650°C	99	118
Ni-Fe-Ce/Al_2O_3	Naphthalene: 5000 mg/m^3, H_2O: 15, CO_2: 10, N_2 carrier	T: 550°C, F: 500l/min	97.2	98
		T: 600°C, F: 500l/min	98	
		T: 650°C, F: 500l/min	97.7	
		T: 700°C, F: 500l/min	98.7	

T = temperature, F = flow rate, GHSV = gas hourly space velocity

2.7.2.1.1 Alkali and Alkaline Earth Metal Catalysts (Dolomite, olivine, CaO, $CaCO_3$ and MgO)

Alkali metal catalysts have been investigated as primary catalysts to improve the quality of the gasification syngas by several researchers over the years. Their presence in biomass ash and their catalytic effects in thermochemical conversion is well documented.[105] These catalysts have however been less effective for carbon conversion and often result in downstream recovery challenges due to their volatility around typical gasification temperatures.[119]

K_2CO_3 supported on perovskite oxide ($LaMn_{(1-x)}Cu_xO_3$) and Al_2O_3 was investigated for in-situ tar removal in a fluidized bed gasifier. In the presence of 10 wt % K_2CO_3 supported on Al_2O_3 and perovskite oxide, the tar concentration was reduced by 53 and 59%, respectively at low gasification temperature (700°C).[120] K_2CO_3 unsupported was less effective resulting only in 20 % reduction of tar content.

Carbonate minerals of Ca and Mg, well known as dolomites, are of great interest in gas cleanup. Several groups have studied dolomites as *in-situ* and *ex-situ* catalysts for tar cleanup and have showed that near complete conversion can be achieved under optimum condition.[81, 112, 121] Corella *et al.*[121] showed that dolomites are equally effective in-situ as ex-situ in tar removal. Calcination of dolomites results in increase in activity because of the increase in surface area and oxide content.[121] Improved dolomite activity can be attained by the addition of other metal oxides such as Fe_2O_3[81, 113], Ni[81]. Furthermore, bimetallic Ni-Pt supported on dolomite showed significantly better performance over various Pt/Al_2O_3 and olivine with extensive cracking of tar based on a GC-MS comparative analysis of uncatalyzed and catalyzed samples.[122] Calcined dolomite catalysts seems to be more active towards tar when the gasifying agent is steam rather than air suggesting that dolomite removes tars via steam reforming primarily.[123, 124] The

drawback of dolomites is that they can easily be eroded limiting their use in fluidized bed reactors as primary or secondary catalyst.[116] Olivine, like dolomite, is a natural mineral catalyst that is composed primarily of magnesium iron and silicon in the chemical formulas of Fe_2SiO_4 or Mg_2SiO_4. Like dolomite, olivine can achieve high conversion (> 90%) for naphthalene.[115] Kuhn *et al.*[115] compared the performance of several olivine catalysts in tar reforming potential with naphthalene and toluene as model compounds., the authors listed the origin, treatment and phase of the Fe atom among factors affecting the activity. Deactivation was observed and was attributed to carbon deposition as well as Fe dispersion. Like dolomites, greater activity was reported for calcined olivine relative to the natural and uncalcined olivine.[116,125] X-ray photoelectron spectroscopy analysis revealed that calcination increased the Fe content on the surface as a potential reason for enhanced activity upon calcination.[116] Ni doping on olivine showed enhancement of the support with conversion increasing from 4 to near 30% at 900°C.[117] Furthermore, steam pretreatment of Ni/Olivine increased conversion near 75 % at the same temperature.

The effectiveness of dolomite and olivine in tar decomposition has motivated researchers to look into the activity of individual oxides (CaO, $CaCO_3$ and MgO) in dolomites. Simell and coworkers [112] investigated the activity towards tar decomposition of CaO and MgO and reported activities in the following order: CaO > CaO–MgO > MgO > $NiMo/Al_2O_3$ indicating that CaO has a greater catalytic role than MgO in dolomite. Fe and Ni impregnated scallop shell ($CaO/CaCO_3$) as well as scallop shell were investigated in steam reforming of biomass tar to enhance the production of primary gases[126]. The authors reported that Ni loading outperformed Fe loading and $CaO/CaCO_3$ showed good activity in steam reforming of tar. In downdraft

gasification of bagasse with CaO, exit tar concentration was reduced by 80% in the presence of 6 wt % of CaO in the bed.

2.7.2.1.2 Transition Metal Based Catalysts

2.7.2.1.2.1 Iron Based Catalysts

Limonite is a naturally occurring iron ore with generic formula as $FeO_x(OH)_y$. They have been used in tar cleanup studies in-situ and ex-situ. Indonesian limonite was used for the decomposition of coal syngas tars resulting in a good tar concentration reduction.[127] Investigations of the activity of the catalyst revealed that transformation from FeOOH to Fe_3O_4 is responsible for the increase in activity. Furthermore, there was evidence that the Indonesian limonite catalyzed the steam reforming reaction. Matsumura and coworkers[128] compared a catalyst containing an Australian yellow yandi limonite against a conventional $NiO–MoO_2/Al_2O_3$ for the decomposition of asphaltene and reported slightly higher conversion for the catalyst containing limonite. Brazilian limonite was also investigated for asphaltene decomposition with still greater activity than the conventional $NiO–MoO_2/Al_2O_3$ catalyst.[129]

In addition to olivine and limonite, other iron containing catalysts that have been studied for tar reduction include iron oxides (FeO[130], Fe_2O_3[112, 130] and Fe_3O_4[130]), ankerite ($CaFe(CO_3)_2$ as a ferrous dolomite), sintered iron ore, and pelletized iron ore. Nordgreen *et al.*[130] investigated the potential of FeO, Fe_2O_3 and Fe_3O_4 and showed that FeO was more effective than Fe_2O_3 and Fe_3O_4. FeO, Fe_2O_4, Fe_3O_4 and sintered ore have very little catalytic activity in tar decomposition.[119, 131]

2.7.2.1.2.2 Nickel Based Catalysts

Nickel-based catalysts, commonly supported on a metal oxide, have been extensively used in biomass gasification tar cleanup.[20, 99, 132] They are not suitable for in-situ tar destruction due to deactivation by coking.[97, 133] However, these catalysts have remarkable activity as secondary catalysts.[134] Buchireddy *et al.*[135] investigated the impregnation effect of nickel on zeolite catalysts and observed noticeable activity improvement that was attributed to the steam reforming catalytic activity of nickel. Dou and coworkers[134] investigated the potential of a NiMo catalyst containing 4% NiO in the conversion of 1-methyl naphthalene and reported nearly 100% conversion at 550^{o}C. Similar conversion was achieved when nickel catalysts treated with various alkali promoters were used in a different study.[99] Miyazawa *et al.*[136] assessed the activity of several nickel supported catalysts and ranked them as follow: Ni/Al_2O_3 > Ni/ZrO_2 > Ni/TiO_2 > Ni/CeO_2 > Ni/MgO suggesting that the support material can enhance the catalytic performance of the nickel catalysts. Another group tested various bimetallic Ni and Fe catalysts supported on alumina and found that the bimetallic catalyst outperformed nickel supported on alumina.[98] Pt appears to be a good promoter of tar reforming catalysts and mixed oxides of Ni, Fe, Pt performed the best among several Ni, Fe and Ce catalysts at 800˚C in naphthalene reforming. Similarly, Sutton *et al.*[137] investigated several Ni-supported catalysts synthesized via wet impregnation or co-precipitation and observed that the co-precipitated catalysts performed slightly better than their counterparts under similar conditions. Following the same logic, nickel supported on dolomite and olivine catalysts have been evaluated and a noticeable improvement of activity was observed upon nickel addition.[81, 115, 138]

2.7.2.1.2.3 Zeolite Based Catalysts

Zeolites are a group of crystalline aluminosilicate minerals whose three-dimensional structures are derived from frameworks of $[SiO_4]^{4-}$ and $[AlO_4]^{5-}$ coordination polyhedra. The catalysts have been extensively used in the petrochemical industry to crack large and complex hydrocarbons. These catalysts should be ideal for tar cracking since they already catalyze the breakdown of hydrocarbons similar to those found in biomass syngas tars. Furthermore, these catalysts are used for tar reforming of biomass pyrolysis with good results[139,140] The increase in the concentration of primary gases is presumably due to steam reforming of pyrolytic tar.[140] Dou *et al.*[134] satisfactorily used Y-zeolite to convert 1-methylnaphthalene and achieved near complete conversion at 550^{o}C. Seven commercial zeolites with different pore sizes and acidity were tested for naphthalene conversion. The authors stated that the naphthalene conversion increased with increasing acidity.[135] Adversely, increasing acidity also resulted in increased coke formation. Other catalyst properties that affected naphthalene conversion are pore size and surface area with both properties resulting in higher conversion. The same authors reported the following order for naphthalene conversion at 750°C with all other reactions being identical: ZY-5.2 (SiO_2/Al_2O_3 = 5.2) > ZY-30 (SiO_2/Al_2O_3 = 30) ≈ ZY-80 (SiO_2/Al_2O_3 = 80) > Zβ (SiO_2/Al_2O_3 = 25) > Na-Chabazite (SiO_2/Al_2O_3 = 4) > ZSM5 (SiO_2/Al_2O_3 = 24) > Si/Al (SiO_2/Al_2O_3 = 28).

2.7.2.2 Catalysts for Ammonia Removal

Ammonia is not easy to decompose under typical gasification temperature without the use of catalysts.[101] In the following subsections, the various groups in ammonia decomposition are reviewed. Table 2.10 summarizes experimental conditions and results obtained in several catalytic ammonia decomposition studies. The most effective active metals are Ni or Ni

promoted with Ce or La, Co or Co-Zn mixed oxide, Ru and Fe while Al_2O_3 and activated carbon are among the most common and effective supports. In addition, limonite is also very effective in NH_3 decomposition. While the experimental conditions vary widely depending on the studies, NH_3 decomposition in the context of hot gas cleanup is typically investigated at temperatures ranging from 450 to 750°C and GHSV ranging from a few thousands to as high as 45,000 h^{-1}.

Table 2.10. Summary of catalytic ammonia decomposition studies

Catalysts	*Gas composition, vol %*	*Reaction conditions*	*Conversion, %*	*Ref*
Ni-Zn/Al_2O_3	NH_3: 0.1, H_2: 11.7, CO: 9.56, CO_2: 5.20, N_2 balance	650°C, GHSV: 5000h^{-1}	95%	141
Fe-Zn/Al_2O_3			20-30	
Co-Zn/Al_2O_3			95%	
5% Ru/Fly ash	NH_3: 100	T: 500°C, F: 100 ml/min	15.3	103
Ru/CMK3-NaOH	NH_3: 100	T: 500°C, WHSV: 30000 ml g^{-1} h^{-1}	50.8	104
Ru/CMK3-KOH			78.9	
Ru/CMK3-$Ca(OH)_2$			48.5	
Ni-Ce/Al_2O_3	NH_3: 100	T: 500°C, WHSV: 30000 ml g^{-1} h^{-1}	~100	142
Ce-Ni/SBA-15	NH_3: 100	T: 650°C, WHSV: 30000 ml g^{-1} h^{-1}	100	97
Ce-Ni/SBA-15		T: 550°C, WHSV: 30000 ml g^{-1} h^{-1}	80-90	
La-Ni/SBA-15		T: 650°C, WHSV: 30000 ml g^{-1} h^{-1}	100	
La-Ni/SBA-15		T: 550°C, WHSV: 30000 ml g^{-1} h^{-1}	80-90	
Fe/Activated carbon	NH_3: 0.20, Balance: He	T: 750°C, GHSV: 45000 h^{-1}	~90	143
Ni/activated carbon			~75	
Ni/activated carbon	NH_3: 100	T: 500°C, GHSV: 6000h^{-1}	~ 60	144
Ru/$LaZrO_2$	NH_3: 100	T: 450, 700°C, WHSV: 4000 ml g^{-1} l^{-1}	80, 100	145
Ru/$LaZrO_2$			40, 100	
15% Ni/Al_2O_3	NH_3: 0.21, CO: 16.5, CO_2: 10.3, CH_4: 4.6, H_2: 16.7, H_2O: 15.1, N_2 balance	T: 850°C, τ: 0.6 s	~ 80	101
Ni-Ru			~ 85	
Ni/ZSM-5	NH_3: 0.10, H_2: 10.5, CO: 28.4, CO_2: 3.6, H_2O 3.1, O_2: 0.008, N_2 balance	T: 300°C, GHSV: 20,000 h^{-1}	~95	146
Ru/CNT	NH_3: 100	T: 500°C, WHSV: 30,000 ml g^{-1} h^{-1}	84.78	100

Ru/CNT				
Rh/CNT			12.53	
Pt/CNT			4.22	
Pd/CNT		T: 450°C, WHSV: 30,000 ml g^{-1} h^{-1}	1.70	
Pd/CNT		T: 500°C, WHSV: 30,000 ml g^{-1} h^{-1}	4.28	
Ni/CNT			8.67	
Fe/CNT			1.94	
Ru/MgO		T: 500°C, WHSV: 150,000 ml g^{-1} h^{-1}	13.39	
Ru/TiO_2			11.30	
Ru/Ac			10.49	
Ru/Al_2O_3			10.79	
Ru/ZrO_2			5.10	
k-Ru/CNT			28.58	
$k\text{-}Ru/ZrO_2$			18.89	
Ni/Al_2O_3	NH_3: 0.06, H_2: 9-11, CO: 12-15,	T: 830°C, P: 20 bar, τ: 1.1 s	38.00	[101].
$Ru\text{-}Al_2O_3$	CO_2: 13-18, CH_4: 5-8, H_2O: 7-15,		~ 28	
Al_2O_3	H_2S: 0.0030-0.0070, N_2 balance		23	
Co_3O_4	NH_3: 0.50, H_2: 11.7, CO: 9.56, CO_2:	T: 650°C, GHSV: 5000h^{-1}	~ 95	[102]
MoO_3	5.20, N_2 balance		~ 96	
NiO			~ 97	
ZrO_2			~30	
WO_3			~20	
ZnO			~20	
Co_3O_4			~20	
MoO_3			~20	
NiO			~20	
Co/ZnO			~95	
Mo/ZnO			~95	

Ni/ZnO			~95	
Ru/Al_2O_3	NH_3: 10, He balance	T: 450°C, F: 200 ml/min	90	[147].
Fe_2O_3	NH_3: 0.17, CO: 17.2, CO_2: 8.0, CH_4: 1.6, H_2: 13.2, H_2O: 25.9, Tar: 0.98, N_2 balance	T: 900°C, τ:0.2-0.3s	87	[112]
$Fe_2O_3/Mg_3Ca(CO_3)_4$			75	
Ni/Al_2O_3			100	
$Mg_3Ca(CO_3)_4$			53	
$Fe_2O_3/Mg_3Ca(CO_3)_4$			53	
Ni/Al_2O_3			100	
Fe/AC	NH_3: 0.20, He balance	T: 750°C, GHSV: 45000 h^{-1}	100	[148]
Fe/AC			100	
Ca/AC			100	
Fe/AC			~50	
Fe/AC	NH_3: 0.20, CO/H_2 = 2, CO_2		~95	
Limonite	NH_3: 0.2, H_2S: 0.0050-0.050, N_2 balance	T: 750°C, GHSV: 45000h^{-1}	100	[149]

T = temperature, F = flow rate, P = pressure, GHSV = gas hourly space velocity, WHSV = weight hourly space velocity

2.7.2.2.2 Transition Metal Based Catalysts

2.7.2.2.2.1 Iron Based Catalysts

Limonite is very effective in ammonia conversion with near complete conversion at 500^{o}C in an inert environment.[153] In the presence of primary gases (CO, H_2 and H_2O), limonite's activity in ammonia decomposition was seemingly reduced and higher temperature (> 750˚C) was required to achieve conversions above 90%.[153] In addition to good catalytic activity, Australian limonite showed resistance to sulfur deactivation in the presence of 50-500 ppmv H_2S.[149]

Leppälahti *et al*.[131] investigated the effectiveness of iron sinter, iron pellet, ferrous dolomite against dolomite limestone, inert silicon carbide and a commercial nickel catalyst as the reference in the decomposition of ammonia. Their results indicated that ferrous catalysts were more active than dolomite and limestone while less active than nickel. An iron doped mesoporous activated carbon, prepared by H_3PO_4 activation of Canadian peat, was synthesized and tested by Donald and co-workers with great success.[154] Under optimum conditions, NH_3 conversions near 90% were obtained for a gas mixture containing 2000 ppmv NH_3 in a balance of helium at 750^{o}C with conversion as high as 90%. Supported iron catalysts have demonstrated greater activity than supported calcium catalysts suggesting that iron is better than calcium in ammonia decomposition.[148]

2.7.2.2.2.2 Nickel Catalysts

Nickel based catalysts, either supported or unsupported, are very effective in NH_3 decomposition, often with conversions exceeding 95%.[20, 102] The selection of the support plays a key role in the activity of supported nickel catalysts: stronger acidity tend to increase catalytic activity[146] and some common supports (ZrO_2[102], MoO_3[102], Al_2O_3[155]) appear to be active in NH_3

decomposition even prior to Ni impregnation. The effectiveness in NH_3 decomposition increases with Ni loading as shown by Mojtahedi and Abbasian[101] who demonstrated that with increasing Ni loading from 2 to 15 wt %, NH_3 conversion increased from 54 to 92% conversion at 850°C. Nassos *et al.*[156] studied the effect of nickel loading on three metal oxide supports, $Ce_{0.9}La_{0.1}O_2$, $Ce_{0.9}Zr_{0.1}O_2$ and γ-Al_2O_3 with nickel loading of 5 and 10 wt %. The ammonia conversion increased with increasing nickel concentration for $Ce_{0.9}La_{0.1}O_2$ and $Ce_{0.9}Zr_{0.1}O_2$. They also observed that γ-Al_2O_3 was not as good of a support as were $Ce_{0.9}La_{0.1}O_2$ and $Ce_{0.9}Zr_{0.1}O_2$. It has also been reported that Ce and La addition to Ni based catalysts improved its performance in NH_3 conversion.[97, 142]

Other metal oxides can also be combined with Ni to improve its performance. Simell *et al.*[112] reported 80% conversion using a nickel monolith catalyst ($NiMo/Al_2O_3$). Upon increasing the temperature to 900^{o}C, complete conversion was achieved. Wang *et al.*[157] investigated hot gas ammonia decomposition in the presence of a nickel based catalyst in an air blown fluidized bed gasifier. A maximum ammonia conversion of 95% was achieved under optimum conditions. Ni–Pt/ Al_2O_3 catalyst was used in the decomposition of ammonia and good activity was observed for pure ammonia decomposition with 97.4% conversion at only 560°C.[158]

While nickel based catalysts are very active in ammonia decomposition, their major drawback is catalyst deactivation due to coking as observed by Wang *et al.*[159] and/or poisoning[160], particularly by H_2S present in syngas.[102]

2.7.2.2.2.3 Ruthenium Catalysts

The use of ruthenium based catalysts for NH_3 decomposition is well documented.[100, 101, 104] Mojtahedi and Abbasian[101] investigated Ru/Al_2O_3 in ammonia decomposition and observed

complete conversion from 800 to 950˚C for a gas mixture containing 1 vol % NH_3, 0.4 vol % H_2 and N_2 as balance. However, the same catalyst was less effective with real syngas achieving only 30 % conversion at 830˚C and 20 bar. Other authors observed that 10 wt.% Ru supported on SiO_2 achieved better ammonia conversion than 10 wt.% Ni/SiO_2 under similar conditions.[161] In fact Ru catalysts with loading less than 10 wt.% on various metal oxide supports (Al_2O_3, SiO_2, ZrO_2, TiO_2, MgO and carbon nanotubes) have been employed for hydrogen production through ammonia decomposition[162-164] with better performance than Ni supported on the same metal oxides under similar conditions. When deposited on the above supports, the following order of activity was observed: Ru/Carbon Nanotubes > Ru/MgO > Ru/TiO_2 ≅ Ru/Al_2O_3 ≅ Ru/ZrO_2.[100]

Ru–Ni catalysts constitute a powerful catalytic system in ammonia decomposition. Such catalytic system has been successfully used in decomposition of ammonia coal gasification syngas with conversion of 90% ammonia conversion at 900°C.[165] Despite its good catalytic activity in ammonia decomposition, Ru suffers from catalyst deactivation by coking and poisoning just like nickel based catalysts previously discussed. Furthermore, Ru seems to promote the side reaction to convert hydrogen to water instead of ammonia.[166]

2.7.2.2.2.4 Other Transition Metal Oxide Catalysts

Juutilainen *et al*.[167] investigated the removal of ammonia by ZrO_2 and ZrO_2/Al_2O_3. In a comparative test with nickel and dolomite catalysts, they reported better ammonia conversion below 650^{o}C for ZrO_2 and ZrO_2/Al_2O_3. Yin *et al*.[100] compared Ni, Fe, Pt, Pd and Rh against Ru supported on carbon nanotubes and reported significantly lower performance for all catalysts relative to Ru. At 500˚C, the same authors reported the following order in activity for ammonia decomposition: Ru > Rh > Ni > Pt ≅ Pd > Fe. Co_3O_4 and MoO_3 achieved similar NH_3 conversion

(~ 95%) at 650°C.[102] It appears that Al_2O_3, as a support, contributes to NH_3 decomposition as Ni impregnation has been shown to only increase NH_3 conversion on alumina from 23 to 38%.[168] Other metal oxides (ZrO_2, WO_3 and ZnO) achieved NH_3 conversion between 20-30% at 650°C.[102]

2.7.2.3 Sorbents for Sulfur Removal

Unlike tars and ammonia, sulfur removal is achieved with the help of a sorbent, commonly a metal oxide, which chemically reacts with sulfur contaminants to produce a metal sulfide according the reaction below.

$$MO + H_2S \rightarrow MS + H_2O \qquad [2.25]$$

This process is referred to, interchangeably as desulfurization, from the point of view of sulfur removal from syngas, or sulfidation, from the point of view of metal oxide conversion to its corresponding metal sulfide.

The most common catalysts employed in desulfurization are metal oxides with ZnO and CuO often regarded as the reference. As such, calcium, zinc and copper based sorbents are discussed in separate sections. Calcium based sorbents are also discussed separately as they are of great interest in gasification due to their relative lower cost when they come in the form minerals such dolomite or limestone. Table 2.11 summarizes desulfurization studies of sulfur contaminants on various catalysts.

Table 2.11. Catalytic desulfurization studies of syngas sulfur (mostly H_2S) contaminants

Catalysts	***Gas composition***	***Reaction conditions***	***Performance***		***Ref***
			Breakthrough time (min)	**Sorbent capacity (gS/gSorbent)**	
Zn-Fe-V-O	H_2S: 1, H_2: 20, H_2O: 7-20, N_2: 72	T: 500-700°C, GHSV: 4000h^{-1}	n/a	0.156-0.324 at 500°C 0.105-0.288 at 700°C	169
$LaFeO_3$/M41	H_2S: 0.33, H_2: 10.5, CO_2 (or CO): 17.1, N_2: 72.1	T: 450-550°C, WHSV: 9000 ml h^{-1} g^{-1}	n/a	0.0035 CO_2 0.0324 with CO	170
La_2ZnO_4/M41		T: 450-550°C, WHSV: 9000 ml h^{-1} g^{-1}	n/a	0.35 CO_2, 0.94 CO (g/100 sorbent)	170
La_2CoO_4/M41		T: 450-550°C, WHSV: 9000 ml h^{-1} g^{-1}	n/a	0.35 with CO_2 0.0153 with CO	170
Ni-Zn/Al_2O_3	H_2S: 1, H_2: 11.7, CO: 9.56, CO_2: 5.20, NH_3: 0.50, N_2 balance	T: 650°C, F: 50 ml/min, GHSV: 5000h^{-1}	250-450	0.13	141
Fe-Zn/Al_2O_3		T: 650°C, F: 50 ml/min, GHSV: 5000h^{-1}	250-450	0.16	141
Co-Zn/Al_2O_3		T: 650°C, F: 50 ml/min, GHSV: 5000h^{-1}	250-450	Better than previos two catalyst but not indicated	141
Zn-Ti	H_2S: 1.5, H_2: 11.7, CO: 9.6, CO_2: 5.2, N_2: balance	T: 480°C, 650°C, F: 50 ml/min, GHSV: 5000h^{-1}	n/a	<0.15 at 480°C 0.15-0.20 at 650°C	171
Co-Zn-T			n/a	0.05-0.17 at 480°C 0.20-0.25 at 650°C	171

ZnO	H_2S: 0.01, He balance	T: 250°C, F: 400ml/min	550	0.48	[172]
Cu-Ce	H_2S: 0.0394, CO: 10.5, H_2: 10.5, CO_2: 8.3, CH_4: 6.3, C_2H_4: 1.7, Benzene: 0.0370, H_2O: 0, 45	T: 700°C, GHSV: 56,000h^{-1}	n/a	0.0004	[173]
		T: 700°C, GHSV: 14,000h^{-1}		0.0005	
Mn/Al_2O_3	H_2S: 0.0394, CO: 10.5, H_2: 10.5, CO_2: 8.3, CH_4: 6.3, C_2H_4: 1.7, Benzene: 0.0370, H_2O: 0, 25-65	T: 700°C, GHSV: 3300h^{-1}	n/a	0.004 (w/ steam) 0.0002 (w steam)	

n/a means not available, T = temperature, F = flow rate, GHSV = gas hourly space velocity, WHSV = weight hourly space velocity

2.7.2.3.1 Alkaline Earth Metal Based Sorbents

Calcium based catalysts, reported to be effective in hot gas desulfurization, are CaO[37, 174], $CaCO_3$[37] and dolomite[37]. The gas-solid reaction of calcium based catalysts and hydrogen sulfide proceeds according to the general metal oxide desulfurization reaction discussed earlier and adapted to CaO and $CaCO_3$ below.

$$CaO + H_2S \leftrightarrow CaS + H_2O \quad [2.26]$$

$$CaCO_3 + H_2S \leftrightarrow CaS + CO_2 + H_2O \quad [2.27]$$

Calcination plays a crucial role in the activity of calcium based catalysts. Uncalcined limestone (i.e. $CaCO_3$) is less effective than fully calcined limestone (i.e. CaO).[37] A similar behavior is observed for dolomite as well although uncalcined dolomite performed better than uncalcined limestone.[37] In dolomite, it was reported that MgO does not bind sulfur although there is strong evidence of a synergistic effect between Mg and Ca: the higher the Mg to Ca ratio, the higher the conversion of Ca to CaS.[37] Both higher temperature and pressure increase H_2S conversion.[175] Conversion of H_2S is inhibited by COS, H_2 and CO, presumably by reducing the number of free active sites[175] and likely by reducing the CaO. One benefit of calcium based sorbents, such as CaO, is that they can absorb both sulfur and halogen species such as chlorine according to the reaction outlined below.[176]

$$CaO + 2HCl \leftrightarrow CaCl_2 + H_2O \quad [2.28]$$

In addition, as other basic metal oxide catalysts of CaO and MgO, have shown activity in tar conversion as discussed above, it is likely that Ca based sorbents can be of use in simultaneous removal of multiple contaminants.

2.7.2.3.2 Transition Metal Based Catalysts

2.7.2.3.2.1 Zinc Based Catalysts

It is well established that zinc oxide and its derivatives are very effective sorbents for hydrogen sulfide removal. Zinc oxide is one the best metal oxide catalysts for desulfurization based on thermodynamic simulations[177] with the ability to reduce hydrogen sulfide concentration to less than 1 ppmv in experimental studies.[172] However, the regeneration of the spent catalyst suffers from several issues. In order to avoid the formation of zinc sulfate, regeneration must be carried out under a reducing gas stream. Under a reducing environment, zinc oxide tends to be reduced to elemental zinc. Furthermore, zinc oxide is prone to elemental zinc volatilization at temperatures above 600^{o}C.[71] These drawbacks significantly limit the long term performance of zinc oxide as a hydrogen sulfide sorbent. As a remedy to these issues, iron oxide and titanium oxide are commonly incorporated with zinc oxide in the catalyst structure. Of the two metal oxides, it appears that the addition of Fe_2O_3 is less effective than that of TiO_2 as a solution for the issues aforementioned.[71] While zinc ferrites are more active than zinc oxide alone, they too are subjected to decomposition under gasification condition.[178] On the other hand, zinc titanates have a similar performance to zinc oxide: Fe_2O_3 synergistically participates in the desulfurization reaction whereas TiO_2 does not.[178] However, TiO_2 improves thermal stability[177], prevents ZnO reduction in the reducing environment of gasification[177, 179] if adequate dispersion is achieved and inhibits zinc sulfate formation[177] in the presence of excess oxygen. Other mixed metal oxide

catalysts of zinc oxide/titanates and other metal oxides such ZrO_2[180], Co_3O_4[171], CuO[181] and MnO[181] have been investigated with promising results. Cobalt, in particular, appears to be a promising promoter for zinc titanates as it has been reported to enhance high (650°C) and medium (480°C) temperature desulfurization.[182]

2.7.2.3.2.2 Copper Based Catalysts

Thermodynamically, copper, along with zinc, is among the most suitable transition metals for hydrogen sulfide absorption. Unlike zinc, copper based sorbents have high sorption capacity under reducing as well as oxidizing environments although unsupported copper oxide is reduced to elemental copper, a less effective sorbent, in gasification environment.[71] Besides reduction, copper oxide suffers from a loss of surface area due to the formation of a sulfide layer.[183] This shortcoming can be alleviated through dispersion on to a support in order to improve its stability and increase the surface area. Dispersion on a support can significantly improve catalytic activity to that of dispersed zinc oxide[184] with the hydrogen sulfide sorption capacity being directly proportional to the quantity of copper oxide dispersed on the support.[185] Copper oxide has been dispersed on γ-Al_2O_3[186], SiO_2[185], ZrO_2[187], V_2O_5[188], Ce[173] and ZnO[181]. However, even supported copper based catalysts can be affected by the presence of hydrogen as evidenced by the decrease in breakthrough time in the presence of equimolar H_2S and H_2 for copper supported on olivine.[189]

2.7.2.3.2.3 Other Transition Metal Oxides

Iron oxide has attracted attention as hydrogen sulfide sorbent due to its thermodynamically favorable properties and relatively low cost.[190] However, in the temperature ranges of interest, iron oxide catalyzes the Boudouard reaction, thus leading to potential catalyst deactivation due to coke formation.[177] Nickel based catalysts, primarily tested for tar and NH_3 removal, can also

remove H_2S as well as other sulfur based contaminants in syngas.[20] The reported H_2S removal capacity is consistent with the well-known poisoning effect of sulfur compounds on Ni based catalysts. Ceria based sorbents, either as active supports or as mixed metal oxides, have been investigated as H_2S sorbents.[173, 191] It appears that ceria sorbent capacity for sulfur is significantly diminished by reduction from H_2 in syngas which can be alleviated by steam in syngas.[173]

2.7.2.4 Sorbents for Hydrogen Halides Removal

The body of research on halide cleanup is not as exhaustive as that of tar, ammonia or hydrogen sulfide in syngas, especially for biomass derived syngas.[74] Due to its abundance, relative to other hydrogen halides in syngas, HCl has been the target of most research investigations.

Hydrogen halides are removed from syngas via dehydrohalogenation. In the specific case of HCl, this process is referred to as dechlorination or dehydrochlorination and proceeds according to the reactions given below:

$$MO + 2HCl \rightarrow MCl_2 + H_2O \quad [2.29]$$

$$MCO_3 + 2HCl \rightarrow MCl_2 + H_2O + CO_2 \quad [2.30]$$

$$M_2CO_3 + 2HCl \rightarrow 2MCl + H_2O + CO_2 \quad [2.31]$$

where M is metal elements. Thermodynamic simulations have indicated that alkaline and alkali earth metals are promising halide sorbents for cleanup temperatures greater than 500^{o}C.[192]

2.7.2.4.1 Alkali Metal Catalysts

Alkali metals of interest in halides removal are Li, Na and K with the following order established in terms of sorbent capability to achieve high HCl removal in temperature ranges for hot gas

cleanup based on thermodynamic modeling.[38] $Na_2O \approx K_2O >> Li_2O$. Na_2O and K_2O are more suitable for high temperature application with less than 5 ppmv of HCl up to 600°C whereas Li_2O is only effective below 200°C.[74] In syngas containing high concentration of CO_2, alkali metal oxides will be converted to their respective carbonates (i.e. Li_2CO_3, Na_2CO_3 and K_2CO_3). Na_2CO_3 tested in a simulated coal syngas with 200 ppmv HCl was effective in achieving a concentration less than 1 ppmv with a breakthrough time near 200 min.[38] Duo *et al*.[193] reported the following order for Na carbonates sorbents: $Na_2CO_3.10H_2O > Na_2CO_3 > NaHCO_3$. In addition to HCl, alkali based sorbents can additionally remove other halides. Na_2CO_3 can achieve complete removal below 600°C for HI and HBr and below 400°C for HF.[74]

2.7.2.4.2 Alkaline Earth Metal Catalysts

Alkaline earth metals of interest as HCl sorbents are Mg, Ca, Sr, Ba. In their oxide form, these elements can be used as sorbent with the following order established in terms of sorbent capability to achieve high HCl removal over in hot gas cleanup based on thermodynamic modeling: BaO > SrO > CaO > MgO. These sorbents are more effective when they are not converted to their corresponding carbonate. $CaCO_3$ was reported to be less effective in HCl removal than CaO.[192, 193] Based on experimental studies on a simulated syngas, the following order was observed for calcium based sorbents: $CaO = Ca(OH)_2 > CaCO_3$.[176, 193]

2.7.2.4.3 Transition Metal Oxides

It appears that select transition metal oxides (MnO, CoO, ZnO, NiO, Y_2O_3, Cu_2O, FeO) can be HCl sorbents albeit less effective than alkali and alkaline earth metals based on a thermodynamic study. These sorbents could be effective for low temperature range dechlorination (<200°C).[74]

2.7.2.5 Trace Metals Removal

Granite *et al*.[194] investigated the removal of mercury (Hg) from nitrogen as well as a gas mixture emulating syngas on solid sorbents of metal oxides of Ir, Pt, Ru, Pd, Rh, Ti and Ag at 204, 288 and 371˚C. In nitrogen, Ir, Pt, Pd and Ru based sorbents performed best at 288˚C with removal efficiencies of 93, 100, 65 and 65%, respectively. Low removal efficiencies were reported at 204 and 371˚C for the sorbents as well as other (Rh, Ti and Ag) sorbents. However, in an emulated syngas mixture (27% H_2, 36% CO, 4% CO_2, 240 ppb mercury, balance N_2), only Pt and Pd based sorbents were effective at the same temperature with removal efficiencies of 100 and 54%, respectively.

Metals can be conjointly removed along with halides in the form of halide salts. For example, the removal of alkali metal vapors often occurs in conjunction with halides as alkali metals tend to combine with halides to form salts (NaCl, KCl etc) in syngas. In a study focusing on alkali metals removal, fly ash, bentonite, kaolin and bauxite were investigated as potential sorbents. The authors reported that all sorbents reduced the release of alkali metals although fly ash and bentonite recorded the best performance.[195]

Kaolinite as well as zeolite were also effective in alkali vapors from syngas with the presence of of H_2O and H_2S enhancing NaCl capture.[196] In another experimental study, several aluminosilicate sorbents (bauxite, zeolites, bentonite, kaolinite) were effective in reducing alkali metal concentrations with kaolinite, bauxite and zeolites achieving the best performance.

2.7.3 Barriers to Biomass Gasification Commercialization

Gasification as a technology has certainly been around for many years and can be consider a "mature" technology since there are existing techniques to solve major problems. However, the maturity of this technology is not across broad. While it is "mature" in coal gasification with

years of large scale demonstration, it has not achieved the same level of maturity for biomass. Compared to coal, biomass gasification is undergoing more research currently. Table 2.2 shows the properties of various biomass feedstocks and coal considered in gasification. Relatively speaking, coal is a "dirtier" feedstock as compared to woody and herbaceous biomass as well as agricultural residue in virtually all contaminants (high sulfur, nitrogen, halides and metals) except for tar where biomass tends to surpass coal due to higher volatile matter.

The lack of maturity in biomass gasification has much to do with the large variability between feedstock that calls for greater fuel flexible systems and/or newer techniques to improve uniformity of feedstock. This task is rendered even more difficult given the nature of biomass supply which is subject to seasonal and regional variability. All these factors translate to the need of more investigations hence the limited maturity of biomass gasification. The main challenges to commercial biomass gasification deployment are grouped into technical, economic and policy barriers.

2.7.3.1 Technical Barriers

2.7.3.1.1 Biomass Logistics

Biomass logistics encompasses harvesting, transporting, storing, and processing of forest materials and agricultural-residues for use in a plant. Many biomass feedstocks considered for gasification are only available seasonally leading to an intermittent supply of fuel and calling for flexible designs to accommodate other feedstocks in the case of unexpected shortage. In addition, feedstock properties can vary significantly depending on the type of biomass (herbaceous biomass, woody biomass or agricultural residue). The variability in biomass creates significant challenges in terms of feedstock pretreatment and feeding depending on the type of

gasification system employed. These challenges are compounded by the limited experience in dealing with such feedstock in large scale operation. For an entrained flow gasifier, for example, very fine particle size (<75μm [57]) is required due to the feeding mode employed by this system, originally designed for coal fed systems. However, while this size can be easily achieved for coal, more energy will be required in the case of biomass to achieve such smaller a size making some to question the suitability of this system for biomass.[57] If on one hand, more energy is spent for size reduction, entrained flow gasifiers have other benefits namely that they can handle high pressures, which in the cases where gasification is coupled with fuel synthesis can results in savings as the syngas need not be pressurized again for use in downstream systems. Furthermore, owing to the high operating temperature, tar levels are significantly lowered while carbon conversion is near complete. In addition, slagging entrained flow gasifiers can handle high ash fuel providing fuel flexibility. In contrast, fluidized bed gasifiers have a lower tolerance for high ash feedstock that render fluidization challenging due to potential bed agglomeration. On the other hand, such systems do not have size reduction requirements as stringent as that required by entrained flow systems but tend to produce more contaminants as they operate at lower temperature. In addition, if the size of the plant is large, biomass availability might require a larger transportation radius which, besides from the economical disadvantages that will be discussed in the economical barriers later, requires adapted technical solutions to biomass operations.

One potential solution to reduce biomass variability is to carry out pretreatments such as torrefaction and densification with pelletizing. For example, torrefaction is a suitable pretreatment to reduce the energy requirement for size reduction. Such an approach cannot only generate energy saving in grinding but will also improve biomass storage ability by reducing

moisture absorption and thus limiting biological activity during storage. This particular enhancement is significant as it dampens the effect of seasonal and regional availability and variability on continuous operation in large scale plants. Densification through pelletizing can also alleviate the variability in feedstock that affects feeding by providing a narrower uniformity in feedstock. However, there are some characteristics of biomass that cannot be improved with current pretreatment techniques, namely ash content. Consequently, ultimately, careful matching between biomass types available regionally and gasification systems is necessary to minimize cost of pretreatment and feeding as well as to ensure fuel flexible designs that can handle not only the main targeted fuel but also other regionally available fuels.

2.7.3.1.2 Product Gas Contaminants

Remediation of contaminants in producer gas is the biggest challenge to commercialization of biomass gasification. This view is corroborated by a recent survey of many experts in biomass gasification who identified tar removal and syngas cleanup as a main hurdle to commercialization.[24] Over the years, various conventional techniques have been utilized to deal with syngas contaminants based on knowledge of such contaminants in coal gasification. While these techniques can be applied to biomass gasification, there is still a need to improve and adapt these techniques to biomass gasification in particular in terms of removal efficiencies. These conventional methods heavily rely on wet scrubbing with a suitable solvent for contaminant removal and are summarized below:

- Tar: wet scrubbing in water (poor)[197], alcohol (good), vegetable oil/biodiesel (good)[197]
- NH_3: wet scrubbing in water (adequate) or dilute acid (good)
- H_2S, COS: wet scrubbing in solvents MEA (adequate), DMEA (adequate), sulfinol (adequate), Selexol (good) and Rectisol (good)
- Halides: wet scrubbing in water
- Trace metals: activated charcoal and condensation

In addition to the conventional techniques, catalytic or "hot gas cleanup" approaches have been investigated to contaminant removal. Select groups of catalysts have demonstrated good activity in tar removal. The elements are:

- **Tars**: Ni/Mo/Pt/zeolites/Fe/Dolomite (Ca/Mg/Fe)/Olivine (Fe)/Limonite (Fe)
- **NH_3**: Ru/Ni/Dolomite/Olivine/Limonite
- **H_2S, COS**: ZnO/Ni/Cu/Fe/Ca

Besides conventional and catalytic methods, operating parameters can be tuned to serve as primary remediation techniques thus reducing the downstream cleanup requirement. This aspect is not well understood and can benefit from further detailed investigations. As it was the case for feedstock pretreatment, careful matching must be done at the onset of plant design and it is vital to carefully consider the end-use of the syngas and tailor the cleanup process to meet the desired goals in order to reduce cost.

2.7.3.1.3 Pilot and Large Scale Demonstration

When we look at the body of literature on gasification, we realize quickly that none of the issues we are dealing with currently are new, never investigated, challenges, even in biomass gasification which has been less studied than coal gasification. Tremendous fundamental research has been conducted on various aspects of gasification. For example, in the case of syngas cleanup, there are few established effective catalysts that have been studied in small scale setup and are commonly accepted as good candidates for hot gas cleanup. Yet, hot gas has remained at the stage of R&D and is generally considered commercially not proven.[24] It is necessary, in order to move forward, to bridge the gap between bench-scale studies and large (pilot) scale demonstration. Despite mentioning those specific technical barriers discussed above,

experts surveyed were optimistic about resolving the challenges related to biomass handling and syngas contaminants and rather suggested that large scale demonstration of existing techniques will help improve knowledge and therefore reduce the risk that currently limits investments in this area. In order to overcome this barrier, a concerted effort must be made between research institutions and funding agencies to drive select activities towards pilot-scale testing of commercially formulated catalysts based on the current R&D knowledge.

2.7.3.2 Economic Barriers

Aside from technical challenges, large commercial developments of biomass gasification projects require significant investment. However, investors weigh potential investment based on risk and rewards. While there is no doubt on the potential rewards, the risk associated with large scale biomass gasification projects is still deemed high. While much of the risk associated with biomass gasification is due to the inherent lack of confidence due to limited demonstration in large scale, some of the well publicized failures over the years have deter investors.[24] Besides the risk associated with large scale biomass gasification projects, most experts agree that the current cost of syngas cleanup technologies are high and need to be reduced. It is estimated that 15-25% cost reduction can be achieved by improving existing syngas cleanup technology.[198] It is generally agreed upon that, in order to benefit from the savings of economies of scale, biomass gasification must be carried out at large scale (100-150 MWe). However, even with the promise of high yield short rotation plantation, this capacity will result in a supply radius greater than 50 km, which is generally accepted as the limit beyond which transportation cost significant impedes the overall economic viability. Hence the issue of biomass supply radius is one to be carefully looked at in the early design stage.

Economic barriers can be lessened by seeking to lower the risk or perceived risk involved with biomass gasification due to developing, but more importantly testing, robust cleanup and feedstock handling solutions in pilot scale and large scale setups. As with all other barriers, careful planning and designing at the onset can minimize significantly issues related with fuel supply and even syngas cleanup by accommodating for fuel flexibility.

2.7.3.3 Policy Barrier

However, governments, both at the state and federal level, can act as a catalyst in the commercialization of biomass gasification. The main way they can do so is by creating incentives for investments through (*i*) taxation policies, (*ii*) agriculture policies/subsidies, and (*iii*) fuel mandates. [199,200] These policies are necessary in the earlier phases of biofuel industry establishment to spread out some of the high risk associated with these newer technologies in the early phases.[24]

2.8 Applications of Gasification Syngas

Producer gas derived from gasification can be used for liquid fuel production via Fischer-Tropsch, chemical synthesis via methanol and other synthesis routes, power generation via fuel cells, gas turbines, steam turbines or internal combustion engines or hydrogen production via fermentation.[201,202, 203] However, prior to its use in these applications, raw producer gas must be rid of gas contaminants discussed in earlier sections. The integrated gasification combined cycle (IGCC) is a prime illustration of this concept.[204] The host of potential application of producer gas is illustrated in Figure 2.24.

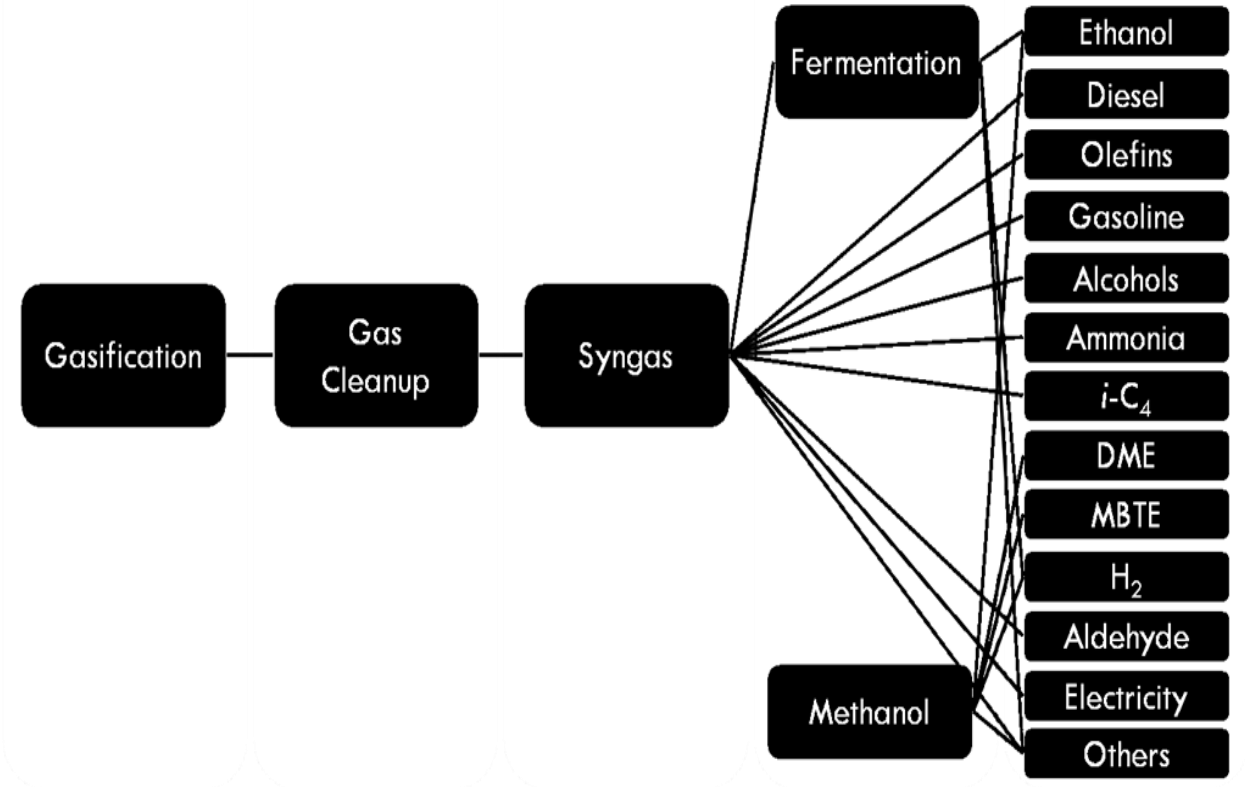

Figure 2.24. Potential application of syngas from biomass gasification upon adequate gas cleanup

Presently, product gas derived from biomass gasification has been utilized in small to medium scale applications, primarily in direct or indirect combustion to generate power with co-production of heat. With the exception of pilot-scale demonstrations, no commercial large scale demonstration of biomass to liquid fuel exists at this moment due to challenges discussed in the previous section.

2.8.1 Power Generation

Product gas derived from biomass gasification can be co-fired in existing coal power plants by injecting the product gas in the combustion zone of the coal boiler. In such a scenario, co-firing

with up to 10% on energy basis is feasible without substantial or costly modifications of the coal boiler.[53] Co-firing with coal is beneficial environmentally in the case of coal combustion as it allows to curb SOx and NOx emissions due to the lower sulfur and nitrogen content of biomass. As fly-ash is a valuable product in coal combustion, it is critical to control the input of biomass ash to the boiler to minimize the impact of biomass ash on the quality of the fly ash.

Alternatively, the product gas can be combusted in a gas engine or turbines or power a steam turbine. With adequate tar removal, modified gas engines can be operated without problems if the gas calorific value is around 5-6 MJ/m^3.[53] This process is referred to as combined heat and power (CHP) or integrated gasification combined cycle (IGCC) when gas or steam turbines are employed in the power production scheme. Producer gas can also power fuel cells in order to produce electricity. This approach is environmentally very benign. Depending on the type of fuel cell, other product gas constituents like CO and CH_4 can also be utilized.

2.8.2 Liquid Fuel

One of the main drivers for the development of sustainable and renewable fuels is the role of transportation fuels in increasing greenhouse emissions in an ever growing automobile market worldwide. Consequently, processes that can produce drop-in liquid transportation fuels are vital to reduce greenhouse gas emissions. The Fischer-Tropsch (FT) process can produce liquid hydrocarbon fuels from syngas as shown by reaction.

$$\left(\frac{n}{2}+m\right)H_2 + mCO \rightarrow C_mH_n + mH_2O \qquad [2.32]$$

The FT process can be conducted at low-temperature or LTFT (200-240^oC) or high-temperature or HTFT (300-350^oC) in the presence of iron or cobalt catalysts. For gasoline synthesis, the HTFT process and iron catalysts are preferred whereas for diesel, cobalt catalysts are preferred in

LTFT process.[7] For iron based catalyst, H_2/CO of 0.6 is preferred whereas cobalt uses H_2/CO of 2.0.[205]

Methanol synthesis occurs by way of CO or CO_2 hydrogenation over a copper-zinc oxide catalyst as illustrated below.

$$H_2 + CO \rightarrow CH_3OH \quad [2.33]$$

$$3H_2 + CO_2 \rightarrow CH_3OH + H_2O \quad [2.34]$$

H_2/CO of 2 is preferred to minimize by-products[206] while CO_2/CO ratio should be around 0.6 to avoid catalyst deactivation or oxidation.[207] Gasoline can then further be produced by reacting methanol over zeolites. Besides FT fuels and methanol, other chemicals and fuels can be produced from syngas as outlined in table 2.12.

Table 2.12. Chemical and fuel synthesis process conditions[208]

Downstream Process	Pressure (bar)	Temperature (°C)	H_2/CO
FT fuels	~20–40[209]	200–240[209]	0.6 for iron catalyst, 2.0 cobalt catalyst[205]
	25–40[208]		
		300–350[209]	0.6 for iron catalyst[205]
		250–350[208]	1.5–2[208]
Methanol	50–100[209]	100–200[205]	2.0[205]
	20–50[210]	200–300[209]	2.0[208]
	50–300[208]	210–290[210]	
		220–450[208]	
DME	26	310[209]	Converted from methanol[209]
	20–50[210]	210–290[210]	
Ethanol	100[209]	275[209]	1.0[209]
Hydrogen	~28[205]	100–200[205]	High[205]
Bio SNG	200–500[208]	300–450[208]	3.0[208]

2.9 Conclusions

This chapter provides a comprehensive review of the literature pertaining to biomass gasification, the effect of feedstock and operating conditions on primary and contaminant gas products, gas cleanup, biomass syngas applications and barriers to its commercialization.

The operating condition (temperature, gasifying agents) is the primary tools for adjusting the gas composition for primary and contaminant gases. While different feedstocks result in different producer gas concentration, the impact of the feedstock on producer gas composition is secondary to the impact of operating conditions on primary gases. However, feedstock has a significant effect on contaminants. Higher volatile matter, nitrogen, sulfur, chlorine and metals in biomass will result in higher concentration of contaminants bearing these elements in producer gas. For primary gases, everything else being constant, as temperature is increased, the concentration of CO and H_2 will typically increase while CO_2, CH_4 and other light hydrocarbons will decrease. In contrast, CO_2 increases as equivalence ratio increases while CO and H_2 typically decrease. Addition of steam at a given temperature and equivalence ratio seems to affect the concentration of H_2 drastically and CO and CO_2 mildly.

For tar, it has been shown that the reduction of volatile matter results in a reduction in tar formation. Increase in temperature reduces tar content. However increasing amount of oxygen (ER) and steam (S/B) are both more effective in reducing tar content of syngas than increasing temperature. Typically, as temperature is increased, NH_3 concentration decreases due to NH_3 decomposition to N_2 and H_2. Equivalence ratio does not appear to have a significant impact on NH_3 concentration. H_2S is mildly affected by equivalence ratio which enhances SOx formation. The concentration of H_2S seems to modestly increase as temperature is increased. It is

consequently concluded that H_2S can only be minimally reduced even if operating conditions are optimized due to the minor effect on its concentration observed over a wide range of temperature, ER and S/B. The impact of operating conditions on hydrogen halides and trace metals is not well understood at this time with fewer modeling and experimental studies compared to other contaminants. Few modeling and experimental studies suggest that temperature and ER drastically reduced hydrogen halide concentration while temperature increases metal halide concentration.

Remediation of contaminants in syngas is the biggest challenge to the commercialization of biomass gasification as corroborated by a recent survey of experts in biomass gasification. Over the years, various cold gas techniques have been utilized to deal with syngas contaminants. These techniques are listed below:

- Tar: wet scrubbing in water or vegetable oil/biodiesel (good)
- NH_3: wet scrubbing in water (good)
- H_2S, COS: wet scrubbing in amine based chemical solvents (MEA, DMEA etc) or physical sorbents (Selexol, Rectisol etc)
- Halides: wet scrubbing in water or caustic water
- Trace metals: condensation or wet scrubbing

While these techniques are considered "mature" for syngas cleanup, there is still room to improve and adapt these techniques for improved energy and contaminant removal efficiencies. In addition to the cold gas cleanup approaches, warm and hot gas cleanup approaches have also been investigated. Based on this review, few catalysts or sorbents have demonstrated good activity in contaminant removal studies. These elements are listed:

- Tars: Ni and Fe based catalysts and mineral catalysts (dolomite, olivine, limonite)
- NH_3: Ru and Ni based catalysts
- H_2S, COS: Zn and Cu based sorbents
- Halides: alkali metal based (Na_2CO_3, K_2CO_3) and Ca based (CaO, $CaCO_3$) sorbents
- Trace metals: clay mineral such as kaolinite and bentonite

In light of the growing importance of hot gas cleanup in gasification and based on this review, few recommendations are suggested for future studies:

It has been observed that many studies are carried out with gas mixtures that are significantly different from syngas, often with a high concentration of a particular contaminant (e.g. 100 % NH_3) and without other syngas components (CO, CO_2, H_2). The utility of contaminant removal studies will be greatly enhanced by selecting gas mixture that closely mimic syngas composition. Furthermore, it is recommended that future works be complemented with kinetic studies in order to provide valuable information necessary to objectively rank catalytic performance.

References

(1) Escobar, J. C.; Lora, E. S.; Venturini, O. J.; Yáñez, E. E.; Castillo, E. F.;Almazan, O. Biofuels: Environment, technology and food security. *Renew. Sust. Energ. Rev.* 2008, 13, 1275-1287.

(2) Hurley, S.; Xu, C.; Preto, F.; Shao, Y.; Li, H.; Wang, J.;Tourigny, G. Catalytic gasification of woody biomass in an air-blown fluidized-bed reactor using Canadian limonite iron ore as the bed material. *Fuel* 2012, 91, 170-176.

(3) Vasudevan, P.; Sharma, S.;Kumar, A. Liquid fuel from biomass: An overview. *J. Sci. Ind. Res.* 2005, 64, 822-831.

(4) Abdoulmoumine, N.; Kulkarni, A.; Adhikari, S.; Taylor, S.;Loewenstein, E. Economic analysis of municipal power generation from gasification of urban green wastes: case study of Fultondale, Alabama, USA. *Biofuels, Bioprod. Biorefin.* 2012, 6, 521-533.

(5) Moens, L. Chapter 9 Renewable feedstocks. In *Sustainability Science and Engineering*, Abraham, M. A., Ed. Elsevier: 2006; Vol. Volume 1, pp 177-199.

(6) Bridgwater, A. The technical and economic feasibility of biomass gasification for power generation. *Fuel* 1995, 74, 631-653.

(7) Brown, R. C. *Thermochemical processing of biomass: conversion into fuels, chemicals and power*. Wiley: New York, New York, 2011; Vol. 12.

(8) Bingyan, X.; Zengfan, L.; Chungzhi, W.; Haitao, H.;Xiguang, Z. Integrated Energy Systems in China - The Cold Northeastern Region Experience - Circulating fluidized bed gasifier for biomass. In Natural Resources Management and Environment Department, United Nation Food and Agricultural Organization: Rome, Italy, 1994.

(9) Li, X. T.; Grace, J. R.; Lim, C. J.; Watkinson, A. P.; Chen, H. P.;Kim, J. R. Biomass gasification in a circulating fluidized bed. *Biomass Bioenergy* 2004, 26, 171 – 193.

(10) van der Drift, A.; van Doorn, J.;Vermeulen, J. W. Ten residual biomass fuels for circulating fluidized-bed gasification. *Biomass Bioenergy* 2001, 20, 45-56.

(11) Narvaez, I.; Orio, A.; Aznar, M. P.;Corella, J. Biomass Gasification with Air in an Atmospheric Bubbling Fluidized Bed. Effect of Six Operational Variables on the Quality of the Produced Raw Gas. *Ind. Eng. Chem. Res.* 1996, 35, 2110-2120.

(12) Cao, Y.; Wang, Y.; Riley, J. T.;Pan, W.-P. A novel biomass air gasification process for producing tar-free higher heating value fuel gas. *Fuel Process. Technol.* 2006, 87, 343-353.

(13) Campoy, M.; Gómez-Barea, A.; Villanueva, A. L.;Ollero, P. Air−Steam Gasification of Biomass in a Fluidized Bed under Simulated Autothermal and Adiabatic Conditions. *Ind. Eng. Chem. Res.* 2008, 47, 5957-5965.

(14) Meng, X.; de Jong, W.; Fu, N.;Verkooijen, A. H. M. Biomass gasification in a 100 kWth steam-oxygen blown circulating fluidized bed gasifier: Effects of operational conditions on product gas distribution and tar formation. *Biomass Bioenergy* 2011, 35, 2910-2924.

(15) Miccio, F.; Ruoppolo, G.; Kalisz, S.; Andersen, L.; Morgan, T. J.;Baxter, D. Combined gasification of coal and biomass in internal circulating fluidized bed. *Fuel Process. Technol.* 2012, 95, 45-54.

(16) Hannula, I.;Kurkela, E. A parametric modelling study for pressurised steam/O2-blown fluidised-bed gasification of wood with catalytic reforming. *Biomass Bioenergy* 2012, 38, 58-67.

(17) Lv, P.; Yuan, Z.; Wu, C.; Ma, L.; Chen, Y.;Tsubaki, N. Bio-syngas production from biomass catalytic gasification. *Energy Convers. Manage.* 2007, 48, 1132-1139.

(18) Campoy, M.; Gómez-Barea, A.; Vidal, F. B.;Ollero, P. Air–steam gasification of biomass in a fluidised bed: Process optimisation by enriched air. *Fuel Process. Technol.* 2009, 90, 677-685.

(19) Cui, H.; Turn, S. Q.; Keffer, V.; Evans, D.; Tran, T.;Foley, M. Study on the fate of metal elements from biomass in a bench-scale fluidized bed gasifier. *Fuel* 2013, 108, 1-12.

(20) Cui, H.; Turn, S. Q.; Keffer, V.; Evans, D.; Tran, T.;Foley, M. Contaminant Estimates and Removal in Product Gas from Biomass Steam Gasification. *Energy Fuels* 2010, 24, 1222-1233.

(21) Devi, L.; Ptasinski, K. J.;Janssen, F. J. J. G. A review of the primary measures for tar elimination in biomass gasification processes. *Biomass Bioenergy* 2003, 24, 125-140.

(22) Abdoulmoumine, N.; Kulkarni, A.;Adhikari, S. Effects of Temperature and Equivalence Ratio on Pine Syngas Primary Gases and Contaminants in a Bench-Scale Fluidized Bed Gasifier. *Ind. Eng. Chem. Res.* 2014, 53, 5767–5777.

(23) Milne, T. A.; Evans, R. J.;Abatzoglou, N. *Biomass gasifier" tars": their nature, formation, and conversion*; NREL/TP-570-25357; National Renewable Energy Laboratory: Golden, Colorado, 1998.

(24) Stefan Heyne, T. L., Magnus Marklund. *Biomass gasification - A synthesis of technical barriers and current research issues for deployment at large scale*; The Swedish Knowledge Centre for Renewable Transportation Fuels: Göteborg, Sweden, 2013.

(25) Rabou, L. P.; Zwart, R. W.; Vreugdenhil, B. J.;Bos, L. Tar in biomass producer gas, the Energy research Centre of the Netherlands (ECN) experience: an enduring challenge. *Energy Fuels* 2009, 23, 6189-6198.

(26) Hosoya, T.; Kawamoto, H.;Saka, S. Pyrolysis gasification reactivities of primary tar and char fractions from cellulose and lignin as studied with a closed ampoule reactor. *J. Anal. Appl. Pyrolysis* 2008, 83, 71-77.

(27) Asmadi, M.; Kawamoto, H.;Saka, S. Gas-and solid/liquid-phase reactions during pyrolysis of softwood and hardwood lignins. *J. Anal. Appl. Pyrolysis* 2011, 92, 417-425.

(28) Frenklach, M.;Wang, H. Detailed Mechanism and Modeling of Soot Particle Formation. In *Soot Formation in Combustion*, Bockhorn, H., Ed. Springer Berlin Heidelberg: Berlin, Germany, 1994; Vol. 59, pp 165-192.

(29) Egsgaard, H.;Larsen, E. In *Thermal Transformation of Light Tar - Specific Routes to Aromatic Aldehydes and PAH*, Proceedings of the 1st World Conference on Biomass for Energy and Industry, Sevilla, Spain, 5–9 June 2000, 2000; James and James: Sevilla, Spain, 2000.

(30) Font Palma, C. Modelling of tar formation and evolution for biomass gasification: A review. *Appl. Energy* 2013, 111, 129-141.

(31) Evans, R. J.;Milne, T. A. Molecular characterization of the pyrolysis of biomass. *Energy Fuels* 1987, 1, 123-137.

(32) Shen, D. K.; Gu, S.;Bridgwater, A. V. Study on the pyrolytic behaviour of xylan-based hemicellulose using TG–FTIR and Py–GC–FTIR. *J. Anal. Appl. Pyrolysis* 2010, 87, 199-206.

(33) Font Palma, C. Model for Biomass Gasification Including Tar Formation and Evolution. *Energy Fuels* 2013, 27, 2693-2702.

(34) Zhou, J.; Masutani, S. M.; Ishimura, D. M.; Turn, S. Q.;Kinoshita, C. M. Release of Fuel-Bound Nitrogen during Biomass Gasification. *Ind. Eng. Chem. Res.* 2000, 39, 626-634.

(35) Zhou, J.; Masutani, S. M.; Ishimura, D. M.; Turn, S. Q.;Kinoshita, C. M. Release of Fuel-Bound Nitrogen during Biomass Gasification. *Industrial & Engineering Chemistry Research* 2000, 39, 626-634.

(36) Abdoulmoumine, N.; Kulkarni, A.;Adhikari, S. Effects of Temperature and Equivalence Ratio on Pine Syngas Primary Gases and Contaminants in a Bench-Scale Fluidized Bed Gasifier. *Ind. Eng. Chem. Res.* 2014, 53, 5767-5777.

(37) Yrjas, P.; Iisa, K.;Hupa, M. Limestone and dolomite as sulfur absorbents under pressurized gasification conditions. *Fuel* 1996, 75, 89-95.

(38) Ohtsuka, Y.; Tsubouchi, N.; Kikuchi, T.;Hashimoto, H. Recent progress in Japan on hot gas cleanup of hydrogen chloride, hydrogen sulfide and ammonia in coal-derived fuel gas. *Powder Technol.* 2009, 190, 340-347.

(39) Bläsing, M.; Schaafhausen, S.;Müller, M. Investigation of alkali induced corrosion of SiC filter candles at high temperature, in gasification environment. *J. Eur. Ceram. Soc.* 2014, 34, 1041-1044.

(40) Carter, C.; Abdoulmoumine, N.; Kulkarni, A.; Adhikari, S.;Fasina, O. Physicochemical properties of thermally treated biomass and energy requirement for torrefaction. *Trans. ASAE.* 2013, 56, 1093-1100.

(41) Bain, R. L. An Introduction to Biomass Thermochemical Conversion. In DOE/NASLUGC Biomass and Solar Energy Workshops: 2004.

(42) Daniel L. Carpenter, R. L. B., Ryan E. Davis, Abhijit Dutta, Calvin J. Feik, Katherine R. Gaston, Whitney Jablonski, Steven D. Phillips, and Mark R. Nimlos. Pilot-Scale Gasification of

Corn Stover, Switchgrass, Wheat Straw, and Wood: 1. Parametric Study and Comparison with Literature. *Ind. Eng. Chem. Res.* 2010, 49, 1859-1871.

(43) Brage, C.; Yu, Q.; Chen, G.;Sjöström, K. Tar evolution profiles obtained from gasification of biomass and coal. *Biomass Bioenergy* 2000, 18, 87-91.

(44) Vogel, K. P. Energy production from forages (or American agriculture—back to the future). *J. Soil Water Conserv.* 1996, 51, 137-139.

(45) Couto, N.; Rouboa, A.; Silva, V.; Monteiro, E.;Bouziane, K. Influence of the biomass gasification processes on the final composition of syngas. *Energy Procedia* 2013, 36, 596-606.

(46) Lv, P. M.; Xiong, Z. H.; Chang, J.; Wu, C. Z.; Chen, Y.;Zhu, J. X. An experimental study on biomass air–steam gasification in a fluidized bed. *Bioresour. Technol.* 2004, 95, 95-101.

(47) Kumar, A.; Eskridge, K.; Jones, D. D.;Hanna, M. A. Steam–air fluidized bed gasification of distillers grains: Effects of steam to biomass ratio, equivalence ratio and gasification temperature. *Bioresour. Technol.* 2009, 100, 2062-2068.

(48) Weiland, F.; Hedman, H.; Marklund, M.; Wiinikka, H.; Öhrman, O.;Gebart, R. Pressurized Oxygen Blown Entrained-Flow Gasification of Wood Powder. *Energy Fuels* 2013, 27, 932-941.

(49) Son, Y.-I.; Yoon, S. J.; Kim, Y. K.;Lee, J.-G. Gasification and power generation characteristics of woody biomass utilizing a downdraft gasifier. *Biomass Bioenergy* 2011, 35, 4215-4220.

(50) Liu, H.; Hu, J.; Wang, H.; Wang, C.;Li, J. Experimental studies of biomass gasification with air. *J. Nat. Gas Chem.* 2012, 21, 374-380.

(51) Cheah, S.; Carpenter, D. L.;Magrini-Bair, K. A. Review of mid-to high-temperature sulfur sorbents for desulfurization of biomass-and coal-derived syngas. *Energy Fuels* 2009, 23, 5291-5307.

(52) Carpenter, D. L.; Bain, R. L.; Davis, R. E.; Dutta, A.; Feik, C. J.; Gaston, K. R.; Jablonski, W.; Phillips, S. D.;Nimlos, M. R. Pilot-Scale Gasification of Corn Stover, Switchgrass, Wheat Straw, and Wood: 1. Parametric Study and Comparison with Literature. *Ind. Eng. Chem. Res.* 2010, 49, 1859-1871.

(53) Boerrigter, H.;Rauch, R. Syngas Production and Utilisation. In *Handbook Biomass Gasification*, Knoef, H. A. M., Ed. Biomass Technology Group: Enschede, The Netherlands, 2006; pp 211-230.

(54) Zhou, J.; Chen, Q.; Zhao, H.; Cao, X.; Mei, Q.; Luo, Z.;Cen, K. Biomass–oxygen gasification in a high-temperature entrained-flow gasifier. *Biotechnol. Adv.* 2009, 27, 606-611.

(55) Higman, C.;Van der Burgt, M. *Gasification*. Gulf Professional Publishing: 2003.

(56) Yang, W.-c. *Handbook of fluidization and fluid-particle systems*. CRC Press: Boca Raton, Florida, 2003; Vol. 91.

(57) Basu, P. *Biomass gasification and pyrolysis: practical design and theory*. Academic press: 2010.

(58) Steynberg, A.;Dry, M. *Fischer-Tropsch Technology*. Access Online via Elsevier: 2004.

(59) Basu, P. *Combustion and gasification in fluidized beds*. CRC Press: 2006.

(60) Saw, W. L.;Pang, S. Co-gasification of blended lignite and wood pellets in a 100kW dual fluidised bed steam gasifier: The influence of lignite ratio on producer gas composition and tar content. *Fuel* 2013, 112, 117-124.

(61) Skoulou, V.; Kantarelis, E.; Arvelakis, S.; Yang, W.;Zabaniotou, A. Effect of biomass leaching on H2 production, ash and tar behavior during high temperature steam gasification (HTSG) process. *Int. J. Hydrogen Energy* 2009, 34, 5666-5673.

(62) Milne, T.; Abatzoglou, N.; Evans, R.; Kemestrie, I.;Laboratory, N. R. E. Biomass gasifier" tars": their nature, formation, and conversion. In National Renewable Energy Laboratory Golden, CO: 1998.

(63) Pfeifer, C.; Puchner, B.;Hofbauer, H. Comparison of dual fluidized bed steam gasification of biomass with and without selective transport of CO_2. *Chem. Eng. Sci.* 2009, 64, 5073-5083.

(64) Gil, J.; Corella, J.; Aznar, M. P.;Caballero, M. A. Biomass gasification in atmospheric and bubbling fluidized bed: Effect of the type of gasifying agent on the product distribution. *Biomass Bioenergy* 1999, 17, 389-403.

(65) Drifta, A. v. d.; Doorna, J. v.;Vermeulenb, J. W. Ten residual biomass fuels for circulating fuidized-bed gasification. *Biomass Bioenergy* 2001, 20, 45-56.

(66) Wilk, V.;Hofbauer, H. Conversion of fuel nitrogen in a dual fluidized bed steam gasifier. *Fuel* 2013, 106, 793-801.

(67) Torres, W.; Pansare, S. S.;Goodwin, J. G. Hot Gas Removal of Tars, Ammonia, and Hydrogen Sulfide from Biomass Gasification Gas. *Cat. Rev. - Sci. Eng.* 2007, 49, 407-456.

(68) Gai, C.; Dong, Y.;Zhang, T. Distribution of sulfur species in gaseous and condensed phase during downdraft gasification of corn straw. *Energy* 2013.

(69) Aigner, I.; Pfeifer, C.;Hofbauer, H. Co-gasification of coal and wood in a dual fluidized bed gasifier. *Fuel* 2011, 90, 2404-2412.

(70) Dias, M.;Gulyurtlu, I. In *H2S and HCl formation during RDF and coal co-gasification: a comparison between the predictions and experimental results*, Proceedings of the biomass gasification technologies workshop MRC Gebze Campus-Tü rkiye, 2008; 2008.

(71) Meng, X.; de Jong, W.; Pal, R.;Verkooijen, A. H. M. In bed and downstream hot gas desulphurization during solid fuel gasification: A review. *Fuel Process. Technol.* 2010, 91, 964-981.

(72) Turn, S. Q.; Kinoshita, C. M.; Ishimura, D. M.;Zhou, J. The fate of inorganic constituents of biomass in fluidized bed gasification. *Fuel* 1998, 77, 135-146.

(73) Kuramochi, H.; Wu, W.;Kawamoto, K. Prediction of the behaviors of H2S and HCl during gasification of selected residual biomass fuels by equilibrium calculation. *Fuel* 2005, 84, 377-387.

(74) Dolan, M. D.; Ilyushechkin, A. Y.; McLennan, K. G.;Sharma, S. D. Halide removal from coal-derived syngas: review and thermodynamic considerations. *Asia-Pac. J. Chem. Eng.* 2011, n/a-n/a.

(75) Porbatzki, D.; Stemmler, M.;Müller, M. Release of inorganic trace elements during gasification of wood, straw, and miscanthus. *Biomass Bioenergy* 2011, 35, S79-S86.

(76) Porbatzki, D.; Stemmler, M.;Müller, M. Release of inorganic trace elements during gasification of wood, straw, and miscanthus. *Biomass and Bioenergy* 2011, 35, Supplement 1, S79-S86.

(77) Konttinen, J.; Backman, R.; Hupa, M.; Moilanen, A.;Kurkela, E. Trace element behavior in the fluidized bed gasification of solid recovered fuels – A thermodynamic study. *Fuel* 2013, 106, 621-631.

(78) Froment, K.; Defoort, F.; Bertrand, C.; Seiler, J. M.; Berjonneau, J.;Poirier, J. Thermodynamic equilibrium calculations of the volatilization and condensation of inorganics during wood gasification. *Fuel* 2013, 107, 269-281.

(79) Woolcock, P. J.;Brown, R. C. A review of cleaning technologies for biomass-derived syngas. *Biomass Bioenergy* 2013, 52, 54-84.

(80) Chen, H.; Namioka, T.;Yoshikawa, K. Characteristics of tar, NOx precursors and their absorption performance with different scrubbing solvents during the pyrolysis of sewage sludge. *Appl Energy* 2011, 88, 5032-5041.

(81) Wang, T.; Chang, J.; Lv, P.;Zhu, J. Novel catalyst for cracking of biomass tar. *Energy Fuels* 2005, 19, 22-27.

(82) Gil, J.; Caballero, M. A.; Martin, J. A.; Aznar, M.-P.;Corella, J. Biomass Gasification with Air in a Fluidized Bed: Effect of the In-Bed Use of Dolomite under Different Operation Conditions. *Ind. Eng. Chem. Res* 1999, 38, 4226-4235.

(83) Zwart, R. *Gas Cleaning Downstream Biomass Gasification: Status Report 2009*; Energy research Centre of the Netherlands: Petten, Netherlands, 2009.

(84) Phuphuakrat, T.; Namioka, T.;Yoshikawa, K. Absorptive removal of biomass tar using water and oily materials. *Bioresour. Technol.* 2011, 102, 543-549.

(85) Resnik, K. P.;Pennline, H. W. Study of an ammonia-based wet scrubbing process in a continuous flow system. *Fuel* 2013, 105, 184-191.

(86) Pinto, F.; Lopes, H.; André, R. N.; Dias, M.; Gulyurtlu, I.;Cabrita, I. Effect of Experimental Conditions on Gas Quality and Solids Produced by Sewage Sludge Cogasification. 1. Sewage Sludge Mixed with Coal. *Energy Fuels* 2007, 21, 2737-2745.

(87) Haslbeck, J. L.; Kuehn, N. J.; Lewis, E. G.; Pinkerton, L. L.; Simpson, J.; Turner, M. J.; Varghese, E.;Woods, M. C. *Cost and Performance Baseline for Fossil Energy Plants Volume 1: Bituminous Coal and Natural Gas to Electricity*; DOE/NETL-2010/1397; National Energy Technology Laboratory: Morgantown, WV, 2013.

(88) Burr, B.;Lyddon, L. A comparison of physical solvents for acid gas removal. In Bryan Research & Engineering, Inc.: Bryan, Texas, 2008.

(89) Kohl, A. L.;Nielsen, R. *Gas purification*. 5th ed.; Gulf Professional Publishing: Houston, TX, 1997.

(90) Mondal, P.; Dang, G. S.;Garg, M. O. Syngas production through gasification and cleanup for downstream applications — Recent developments. *Fuel Process. Technol.* 2011, 92, 1395-1410.

(91) Allegue, L. B.;Hinge, J. *Biogas and bio-syngas upgrading*; Danish Technological Institute: Aarhus, Denmark, 2012.

(92) Paasen, S. v.; Cieplik, M.;Phokawat, N. *Gasification of non-woody biomass - Economic and Technical Perspectives of*
Chlorine and Sulphur Removal from Product Gas; ECN-C-06-032; Energy Research Centre of the Netherlands (ECN): Petten, Netherlands, 2006.

(93) Kirk, R. E.;Othmer, D. F. Encyclopedia of Chemical Technology. In 5th ed.; Wiley-Interscience Publication: New York, New York, 2004; Vol. 20.

(94) Salo, K.;Mojtahedi, W. Fate of alkali and trace metals in biomass gasification. *Biomass Bioenergy* 1998, 15, 263-267.

(95) Stevens, D. J. *Hot Gas Conditioning: Recent Progress With Larger-Scale Biomass Gasification Systems*; NREL/SR-510-29952; National Renewable Energy Laboratory: Golden, Colorado, 2001.

(96) Yung, M. M.; Jablonski, W. S.;Magrini-Bair, K. A. Review of Catalytic Conditioning of Biomass-Derived Syngas. *Energy Fuels* 2009, 23, 1874-1887.

(97) Liu, H.; Wang, H.; Shen, J.; Sun, Y.;Liu, Z. Promotion effect of cerium and lanthanum oxides on Ni/SBA-15 catalyst for ammonia decomposition. *Catal. Today* 2008, 131, 444-449.

(98) Ferella, F.; Stoehr, J.; Michelis, I. D.;Hornung, A. Zirconia and alumina based catalysts for steam reforming of naphthalene. *Fuel* 2013, 105, 614-629.

(99) Zhang, R.; Brown, R. C.; Suby, A.;Cummer, K. Catalytic destruction of tar in biomass derived producer gas. *Energy Convers. Manage.* 2004, 45, 995-1014.

(100) Yin, S.-F.; Zhang, Q.-H.; Xu, B.-Q.; Zhu, W.-X.; Ng, C.-F.;Au, C.-T. Investigation on the catalysis of COx-free hydrogen generation from ammonia. *J. Catal.* 2004, 224, 384-396.

(101) Mojtahedi, W.; Ylitalo, M.; Maunula, T.;Abbasian, J. Catalytic decomposition of ammonia in fuel gas produced in pilot-scale pressurized fluidized-bed gasifier. *Fuel Process. Technol.* 1995, 45, 221-236.

(102) Park, J. J.; Park, C. G.; Jung, S. Y.; Lee, S. C.; Ragupathy, D.;Kim, J. C. A study on Zn-based catal-sorbents for the simultaneous removal of hydrogen sulfide and ammonia at high temperature. *Res. Chem. Intermed.* 2011, 37, 1193-1202.

(103) Ng, P. F.; Li; Wang, S.; Zhu, Z.; Lu, G.;Yan, Z. Catalytic Ammonia Decomposition over Industrial-Waste-Supported Ru Catalysts. *Environ. Sci. Technol.* 2007, 41, 3758-3762.

(104) Li, L.; Wang, S.; Zhu, Z.; Yao, X.;Yan, Z. Catalytic decomposition of ammonia over fly ash supported Ru catalysts. *Fuel Process. Technol.* 2008, 89, 1106-1112.

(105) Bridgwater, A. Catalysis in thermal biomass conversion. *Appl. Catal., A* 1994, 116, 5-47.

(106) Sutton, D.; Kelleher, B.;Ross, J. R. H. Review of literature on catalysts for biomass gasification. *Fuel Process. Technol.* 2001, 73, 155-173.

(107) Coll, R.; Salvado, J.; Farriol, X.;Montane, D. Steam reforming model compounds of biomass gasification tars: conversion at different operating conditions and tendency towards coke formation. *Fuel Process. Technol.* 2001, 74, 19-31.

(108) Twigg, M. *Catalyst handbook*. CSIRO: 1989.

(109) Devi, L.; Ptasinski, K. J.;Janssen, F. J. J. G. A review of the primary measures for tar elimination in biomass gasification processes. *Biomass and Bioenergy* 2003, 24, 125-140.

(110) Leppälahti, J.;Kurkela, E. Behaviour of nitrogen compounds and tars in fluidized bed air gasification of peat. *Fuel* 1991, 70, 491-497.

(111) Link, S.; Arvelakis, S.; Paist, A.; Martin, A.; Liliedahl, T.;Sjöström, K. Atmospheric fluidized bed gasification of untreated and leached olive residue, and co-gasification of olive residue, reed, pine pellets and Douglas fir wood chips. *Appl. Energy* 2012, 94, 89-97.

(112) Simell, P.; Kurkela, E.; Ståhlberg, P.;Hepola, J. Catalytic hot gas cleaning of gasification gas. *Catal. Today* 1996, 27, 55-62.

(113) Orio, A.; Corella, J.;Narvaez, I. Performance of different dolomites on hot raw gas cleaning from biomass gasification with air. *Ind. Eng. Chem. Res* 1997, 36, 3800-3808.

(114) Dou, B.; Gao, J.; Sha, X.;Baek, S. W. Catalytic cracking of tar component from high-temperature fuel gas. *Appl. Therm. Eng.* 2003, 23, 2229-2239.

(115) Kuhn, J.; Zhao, Z.; Felix, L.; Slimane, R.; Choi, C.;Ozkan, U. Olivine catalysts for methane-and tar-steam reforming. *Appl. Catal., B* 2008, 81, 14-26.

(116) Devi, L.; Ptasinski, K.;Janssen, F. Pretreated olivine as tar removal catalyst for biomass gasifiers: investigation using naphthalene as model biomass tar. *Fuel Process. Technol.* 2005, 86, 707-730.

(117) Michel, R.; Łamacz, A.; Krzton, A.; Djéga-Mariadassou, G.; Burg, P.; Courson, C.;Gruber, R. Steam reforming of α-methylnaphthalene as a model tar compound over olivine and olivine supported nickel. *Fuel* 2013, 109, 653-660.

(118) D'Orazio, A.; Di Carlo, A.; Dionisi, N.; Dell'Era, A.;Orecchini, F. Toluene steam reforming properties of CaO based synthetic sorbents for biomass gasification process. *International Journal of Hydrogen Energy* 2013, 38, 13282-13292.

(119) Xu, C.; Donald, J.; Byambajav, E.;Ohtsuka, Y. Recent advances in catalysts for hot-gas removal of tar and NH3 from biomass gasification. *Fuel* 2010, 89, 1784-1795.

(120) Kim, Y.-K.; Park, J.-I.; Jung, D.; Miyawaki, J.; Yoon, S.-H.;Mochida, I. Low-temperature catalytic conversion of lignite: 1. Steam gasification using potassium carbonate supported on perovskite oxide. *J. Ind. Eng. Chem.* 2014, 20, 216-221.

(121) Corella, J.; Aznar, M.-P.; Gil, J.;Caballero, M. A. Biomass Gasification in Fluidized Bed: Where To Locate the Dolomite To Improve Gasification? *Energy Fuels* 1999, 13, 1122-1127.

(122) Sun, Y.; Jiang, J.; Kantarelis, E.; Xu, J.; Li, L.; Zhao, S.;Yang, W. Development of a bimetallic dolomite based tar cracking catalyst. *Catal. Commun.* 2012, 20, 36-40.

(123) Perez, P.; Aznar, P.; Caballero, M.; Gil, J.; Martin, J.;Corella, J. Hot Gas Cleaning and Upgrading with a Calcined Dolomite Located Downstream a Biomass Fluidized Bed Gasifier Operating with Steam- Oxygen Mixtures. *Energy Fuels* 1997, 11, 1194-1203.

(124) Corella, J.; Orio, A.;Toledo, J. Biomass gasification with air in a fluidized bed: Exhaustive tar elimination with commercial steam reforming catalysts. *Energy Fuels* 1999, 13, 702-709.

(125) Hu, G.; Xu, S.; Li, S.; Xiao, C.;Liu, S. Steam gasification of apricot stones with olivine and dolomite as downstream catalysts. *Fuel Process. Technol.* 2006, 87, 375-382.

(126) Guan, G.; Chen, G.; Kasai, Y.; Lim, E. W. C.; Hao, X.; Kaewpanha, M.; Abuliti, A.; Fushimi, C.;Tsutsumi, A. Catalytic steam reforming of biomass tar over iron- or nickel-based catalyst supported on calcined scallop shell. *Appl. Catal., B* 2012, 115–116, 159-168.

(127) Li, L.; Morishita, K.;Takarada, T. Light fuel gas production from nascent coal volatiles using a natural limonite ore. *Fuel* 2007, 86, 1570-1576.

(128) Matsumura, A.; Sato, S.; Kondo, T.; Saito, I.;de Souza, W. Hydrocracking Marlim vacuum residue with natural limonite. Part 2: experimental cracking in a slurry-type continuous reactor. *Fuel* 2005, 84, 417-421.

(129) Matsumura, A.; Kondo, T.; Sato, S.; Saito, I.;de Souza, W. Hydrocracking Brazilian Marlim vacuum residue with natural limonite. Part 1: catalytic activity of natural limonite. *Fuel* 2005, 84, 411-416.

(130) Nordgreen, T.; Liliedahl, T.;Sjöström, K. Metallic iron as a tar breakdown catalyst related to atmospheric, fluidised bed gasification of biomass. *Fuel* 2006, 85, 689-694.

(131) Leppälahti, J.; Simell, P.;Kurkela, E. Catalytic conversion of nitrogen compounds in gasification gas. *Fuel Process. Technol.* 1991, 29, 43-56.

(132) Dou, B.; Gao, J.; Sha, X.;Baek, S. W. Catalytic cracking of tar component from high-temperature fuel gas. *Applied thermal engineering* 2003, 23, 2229-2239.

(133) Huber, G. W.; Iborra, S.;Corma, A. Synthesis of Transportation Fuels from Biomass: Chemistry, Catalysts, and Engineering. *Chem. Rev.* 2006, 106, 4044-4098.

(134) Dou, B.; Gao, J.; Sha, X.;Baek, S. Catalytic cracking of tar component from high-temperature fuel gas. *Appl. Therm. Eng.* 2003, 23, 2229-2239.

(135) Buchireddy, P. R.; Bricka, R. M.; Rodriguez, J.;Holmes, W. Biomass Gasification: Catalytic Removal of Tars over Zeolites and Nickel Supported Zeolites. *Energy Fuels* 2010, 24, 2707-2715.

(136) Miyazawa, T.; Kimura, T.; Nishikawa, J.; Kado, S.; Kunimori, K.;Tomishige, K. Catalytic performance of supported Ni catalysts in partial oxidation and steam reforming of tar derived from the pyrolysis of wood biomass. *Catal. Today* 2006, 115, 254-262.

(137) Sutton, D.; Kelleher, B.; Doyle, A.;Ross, J. Investigation of nickel supported catalysts for the upgrading of brown peat derived gasification products. *Bioresour. Technol.* 2001, 80, 111-116.

(138) Swierczynski, D.; Libs, S.; Courson, C.;Kiennemann, A. Steam reforming of tar from a biomass gasification process over Ni/olivine catalyst using toluene as a model compound. *Appl. Catal., B* 2007, 74, 211-222.

(139) Agblevor, F.; Beis, S.; Mante, O.;Abdoulmoumine, N. Fractional Catalytic Pyrolysis of Hybrid Poplar Wood. *Ind. Eng. Chem. Res* 2010, 49, 3533-3538.

(140) Kaewpanha, M.; Guan, G.; Hao, X.; Wang, Z.; Kasai, Y.; Kakuta, S.; Kusakabe, K.;Abudula, A. Steam reforming of tar derived from the steam pyrolysis of biomass over metal catalyst supported on zeolite. *J. Taiwan Inst. Chem. Eng.* 2013, 44, 1022-1026.

(141) Jung, S. Y.; Lee, S. J.; Park, J. J.; Lee, S. C.; Jun, H. K.; Lee, T. J.; Ryu, C. K.;Kim, J. C. The simultaneous removal of hydrogen sulfide and ammonia over zinc-based dry sorbent supported on alumina. *Sep. Purif. Technol.* 2008, 63, 297-302.

(142) Zheng, W.; Zhang, J.; Ge, Q.; Xu, H.;Li, W. Effects of CeO2 addition on Ni/Al2O3 catalysts for the reaction of ammonia decomposition to hydrogen. *Appl. Catal., B* 2008, 80, 98-105.

(143) Donald, J.; Xu, C.; Hashimoto, H.; Byambajav, E.;Ohtsuka, Y. Novel carbon-based Ni/Fe catalysts derived from peat for hot gas ammonia decomposition in an inert helium atmosphere. *Appl. Catal., A* 2010, 375, 124-133.

(144) Zhang, H.; Alhamed, Y. A.; Kojima, Y.; Al-Zahrani, A. A.; Miyaoka, H.;Petrov, L. A. Structure and catalytic properties of Ni/MWCNTs and Ni/AC catalysts for hydrogen production via ammonia decomposition. *Int. J. Hydrogen Energy* 2014, 39, 277-287.

(145) Lorenzut, B.; Montini, T.; Pavel, C. C.; Comotti, M.; Vizza, F.; Bianchini, C.;Fornasiero, P. Embedded Ru@ZrO2 Catalysts for H2 Production by Ammonia Decomposition. *ChemCatChem* 2010, 2, 1096-1106.

(146) Ozawa, Y.;Tochihara, Y. Catalytic decomposition of ammonia in simulated coal-derived gas over supported nickel catalysts. *Catal. Today* 2011, 164, 528-532.

(147) Prasad, V.; Karim, A.; Arya, A.;Vlachos, D. Assessment of overall rate expressions and multiscale, microkinetic model uniqueness via experimental data injection: Ammonia decomposition on Ru/γ-Al2O3 for hydrogen production. *Ind. Eng. Chem. Res* 2009, 48, 5255-5265.

(148) Ohtsuka, Y.; Xu, C.; Kong, D.;Tsubouchi, N. Decomposition of ammonia with iron and calcium catalysts supported on coal chars. *Fuel* 2004, 83, 685-692.

(149) Tsubouchi, N.; Hashimoto, H.;Ohtsuka, Y. Sulfur tolerance of an inexpensive limonite catalyst for high temperature decomposition of ammonia. *Powder Technol.* 2008, 180, 184-189.

(150) Corella, J.; Toledo, J. M.;Padilla, R. Olivine or Dolomite as In-Bed Additive in Biomass Gasification with Air in a Fluidized Bed: Which Is Better? *Energy Fuels* 2004, 18, 713-720.

(151) Bjoerkman, E.;Sjoestroem, K. Decomposition of ammonia over dolomite and related compounds. *Energy Fuels* 1991, 5, 753-760.

(152) Simell, P. A.; Hirvensalo, E. K.; Smolander, V. T.;Krause, A. O. I. Steam reforming of gasification gas tar over dolomite with benzene as a model compound. *Ind. Eng. Chem. Res* 1999, 38, 1250-1257.

(153) Tsubouchi, N.; Hashimoto, H.;Ohtsuka, Y. Catalytic performance of limonite in the decomposition of ammonia in the coexistence of typical fuel gas components produced in an air-blown coal gasification process. *Energy Fuels* 2007, 21, 3063-3069.

(154) Donald, J.; Xu, C.; Hashimoto, H.; Byambajav, E.;Ohtsuka, Y. Novel carbon-based Ni/Fe catalysts derived from peat for hot gas ammonia decomposition in an inert helium atmosphere. *Applied Catalysis A: General* 2010, 375, 124-133.

(155) Mojtahedi, W.;Abbasian, J. Catalytic decomposition of ammonia in a fuel gas at high temperature and pressure. *Fuel* 1995, 74, 1698-1703.

(156) Nassos, S.; Elm Svensson, E.; Boutonnet, M.;Järås, S. The influence of Ni load and support material on catalysts for the selective catalytic oxidation of ammonia in gasified biomass. *Appl. Catal., B* 2007, 74, 92-102.

(157) Wang, W.; Padban, N.; Ye, Z.; Olofsson, G.; Andersson, A.;Bjerle, I. Catalytic Hot Gas Cleaning of Fuel Gas from an Air-Blown Pressurized Fluidized-Bed Gasifier. *Ind. Eng. Chem. Res* 2000, 39, 4075-4081.

(158) Chellappa, A.; Fischer, C.;Thomson, W. Ammonia decomposition kinetics over Ni-Pt/Al2O3 for PEM fuel cell applications. *Appl. Catal., A* 2002, 227, 231-240.

(159) Wang, W.; Padban, N.; Ye, Z.; Andersson, A.;Bjerle, I. Kinetics of Ammonia Decomposition in Hot Gas Cleaning. *Ind. Eng. Chem. Res* 1999, 38, 4175-4182.

(160) Depner, H.;Jess, A. Kinetics of nickel-catalyzed purification of tarry fuel gases from gasification and pyrolysis of solid fuels. *Fuel* 1999, 78, 1369-1377.

(161) Li, X. K.; Ji, W. J.; Zhao, J.; Wang, S. J.;Au, C. T. Ammonia decomposition over Ru and Ni catalysts supported on fumed SiO2, MCM-41, and SBA-15. *J. Catal.* 2005, 236, 181-189.

(162) Choudhary, T.; Sivadinarayana, C.;Goodman, D. Production of COx-free hydrogen for fuel cells via step-wise hydrocarbon reforming and catalytic dehydrogenation of ammonia. *Chem. Eng. J.* 2003, 93, 69-80.

(163) Yin, S.; Xu, B.; Zhou, X.;Au, C. A mini-review on ammonia decomposition catalysts for on-site generation of hydrogen for fuel cell applications. *Appl. Catal., A* 2004, 277, 1-9.

(164) Zhang, J.; Xu, H.; Ge, Q.;Li, W. Highly efficient Ru/MgO catalysts for NH_3 decomposition: Synthesis, characterization and promoter effect. *Catal. Commun.* 2006, 7, 148-152.

(165) Ozawa, Y.;Tochihara, Y. Catalytic decomposition of ammonia in simulated coal-derived gas. *Chem. Eng. Sci.* 2007, 62, 5364-5367.

(166) Ozawa, Y.;Tochihara, Y. Catalytic decomposition of ammonia in simulated coal-derived gas. *Chemical Engineering Science* 2007, 62, 5364-5367.

(167) Juutilainen, S. J.; Simell, P. A.;Krause, A. O. I. Zirconia: Selective oxidation catalyst for removal of tar and ammonia from biomass gasification gas. *Appl. Catal., B* 2006, 62, 86-92.

(168) Mojtahedi, W.; Ylitalo, M.; Maunula, T.;Abbasian, J. Catalytic decomposition of ammonia in fuel gas produced in pilot-scale pressurized fluidized-bed gasifier. *Fuel Processing Technology* 1995, 45, 221-236.

(169) Akyurtlu, J. F.;Akyurtlu, A. Hot gas desulfurization with vanadium-promoted zinc ferrite sorbents. *Gas Sep. Purif.* 1995, 9, 17-25.

(170) Liu, B.; Wan, Z.; Zhan, Y.;Au, C. Desulfurization of hot coal gas over high-surface-area LaMeOx/MCM-41 sorbents. *Fuel* 2012, 98, 95-102.

(171) Jun, H. K.; Lee, T. J.; Ryu, S. O.;Kim, J. C. A study of Zn-Ti based H_2S removal sorbents promoted with cobalt oxides. *Ind. Eng. Chem. Res* 2001, 40, 3547-3556.

(172) Rosso, I.; Galletti, C.; Bizzi, M.; Saracco, G.;Specchia, V. Zinc oxide sorbents for the removal of hydrogen sulfide from syngas. *Ind. Eng. Chem. Res* 2003, 42, 1688-1697.

(173) Cheah, S.; Parent, Y. O.; Jablonski, W. S.; Vinzant, T.;Olstad, J. L. Manganese and ceria sorbents for high temperature sulfur removal from biomass-derived syngas – The impact of steam on capacity and sorption mode. *Fuel* 2012, 97, 612-620.

(174) Heesink, A. B. M.;Van Swaaij, W. P. M. The sulphidation of calcined limestone with hydrogen sulphide and carbonyl sulphide. *Chem. Eng. Sci.* 1995, 50, 2983-2996.

(175) Heesink, A. B. M.;Van Swaaij, W. P. M. The sulphidation of calcined limestone with hydrogen sulphide and carbonyl sulphide. *Chemical Engineering Science* 1995, 50, 2983-2996.

(176) Wang, W.; Ye, Z.;Bjerle, I. The kinetics of the reaction of hydrogen chloride with fresh and spent Ca-based desulfurization sorbents. *Fuel* 1996, 75, 207-212.

(177) Elseviers, W. F.;Verelst, H. Transition metal oxides for hot gas desulphurisation. *Fuel* 1999, 78, 601-612.

(178) Lew, S.; Sarofim, A. F.;Flytzani-Stephanopoulos, M. Sulfidation of zinc titanate and zinc oxide solids. *Ind. Eng. Chem. Res* 1992, 31, 1890-1899.

(179) Jothimurugesan, K.;Gangwal, S. K. Regeneration of Zinc Titanate H_2S Sorbents. *Ind. Eng. Chem. Res* 1998, 37, 1929-1933.

(180) Sasaoka, E.; Sada, N.; Manabe, A.; Uddin, M. A.;Sakata, Y. Modification of ZnO−TiO2 High-Temperature Desulfurization Sorbent by ZrO2 Addition. *Ind. Eng. Chem. Res.* 1999, 38, 958-963.

(181) Bu, X.; Ying, Y.; Zhang, C.;Peng, W. Research improvement in Zn-based sorbent for hot gas desulfurization. *Powder Technol.* 2008, 180, 253-258.

(182) Jun, H. K.; Lee, T. J.; Ryu, S. O.;Kim, J. C. A study of Zn-Ti-based H_2S removal sorbents promoted with cobalt oxides. *Ind. Eng. Chem. Res.* 2001, 40, 3547-3556.

(183) Kyotani, T.; Kawashima, H.; Tomita, A.; Palmer, A.;Furimsky, E. Removal of H2S from hot gas in the presence of Cu-containing sorbents. *Fuel* 1989, 68, 74-79.

(184) Ko, T.-H.; Chu, H.;Chaung, L.-K. The sorption of hydrogen sulfide from hot syngas by metal oxides over supports. *Chemosphere* 2005, 58, 467-474.

(185) Karvan, O.;Atakül, H. Investigation of CuO/mesoporous SBA-15 sorbents for hot gas desulfurization. *Fuel Process. Technol.* 2008, 89, 908-915.

(186) Buelna, G.;Lin, Y. S. Characteristics and desulfurization-regeneration properties of sol–gel-derived copper oxide on alumina sorbents. *Sep. Purif. Technol.* 2004, 39, 167-179.

(187) Baeza, P.; Aguila, G.; Gracia, F.;Araya, P. Desulfurization by adsorption with copper supported on zirconia. *Catal. Commun.* 2008, 9, 751-755.

(188) Bineesh, K. V.; Kim, D.-K.; Kim, M.-I. L.;Park, D.-W. Selective catalytic oxidation of H2S over V2O5 supported on TiO2-pillared clay catalysts in the presence of water and ammonia. *Appl. Clay Sci.* 2011, 53, 204-211.

(189) Hachimi, A.; Vilcocq, L.; Courson, C.;Kiennemann, A. Study of olivine supported copper sorbents performances in the desulfurization process in link with biomass gasification. *Fuel Process. Technol.* 2014, 118, 254-263.

(190) Wang, J.; Zhang, Y.; Han, L.; Chang, L.;Bao, W. Simultaneous removal of hydrogen sulfide and mercury from simulated syngas by iron-based sorbents. *Fuel* 2011.

(191) Zeng, Y.; Kaytakoglu, S.;Harrison, D. Reduced cerium oxide as an efficient and durable high temperature desulfurization sorbent. *Chem. Eng. Sci.* 2000, 55, 4893-4900.

(192) Krishnan, G. N.; Gupta, R.;Ayala, R. *Development of Disposable Sorbents for Chloride Removal from High Temperature Coal-Derived Gases*; DE-AC21-93MC30005; National Energy Technology Laboratory: Morgantown, WV, 1999.

(193) Duo, W.; Kirkby, N.; Seville, J.; Kiel, J.; Bos, A.;Den Uil, H. Kinetics of HCl reactions with calcium and sodium sorbents for IGCC fuel gas cleaning. *Chem. Eng. Sci.* 1996, 51, 2541-2546.

(194) Granite, E. J.; Myers, C. R.; King, W. P.; Stanko, D. C.;Pennline, H. W. Sorbents for Mercury Capture from Fuel Gas with Application to Gasification Systems. *Ind. Eng. Chem. Res* 2006, 45, 4844-4848.

(195) Bläsing, M.;Müller, M. Investigation of the effect of alkali metal sorbents on the release and capture of trace elements during combustion of straw. *Combust. Flame* 2013, 160, 3015-3020.

(196) Inai, M.;Ronhunshu, K. K. Alkali metal vapor removal from coal gasification flue gases. *Fuel Energ. Abstr.* 2000, 41, 313.

(197) Phuphuakrat, T.; Namioka, T.;Yoshikawa, K. Absorptive removal of biomass tar using water and oily materials. *Bioresource Technology* 2011, 102, 543-549.

(198) Craig, K. Thermochemical Platform Overview. In *Second Meeting of S - 1007*, U.S. Department of Energy by Midwest Research Institute Battelle: Washington, DC, 2003.

(199) E Gnansounou , D. B., A Dauriat In *Promoting bioethanol production through clean development mechanism: findings and lessons learnt from ASIATIC project*, 7th IAEE European energy conference, Bergen, Norway, August 28–30, 2005., 2005; Bergen, Norway, 2005.

(200) Bridgwater, A. V. Renewable fuels and chemicals by thermal processing of biomass. *Chem. Eng. J.* 2003, 91.

(201) Tijmensen, M.; Faaij, A.; Hamelinck, C.;van Hardeveld, M. Exploration of the possibilities for production of Fischer Tropsch liquids and power via biomass gasification. *Biomass Bioenergy* 2002, 23, 129-152.

(202) Tijmensen, M. J. A.; Faaij, A. P. C.; Hamelinck, C. N.;van Hardeveld, M. R. M. Exploration of the possibilities for production of Fischer Tropsch liquids and power via biomass gasification. *Biomass Bioenergy* 2002, 23, 129-152.

(203) Henstra, A. M.; Sipma, J.; Rinzema, A.;Stams, A. J. M. Microbiology of synthesis gas fermentation for biofuel production. *Curr. Opin. Biotechnol.* 2007, 18, 200-206.

(204) McKendry, P. Energy production from biomass (part 1): overview of biomass. *Bioresour. Technol.* 2002, 83, 37-46.

(205) J.P. Ciferno, J. J. M. Benchmarking biomass gasification technologies for fuels, chemicals and hydrogen production. In U.S. Department of Energy National Energy Technology Laboratory: 2002.

(206) Brown, R. C.;Stevens, C. *Thermochemical Processing of Biomass: Conversion Into Fuels, Chemicals and Power*. Wiley: 2011; Vol. 11.

(207) Ciferno, J. P.;Marano, J. J. *Benchmarking biomass gasification technologies for fuels, chemicals and hydrogen production*; US Department of Energy National Energy Technology Laboratory: Morgantown, WV, 2002.

(208) Göransson, K.; Söderlind, U.; He, J.;Zhang, W. Review of syngas production via biomass DFBGs. *Renew. Sust. Energ. Rev.* 2011, 15, 482-492.

(209) Zhang, W. Automotive fuels from biomass via gasification. *Fuel Process. Technol.* 2010, 91, 866-876.

(210) K. Dowaki, Y. G. Life cycle inventory analysis on Bio-DME and/or Bio-MeOH products through BLUE tower process. *Int. J. Life Cycle Assess.* 2009, 14, 611–620.

Chapter 3

Effect of Temperature and Equivalence Ratio on Primary Gases and Contaminants in an Atmospheric Air Blown Bench-Scale Fluidized Bed Gasifier

Abstract

Effects of equivalence ratio (ER = 0.15, 0.25 and 0.35 at 934°C) and temperature (790, 934 and 1078°C at 0.25ER) were investigated in air gasification of loblolly pine for primary gases and contaminants. CO and H_2 increased while CO_2 and CH_4 decreased from 790 to 1078°C. Opposite trends were observed for ER. Based on overall contaminant weight, tar was highest at all temperatures (7.81, 8.24 and 8.93 g/kg dry biomass) and ERs (13.08, 8.24 and 2.51 g/kg dry biomass). NH_3 varied from 1.63 to 1.00 g/kg dry biomass between 790 and 1078°C and 1.76 to 1.47 g/kg dry biomass between 0.15 to 0.35 ERs. H_2S ranged between 0.13 and 0.17 g/kg dry biomass from 790 to 1078°C and 0.154 to 0.18 g/kg dry biomass from 0.15 to 0.35 ER. Finally, HCl yields ranged from 13.63 to 0 mg/kg dry biomass and 11.51 to 0.28 mg/kg dry biomass over the range of temperature and ER, respectively.

3.1 Introduction

Energy and fuel production from renewable feedstocks is a critical research area today because of the forecasted depletion of crude oil reserves and the growing concern of irreversible environmental damage caused by greenhouse gases.[1] In particular, conversion of biomass to biofuel and energy through gasification is particularly very attractive as it has the potential to produce mixed alcohols, gasoline and diesel via Fischer-Tropsch, gasoline via methanol synthesis as well as electricity via internal combustion engine, steam and gas turbines.[2]

In gasification of biomass, the starting solid fuel is converted into two main product streams: gaseous product stream known as syngas or producer gas and a solid residue stream known as char. Syngas contains CO, CO_2, H_2, CH_4, and inert N_2, the proportion of which varies depending on the gasifying agent, along with light hydrocarbons (C_2-C_6) and H_2O. In addition to the primary gaseous products (CO, H_2, CO_2, CH_4), syngas typically contains a small but nonetheless significant amount of contaminants. Contaminants are condensable organic tars (MW >78), nitrogenous compounds (NH_3, HCN & N_xO_y), sulfur containing compounds (H_2S, COS and CS_2), hydrogen halides (HCl, HF etc) and trace amount of metals (Na, K and other trace metals) as shown in Figure 3.1.

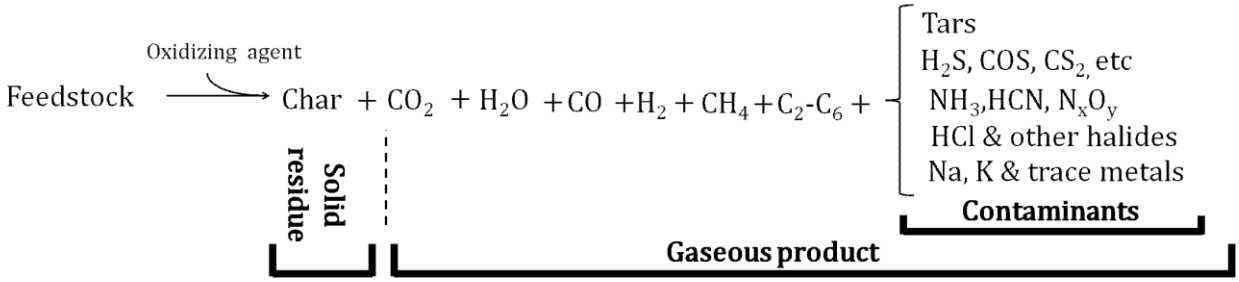

Figure 3.1. Representation of the overall gasification product distribution

The presence of these contaminants is problematic as they result in severe complications in operation ranging from equipment fouling, corrosive degradation, catalyst deactivation and undesirable emissions.[3] The major technical challenge to syngas utilization is the presence of these contaminants.[4] The concentrations of contaminants vary depending on the nature and properties of the starting solid fuel, the operating conditions (temperature, gasifying agent, pressure and catalyst) and the type of gasifier.

In recent years, various studies investigated the effect of temperature[3, 5-9], ER[3, 5-7, 9] and S/B[3, 5-8] on primary gas products in fluidized bed gasifiers. In addition, few studies have explored the effect of these conditions on few contaminants.[3, 8-11] However, of these studies, only few investigated the effect of gasification conditions on primary gases and major contaminants over a wide range of temperature and equivalence ratio. Consequently, there is a limited understanding of the effect of gasification conditions, like temperature and ER, on major contaminants over a wide range of conditions in biomass gasification.

The current study was undertaken to address this issue by investigating the role of gasification parameters (temperature and equivalence ratio) on the fate of not only primary gases and product distribution but also major contaminants over a wide range of temperature and ER. Specifically, the objective of this study is to assess the effect of gasification temperature (790, 934 and 1078^{o}C) and equivalence ratio (0.15, 0.25 and 0.35) on the concentrations of primary gases (CO, CO_2, CH_4, H_2), product distribution (gas, condensable liquid and char) and contaminants (tar, NH_3, HCN, H_2S and HCl) in pine syngas produced from an air-blown bench-scale atmospheric fluidized bed gasifier. For statistical analysis, a one-way analysis of variance (ANOVA) was carried out to ascertain whether or not concentrations at various temperature and equivalence ratios were significantly different.

3.2 Materials and Methods

3.2.1 Material Characterization

Pine wood was secured from a local chipping plant in Opelika, AL, air dried, ground and sieved through a 850μm screen opening prior to any characterization. Ultimate and proximate analyses were performed for raw pine wood. Ultimate analysis was carried out by a CHNS/O elemental analyzer (Perkin Elmer, Model 2400, Waltham, MA) while the higher heating value (HHV) was determined with a bomb calorimeter (IKA Bomb Calorimeter, Model C-200, Wilmington, NC).

3.2.1.1 Gasification Experimental Setup

All the gasification experiments were conducted on a bench-scale fluidized bed gasification reactor depicted in Figure 3.2 with O_2 and N_2 as oxidizing and fluidization gases, respectively.

The gasifier consists of a biomass hopper equipped with a twin screw auger, an injection screw, a bubbling fluidized bed reactor, a high temperature filter maintained at 350°C, two condensers in series cooled by a mixture of ethylene glycol and water maintained near -5°C by a circulating chiller, an electrostatic precipitator with 20 kV supply to the rod, an activated charcoal filter and finally a gas analysis rig and impinger train. The fluidized bed reactor consisted of 50 mm (2 inches) and 100 mm (4 inches) diameter and 0.58 m (22.75 inches) and 0.20 m (8 inches) length for bed and freeboard, respectively. The total height of reactor is 0.78 m.

The equivalence ratio is defined as ratio of the actual oxygen to biomass (dry and ash free basis) mass flow rate by that required stoichiometrically for complete combustion as outlined in eq. 1 below where subscripts a and s stand for actual and stoichiometric, respectively.

$$ER = \frac{[\dot{m}_{O_2}/\dot{m}_{biomass,dry}]_a}{[\dot{m}_{O_2}/\dot{m}_{biomass,dry}]_s} \quad (3.1)$$

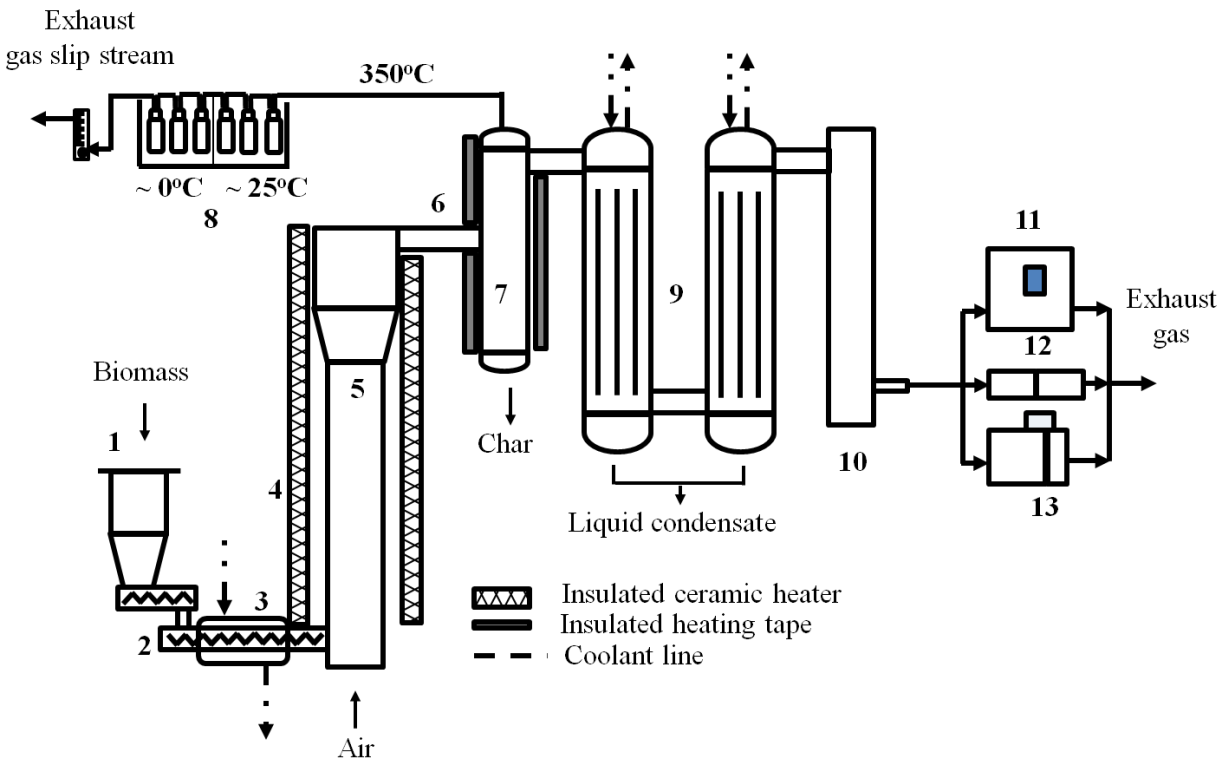

Figure 3.2. Schematic of bench-scale fluidized bed gasification set-up. **1.** Biomass hoper, **2**. Injection screw, **3.** Heat exchanger, **4.** Gasifier heaters, **5.** Fluidized bed gasifier, **6.** Filter heaters, **7.** High temperature filter, **8.** Impinger train for tar sampling, **9.** Condensers, **10.** Electrostatic precipitator, **11.** Gas analyzer for CO, CO_2, CH_4 and H_2, **12.** FTIR for NH_3, HCN and HCl and **13.** FPD GC for H_2S.

3.2.1.1.1 Product sampling and analysis

Three product streams are analyzed during the experiments. Char is collected from both the gasifier and the high temperature filter (Figure 3.2, label#5 and #7). The total amount of char after each experiment is determined by weighing the bed material in the gasifier and the char in the filter minus the sand used for fluidization. The syngas exiting the high temperature filter is

cooled as it passes through the condensers (Figure 3.2, label#9) and a liquid condensate is collected at the bottom. Finally, the gaseous product is sent to an analysis rig before it is vented. The yield of char and liquid condensate is determined gravimetrically and that of the gaseous product obtained by difference.

The gaseous product is analyzed both for primary components as well as gas phase contaminants (NH_3, HCN, H_2S, HCl and HF). The concentrations of primary gases (CO, CO_2, CH_4 and H_2) along with oxygen were measured real-time using a gas analyzer (NOVA, Niagara Falls, NY). In addition, an FTIR gas analyzer fitted with a 4m gas cell and a liquid cooled MCT detector was used to measure in real time gas phase NH_3, HCN, HCl, HF, C_2H_2, C_2H_4 and H_2O (IMAAC, Austin, TX). Furthermore, a sample of syngas was collected in a tedlar bag and analyzed with a GC equipped with a flame photometric detector (Agilent, Santa Clara, CA) using a CP-Sil-8 CB column.

3.2.1.1.1 Tar sampling and analysis

Tar sampling and analysis was conducted on selected runs. A tar sampling rig consisting of six impingers was used.[12] The first five impingers were each filled with approximately 50 mL of isopropanol while the last one was kept empty to capture entrained liquid. The first three impingers were kept at room temperature while the last three were maintained approximately at 0^oC. The tar concentration, in mg/Nm^3, was determined gravimetrically. A sample mixture of all six impingers was created and analyzed on an Agilent GC-MS (Agilent, Santa Clara, CA) equipped with a mass spectrometer and a DB-1701 column (30m, 0.25mm, 0.25um, Agilent,

Santa Clara, CA). The GC inlet and MS detector temperature were both maintained at 250^{o}C and the oven ramped at 8^{o}C/min to 250^{o}C.

3.2.1.2 Experimental Design and Statistical Analysis

The effects of temperature (790, 934 and 1078^{o}C) at equivalence ratio of 0.25 and equivalence ratio (0.15, 0.25 and 0.35) at 934°C were analyzed using a one-way ANOVA at an alpha of 5%. The levels of temperature (790, 934 and 1078^{o}C) and equivalence ratio (0.15, 0.25 and 0.35) were selected far apart deliberately to ensure that variation in responses (primary gases and contaminants) would be present, if the response is indeed affected by temperature and equivalence ratio. In the case of temperature, the original experimental design aimed for a lower temperature range. However, due to unforeseen technical challenges, the present temperature range was used instead. All experiment conditions were repeated at least three times with a maximum of five replicates at the center point condition (934°C and 0.25 ER). The data was treated by an unbalanced ANOVA and all statistical analyses were performed using Microsoft Excel Data Analysis Tool and the statistical software JMP.[13] Furthermore, in order to eliminate confounding factors that might affect statistical analysis and interpretation, all statistical analyses were performed on product yield (g/kg dry biomass and mg/kg dry biomass for HCl) in order to account for the variation in moisture content as well as feeding rate between runs. Tukey-HSD multiple comparison test was performed on statistically significant factor.

3.3 Results and Discussion

3.3.1 Biomass Characterization

Pine wood sawdust was fully characterized prior to its use in the gasification experiments. Its physical and chemical properties are detailed in Table 3.1 and are consistent with other sawdust pine properties.[14]

Table 3.1. Pine physical and chemical properties

Moisture Content, (wt % wet.basis).	7.94 ± 0.16
Higher Heating Value, MJ/kg	20.18 ± 0.21
Proximate Analysis (wt %, dry)	
Ash content	0.34 ± 0.01
Fixed carbon	16.52 ± 0.03
Volatile matter	83.14 ± 0.03
Ultimate Analysis (wt %, dry)	
C	47.14 ± 0.18
H	6.52 ± 0.04
N	0.44± 0.10
S	0.10
O†	45.46 ± 0.24

† Oxygen value was obtained by difference

3.3.2 Syngas Composition Profiles

Figures 3.3 and 3.4 illustrate mean gas profile observed during the run on a fluidized bed gasifier for three temperatures (790, 934 and 1078°C) and three equivalence ratios (0.15, 0.25 and 0.35). The time to steady state varied significantly and as temperature was increased, it decreased. It is believed that this variation in time to steady state underscores heat transfer variation at different

temperature. At higher temperature, due to the higher heating rate of the entering biomass, biomass decomposition is achieved much faster leading to faster steady state.

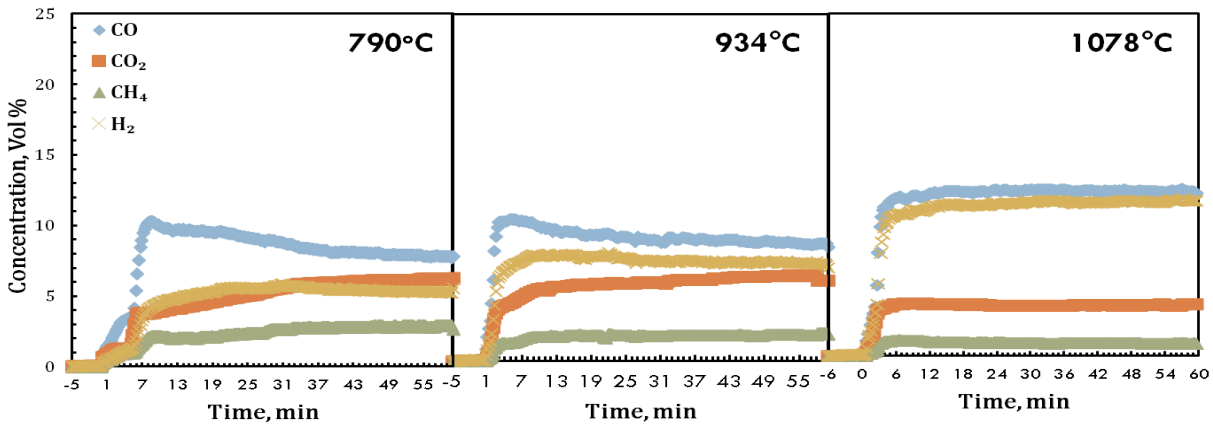

Figure 3.3. Primary gas composition profile at 790, 934 and 1078°C for ER = 0.25

A similar trend is observed in Figure 3.4 where as equivalence ratio is increased, steady state is achieved faster. In this case, it is likely that as equivalence ratio is increased, bulk phase mass transfer is improved due to greater oxygen availability for reaction resulting in faster achievement of steady state.

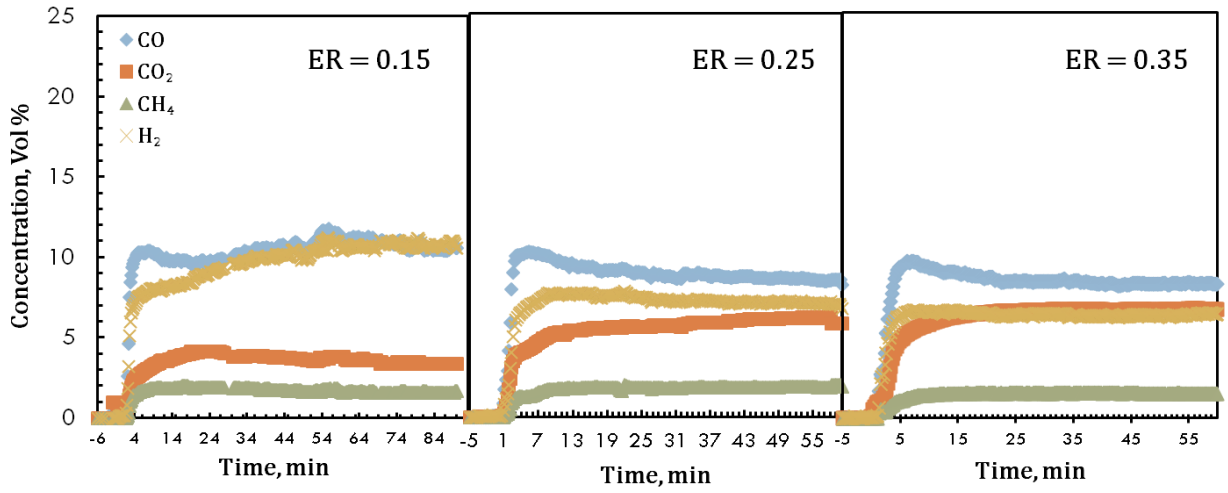

Figure 3.4. Primary gas composition profile at ER of 0.15, 0.25 and 0.35 at 934^{o}C

It should be noted that run times were adjusted to ensure that steady state is achieved for each experiment and only steady state values were used for calculations and comparisons.

3.3.3 Effect of Temperature and ER on Product Distribution

Temperature and ER play important roles in the final gasification product distribution as evidenced in Figure 3.5. An increase in temperature results in greater biomass conversion to gaseous product while both liquid condensate and char products decrease. As temperature is increased, it is expected that carbon rich char conversion will be enhanced by the endothermic char gasification reactions (R1-R4). The reactions can also explain the decrease in liquid condensate (mostly H_2O) formation as temperature is increased. This hypothesis is further corroborated by an increase in CO and H_2 and a decrease in CO_2 as temperature is increased as discussed in the next section.

Water-gas $C + H_2O \leftrightarrow CO + H_2$ [3.1]

Boudouard $C + CO_2 \leftrightarrow 2CO$ [3.2]

The yields of char were 6.07, 3.65, 4.09 wt % dry biomass for 790, 934 and 1078°C, respectively and similar to others reported values.[15] This variation, though noticeable, was not statistically significant ($F(2, 12) = 3.57$, $P = 0.07$). In contrast, the yields of liquid condensate were significantly affected by temperature ($P = 0.001$) and were 20.87, 16.93, 11.75 wt % dry biomass for 790, 934 and 1078°C. Syngas production was also significantly affected by temperature syngas ($P < 0.003$) as its yields increased from 73.06, 79.42 and 84.16 wt % dry biomass as temperature was increased from 790, 934 and 1078°C, respectively.

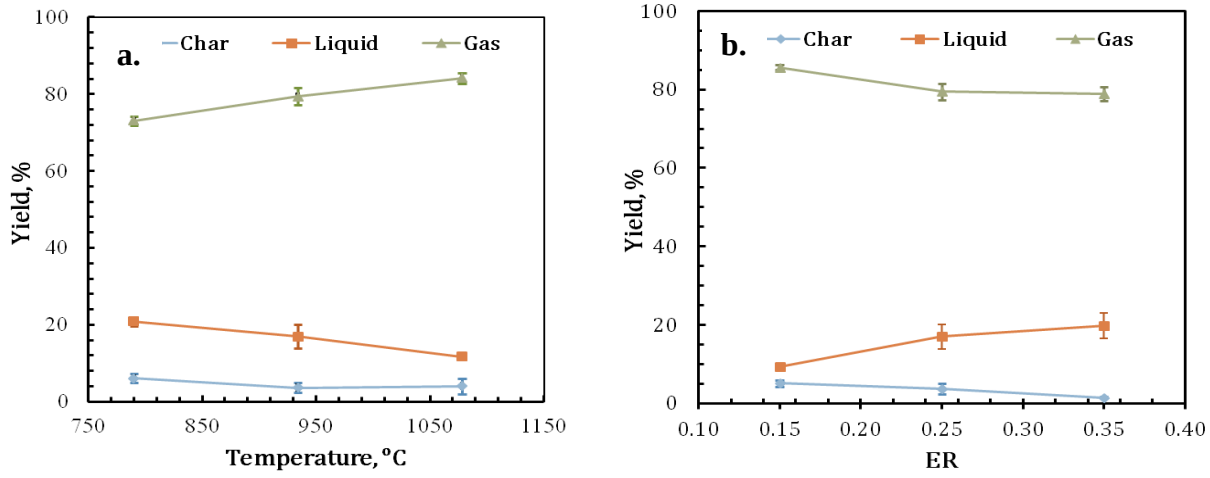

Figure 3.5. Effect of (**a**) temperature (790, 934 and 1078°C at ER = 0.25) and (**b**) ER (0.15, 0.25 and 0.35 at 934°C) on gasification product distribution. Note: Error bars represent standard deviations.

The occurrence of oxidation reactions largely account for the variation observed in product yields over equivalence ratio. As equivalence ratio is increased, both char and dry syngas yields decrease while liquid condensate yield increased. The decrease in char yield is likely due to char oxidation reactions (R3 and R4) due to increasing oxygen presence as ER is increased.

$$C + O_2 \rightarrow CO_2 \quad [3.3]$$

$$C + 0.5O_2 \rightarrow CO \quad [3.4]$$

Furthermore, the increase in liquid condensate can also be explained by H_2 oxidation to H_2O by the reaction depicted below (R5).

$$H_2 + 0.5O_2 \rightarrow H_2O \quad [3.5]$$

These hypotheses are corroborated by an observed increase in CO_2 and decrease in H_2 concentrations as discussed in next section. Analysis of variance shows that the decrease in char yield is statistically significant ($P < 0.001$) indicating that ER does indeed result in a change in char yield that is large enough to have solely occurred due to experimental variations. However that of dry gas was not ($F(2, 14) = 3.82$, $P = 0.052$).The yields of these two products were 5.03, 3.65 and 1.26 wt % dry biomass and 85.67, 79.42 and 80.57 wt % dry biomass for char and dry gas, respectively at 0.15, 0.25 and 0.35 ER. As indicated earlier in this section, the decreasing

trends for char and dry gas are due to greater char and H_2 oxidation to gases and water, respectively. Therefore, the liquid condensate product increased by 9.30, 16.93 and 18.17 wt % as ER was increased. This increase was statistically significant (P = 0.003).

3.3.4 Effect of Gasification Temperature and ER on Primary Gas Constituents

The effects of temperature and equivalence ratio were evaluated for all light gases and summarized in Table 3.2 and 3.3.

Table 3.2. Effect of temperature on primary gas composition at ER = 0.25

	Temperature, °C		
Yield, g/kg dry biomass Mean (SD)	**790**	**934**	**1078**
CO	379.63 (32.48) ^{A1}	434.72 (19.92) ^{A1}	646.98 (119.24) ^{A2}
CO_2	463.95 (25.15) ^{B1}	431.58 (39.03) ^{B1}	311.83 (28.12) ^{B2}
CH_4	85.80 (16.68) ^{C1}	53.69 (3.12) ^{C2}	29.23 (3.97) ^{C3}
H_2	17.45 (3.40) ^{D1}	25.73 (1.50) ^{D2}	42.70 (1.07) ^{D3}
C_2H_2	6.09 (1.36) $^{E1, E2}$	7.03 (0.40) ^{E1}	4.35 (*0.45)* ^{E2}
C_2H_4	51.97(12.39)	37.32(15.74)	13.70(4.74)

Means without superscripts are not statistically different (P-value > 0.05) based on a one-way ANOVA test. Means not connected by the same superscript are significantly different at the 0.05 level based on Tukey HSD Post Hoc test. [†]Yields are reported as mg/kg dry biomass and SD stands for "standard deviation"

Table 3.3. Effect of equivalence ratio on primary gas composition at 934°C

	ER		
Yield, g/kg dry biomass Mean (SD)	**0.15**	**0.25**	**0.35**
CO	519.02 (44.38) ^{1A}	434.72 (19.92) ^{1B}	460.65 (60.95) ^{1C}
CO_2	266.76 (29.77) ^{2A}	431.58 (39.03) ^{2B}	591.89 (44.80) ^{2C}
CH_4	46.76 (1.98)	53.69 (3.12)	49.31 (8.46)
H_2	35.60 (3.46) ^{3A}	25.73 (1.50) ^{3B}	24.03 (3.70) ^{3B}
C_2H_2	7.79 (0.13)	7.03 (0.40)	6.68 (0.71)
C_2H_4	74.28 (20.74)	37.32 (15.74)	43.31 (16.30)

Means without superscripts are not statistically different (P-value > 0.05) based on a one-way ANOVA test. Means not connected by the same superscript are significantly different at the 0.05 level based on Tukey HSD Post Hoc test. [†]Yields are reported as mg/kg dry biomass and SD stands for "standard deviation".

Primary gases over temperature

Temperature has a noticeable effect on the concentration of light gases as evidenced in Figure 3.6. The effect of temperature was statistically significant for all light gases except for C_2H_4 (*F(2, 7) = 5.32, P = 0.06*). It is known that the Boudouard and water-gas reactions [R1 and R2], both contributing to CO and H_2 formation, are favored at higher temperature.[16] The effect of temperature on these reactions likely explains our findings where, as temperature is increased, CO and H_2 increased while CO_2 decreased. Over the same temperature range, CH_4 yield and concentration decreased probably due to thermal cracking at higher temperature as char methanation reaction rate [R6] is relatively slow and other methanation reactions [R6, R7, R8] are not favored at higher temperature.[16]

$$C + 2H_2 \leftrightarrow CH_4 \quad [3.6]$$

$$2C + 2H_2O \leftrightarrow CO_2 + CH_4 \quad [3.7]$$

$$CO + 3H_2 \leftrightarrow H_2O + CH_4 \quad [3.8]$$

The yield of primary gases is comparable to other published results for air-blown gasifier[7] and the primary gas product trends are similar to trends reported by Aljbour and Kawamoto.[6]

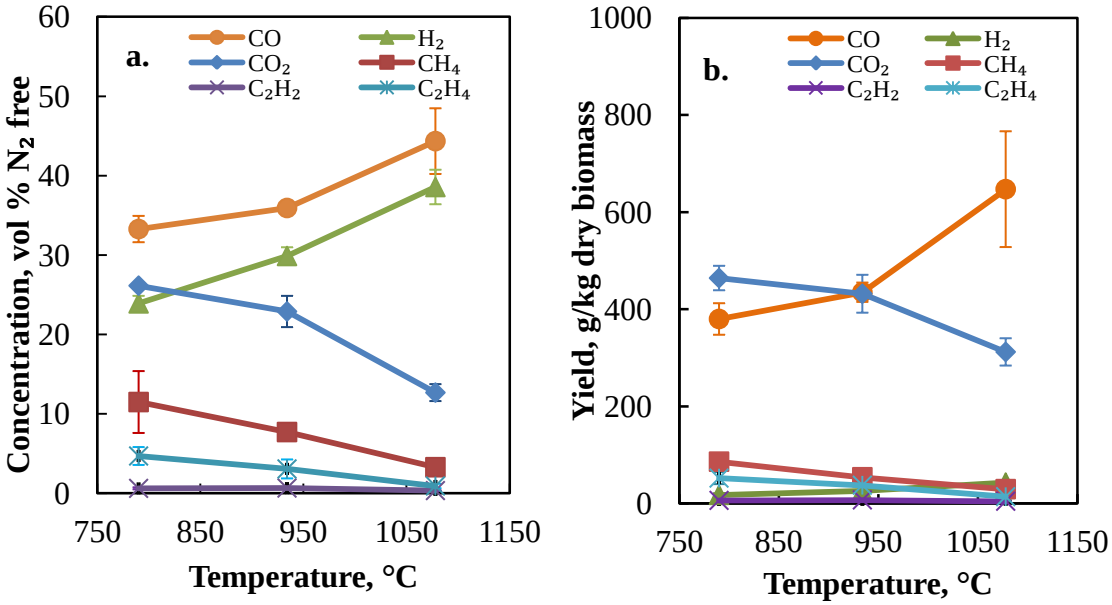

Figure 3.6. Effect of gasification temperature (790, 934 and 1078˚C at ER = 0.25) on (**a**) concentration and (**b**) yield of primary gases in pine gasification. *Note*: N_2 concentration was 76.34, 75.61 and 71.45 vol % for 790, 934 and 1078˚C. Error bars represent standard deviations.

Primary gases over equivalence ratio

Besides temperature, equivalence ratio also plays a crucial role in the composition of primary gases. Equivalence ratio had a significant effect on the concentration of CO ($P = 0.03$), CO_2 ($P < 0.01$) and H_2 ($P < 0.01$) as shown in Figure 3.7. However, CH_4, C_2H_2 and C_2H_4 were not significantly impacted by increasing equivalence ratio. As equivalence ratio is increased, the concentration of CO and H_2 decreased while CO_2 increased due to increasing partial oxidation as well as char oxidation. The decrease in H_2 and CO can be explained by further oxidation to H_2O and CO_2 by oxidation reactions of H_2 [R5] and CO shown below as [R9].

$$CO + 0.5O_2 \rightarrow CO_2 \qquad [3.9]$$

The increase in both CO_2 and product liquid yield over the same range of equivalence ratios corroborates this hypothesis. Other investigators have reported similar trends as well.[6] CH_4 remained roughly unchanged and consequently, ER did not affect its yield (*F(2,14) = 2.14, P = 0.16*). Other investigators have also observed that ER has minimal impact on CH_4 concentration.[5] It is believed that free oxygen would be primarily consumed by other char, CO and H_2 oxidation reactions thus resulting in statistically insignificant effects on CH_4. Furthermore, equivalence ratio did not have any significant effect on the concentration of C_2H_2 (*F(2,9) = 2.85, P = 0.12*) and C_2H_4 (*F(2, 6) = 2.94, P = 0.16)* within the limits of this study. Comparison of the primary gas concentrations in this study and data available in the literature is presented below in Table 3.4.

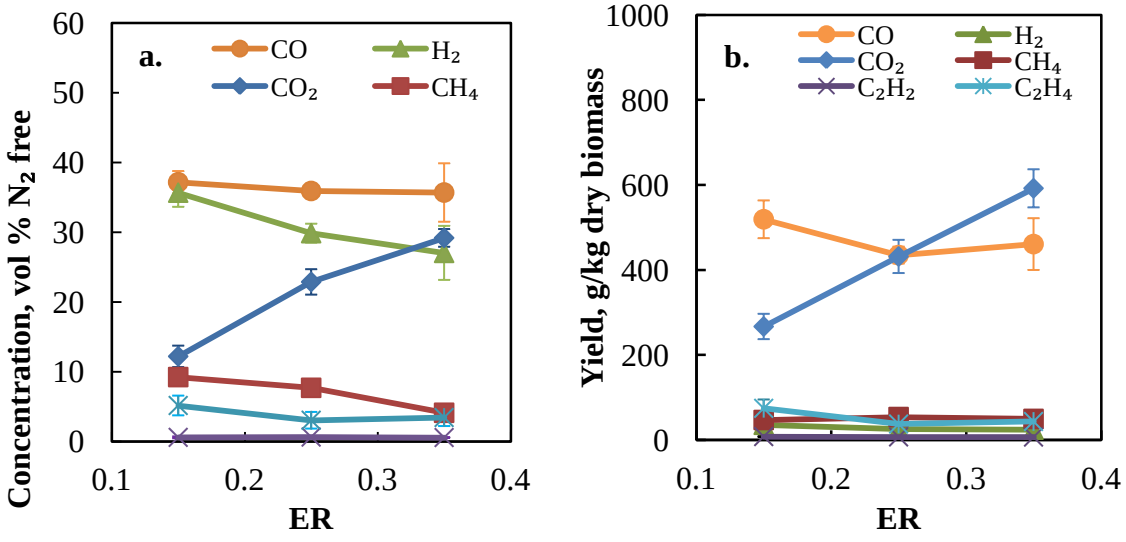

Figure 3.7. Effect of ER (0.15, 0.25 and 0.35 at 934°C) on (**a**) concentration and (**b**) yield of primary gases in pine gasification. *Note:* N_2 content was 71.92, 75.64, 77.54 vol % at 0.15, 0.25 and 0.35 ER. Error bars represent standard deviations.

Table 3.4. Comparison of primary gas concentrations with study under similar conditions

	Others			***Present study***		
ER	0.35	0.36	0.27	0.35	0.25	0.35
Temperature (°C)	812[7]	790[9]	805[15]	790	790	934
Gas composition, vol % N_2 free						
CO	35.3	31.2	35.41	34.7	34.67	35.8
H_2	19.5	22.8	25.35	23.9	24.90	26.6
CO_2	33.8	35.97	29.98	31.5	27.23	30.4
CH_4	11.4	6.47	10.46	10.3	11.95	7.2

3.3.5 Effect of Temperature and ER on Syngas Contaminants

Contaminants are a major concern for downstream applications in which syngas might be used as a feed. Therefore, it is important to determine the concentration of these contaminants as well as the effect of temperature and ER on these compounds. Table 3.5 and Table 3.6 summarize the concentrations of contaminants at different temperatures and equivalence ratio.

Table 3.5. Effect of temperature on contaminants at ER = 0.25

	Temperature, °C		
Yield, g/kg dry biomass Mean (SD)	**790**	**934**	**1078**
H_2S	0.13 (0.005)^{A1}	0.16 (0.011)^{A1,A2}	0.17 (0.015)^{A2}
NH_3	1.63 (0.23)^{B1}	1.47 (0.19)^{B1,B2}	1.00 (0.11)^{B2}
HCN	0.24 (0.02)^{C1,C2}	0.26 (0.04)^{C2}	0.14 (0.01)^{C3}
HCl†	13.63 (5.00)^{D1}	8.89 (2.22)^{D1}	n.d

Means without superscripts are not statistically different (P-value > 0.05) based on a one-way ANOVA test. Means not connected by the same superscript are significantly different at the 0.05 level based on Tukey HSD Post Hoc test. †Yields are reported as mg/kg dry biomass. n.d stands for not detected (i.e. below the instrument accurate detection limit) and SD for "standard deviation".

Table 3.6. Effect of equivalence ratio on contaminants at 934°C

	ER		
Yield, g/kg dry biomass *Mean (SD)*	**0.15**	**0.25**	**0.35**
H_2S	0.18 (0.03)	0.16 (0.01)	0.15 (0.04)
NH_3	1.76 (0.13)	1.47 (0.19)	1.54 (0.14)
HCN	0.24 (0.02)	0.26 (0.04)	0.26 (0.02)
HCl†	11.51 (0.44) [1A]	8.89 (2.23) [1A]	0.28 (0.55) [1B]

Means without superscripts are not statistically different (P-value > 0.05) based on a one-way ANOVA test. Means not connected by the same superscript are significantly different at the 0.05 level based on Tukey HSD Post Hoc test. †Yields are reported as mg/kg dry biomass. SD stands for "standard deviation".

3.3.5.1 Tar

The gravimetric tar analysis at different temperatures and equivalence ratios is shown in Figure 3.8. Tar yield decreases with increase in temperature with yields of 9.7, 9.0 and 7.4 g/Nm^3 for 790, 934 and 1078°C, respectively and 13.6, 9.0 and 2.5 g/Nm^3 for ER of 0.15, 0.25 and 0.35. Both follow expected trends and values for fluidized bed gasifier. Due to significant decrease in tar yield as ER is increased, it can be concluded that oxidation is more effective than thermal cracking for tar mitigation.

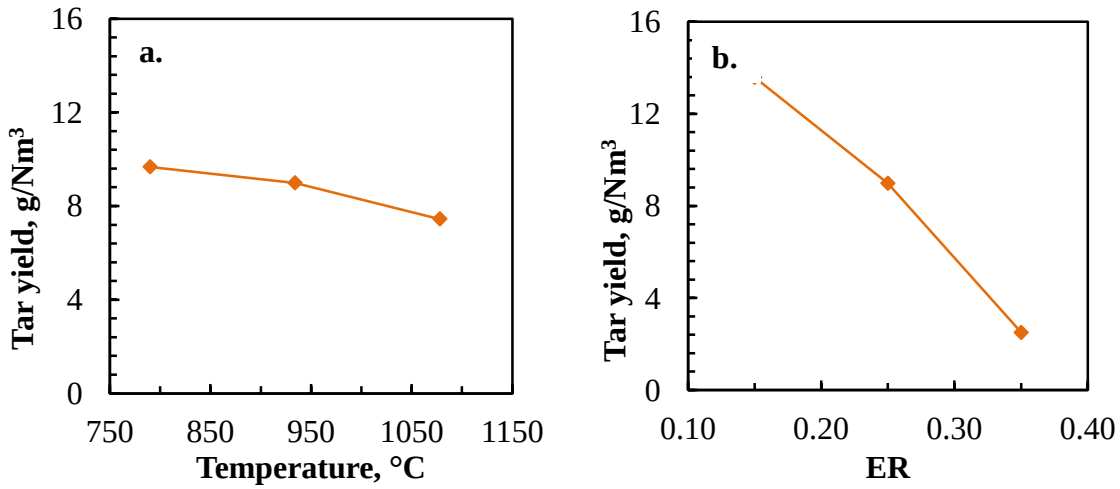

Figure 3.8. Effect of (**a**) temperature (790, 934 and 1078°C at ER = 0.25) and (**b**) ER (0.15, 0.25 and 0.35 at 934°C) on gravimetric tar yield

Gasification tars are composed of several groups of compounds. Tar compounds such as toluene, anthracene, indene, nathphtalene, pyrene, fluoranthene and biphenylene were detected in the impinger solvents in addition to benzene. While benzene is technically not a tar compound, it was included here as its concentrations are significantly higher than all other compounds detected in solvent. Table 3.7 and Table 3.8 show the effect of temperature and ER on the yield of GC detected tar compounds. As temperature increased from 790 to 1078°C, the concentration of toluene, biphenylene, anthrecene, fluoranthene and pyrene were reduced to below detection limit. Benzene was detected at high concentrations at all temperature whereas naphthalene was only detected at 790 and 934°C. Benzene and naphthalene increased as temperature increased. Such trend with increasing temperature has been reported by Brage *et al*. (1996). Furthermore,

benzene and naphthalene were dominant constituents in agreement with other studies [11, 17, 18] with benzene accounting for at least 65 wt % of the GC detected compounds.

Table 3.7. Tar yield (mg kg^{-1} dry biomass) of GC detectable compounds at three different temperatures (ER = 0.25)

Temperature, °C	**790**		**934**		**1078**	
Compounds	Mean	SD	Mean	SD	Mean	SD
Benzene	1175.93	4.98	2239.52	1.71	2530.47	0.26
Toluene	337.01	0.20	n.d	n.d	n.d	n.d
Naphthalene	0.93	0.02	5.06	0.26	n.d	n.d
Biphenylene	1.52	N/A	n.d	n.d	n.d	n.d
Anthracene	5.78	0.19	n.d	n.d	n.d	n.d
Fluoranthene	2.92	0.21	n.d	n.d	n.d	n.d
Pyrene	294.11	0.05	n.d	n.d	n.d	n.d

n.d stands for "not detected", N/A for "not available" and SD for "standard deviation"

At the same temperature (934°C) and lowest equivalence ratio (0.15 ER), the overall tar concentration was highest as would be expected since lower equivalence ratio is closer to pyrolysis conditions. However, as equivalence ratio increased from 0.15 to 0.35, the concentrations of biphenylene, diphenylethyne, fluoranthene and pyrene were reduced below detection limits, suggesting that other compounds have been oxidized and converted to primary gases.

Table 3.8. Tar yield (mg kg^{-1} dry biomass) of GC detectable compounds at three different equivalence ratio (934˚C)

ER	**0.15**		**0.25**		**0.35**	
Compounds	Mean	SD	Mean	SD	Mean	SD
Benzene	2430	0.62	2240	1.71	2300	1.90
Naphthalene	11.0	0.02	5.06	0.26	9.83	0.73

Biphenylene	2.84	N/A	n.d	n.d	n.d	n.d
Diphenylethyne	2.70	0.09	n.d	n.d	n.d	n.d
Fluoranthene	2.72	N/A	n.d	n.d	n.d	n.d
Pyrene	659	N/A	n.d	n.d	n.d	n.d

n.d stands for "not detected", N/A for "not available" and SD for "standard deviation"

It should be noted that gravimetric and GC analyses provide similar indication of tar yield albeit with different magnitude since GC analysis can only detect at best only a fraction of syngas tar compounds because of the wide variety of compounds. Figure 3.9 shows the variation of tar yield measured gravimetrically and by GC analysis over temperature and equivalence ratio. Both gravimetric and GC tar yields increase as temperature is increased and decrease as equivalence ratio is increased. The increase in tar yield can be explained by the greater increase in syngas production per unit mass of biomass gasified. As temperature is increased from 790 to 1078°C, syngas production is noticeably increased from 0.81 to 1.20 Nm^3/kg dry biomass. Simultaneously, tar concentration decreased as temperature was increased, although not drastically with only 2.2 g/Nm^3 decrease for a 288°C increase in temperature. The lower effect of temperature on concentration of tar is most likely due to predominance of tertiary formation reactions. While both primary and secondary tars are decomposed between 790 and 1078°C, tertiary tar formation increases over that same range resulting in an overall modest decrease in tar concentration.[19] This hypothesis seems to be well explained by the results where as temperature increased, only tertiary tar compounds (benzene and naphthalene) were detected in the GC analysis. Therefore, even though the tar concentration is decreasing over the studied

temperature range as shown in Figure 3.8, the syngas yield increases faster resulting in a net tar yield increase as shown in Figure 3.9. In contrast, as ER is increased, syngas yield is only modestly affected while tar concentrations were significantly decreased as seen in Figure 3.8 and hence the noticeable decrease in tar yields in Figure 3.9. It can be concluded from these results that oxidation is more effective than thermal cracking in tar remediation. Furthermore, it appears that benzene is by far the most dominant tar compounds.

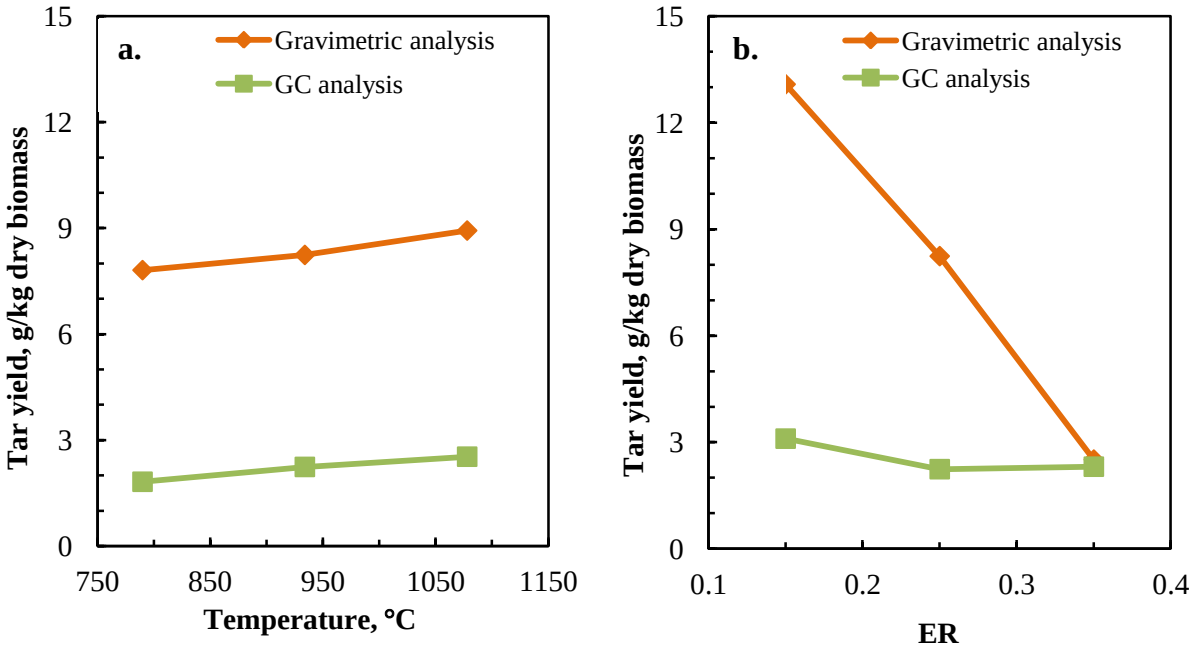

Figure 3.9. Effect of (**a**) temperature (790, 934 and 1078°C at ER = 0.25) and (**b**) ER (0.15, 0.25 and 0.35 at 934°C) on tar yield determined gravimetrically and by GC analysis. *Note:* GC tar yield includes all detected compounds in tables 7 and 8.

3.3.5.2 Nitrogen Contaminants: NH_3 and HCN

Under the limited oxygen environment of gasification, fuel bound nitrogen evolves primarily as NH_3 and N_2 with a lesser fraction converted to HCN and various other N_xO_y products.[20] Table

3.9 shows the fraction of nitrogen from pine that is converted to NH_3 and HCN at various temperatures and ERs.

Table 3.9. Effects of temperature and ER on fuel-bound nitrogen conversion to NH_3 and HCN

Mean (SD)	**Temperature, °C (at ER = 0.25)**			**ER (at 934°C)**		
	790	**934**	**1078**	**0.15**	**0.25**	**0.35**
$\frac{N(NH_3)}{N_{fuel}}$, wt %	27.52 (3.99)	25.22 (5.10)	18.72 (1.97)	31.11 (5.00)	33.92 (6.27)	30.57 (3.46)
$\frac{N(HCN)}{N_{fuel}}$, wt %	1.75 (0.21)	1.51 (0.30)	1.67 (0.17)	2.71 (0.24)	2.13 (1.29)	3.93 (1.04)

SD stands for "standard deviation".

NH_3 and HCN over temperature

As shown in figures 3.10 and 3.11, the yields and concentrations of NH_3 are 1.63, 1.47 and 1.00 g/kg dry biomass and 563.81, 434.42 and 309.66 ppmv at 790, 934 and 1078°C, respectively. This decrease over temperature is statistically significant ($F(2,7) = 9.57, P = 0.02$). Over the same range, HCN yields and concentrations were 0.24, 0.26 and 0.14 g/kg dry biomass and 51.92, 55.37 and 27.66 ppmv. Similarly, statistical analysis revealed HCN was significantly affected by temperature ($F(2, 7) = 2.32, P = 0.003$).

Overall, the evolution of fuel-bound nitrogen to NH_3 was reduced from 27.52% at 790°C to 18.72% at 1078°C for NH_3. The contribution of fuel nitrogen to HCN was significantly lower and was not significantly changed over the same temperature range, as shown in Table 3.9.

As temperature is increased, a decrease in concentration of NH_3 and HCN is expected as NH_3 and HCN undergo decomposition. Overall, our results are consistent with other reports where

similar trends were observed as temperature increased.[10, 21] The decrease in NH_3 concentration is mostly likely due to thermal decomposition to N_2 and H_2 according to reaction [R8] depicted below. As temperature is increased, the fraction of fuel nitrogen converted to NH_3 decreased but remained roughly unchanged for HCN.

$$2NH_3 \leftrightarrow N_2 + 3H_2 \qquad [3.10]$$

NH_3 and HCN over ER

The effect of equivalence ratio was not statistically significant for NH_3 and HCN as evidenced in figures 3.10 and 3.11. The limited impact of equivalence ratio on NH_3 and HCN was consistent with previous report by Zhou *et al*. (2000) although a decreasing trend was observed for HCN. As illustrated in Table 3.9, the fraction of fuel nitrogen converted to NH_3 and HCN does not vary significantly with increasing ER in this study and others.[20]

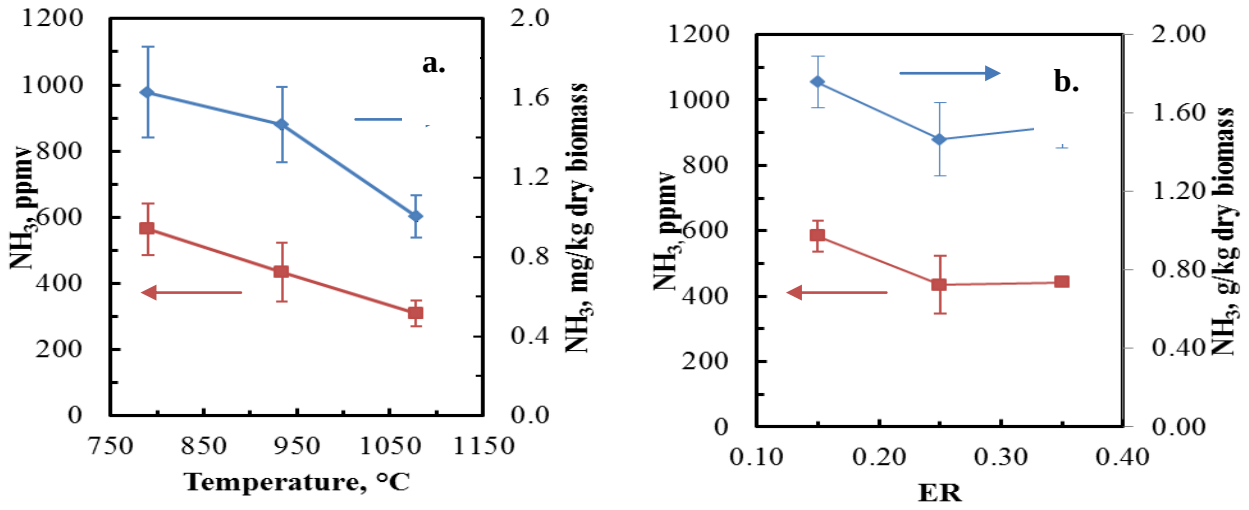

Figure 3.10. Effect of (**a**) temperature (790, 934 and 1078°C at ER = 0.25) and (**b**) ER (0.15, 0.25 and 0.35 at 934°C) on the concentration and yield of NH_3. Note: Error bars represent standard deviations.

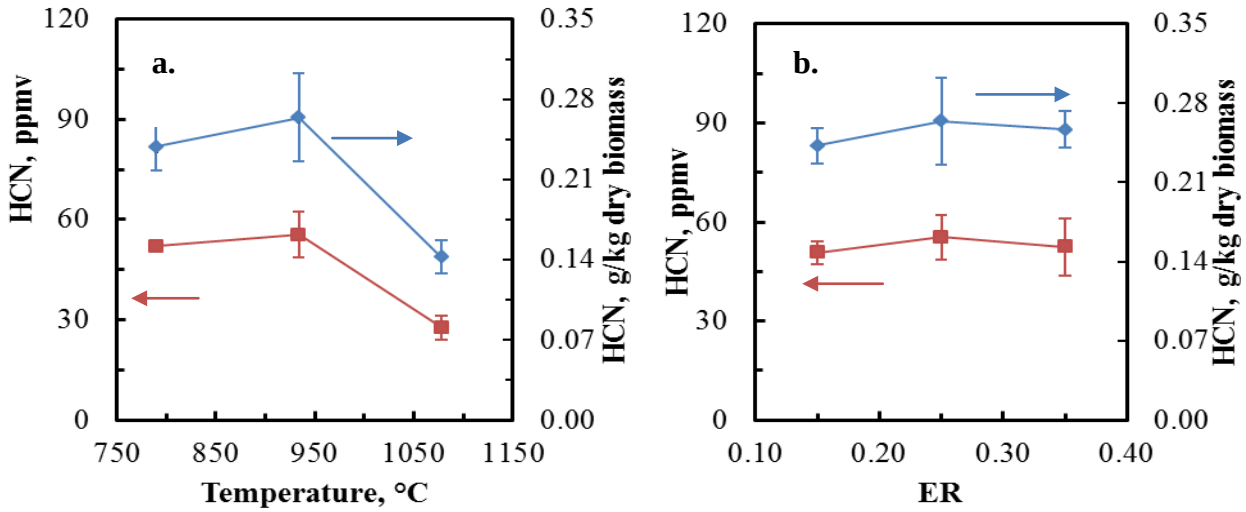

Figure 3.11. Effect of (**a**) temperature (790, 934 and 1078°C at ER = 0.25) and (**b**) ER (0.15, 0.25 and 0.35 at 934°C) on the concentration and yield of HCN. Note: Error bars represent standard deviations.

Equivalence ratio had a smaller effect on NH_3 yield when compared to temperature. Similar conclusions were drawn from the results of other investigators as well.[21,10] In the presence of increasing amount of oxygen, as there is at higher equivalence ratio, the expected NH_3 and HCN conversion route will be via oxidation to NO_x, N_2 and H_2O. However, the smaller effect observed on NH_3 or HCN as ER is increased suggest that additional oxygen participated in other oxidation reactions (ex. char oxidation reactions) rather than NH_3 and HCN oxidation.

Overall, the trends and concentrations of NH_3 and HCN are comparable to reports by other investigators as shown in Table 3.10, after factoring in the difference in fuel bound nitrogen.[10, 21, 22]

Table 3.10. Comparison of NH_3 syngas concentration for feedstock with different nitrogen content during air gasification[22]

Feedstock	**Willow**	**Wood[a]**	**Wood[b]**	**Wood[b]**	**Present study**
Temperature, °C	827	847	861	805	790
ER	0.37	0.37	0.38	0.43	0.35
N-fuel, wt % daf basis	0.88	0.46	0.26	1.16	0.44
NH_3, vol% N_2 free basis	0.18	0.21	0.13	0.31	0.15

daf stands for "dry ash free". [a] demolition wood and [b]park wood

3.3.5.3 Sulfur Contaminants: H_2S

Fuel bound sulfur is released during gasification primarily as H_2S which has a significant deactivation effect on catalysts even at relatively low concentrations. It is therefore important to know the concentration of sulfur containing contaminants in syngas. Table 3.11 shows the fraction of fuel bound sulfur that is released as H_2S at various conditions.

Table 3.11. Effects of temperature and ER on fuel-bound sulfur conversion to H_2S

Mean (SD)	**Temperature, °C (at ER = 0.25)**			**ER (at 934°C)**		
	790	**934**	**1078**	**0.15**	**0.25**	**0.35**
$\frac{N(H_2S)}{S_{fuel}}$, wt %	12.13 (0.41)	14.21 (1.51)	16.63 (0.17)	16.96 (1.84)	15.14 (1.43)	14.48 (0.48)

The concentrations of H_2S were 0.13 (21.70ppmv), 0.16 (25.02ppmv) and 0.17 (27.18ppmv) g/kg dry biomass for 790, 934 and 1078°C, respectively. The increase of H_2S as temperature is increased is likely due to greater devolatilization of fuel bound sulfur which, in the reducing environment of gasification, will likely lead to H_2S formation. From Table 3.11 and Figure 3.12, while both temperature and ER affect H_2S formation, it is clear that that this impact is minor. This increase over the range of temperatures studied is statistically significant based on a one-way analysis of variance (*F(2, 8) = 8.25, P = 0.026*). Similar increasing trends as temperature is increased were observed for woody biomass previously.[8, 23]

As equivalence ratio increased, H_2S concentrations were 0.18 (31.49 ppmv), 0.16 (25.02 ppmv) and 0.15 (23.54 ppmv) g/kg dry biomass for 0.15, 0.25 and 0.35 ER at 934°C. This decrease in H_2S is most likely due to H_2S oxidation to sulfur oxides. While noticeable, this variation was not statistically significant over the range of equivalence ratio underscoring the minor impact of ER on H_2S concentration. The concentrations of H_2S is within the range of published results [8, 24] with an increasing trend as ER increased for coal and refuse derived fuel as well as cedar wood.[10, 25] This variation of yield of H_2S over the range of equivalence ratio was not statistically significant as well (*F(2, 6) = 1.21, P = 0.36*) suggesting temperature or equivalence ratio cannot be used as in-situ H_2S remediation approaches.

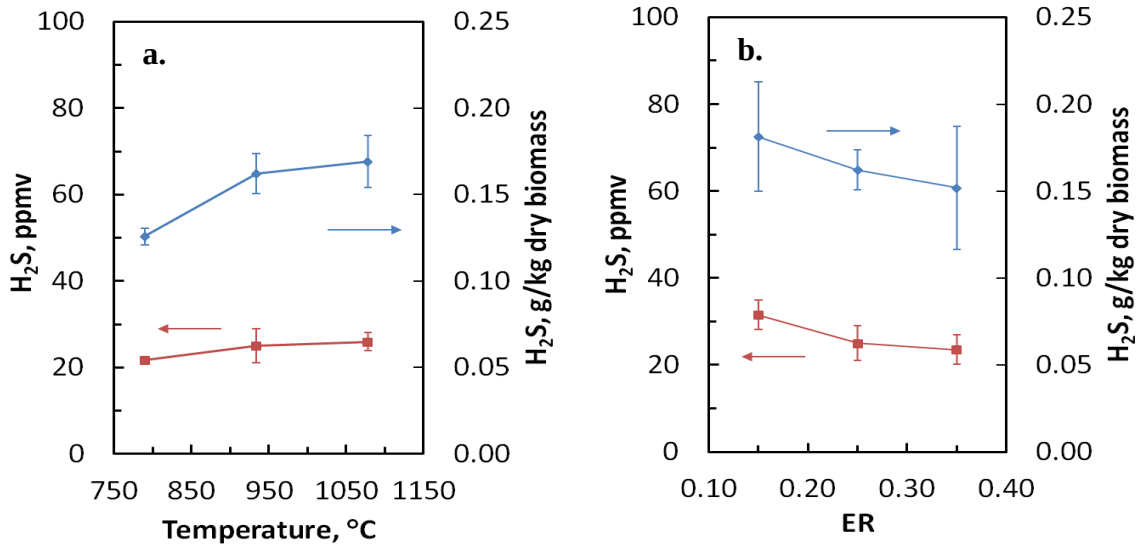

Figure 3.12. Effect of (**a**) temperature (790, 934 and 1078°C at ER= 0.25) and (**b**) ER (0.15, 0.25 and 0.35 at 934°C) on concentration and yield of H_2S. Note: Error bars represent standard deviations.

3.3.5.4 Hydrogen Halides: HCl

Chlorine is a micronutrient necessary in plant and act as catalysts in photosynthesis and enzymatic processes related to plant growth.[26]

The yields and concentrations of HCl were 13.63 and 8.89 mg/kg dry biomass and 2.20 and 1.39 ppmv at 790 and 934°C, respectively and undetectable at higher temperature. Temperature had a significant effect on the concentration of HCl ($F(2,9) = 15.57, P = 0.003$).

Equivalence ratio had a similar decreasing effect on HCl where the yields and concentrations were 11.51, 8.89 and 0.28 mg/kg dry biomass and 1.79, 1.39 and 0.03 ppmv for 0.15, 0.25 and 0.35, respectively. This decrease was statistically significant ($F(2,9) = 49.42, P < 0.001$). HCl

concentration in coal syngas is reported to range between 40-600ppmv. In comparison, the concentrations of HCl and HF are significantly lower in our study. Since it is known that the concentration of HCl in syngas depends on the chloride concentration in the fuel, such a difference should be expected since coal fuels have considerably higher chloride concentrations than woody biomass.[27, 28]

As seen in Figure 3.13, the concentrations of HCl decreases from 790 to 934°C before dipping below detection limit at 1078°C. This decrease is probably due to the conversion of HCl to alkali chloride at temperatures above 790°C.[25, 29] Indeed, a thermodynamic modeling study showed that, in the vicinity of 800°C, chlorine is speciated almost completely as HCl but will appear as NaCl, or other alkali halides vapors as temperature is increased.[30]

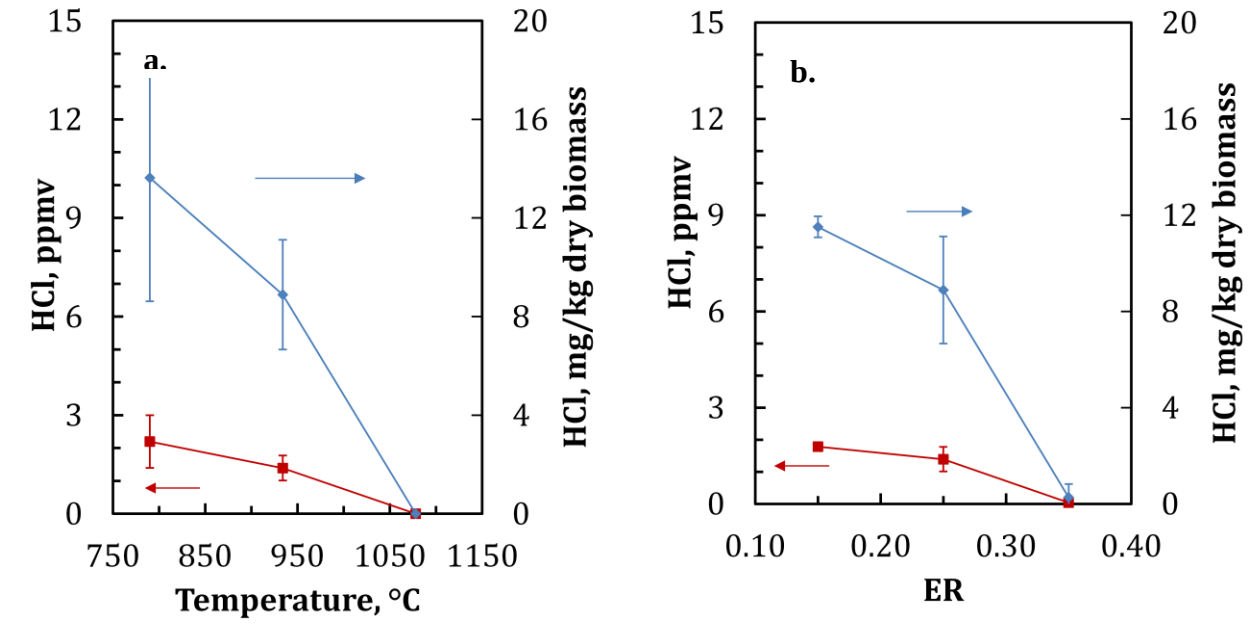

Figure 3.13. Effect of (**a**) temperature (790, 934 and 1078^{o}C at ER = 0.25) and (**b**) ER (0.15, 0.25 and 0.35 at 934˚C) on concentration and yield of HCl. Note: Error bars represent standard deviations.

Similarly, as equivalence ratio is increased, HCl decreases significantly. There is little information available on the effect of equivalence ratio on the concentration of HCl, or other hydrogen halides, in biomass derived syngas. However, studies on coal and refuse derived fuel as well as on cedar wood indicated that HCl formation was not affected as equivalence ratio was varied.[10, 25] It was suggested that the neutralization of alkali species in syngas to alkali hydroxides like NaOH and KOH at higher equivalence ratio might have impeded the formation of alkali halides that caused HCl decrease.[25] In the current study, it is possible that greater volatilization of biomass as equivalence ratio increased led to higher concentration of alkali vapors, which were not neutralized to alkali hydroxide, thus resulting in a decrease in HCl concentration as equivalence ratio increased.

3.4 Conclusions

The present parametric study indicate that temperature and equivalence ratio have a significant effect on primary gases and contaminants. The results presented in this study can serve as a benchmark for understanding how operating conditions affect product distribution, primary gas and contaminant composition during air gasification of pine and similar woody biomass. As such, the results reported in this paper can used as a guideline to predict how changes in operating conditions will impact gasification products of interest.

The following conclusions can be made:

As temperature is increased, it appears that the time required to achieve steady state decreased potentially indicating that heat transfer to the solid fuel is achieved faster. Gas yield increased due to greater biomass decomposition while the liquid condensate and char yield reciprocally decreased. For primary gases, the concentration and yield of CO and H_2 increased significantly due to the Boudouard and water-gas reactions while CO_2 decreased simultaneously. At the same time, CH_4 decreased slightly. The tar concentration in syngas (g/Nm^3) slightly decreased as temperature is increased. However, due to the greater increase of syngas, an increase in the yield of tar (g/kg dry biomass) was observed. Overall, H_2S concentration and yield increased while NH_3, HCN and HCl concentrations and yields decreased.

As ER increased*, g*as and char yields decreased while liquid yield increased due to greater oxidation. Furthermore, CO and H_2 decreased due to oxidation to CO_2 and H_2O while CH_4 is not significantly affected. Equivalence ratio does not significantly affect the concentration of contaminants except for tar and HCl which recorded drastic reduction as equivalence ratio is increased. While changes in concentrations were noticeable for H_2S, NH_3 and HCN as ER was changed, this variation was not statistically significantly.

References

(1) Escobar, J. C.; Lora, E. S.; Venturini, O. J.; Yáñez, E. E.; Castillo, E. F.;Almazan, O. Biofuels: Environment, technology and food security. *Renewable Sustainable Energy Rev.* 2008, 13, 1275-1287.

(2) Huber, G. W.; Iborra, S.;Corma, A. Synthesis of Transportation Fuels from Biomass: Chemistry, Catalysts, and Engineering. *Chem. Rev.* 2006, 106, 4044-4098.

(3) Li, X. T.; Grace, J. R.; Lim, C. J.; Watkinson, A. P.; Chen, H. P.;Kim, J. R. Biomass gasification in a circulating fluidized bed. *Biomass Bioenergy* 2004, 26, 171-193.

(4) Stefan Heyne, T. L., Magnus Marklund. *Biomass gasification - A synthesis of technical barriers and current research issues for deployment at large scale*; The Swedish Knowledge Centre for Renewable Transportation Fuels: Göteborg, Sweden, 2013.

(5) Kumar, A.; Eskridge, K.; Jones, D. D.;Hanna, M. A. Steam–air fluidized bed gasification of distillers grains: Effects of steam to biomass ratio, equivalence ratio and gasification temperature. *Bioresour. Technol.* 2009, 100, 2062-2068.

(6) Aljbour, S. H.;Kawamoto, K. Bench-scale gasification of cedar wood – Part I: Effect of operational conditions on product gas characteristics. *Chemosphere* 2013, 90, 1495-1500.

(7) Campoy, M.; Gómez-Barea, A.; Vidal, F. B.;Ollero, P. Air–steam gasification of biomass in a fluidised bed: Process optimisation by enriched air. *Fuel Process. Technol.* 2009, 90, 677-685.

(8) Carpenter, D. L.; Bain, R. L.; Davis, R. E.; Dutta, A.; Feik, C. J.; Gaston, K. R.; Jablonski, W.; Phillips, S. D.;Nimlos, M. R. Pilot-Scale Gasification of Corn Stover, Switchgrass, Wheat Straw, and Wood: 1. Parametric Study and Comparison with Literature. *Ind. Eng. Chem. Res.* 2010, 49, 1859-1871.

(9) Narvaez, I.; Orio, A.; Aznar, M. P.;Corella, J. Biomass Gasification with Air in an Atmospheric Bubbling Fluidized Bed. Effect of Six Operational Variables on the Quality of the Produced Raw Gas. *Ind. Eng. Chem. Res.* 1996, 35, 2110-2120.

(10) Aljbour, S. H.;Kawamoto, K. Bench-scale gasification of cedar wood – Part II: Effect of Operational conditions on contaminant release. *Chemosphere* 2013, 90, 1501-1507.

(11) Cui, H.; Turn, S. Q.; Keffer, V.; Evans, D.; Tran, T.;Foley, M. Contaminant Estimates and Removal in Product Gas from Biomass Steam Gasification. *Energy Fuels* 2010, 24, 1222-1233.

(12) J.P.A. Neeft; H.A.M. Knoef; U. Zielke; K. Sjöström; P. Hasler; P.A. Simell; M.A. Dorrington; L. Thomas; N. Abatzoglou; S. Deutch, C. G.; G.J. Buffinga; C. Brage;Suomalainen, M. *Guideline for Sampling and Analysis of Tar and Particles in Biomass Producer Gases*; US Department of Energy (DOE): 2005.

(13) *JMP User Guide*, Version 8; SAS Institute, Inc.: Cary, NC, 2008.

(14) Lv, P.; Xiong, Z.; Chang, J.; Wu, C.; Chen, Y.;Zhu, J. An experimental study on biomass air–steam gasification in a fluidized bed. *Bioresour. Technol.* 2004, 95, 95-101.

(15) Campoy, M.; Gómez-Barea, A.; Villanueva, A. L.;Ollero, P. Air−Steam Gasification of Biomass in a Fluidized Bed under Simulated Autothermal and Adiabatic Conditions. *Ind. Eng. Chem. Res.* 2008, 47, 5957-5965.

(16) Basu, P. *Biomass gasification and pyrolysis: practical design and theory*. Academic press: 2010.

(17) Brage, C.; Yu, Q.;Sjöström, K. Characteristics of evolution of tar from wood pyrolysis in a fixed-bed reactor. *Fuel* 1996, 75, 213-219.

(18) de Sousa, L. C. R. Gasification of wood, urban wastewood (Altholz) and other wastes in a fluidised bed reactor. Ph.D. Dissertation, Swiss Federal Institute of Technology, Zürich, Germany, 2001.

(19) Milne, T. A.; Abatzoglou, N.;Evans, R. J. *Biomass gasifier" tars": their nature, formation, and conversion*; NREL/TP-570-25357; National Renewable Energy Laboratory: Golden, CO, 1998.

(20) Zhou, J.; Masutani, S. M.; Ishimura, D. M.; Turn, S. Q.;Kinoshita, C. M. Release of fuel-bound nitrogen during biomass gasification. *Ind. Eng. Chem. Res.* 2000, 39, 626-634.

(21) Zhou, J.; Masutani, S. M.; Ishimura, D. M.; Turn, S. Q.;Kinoshita, C. M. Release of Fuel-Bound Nitrogen during Biomass Gasification. *Ind. Eng. Chem. Res* 2000, 39, 626-634.

(22) Drift, A. v. d.; Doorn, J. v.;Vermeulen, J. W. Ten residual biomass fuels for circulating fuidized-bed gasification. *Biomass Bioenergy* 2001, 20, 45-56.

(23) Kuramochi, H.; Wu, W.;Kawamoto, K. Prediction of the behaviors of H_2S and HCl during gasification of selected residual biomass fuels by equilibrium calculation. *Fuel* 2005, 84, 377-387.

(24) Valin, S.; Ravel, S.; Guillaudeau, J.;Thiery, S. Comprehensive study of the influence of total pressure on products yields in fluidized bed gasification of wood sawdust. *Fuel Process. Technol.* 2010, 91, 1222-1228.

(25) Dias, M.;Gulyurtlu, I. In *H_2S and HCl formation during RDF and coal co-gasification: a comparison between the predictions and experimental results*, Proceedings of the Biomass Gasification Technologies Workshop, Gebze, Turkey, 9-11 April 2008.

(26) Korbee, R.; Kiel, J. H. A.; Zevenhoven, M.; Skrifvars, B.; Jensen, P. A.;Frandsen., F. J. In *Investigation of Biomass Inorganic Matter by Advanced Fuel Analysis and Conversion Experiments*, Proceedings of the Power Production in the 21st Century: Impacts of Fuel Quality and Operations, Snowbird, UT, Oct 28 - Nov 2, 2001; Snowbird, UT, 2001.

(27) Duong, D. N.; Tillman, D. A.; NA, F. W.;Clinton, N. In *Chlorine Issues with Biomass Cofiring in Pulverized Coal Boilers: Sources, Reactions, and Consequences–A Literature Review*, Proceedings of the 34th International Technical Conference on Coal Utilization and Fuel Systems, Clearwater FL, 2009.

(28) Krishnan, G. N.; Gupta, R.;Ayala, R. In *Development of Disposable Sorbents for Chloride Removal from High-Temperature Coal-Derived Gases*, Proceeding of the Advanced Coal-Fired Power Systems, Morgantown, WV, July 16-18, 1996.

(29) Kuramochi, H.; Nakajima, D.; Goto, S.; Sugita, K.; Wu, W.;Kawamoto, K. HCl emission during co-pyrolysis of demolition wood with a small amount of PVC film and the effect of wood constituents on HCl emission reduction. *Fuel* 2008, 87, 3155-3157.

(30) Dolan, M. D.; Ilyushechkin, A. Y.; McLennan, K. G.;Sharma, S. D. Halide removal from coal-derived syngas: review and thermodynamic considerations. *Asia-Pac. J. Chem. Eng.* 2012, 7, 171-181.

Chapter 4

Effects of Temperature and Equivalence Ratio on Mass Balance and Energy Analysis in Pine Air Gasification

Abstract

The effect of temperature (790, 934 and 1078°C) and equivalence ratio (0.15, 0.25 and 0.35) was assessed on the performance of an air blown bubbling fluidized bed gasifier by considering the mass and carbon balances as well as the energy flows and efficiencies and the producer gas heating value.

Mass balance closures ranged from 94.73 to 96.72 % and from 89.82 to 96.93 % as temperature and ER increased, respectively. In addition, the carbon closures ranged from 80.77 to 92.29 % and from 79.09 and 87.13 % as temperature and ER increased, respectively. Carbon conversion efficiency to gas product ranged from 72.26 to 84.32 % as temperature increased and from 72.26 to 84.66 % as equivalence ratio increased. Carbon flow analysis showed that the char product streams retained 10.26 to 6.94 % and 8.82 to 2.13 % of the carbon feed to the gasifier as temperature and equivalence ratio increases, respectively. The carbon content in the liquid condensate was minimal compared to the carbon in other product streams and accounted for less than 0.1 % of the carbon input to the gasifier at all conditions.

The cold and hot gas efficiencies increase from 56.12 to 67.45 % and from 67.51 to 83.83 % as temperature is increased and in contrast decreased from 63.85 to 52.84 % and from 78.06 to 73.00 % as equivalence ratio increase, respectively. The heating value of producer gas increased

from 4.93 to 5.73 MJ/m^3 with increasing temperature and decreased from 7.11 to 3.28 MJ/m^3 with increasing equivalence ratio.

4.1 Introduction

During gasification, a carbonaceous fuel is converted at high temperature (650-1200˚C) into gas, char and liquid condensate, if the gas product is cooled, in the presence of sub-stoichiometric quantity of oxygen provided by the gasifying agents. Typically, it is desired to maximize carbon and energy transfer from biomass into primary gas products (CO, H_2, CO_2, CH_4). The performance of a given gasification process is commonly measured by carbon conversion, cold and hot gas efficiencies as well as mass and energy balances, if sufficient information is available on the process. Together, these performance indicators permit to gauge process efficiency, validate process data or provide design and engineering tools. It is consequently very useful to establish these performance criteria for a range of process conditions.

Few studies have carried out detailed mass and energy balances during air gasification of biomass in fluidized bed gasification systems.[1-3] In addition, several studies have reported carbon conversion and energy efficiencies for various process conditions and feedstocks in fluidized bed biomass gasification.[1, 4-9] However, limited information is available on the effect of temperature and equivalence ration on the distribution and flow of material and energy in the output streams. This chapter addresses this limitation and details the effect of temperature (790, 934 and 1078˚C) and equivalence ratios (0.15, 0.25 and 0.35) on the distribution and flow material and energy during air gasification of pine.

4.2 Materials and Methods

4.2.1 Experimental Setup and Product Sampling

The gasification experimental setup was previously discussed in 0. The control volume, the input and output streams considered for material balance and energy analysis in this study are shown in Figure4.1. Material enters the systems in the form biomass as pine, gasifying agent as oxygen (O_2) and fluidization gas as nitrogen (N_2). Material exits the system in the form of biomass residue as char, liquid condensate, and gas as non-condensable gases (primary gases and contaminants) and tar.

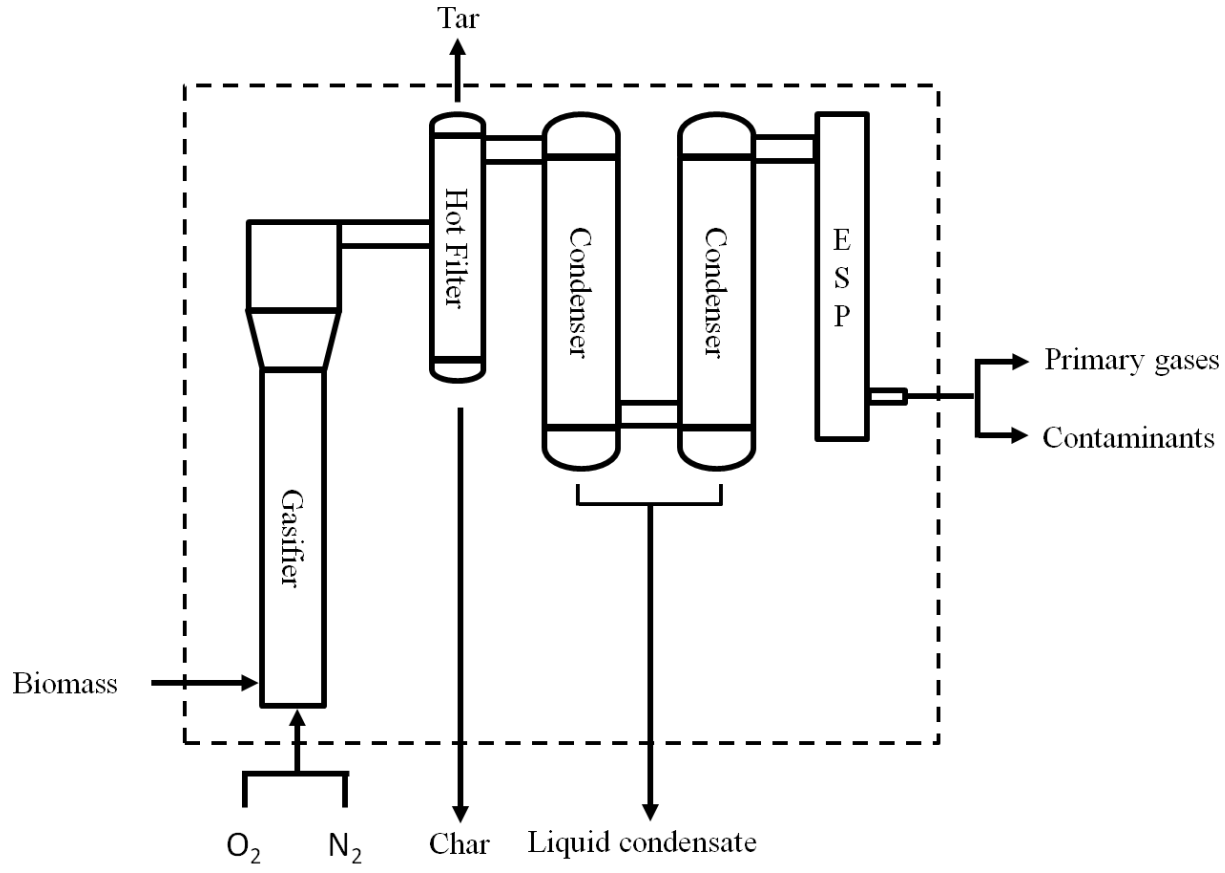

Figure 4.1. Material balance input and output streams

In this study, O_2 and N_2 are supplied separately, the first as the oxidizing medium and the second as the fluidization medium. This approach was taken to decouple fluidization, essential to avoid feeding issues, and gasification which requires an oxidizing agent. Based on preliminary experimental trials, it was established that the suitable nitrogen flow rate for proper fluidization and biomass feeding was near 16.5 l/min. This nitrogen flow rate was thus maintained constant in subsequent experiments while oxygen flow rate was varied to obtain the desired equivalence ratio. The composition of oxygen and nitrogen varied from 5.25 and 94.75 wt % at 0.15 ER and 9.52 and 90.48 wt % at 0.35 ER, respectively. This resulted in a nitrogen enriched gasifying agent and a higher than typical inert gas content when compared to air gasification. As air contains 23 and 77 wt% of oxygen and nitrogen, the higher nitrogen content diluted the gas concentrations. In order to eliminate ambiguity and allow for comparison with reported results for air gasification, the inert nitrogen was adjusted to achieve a normal O_2/N_2 composition in air. This approach does not affect the material balance since nitrogen, being inert in the process, simply enters and exits the control volume. However, for the energy analysis, the volumetric heating value of the producer gas is reported on an air equivalent basis.

4.2.2 Material Characterization

Pine wood was secured from a local chipping plant in Opelika, AL, air dried, ground and sieved through a 850 μm screen opening prior to any characterization. Ultimate and proximate analyses were performed for raw pine wood. Ultimate analysis was carried out by a CHNS/O elemental

analyzer (Perkin Elmer, Model 2400, Waltham, MA) while the higher heating value of pine (HHV_{pine}) was determined with a bomb calorimeter (IKA Bomb Calorimeter, Model C-200, Wilmington, NC). The elemental composition of char product stream was determined using a CHNS/O analyzer while the carbon content in the liquid condensate was determined using a total organic carbon (TOC) analyzer (TOC-L Analyzer, Shimadzu Scientific Instruments Inc., Columbia, MD). As elemental analysis on char samples with high ash content was challenging due to rapid deactivation of CHNS oxidation columns, only the samples with lowest char content were analyzed to avoid this issue. The higher heating value of char (HHV_{char}) was determined using the Milne equation depicted below in eq. 4.1.

$$\mathrm{HHV_{Milne,dry}} = 0.341\mathrm{C} + 1.322\mathrm{H} + 0.12\mathrm{O} - 0.12\mathrm{N} + 0.0686\mathrm{S} - 0.0153\mathrm{ash} \quad (4.1)$$

where C, H, N, O, S and ash are the mass and the ash fractions in wt % of dry material and HHV the heating value for dry material in MJ/kg.

The primary gas concentrations were determined using a gas analyzer equipped with NDIR and TCD detectors (NOVA, Niagara Falls, NY). Non-condensable gas contaminants were measured with an FT-IR fitted with a 4 m gas cell and a liquid cooled MCT detector (IMAAC, Austin, TX). For all non-condensable gases, only steady state concentrations were considered. Tar, due to its condensable nature and its significance in biomass gasification, was measured using a slip stream out of the hot filter. The gas was scrubbed through five impinger bottles each containing 50 ml of isopropanol at a flow rate of 2 l/min and the tar content determined gravimetrically.

4.2.3 Mass Balance and Energy Analysis

The material and energy balance was conducted using 100 g as the basis of calculation. This is an arbitrary value selected for convenience. However, all values can be scaled up or down by applying a factor to this basis.

4.2.3.1 Mass and Carbon Balance

The material and carbon flows for all input and output streams were considered for the purpose of this mass balance. Using the law of conservation of mass, shown in eq. 4.2, material balances were carried out for all process conditions.

$$\sum m_{in} = \sum m_{out} \tag{4.2}$$

where m_{in} and m_{out} are the mass of input and output streams, respectively. In addition, the carbon flow and balance was also carried. The application of the law of mass conservation to the control volume results in the following mass and carbon balance equations shown by eqs. 4.3 and 4.4 below.

$$m_{pine}^{in} + m_{O_2}^{in} + m_{N_2}^{in} = m_{primary\ gas}^{out} + m_{contaminants}^{out} + m_{char}^{out} + m_{liquid\ condensate}^{out} \tag{4.3}$$

$$m_{pine,c}^{in} = m_{primary\ gas,c}^{out} + m_{char,c}^{out} + m_{liquid\ condensate,c}^{out} \tag{4.4}$$

where m_{pine}^{in}, $m_{O_2}^{in}$, $m_{N_2}^{in}$represent the mass input in grams of pine, oxygen and nitrogen to the system, $m_{primary\ gas}^{out}$, $m_{contaminants}^{out}$, m_{char}^{out}, $m_{liquid\ condensate}^{out}$ represent the mass output of gas, total contaminants including tar, char and liquid condensate, $m_{pine,c}^{in}$ represents the mass input in grams of carbon from pine and $m_{primary\ gas,c}^{out}$, $m_{char,c}^{out}$ and $m_{liquid\ condensate,c}^{out}$represent the

mass output in grams of carbon in the gas, char and liquid condensate streams. For the input streams, pine is the only source of carbon input and therefore, only this stream was considered. For the output streams, the carbon input from pine is partitioned into all product streams. For the gas product streams, only carbon from the primary gases was considered. It is noteworthy to indicate that carbon present in tar is not accounted for in the carbon balance as the tar carbon fraction is unknown. However, this omission should not significantly impact the carbon balance accuracy as tar only accounts for 0.83 g/100g biomass, at most, in this study.

In material balance analysis, it is possible to have a discrepancy due measurement error. The accuracy in input and output measurements is assessed by the mass and carbon balance closures, the mass ratio of output to input represented by eqs. 4.5 and 4.6 below.

$$\emptyset_{mass}, \% = 100 \times \frac{\sum m_j^{out}}{\sum m_i^{in}} \tag{4.5}$$

$$\emptyset_c, \% = 100 \times \frac{\sum m_{j,c}^{out}}{\sum m_{i,c}^{in}} \tag{4.6}$$

where $\emptyset_{mass}$and $\emptyset_c$represent mass and carbon balance closures, *i* and *j* represent input and output streams, respectively.

4.2.3.2 Carbon Conversion Efficiency

In addition to the mass and carbon balance, the carbon conversion efficiency to primary gases was also determined as it is a widely reported parameter in gasification studies. The carbon conversion efficiency, η_c, is defined as the mass of carbon in the primary gases over the mass of carbon from biomass supplied to the gasifier as shown in eq. 4.7.

$$\eta_c = \frac{\sum(w_{s,c}^{out} \times m_s^{out})}{m_{pine,c}^{in}} \quad (4.7)$$

where $w_{s,c}^{out}$, defined eq. 4.8 is the mass fraction of carbon baring species (s = CO, CO_2, CH_4, C_2H_2 and C_2H_4) and m_s^{out} is the mass output of the corresponding species in the primary gas output stream.

$$w_{s,c}^{out} = \frac{12n}{MW_s} \quad (4.8)$$

where n and MW_s are the number of carbon and molecular weight of gas species s. $w_{CO,c}^{out}$, $w_{CO_2,c}^{out}$, $w_{CH_4,c}^{out}$, $w_{C_2H_2,c}^{out}$ and $w_{C_2H_4,c}^{out}$.are 0.43, 0.27, 0.75, 0.92 and 0.86, respectively.

4.2.3.3 Energy Analysis

The energy balance in this study examines the flow of gross energy (HHV) as well as exergy from biomass into the product streams of the control volume. The expression of the energy analysis is represented by eq. 4.9 below:

$$(E_{HHV})_{pine}^{in} = (E_{HHV})_{gas}^{out} + (E_{HHV})_{char}^{out} + (E_{HHV})_{loss} \quad (4.9)$$

where $(E_{HHV})_{pine}^{in}$ is the heating value of pine and $(E_{HHV})_{gas}^{out}$ and $(E_{HHV})_{char}^{out}$ represent the heating value of the gas and char output streams and $(E_{HHV})_{loss}$ represents the heating value loss expressed in kJ. Using the specific heating values of pine and char discussed in 4.2.2 gives rise to the following expressions:

$$(E_{HHV})_{pine}^{in} = m_{pine}^{in} \times HHV_{pine} \quad (4.10)$$

$$(E_{HHV})_{gas}^{out} = \sum(m_s^{out} \times HHV_s) \quad (4.11)$$

$$(E_{HHV})_{char}^{out} = m_{char}^{out} \times HHV_{char} \quad (4.12)$$

where HHV_s represents the specific higher heating value of gas species (s = CO, H_2, CH_4, C_2H_2 and C_2H_4) and are reported in Table A3.1 in Appendix A3.

4.2.3.4 Cold and Hot Gas Efficiencies and Volumetric Gas Heating Value

Cold and hot gas efficiencies are widely reported in gasification studies and are therefore calculated in this study. The cold gas efficiency ($\eta_{cold\ gas}$) and hot gas efficiency ($\eta_{hot\ gas}$) are expressed by eqs. 4.13 and 4.14.

$$\eta_{cold\ gas} = 100 \times \frac{(E_{HHV})_{primary\ gas}^{out}}{(E_{HHV})_{pine}^{in}} \quad (4.13)$$

$$\eta_{cold\ gas} = 100 \times \frac{(E_{HHV})_{primary\ gas}^{out} + Q_{primary\ gas}^{out}}{(E_{HHV})_{pine}^{in}} \quad (4.14)$$

where $Q_{primary\ gas}^{out}$, expressed in eq. 4.15, is the sensible heat of the primary gas output in kJ.

$$Q_{primary\ gas}^{out} = \sum m_{s,primary\ gas}^{out} \times C_{p,s,primary\ gas} \times (T^{out} - 298) \quad (4.15)$$

where $C_{p,s,\ primary\ gas}$ (kJ/g K) is the individual specific heat of the primary gas species s (s = CO, CO_2, CH_4, H_2, N_2) and T^{out} (K) is the exit gas temperature. The specific heat capacity was determined using the Shomate equation illustrated below in eq. 4.16.

$$C_{p,s} = A + BT' + CT'^2 + DT'^3 + \frac{E}{T'^2} \quad (4.16)$$

with the coefficients *A, B, C, D* and *E* taken from the National Institute of Standards and Technology (NIST) database[10] and T' is defined as $T^{out}/_{1000}$. The coefficients of the Shomate equations are listed in Table A3.1 in Appendix A3.1. In addition to the energy efficiencies, the volumetric producer gas energy content is also commonly determined in experimental studies and is therefore evaluated as expressed in eq. 4.17.

$$Q_v^{out} = \frac{\sum HHV_s^{out}}{\sum\left(m_s^{out}/\rho_s\right)} \tag{4.17}$$

where Q_v^{out} is the volumetric heating value of the producer gas and ρ_s is the density of gas species s listed in Appendix A3 in Table A3.2. Sample mass and energy balance calculations are provided in Appendix A3.

4.3 Results and Discussion

4.3.1 Effect of Temperature and Equivalence Ratio on Products

Previously, the effect of temperature and ER on the yields of char and liquid condensate were discussed in detailed in Chapter 3. Table 4.2 and Table 4.2 summarize the effect of temperature and equivalence ratio on the char and liquid condensate product streams. The total organic carbon analysis of the liquid condensate showed that minimal carbon is contained in this product stream. The carbon concentrations are 0.29, 0.49 and 0.91 mg C/g condensate for 0.15, 0.25 and

0.35 equivalence ratios and 1.93, 0.49 and 0.15 mg C/g condensate for 790, 934 and 1078°C, respectively.

Table 4.1. Effect of temperature on char and liquid condensate product streams at 0.25 ER

	Temperature, °C		
Means (SD)	**790**	**934**	**1078**
Primary gases (g/100 g pine)			
CO	37.96 (3.25)	43.47 (1.99)	64.70 (11.92)
CO_2	46.40 (2.52)	43.16 (3.90)	31.18 (2.81)
CH_4	8.58 (1.67)	5.37 (0.31)	2.92 (0.40)
H_2	1.75 (0.34)	2.57 (0.15)	4.27 (0.11)
C_2H_2	0.61 (0.14)	0.70 (0.04)	0.44 (*0.05)*
C_2H_4	5.20(1.24)	3.73 (1.57)	1.37 (0.47)
N_2 (*air equivalent*)	93.44 (3.56)	99.51 (10.90)	94.69 (0.91)
Char (g/100 g pine)	6.07 (1.20)	3.65 (1.27)	4.09 (2.02)
Liquid condensate (g/100 g pine)	20.87 (1.20)	16.93 (3.08)	11.75 (0.67)
Values in parentheses indicate standard deviations			

Table 4.2.. Effect of equivalence ratio on char and liquid condensate product streams at 934°C

	ER		
Mean (SD)	**0.15**	**0.25**	**0.35**
Primary gas (g/100g)			
CO	51.90 (4.44)	434.72 (19.92)	460.65 (60.95)
CO_2	26.68 (2.98)	431.58 (39.03)	591.89 (44.80)
CH_4	4.68 (0.20)	53.69 (3.12)	49.31 (8.46)
H_2	3.56 (0.35)	25.73 (1.50)	24.03 (3.70)
C_2H_2	0.78 (0.01)	7.03 (0.40)	6.68 (0.71)
C_2H_4	7.43 (2.07)	37.32 (15.74)	43.31 (16.30)
N_2	58.40 (2.60)	99.51 (10.90)	
Char (g/g pine)	5.03 (0.77)	3.65 (1.27)	1.21 (0.32)
Liquid condensate (g/g pine)	9.30 (0.58)	16.93 (3.08)	18.17 (4.42)
Values in parentheses indicate standard deviations			

The effect of the temperature and equivalence ratio on the ultimate and proximate analyses on char samples are summarized in Table 4.3 and Table 4.4. It was observed that ash content of char samples varied widely from 4.47 to 64.63 wt%, as received for all samples. For reference, the ash content in pine was only 0.34 wt %. This increase in char ash content is due to two principal reasons: ash accumulation in char stream as biomass is decomposed into gas products and fine bed material (sand) entrainment into char filter.

Table 4.3. Properties of char collected at different temperatures at ER = 0.25

		Temperature, °C		
Mean (SD)	**Pine**	**790**	**934**	**1078**
Elements, wt % dry				
C	47.14 (0.18)	82.87 (1.60)	85.38 (3.64)	81.56 (1.16)
H	6.52 (0.04)	1.33 (0.04)	0.34 (0.02)	0.96 (0.11)
N	0.44 (0.10)	0.42 (0.03)	0.31 (0.02)	0.35 (0.03)
S	0.10	n/a	n/a	n/a
O[a]	45.46 (0.24)	9.15 (1.63)	4.38 (3.65)	1.37 (0.88)
Ash, wt % dry	0.34 (0.01)	6.22 (0.0045)	9.59 (0.01)	15.75 (0.35)
HHV, MJ/kg dry basis	20.18 (0.21)	28.78 (0.79)[b]	28.86 (1.66)[b]	28.63 (0.39)[b]

[a] Oxygen was determined by difference, [b] Heating values determined using the Milne formula. Values in parentheses represent standard deviations.

Table 4.4. Properties of char collected at different equivalence ratios at 934°C

		ER		
Mean (SD)	**Pine**	**0.15**	**0.25**	**0.35**
Elements, wt % dry				
C	47.14 (0.18)	84.12 (3.39)	85.39 (3.65)	81.24 (3.7)
H	6.52 (0.04)	0.37 (0.12)	0.35 (0.03)	0.42 (0.2)

N	0.44 (0.10)	0.24 (0.06)	0.31 (0.03)	0.2 (0.05)
S	0.10	n/a	n/a	n/a
O [a]	45.46 (0.24)	9.87 (4.15)	4.38 (3.65)	8.26 (3.56)
Ash, wt % dry	0.34 (0.01)	5.43 (1.21)	9.6 (0.01)	9.91 (0.04)
HHV, MJ/kg dry basis	20.18 (0.21)	27.87 (1.70)[b]	28.86 (1.66)[b]	27.08 (1.60)[b]

[a] Oxygen was determined by difference, [b] Heating values determined using the Milne formula. Values in parentheses represent standard deviations.

The elemental composition of char at various temperature and equivalence ratio did not show any clear trend. All samples have higher carbon content (> 80 wt %, dry basis) while other elements, oxygen in particular, are significantly lower relative to their initial concentration in pine. The elemental compositions as well as the higher heating values, determined using the Milne formula, are similar to values reported in by Energy Research Center of the Netherlands (ECN) Phyllis2 database for various biomass char samples.[11]

4.3.2 Effect of Temperature and Equivalence Ratio on Mass and Carbon Balance

The mass and carbon balances were determined for all process conditions by accounting for mass input and output from all streams. The mass balance closure was 97.47, 94.73 and 96.72 % for 790, 934 and 1078˚C and 89.82, 94.73 and 96.93 % for 0.15, 0.25 and 0.35 ER, respectively. These mass balance closures are similar to mass balance closure results reported by other investigators.[1, 2, 5] Additionally, carbon closures were 97.47, 94.73 and 96.72 % for 790, 934 and 1078˚C and 87.29, 80.77 and 92.29 % for 0.15, 0.25 and 0.35 ER, respectively. Other studies have reported similarly carbon balance closures[2, 5] although higher closures have been reported

by van der Drift and coworkers when carbon-rich light hydrocarbons were included in the carbon balance.

Among all product streams, producer gas accounted for the highest proportion of carbon relative to the carbon input from biomass. The carbon conversion efficiency to product gas was 76.06, 72.26 and 84.32 % for 790, 934 and 1078˚C and 74.10, 72.26 and 84.66 % for ER of 0.15, 0.25 and 0.35, respectively. In Chapter 3, it was observed that, as temperature and equivalence ratio increased, the proportion of pine converted to non-condensable gas product also increases due the promotion of the Boudouard and water gas reaction as well as oxidation reactions, resulting in increasing carbon conversion efficiency. Figure 4.2 shows a comparison of the carbon conversion efficiencies achieved in this study and values reported by various authors for fluidized bed systems during air gasification. The results from this study are within the range of values reported for bubbling fluidized bed reactors[5, 6, 12] but lower than circulating fluidized bed reactors which typically achieve higher carbon conversion efficiency.

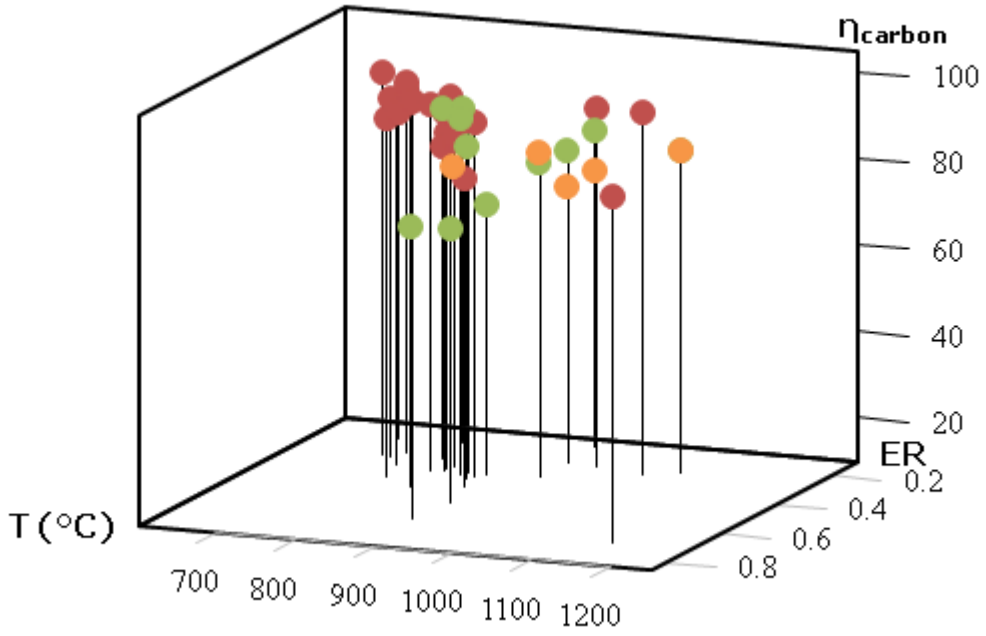

Figure 4.2. Carbon conversion efficiency in this study compared with several reports in woody biomass air gasification in bubbling fluidized bed reactors. Orange points represent data from this study, green points represent data for bubbling fluidized bed and red points represent data for circulating fluidized bed [1, 4-6, 12, 13]

Carbon distribution in the product streams is shown in Figure 4.3 and Figure 4.4 for temperature and equivalence ratio, respectively. For both temperature and equivalence ratio, carbon in the gas stream accounted for the largest percentage (74-85 %) of carbon fed to the gasifier, followed by carbon in the char stream. Carbon in liquid condensate is minor with less than 0.1% of feed carbon for all conditions. The carbon unaccounted for in the carbon balance ranged from 18.45 to 8.73 % and 18.45 to 13.17 % for temperature and equivalence ratio, respectively. The unaccounted carbon is likely present as uncollected product from the gasifier, carbon in the tar

product stream, which is not included in the carbon balance, as well as in other carbon baring gas species such as C_2-C_6 compounds, which are not measured in this study. Nonetheless, the results in this study are similar comparable to other results reported when Carpenter and coworkers[2]. Figure 4.5 illustrates the mass and carbon balance of the process at 934°C and 0.25 ER. Similar mass and energy balance diagrams are shown in figures A3.1, A3.2, A3.3 and A3.4 in Appendix A3.

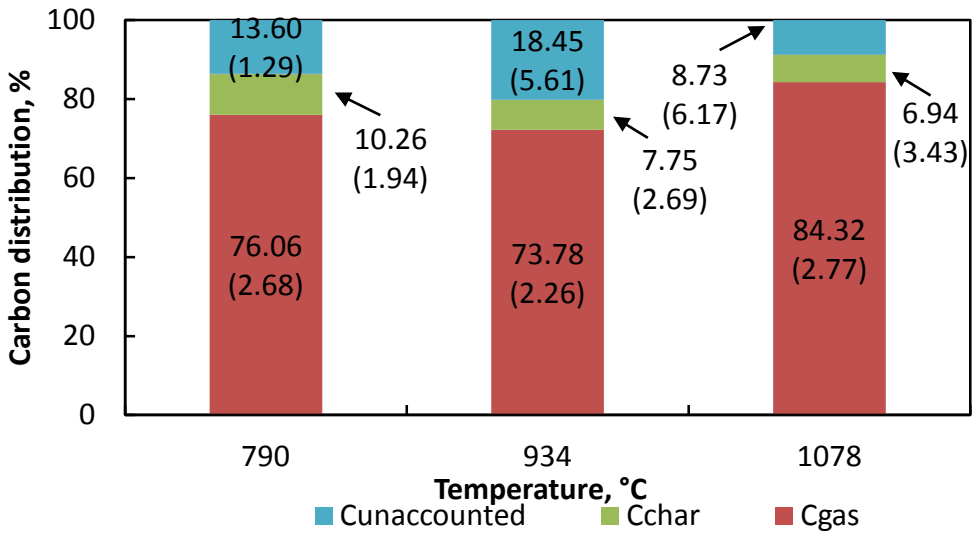

Figure 4.3. Effect of temperature on carbon distribution in product streams

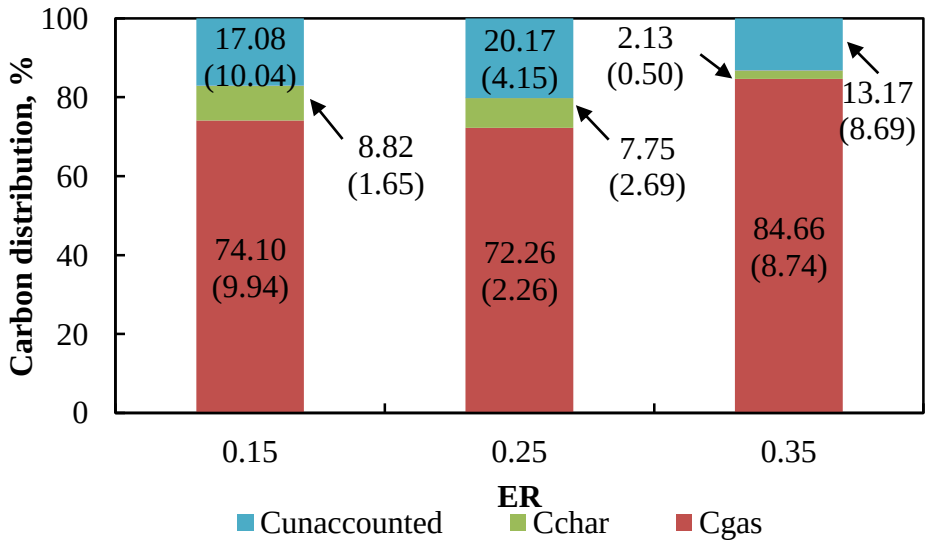

Figure 4.4. Effect of equivalence ratio on carbon distribution in product streams

Carbon balance	Mean	SD
In, g	46.99	0.00
Out, g	37.95	1.95
Discrepency, g	9.04	1.95
Closure, %	80.77	4.15

Mass balance	Mean	SD
In, g	223.91	6.51
Out, g	212.12	7.53
Discrepency, g	11.79	4.55
Closure, %	94.73	2.05

Tar, g	0.88

Carbon flow	Mean	SD
C_{gas}, g	33.96	1.06
C_{char}, g	3.55	1.39
Cl_{iquidr} g	0.01	0.00
$C_{unaccountedr}$ g	9.48	1.95

Energy efficiency	Mean	SD
η_{cold}, %	56.47	2.56
η_{hotr} %	73.83	2.97

Energy flow	Mean	SD
E_{gas}, kJ	1131.53	51.67
E_{char}, kJ	125.19	49.00
E_{loss}, kJ	761.28	90.22

Heating value, MJ/m^3	5.26	0.16

	Basis
Biomass, g	100
C, g	46.99

	Mean	SD
$HHV_{biomass}$, kJ	2018	21

	Mean	SD
Char, g	4.36	1.51
C, g	3.64	1.24

	Mean	SD
HHV_{char}, kJ	128.45	44.55

	Mean	SD
Gasifying agent, g	129.12	14.03

	Mean	SD
Liquid condensate, g	19.63	2.23
C, g	0.676	0.077

Primary gas components	Mean	SD
CO, g	43.47	1.99
CO_2, g	43.16	3.90
CH_4, g	5.37	0.31
H_2, g	2.57	0.15
C_2H_2, g	0.28	0.37
C_2H_4, g	0.37	0.16
N_2, g	99.04	10.76
Total primary gases, g	193.94	15.74
η_{carbon}	73.78	4.24
C, g	34.67	1.99

Contaminants	Mean	SD
H_2S, g	0.016	0.00
NH_3, g	0.180	0.04
HCN, g	0.026	0.00
HCl, g	0.001	0.00
Total contaminants, g	0.11	0.12

Carbon distribution	Mass, g		Carbon distribution	wt %	
	Mean	SD		Mean	SD
Gas	34.67	1.99	Gas	73.78	4.24
Char	3.64	1.24	Char	7.75	2.63
Liquidi condensate	0.68	0.08	Liquidi condensate	1.44	0.16

Figure 4.5. Process mass, carbon and energy balance diagram at 934°C and 0.25 ER

4.3.3 Effect of Temperature and Equivalence Ratio on Energy Analysis

Energy analysis of the process at all conditions was carried out by considering the energy distribution in the product streams, the energy efficiencies ($\eta_{cold\ gas}$ and $\eta_{hot\ gas}$) and the heating value of the producer. The process energy flows are shown in Figure 4.6 and Figure 4.7. As temperature and equivalence ratio increased, the char energy output decreases from 170.44 to 117.95 kJ and from 146.62 to 34.51 kJ. The decrease in char energy flow is due to the decrease in char yield as both temperature and equivalence ratios are increased due to greater biomass decomposition and thus lower char production.

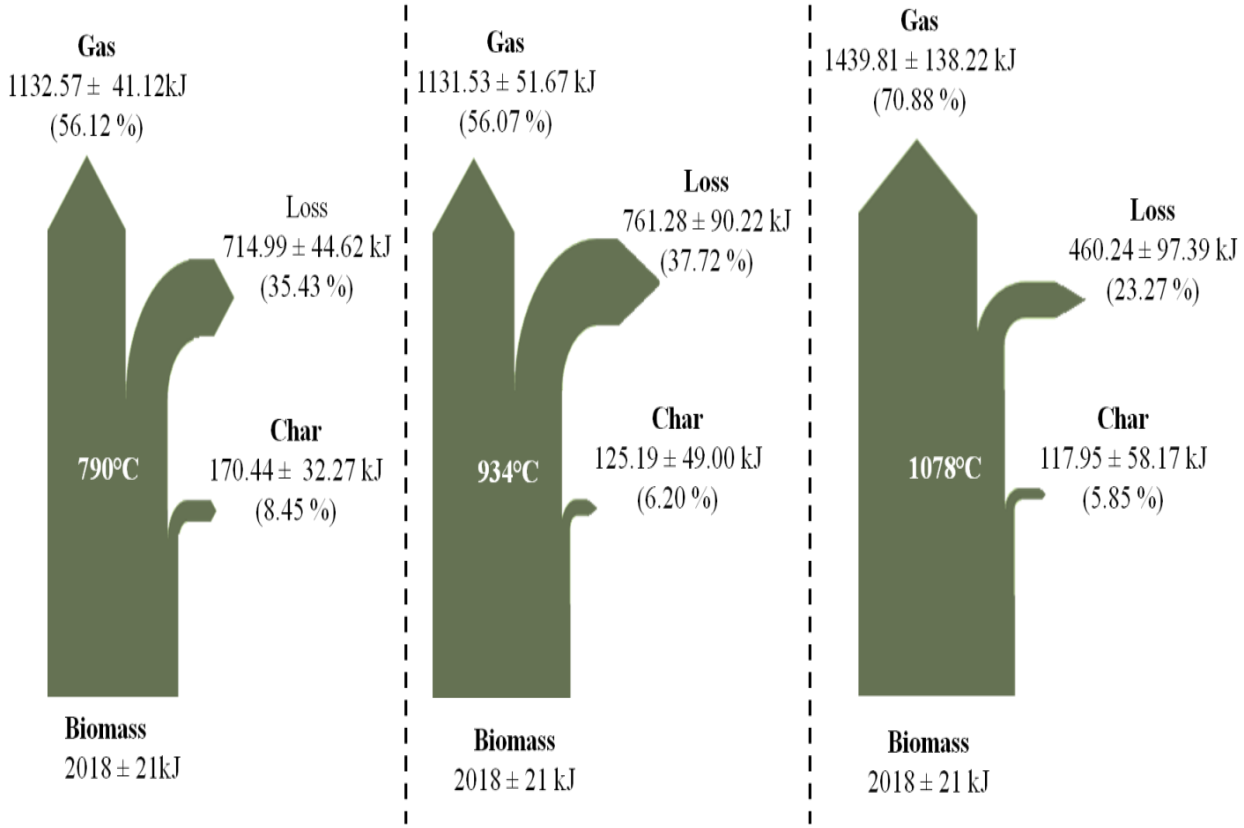

Figure 4.6. Effect of temperature on energy flow illustrated by Shankey diagrams.

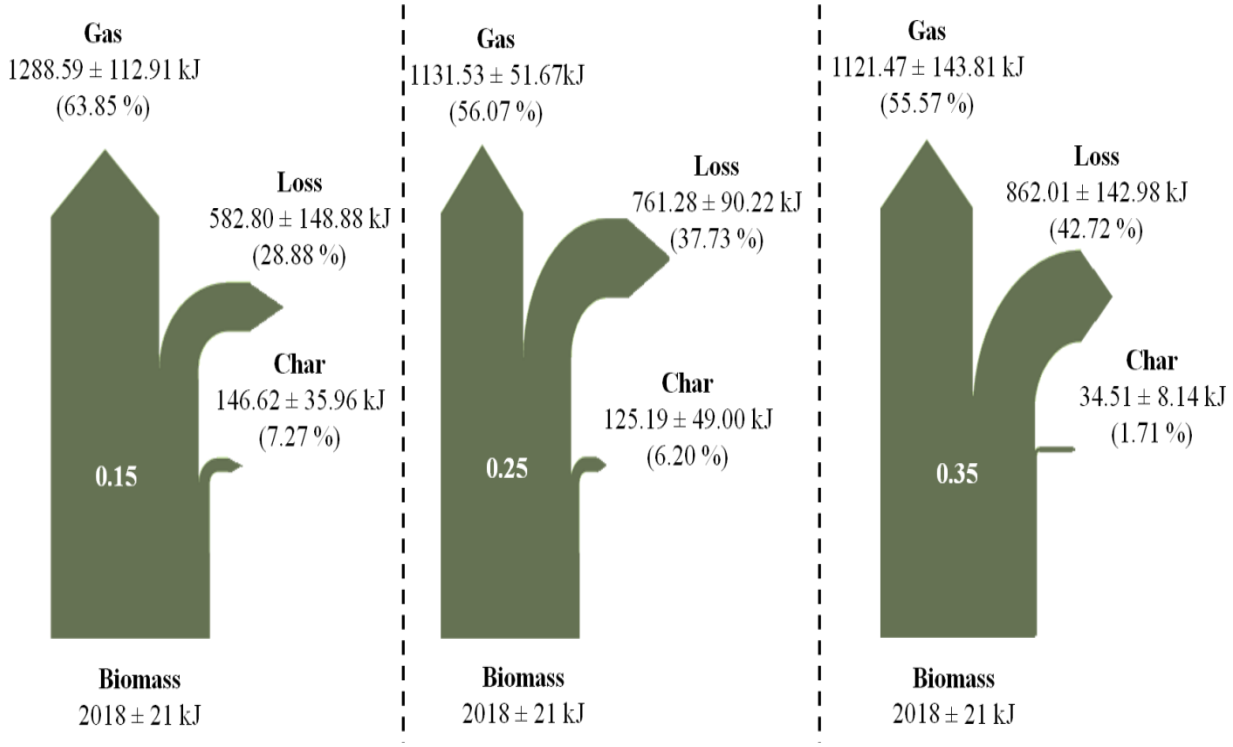

Figure 4.7. Effect of equivalence ratio on energy flow illustrated by Shankey diagrams.

The total producer gas energy output varied from 1132.57 to 1439.81 kJ as temperature increased and from 1288.59 to 1121.47 kJ as equivalence ratio increased. The increase in producer gas energy output is due to the increase in CO and H_2 and decrease in CO_2 as temperature is increased as observed in several studies.[14] In contrast, the producer gas energy output decreased as equivalence ratio is increased due to increased oxidation of CO and H_2 to CO_2 and H_2O as reported previously in Chapter 3.

The energy loss represents heat loss from the systems as well as energy contained in contaminants, tar in particular as well as other gaseous species. The energy losses vary from

37.72 to 23.27 % and 28.88 to 42.72 % of the total biomass energy content as temperature and equivalence ratio is increased, respectively. The decrease in energy loss as temperature is increased is due to the increase in gas energy flow. In contrast, the energy loss increases with equivalence ratio due to the reduction in the concentrations of CO and H_2, the increase in CO_2 concentration, the increase in liquid condensate and the decrease in the char energy. The energy loss at 790°C is similar to figures reported at similar conditions by Lim and coworkers[15].

Cold and hot gas efficiencies are two common thermodynamic efficiencies utilized to access the performance of gasification. Figure 4.8 and Figure 4.9 show the effect of temperature and equivalence ratio on the cold and hot gas efficiencies as well as on the heating value of the producer. As temperature is increased, both cold gas and hot gas efficiencies increase in a similar fashion from 56.12 to 67.45 and from 67.51 to 83.83 %, respectively. The increase in gas efficiencies as temperature is increased is due to the increase in CO and decrease in CO_2 concentrations over the same range of temperature as previously shown in Chapter 3.

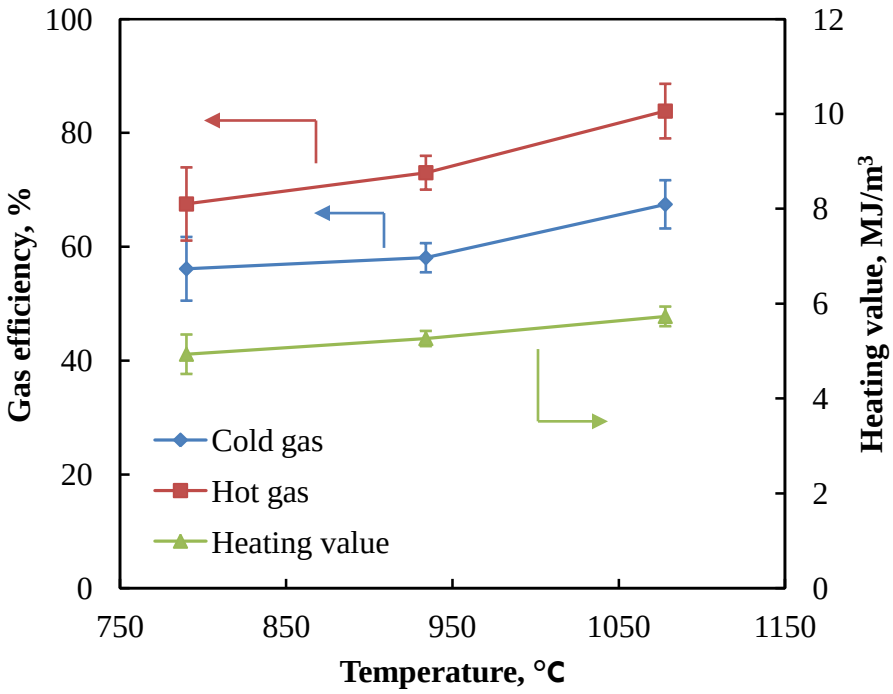

Figure 4.8. Effect of temperature on cold and hot gas efficiencies and heating value of producer gas

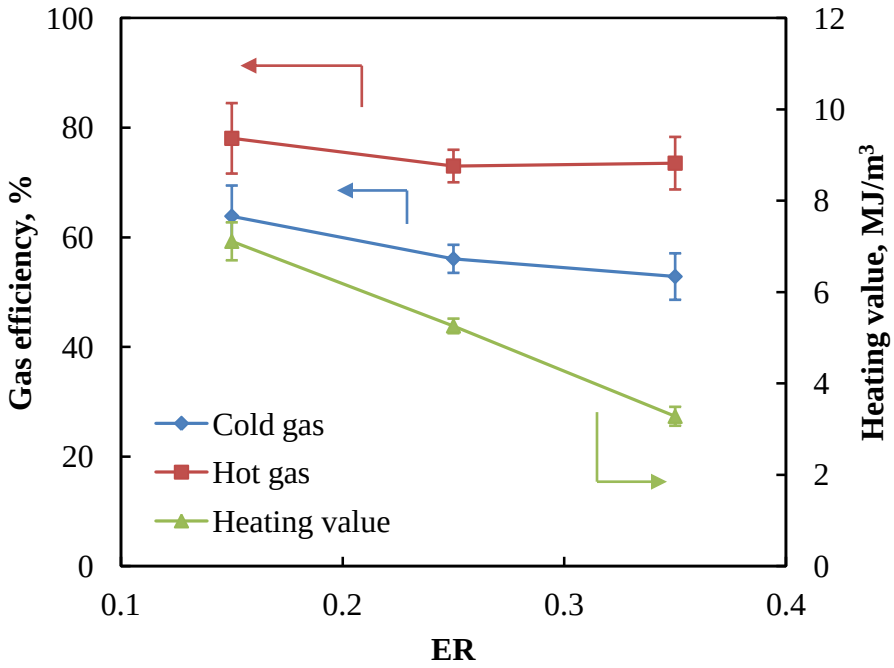

Figure 4.9. Effect of equivalence ratio on cold, hot gas efficiencies and gas heating value

The cold and hot gas efficiencies in this study fall in the range of values reported in other studies as illustrated in Figure 4.10. The heating value of the producer gas increased slightly from 4.93, 5.26 and 5.73 MJ/m^3 for 790, 934 and 1078°C and 7.11, 5.26 and 3.28 MJ/m^3 for 0.15, 0.25 and 0.35 ER, respectively. In this case also, the increase in heating value of the syngas is due to the increase in CO and H_2 as temperature is increased as observed in Chapter 3. In contrast, CO and H_2 decrease as ER increases while CO_2 increases thus decreasing the heating value of the gas product. The producer gas heating values in this study are similar to values reported for air gasification where energy content ranges from 2.93[12] to 6.3 MJ/m.[3,16]

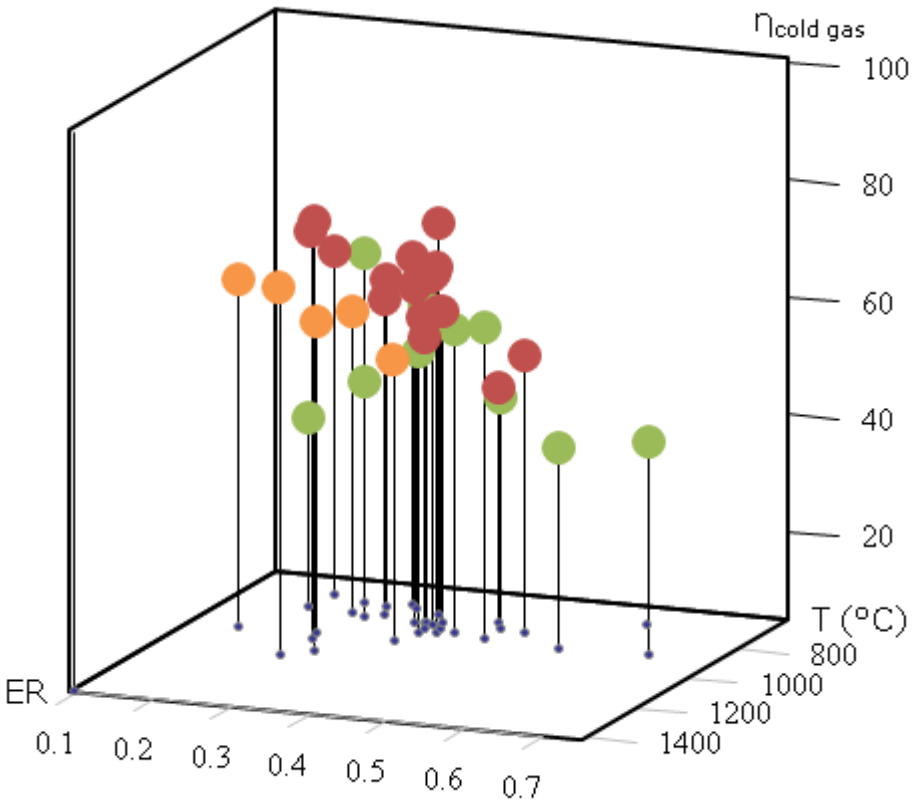

Figure 4.10. Cold gas efficiency in this study compared with several reports in woody biomass air gasification in fluidized bed reactors. Orange points represent data from this study, green points data for bubbling fluidized bed gasifiers and red points data for circulating fluidized bed gasifiers[1, 4-6, 12, 13]

4.4 Conclusions

The mass and energy balance of pine was analyzed at three temperatures (790, 934 and 1078°C) and ER (0.15, 0.25 and 0.35) during air gasification. Mass balance closures were 97.47, 94.73 and 96.72 % and 89.82, 94.73 and 96.93 % as temperature and ER increased. In addition, the carbon closures were 87.29, 80.77 and 92.29 % and 79.09, 80.77 and 87.13 % as temperature and

ER increased. Carbon conversion efficiency to gas product ranged from 72.26 to 84.32 % as temperature increased and from 72.26 to 84.66 as equivalence ratio increased. Carbon flow analysis showed that the char product streams retained 10.26 to 6.94 % and 8.82 to 2.13 % of the carbon feed to the gasifier as temperature and equivalence ratio increases, respectively. The carbon content in the liquid condensate was minimal compared to the carbon in other product streams and accounted for less than 0.1 % of the carbon input to the gasifier at all conditions.

The cold and hot gas efficiencies increase from 56.12 to 67.45 % and from 67.51 to 83.83 % as temperature is increased due primarily to an increase in CO and H_2 concentrations enhanced by the Boudouard reaction. In contrast, cold and hot gas efficiencies decreased as equivalence ratio increase due to the decrease in CO and H_2 concentrations. This decrease is due to greater oxidation of CO to CO_2 and H_2 to H_2O as oxygen availability is increased. The heating value of producer gas increased with increasing temperature and decreased with increasing equivalence ratio for similar reasons as the cold and hot gas efficiencies.

Nomenclature

Symbol	Units	Description
HHV_{pine}	kJ/g	Specific higher heating value of pine
HHV_{char}	kJ/g	Specific higher heating value of char
HHV_s	kJ/g	Specific higher heating value of gas species s
m_{pine}^{in}	g	Mass input of pine to the control volume
$m_{O_2}^{in}$	g	Mass input of oxygen to the control volume
$m_{N_2}^{in}$	g	Mass input of nitrogen to the control volume
$m_{primary\ gas}^{out}$	g	Mass output of primary gas from the control volume
$m_{contaminants}^{out}$,	g	Mass output of contaminants from the control volume
m_{char}^{out},	g	Mass output of char from the control volume
$m_{liquid\ condensate}^{out}$	g	Mass output of liquid condensate from the control volume
c		Subscript denotation for carbon
$m_{pine,c}^{in}$	g	Mass input of carbon from pine
$m_{primary\ gas,c}^{out}$,	g	Mass output of carbon from primary gases
$m_{char,c}^{out}$	g	Mass output of carbon from char
$m_{liquid\ condensate,c}^{out}$	g	Mass output of carbon from liquid condensate
$\emptyset_{mass}$	%	Mass balance closure
$\emptyset_c$	%	Carbon balance closure
S		Gas species in primary gas
η_c	%	Carbon conversion efficiency
m_s^{out}	g	Mass output of the gas species s in primary gas
$m_{s,c}^{out}$		Mass output of carbon for carbon baring species s (*s* = CO, CO_2, CH_4, C_2H_2 and C_2H_4)
$w_{s,c}^{out}$		Mass fraction of carbon baring species (*s* = CO, CO_2, CH_4, C_2H_2 and C_2H_4)
N		Number of carbon in carbon baring species
MWs	g/gmol	Molecular weight of gas species s
$(E_{HHV})_{pine}^{in}$	kJ	Higher heating value of pine input stream
$(E_{HHV})_{primary\ gas}^{out}$	kJ	Higher heating value of the primary gas output stream
$(E_{HHV})_{char}^{out}$	kJ	Higher heating value of char output stream
$(E_{HHV})_{loss}^{out}$	kJ	Higher heating value unaccounted
$\eta_{cold\ gas}$	%	Cold gas efficiency
$\eta_{hot\ gas}$	%	Hot gas efficiency
$Q_{primary\ gas}^{out}$	kJ	Sensible heat of the primary gas output

Q_s^{out}	kJ	Sensible heat of species s in primary gas
T^{out}	K	Exit gas temperature
A, *B*, *C*, *D* and *E*		Coefficients of Shomate specific heat capacity equation
T'	K/1000	Temperature in the Shomate specific heat capacity equation
$C_{p,s,primary\ gas}$	kJ/g K	Specific heat capacity of gas species s
Q_v^{out}	MJ/m^3	Volumetric heating value of primary gas, reported on an air equivalent basis
ρ_s	g/cm^3	Density of the primary gas species s
$C_{pine,c}^{in}$	gC/g pine	Carbon mass fraction of pine as determined by ultimate analysis
$C_{char,c}^{out}$	gC/g char	Carbon mass fraction of char as determined by ultimate analysis
$C_{liquid\ condensate,c}^{out}$	mgC/g liquid	Carbon mass fraction of liquid condensate as determined by total organic carbon (TOC) analysis

References

(1) van der Drift, A.; van Doorn, J.;Vermeulen, J. W. Ten residual biomass fuels for circulating fluidized-bed gasification. *Biomass Bioenergy* 2001, 20, 45-56.

(2) Carpenter, D. L.; Bain, R. L.; Davis, R. E.; Dutta, A.; Feik, C. J.; Gaston, K. R.; Jablonski, W.; Phillips, S. D.;Nimlos, M. R. Pilot-Scale Gasification of Corn Stover, Switchgrass, Wheat Straw, and Wood: 1. Parametric study and comparison with literature. *Ind. Eng. Chem. Res.* 2010, 49, 1859-1871.

(3) Lysenko, S.; Sadaka, S.;Brown, R. C. Comparison of mass and energy balances for air blown and thermally ballasted fluidized bed gasifiers. *Biomass Bioenergy* 2012, 45, 95-108.

(4) Li, X. T.; Grace, J. R.; Lim, C. J.; Watkinson, A. P.; Chen, H. P.;Kim, J. R. Biomass gasification in a circulating fluidized bed. *Biomass Bioenergy* 2004, 26, 171 – 193.

(5) Campoy, M.; Gómez-Barea, A.; Vidal, F. B.;Ollero, P. Air–steam gasification of biomass in a fluidised bed: Process optimisation by enriched air. *Fuel Process. Technol.* 2009, 90, 677-685.

(6) Campoy, M.; Gómez-Barea, A.; Villanueva, A. L.;Ollero, P. Air−steam gasification of biomass in a fluidized bed under simulated autothermal and adiabatic conditions. *Ind. Eng. Chem. Res.* 2008, 47, 5957-5965.

(7) Hannula, I.;Kurkela, E. A parametric modelling study for pressurised steam/O2-blown fluidised-bed gasification of wood with catalytic reforming. *Biomass Bioenergy* 2012, 38, 58-67.

(8) Miccio, F.; Ruoppolo, G.; Kalisz, S.; Andersen, L.; Morgan, T. J.;Baxter, D. Combined gasification of coal and biomass in internal circulating fluidized bed. *Fuel Process. Technol.* 2012, 95, 45-54.

(9) Meng, X.; De Jong, W.; Fu, N.;Verkooijen, A. H. Biomass gasification in a 100 kWth steam-oxygen blown circulating fluidized bed gasifier: Effects of operational conditions on product gas distribution and tar formation. *Biomass Bioenergy* 2011, 35, 2910-2924.

(10) Burgess, D. R.; Afeefy, H. Y.; Liebman, J. F.;Stein, S. E. *Gas Phase Thermochemistry Data*. *In* NIST Chemistry WebBook; Mallard, W. G.; Linstrom, P. J. eds. NIST Standard Reference Database Number 69; National Institute of Standards and Technology: Gaithersburg, MD, 2005, Methane (http://webbook.nist.gov).

(11) Netherlands, E. R. C. o. t. Phyllis2 Database for biomass and waste. In Energy Research Center of the Netherlands.

(12) Cao, Y.; Wang, Y.; Riley, J. T.;Pan, W.-P. A novel biomass air gasification process for producing tar-free higher heating value fuel gas. *Fuel Process. Technol.* 2006, 87, 343-353.

(13) Bingyan, X.; Zengfan, L.; Chungzhi, W.; Haitao, H.;Xiguang, Z. Integrated Energy Systems in China - The Cold Northeastern Region Experience - Circulating fluidized bed gasifier for biomass. In Natural Resources Management and Environment Department, United Nation Food and Agricultural Organization: Rome, Italy, 1994.

(14) Zhou, J.; Masutani, S. M.; Ishimura, D. M.; Turn, S. Q.;Kinoshita, C. M. Release of Fuel-Bound Nitrogen during Biomass Gasification. *Ind. Eng. Chem. Res.* 2000, 39, 626-634.

(15) Lim, M. T.;Alimuddin, Z. Bubbling fluidized bed biomass gasification - Performance, process findings and energy analysis. *Renew. Energ.* 2008, 33, 2339-2343.

(16) Narvaez, I.; Orio, A.; Aznar, M. P.;Corella, J. Biomass Gasification with Air in an Atmospheric Bubbling Fluidized Bed. Effect of Six Operational Variables on the Quality of the Produced Raw Gas. *Ind. Eng. Chem. Res.* 1996, 35, 2110-2120.

Chapter 5
Vanadium Oxide Based Sorbents for Hydrogen Sulfide Adsorption

Abstract

Hydrogen sulfide removal from syngas is very important due to its severe poisoning effect on catalysts. It is also known to be a precursor for SOx formation and thus potentially harmful for the environment.

This chapter focuses on hydrogen sulfide removal using vanadium oxide based sorbents. Five sorbents (V_2O_5, 5 wt% ZnO/V_2O_5, 10 wt% ZnO/V_2O_5 and 10 wt% ZnO-10 wt% SrO/ V_2O_5) were investigated for H_2S removal. In the absence of syngas, V_2O_5 was an effective H_2S sorbent in temperature ranges of 50 to 350˚C. At 50˚C, H_2S was removed below detection limit by V_2O_5 for more than 5 days at 1500 ml/g h WHSV. As temperature increased and gas space velocity was increased to 12,000 ml/h g, the breakthrough time increased to 36, 95 and 140 min at 50, 150 and 250˚C, respectively for V_2O_5. Bulk V_2O_5 was less effective in H_2S removal when syngas constituents were introduced along with H_2S due to competitive adsorption of other syngas constituents as H_2S adsorption was not observed. However, subsequent ZnO and SrO impregnation to produce 10wt% ZnO/V_2O_5 and 10wt% ZnO-10wt% SrO/V_2O_5 improved the performance and increased the breakthrough time from 0 to 20 min in the presence of syngas constituents. This sorbent formula outperformed ZnO, commonly considered one of the best H_2S sorbent, at the same temperature. The following order was observed for sorbents: V_2O_5 < ZnO <

10 wt% ZnO/V_2O_5 < 10 wt% ZnO-10 wt% SrO/V_2O_5. XRD characterization of spent V_2O_5 sorbent interestingly revealed that adsorption rather than sulfidation is the mode of H_2S removal.

5.1 Introduction

Biomass gasification yields primary gases (CO, H_2, CO_2, CH_4) and contaminants (tar, NH_3, HCN, H_2S, COS, trace metals and various other minors compounds). Of all the sulfurous contaminant species, H_2S is the most abundant. Its abatement is important in gas cleanup to reduce *i*) human health hazards as short (30 to 60 min) exposure to concentration in the range of 500 to 700 ppm can lead to death[1], *ii*) environmental concerns because sulfur species from syngas act as precursors to the formation of SOx, the primary cause of acid rain, *iii*) material corrosion and *iv*) catalyst deactivation by poisoning. To avoid catalyst deactivation, its removal to part per billion levels is necessary particularly if syngas is used as a feed in fuel synthesis. Current commercial processes for the removal of H_2S from syngas involve wet processes (i.e. scrubbing) where sulfur impurities are removed by scrubbing syngas in chemical or physical solvents as discussed previously in 0. While the conventional wet scrubbing approach can achieve high sulfur removal efficiency (>99 %), they result in an overall decrease in efficiency due to gas cooling.

Dry processes for H_2S removal from syngas rely on sorbents which can be operated at higher temperature thus improving the process efficiency. Common sorbents are metal oxides and operate in two distinct fashions: chemical reaction by sulfidation to convert metal oxides to metal sulfides and adsorption.

Hydrogen sulfide removal from coal derived syngas has been extensively studied with various metals oxides.[2, 3] Based on thermodynamic modeling, it has previously been established that Ca,

Sr, Ba, V, Mo, W, Mn, Fe, Co, Cu and Zn could produce sorbents with high sulfur adsorption capacity in their oxide form.[4] Of all these elements, Zn, Cu and Fe based catalysts have been the most studied for sulfur removal with zinc and copper based sorbents regarded as the most effective. Based on a literature survey, among the potential sorbents listed above, oxides of Sr and V have not received considerable attention as sorbents for H_2S. Therefore, in this study, ZnO, SrO and V_2O_5 based sorbents have been selected for testing for H_2S removal. Five catalysts (V_2O_5, 5wt% ZnO/V_2O_5, 10wt% ZnO/V_2O_5 and 10 wt% ZnO-10 wt% SrO/V_2O_5) were investigated for H_2S removal in the presence of an inert gas or a gas mixture that emulate the composition of biomass derived syngas.

5.2 Materials and Methods

5.2.1 Catalyst Synthesis and Characterization

Vanadium oxide (V_2O_5) was purchased from Alfa Aeasar (Alfa Aesar, Ward Hill, Massachusetts). Since the catalyst obtained from Alfa Aeasar had a narrower range of particle size, it was first pelletized using an IKA pellet press (Model C21, IKA Works Inc., Wilmington, North Carolina). In order to enhance adhesion, minor amount of water was added to produce a paste which resulted in well-formed pellets. The pellets were then dried in an oven at 105°C overnight before they were crushed in a mortar. Crushed pellet fragments were subsequently sieved into three particle size groups: 0.18 mm < d_1 < 0.30 mm, 0.30 < d_2 < 0.42, 0.42 < d_3 < 0.85 using four different sieve sizes (20, 40, 50 and 80 mesh size). Zinc oxide (ZnO) was obtained in the form of $ZnO.6H_2O$ from Sigma Aldrich (Sigma Aldrich, St. Louis, MO).

Catalysts of ZnO supported on V_2O_5 were synthesized in the following manner. For a given zinc (Zn) loading (*i.e.* 5 and 10 % loading), the appropriate amount of ZnO is measured and dissolved in water using a relative ratio of 1g of total catalyst in 10 ml of water. The mixture was heated to 80°C under constant stirring to ensure complete dissolution of ZnO. This step was followed with the addition of V_2O_5, still under constant stirring for at least 15 minutes. After uniform mixing is satisfactorily observed visually, the paste is dried in an oven at 200°C for 2h. ZnO and SrO supported on V_2O_5 (10 wt% ZnO-10 wt% SrO/V_2O_5) were synthesized using a similar procedure as that used for ZnO/V_2O_5 catalysts with ZnO.6H_2O and SrO dissolved in water simultaneously before V_2O_5 was added. All catalysts were calcined in bulk at 500°C for 5h in a muffler furnace. Figure 5.1 and Figure 5.2 show the synthesis flow diagram and SEM images of calcined sorbents. All catalysts were characterized for elemental chemical composition using a Zeiss EVO 50 SEM-EDS (Carl Zeiss AG, Oberkochen, Germany). The sample preparation consists of evenly dispersing the sorbent on a double sided carbon tape glued to a sample holder. The sample dispersion was carried so as to achieve monolayer coverage. SEM imaging was performed at a working distance between 8.5 and 9 mm and an electron gun voltage of 20 kV. For EDS analysis, the sample was divided in four quadrants with four runs for each sorbent. BET surface area and pore volume analysis was performed by physisorption using an Autosorb-iQ gas sorption instrument (Quantachrome Instruments, Boynton Beach, FL). The sorbent samples were heated to 80˚C at 5˚C/min to 350˚C and outgassed at 350˚C for 10 h prior to initiating the physorption experiments using a 20 points adsorption and desorption profile.

The molecular structure of fresh and spent sorbents were determined using an X-ray diffractometer (XRD) equipped with a lynxeye detector side filtered Cu Kα radiation (λ = 1.5406 Å), a 30 KV and 10 mA x-ray generator (D2 Phaser model, Bruker Corporation, Billerica, MA). The diffractograms were registered in the 2θ range between 10° and 90° with a step time of 0.4s and total step of 5000. Prior to the analysis, all samples were finely grounded in a mortar, placed in the sample holder and positioned in the chamber of the diffractometer. The diffraction patterns were analyzed using Crystallography Open Database (Rev 44788 2013-01-07).

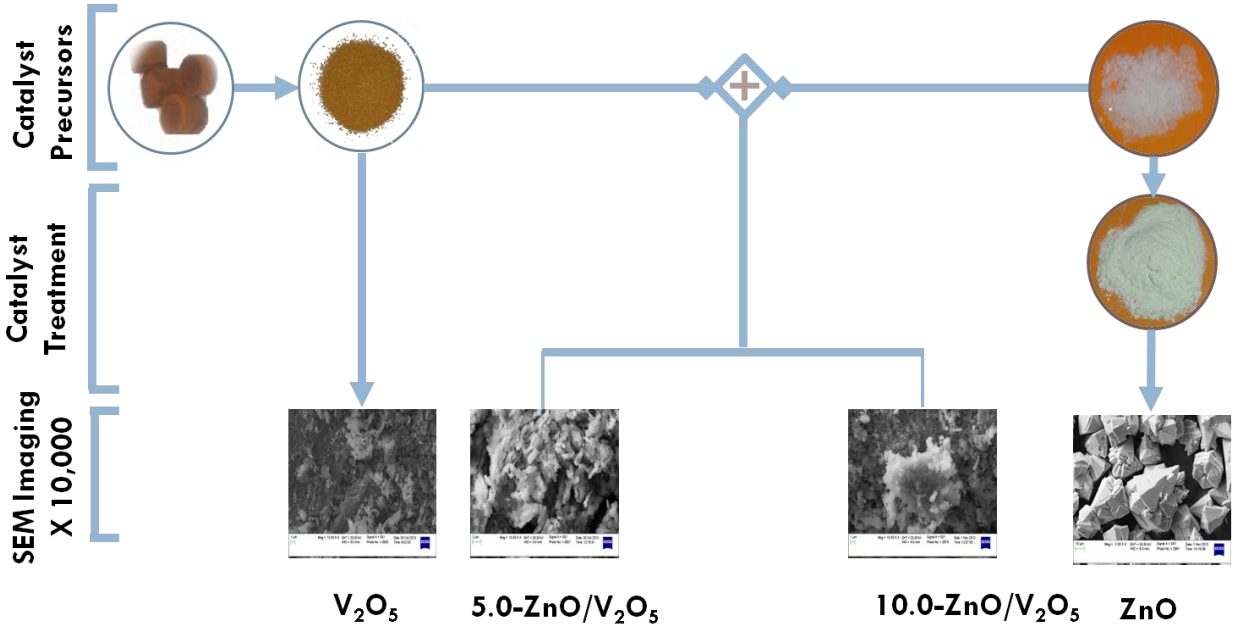

Figure 5.1. Synthesis flow diagram of ZnO supported V_2O_5 sorbents and SEM images at 10000 magnification

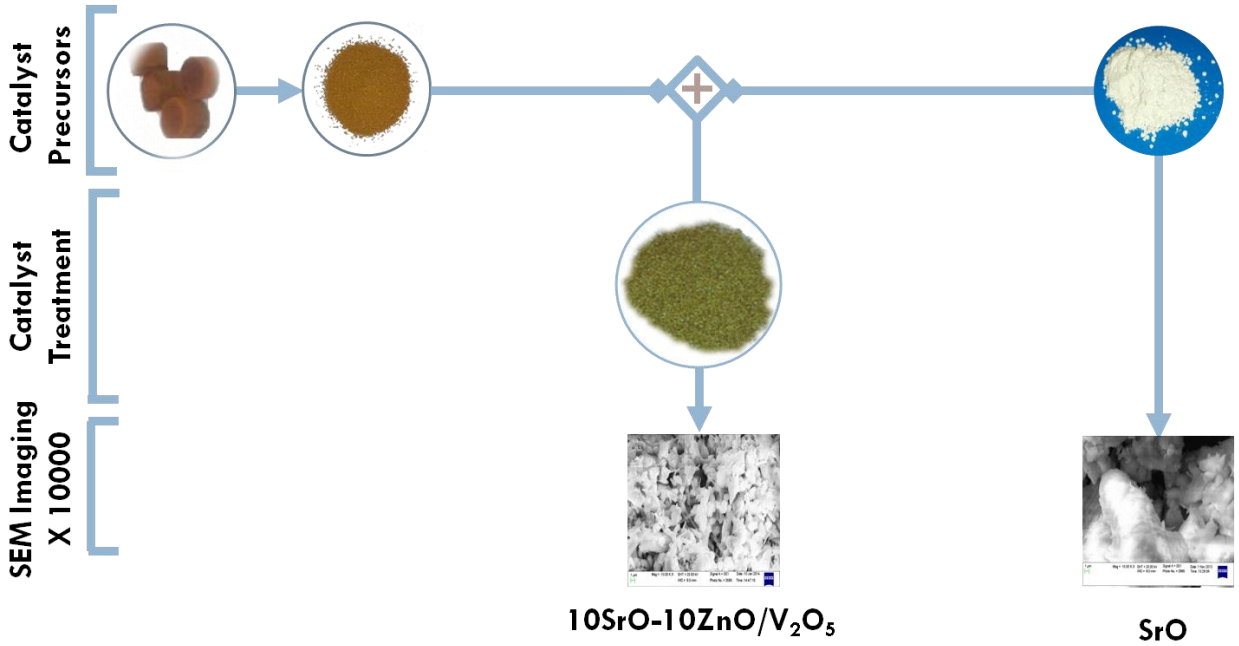

Figure 5.2. Synthesis flow diagram of SrO and ZnO supported V_2O_5 sorbents and SEM images at 10000 magnification

5.2.2 Experimental Setup and Sorption Experiments

The fixed-bed reactor system employed in the removal of H_2S is shown in Figure 5.3. The system consists of a gas cylinder, mass flow controller, a tubular reactor maintained in furnace (Lindberg Blue M model, Thermo Scientific, Waltham, MA), a bypass loop utilized for GC calibration and GC for gas analysis. The analytical instrument was an Agilent GC (Model 7890 A, Agilent, Santa Clara, CA) equipped with a gas sampling valve, a flame photometric detector (FPD) and a CP-Sil 8 CB column with dimensions as 25 m x 0.25 mm x 0.25 µm (CP-Sil 8 CB, Agilent, Santa Clara, CA). The gas sampling valve, GC inlet and detector temperature were maintained at 100, 250 and 300^{o}C, respectively while the GC oven temperature was maintained at 30^{o}C for 5 min. The fixed bed column was made of quartz with 0.45 inch internal diameter and

0.50 inch external diameter. The sorbent bed was maintained in the reactor by two quartz wool porous plugs. In order to measure the bed temperature, the thermocouple was inserted from the bottom the quartz reactor, through the bottom porous plug and into the middle of the bed so as to obtain a representative sorbent temperature. The gas mixtures were used in the present study as shown in Table 5.1. In order to ensure that experiments were conducted in the absence of mass transfer, external and internal mass transfer limitations studies were conducted. These studies were carried out using gas mixture #1 at 250˚C using 50, 75 and 100 ml/min flow rates and d_1, d_2 and d_3 particle size ranges.

The breakthrough concentration is typically defined as 1% of the inlet H_2S concentration in sulfidation experiments. Therefore, the breakthrough capacity was chosen as 1.02 ppmv of H_2S in inert gas and 1.10 ppmv in syngas. The breakthrough time is the time at which outlet concentration of H_2S exceeds that of the breakthrough concentration.

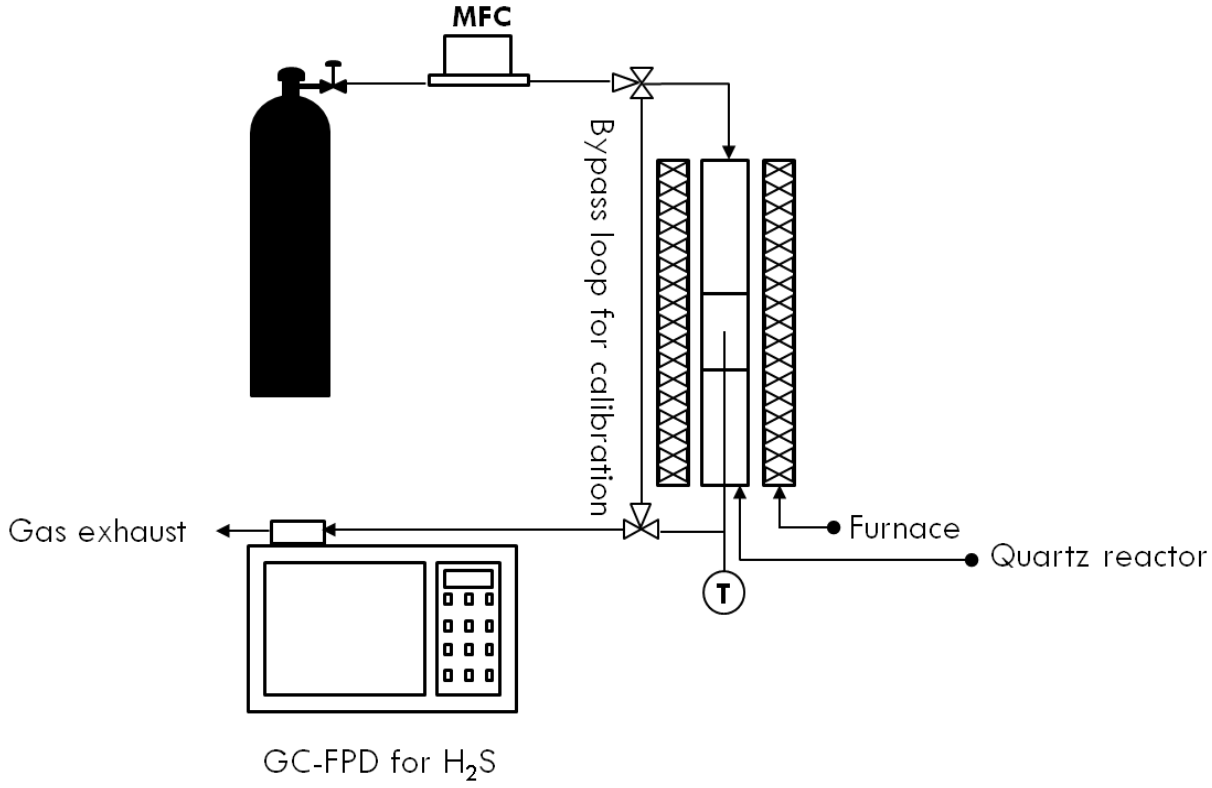

Figure 5.3. Schematic of fixed bed experimental setup for H_2S removal

Table 5.1. Composition of gas mixtures tested in H_2S removal

Gas mixtures	*#1*	*#2*
Main syngas constituents, vol %		
CO	0	30
CO_2	0	5
CH_4	0	5
H_2	0	30
Inert	balance	balance
Contaminant, ppmv		
H_2S	*102*	*110*

Mass transfer limitation was assessed by considering two distinct transport phenomena: external (also called bulk phase or interphase) mass transfer or diffusion limitation and internal (also called intraphase) mass transfer or diffusion limitation. External mass transfer limitation is due to the presence of a concentration gradient at the boundary layer of the catalyst and the bulk phase. It is experimentally determined by varying the gas flow rate and catalyst amount while maintaining the gas space velocity constant as show in 5.4.

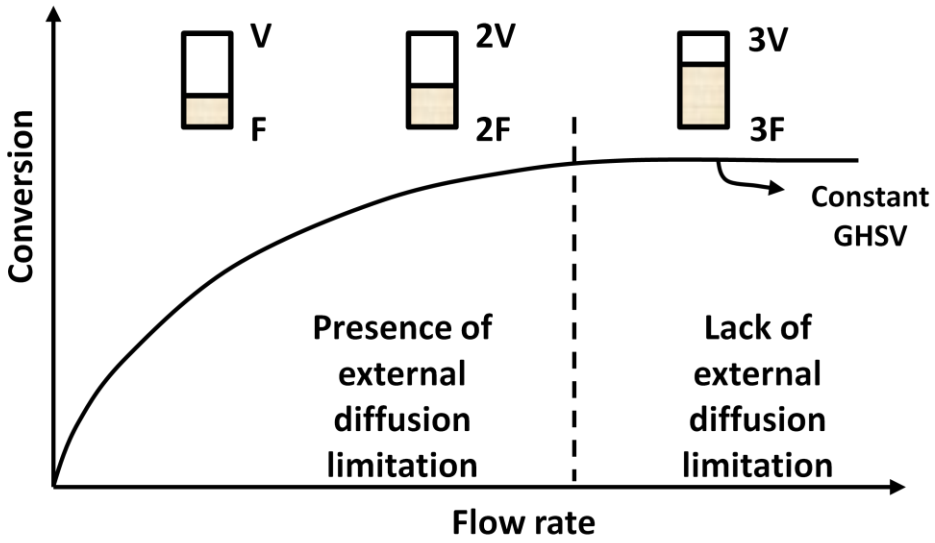

Figure 5.4. External mass transfer elucidation assessment. Adapted from Perego *et al*.[5]

Internal diffusion limitation arises due the presence of concentration gradient in the catalysts. The presence of concentration gradient can be minimized by decreasing the catalysts diameter. As such, minimal internal mass transfer limitation is achieved by reducing the particle diameter while maintaining a constant gas space velocity as illustrated in Figure 5.5. The fraction of

particle size beyond which no increase in conversion is observed is the largest particle size fraction on which reaction can be carried on in order to avoid confounding effect introduced by internal mass transfer.[5]

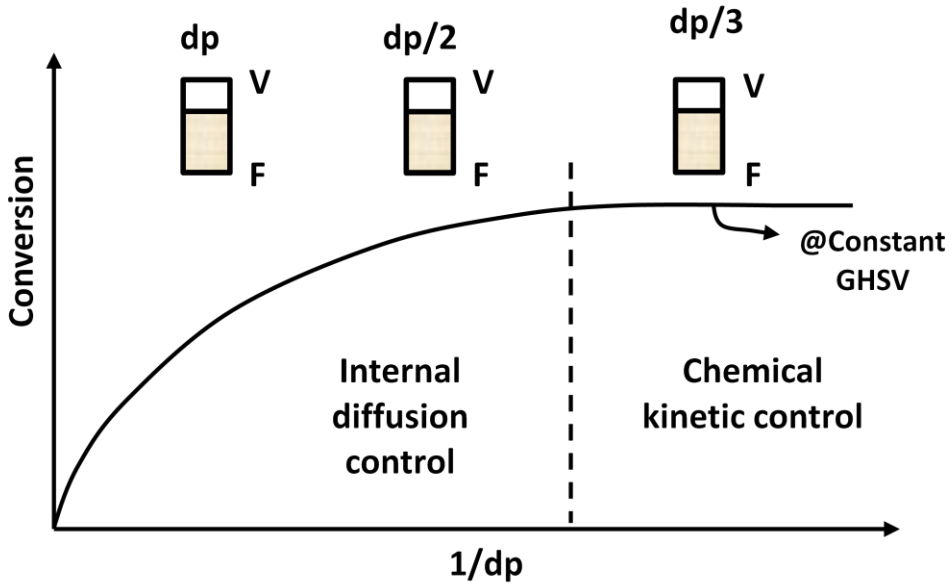

Figure 5.5. Internal mass transfer assessment. Adapted from Perego *et al.* [5]

In this study, the external mass transfer limitation was assessed using flow rates and catalyst masses of 50 ml/min and 0.25 g, 75 ml/min and 0.375 g and 100 ml/min and 0.50 g. The lowest limit of catalyst mass, 0.25 g, was chosen in order to ensure that the sorbent height was appropriate to avoid channeling. For catalyst mass below 0.25 g, it can visually be observed that uniform coverage is not achieved and will thus result in bypassing at locations. For internal mass transfer assessment, d_1, d_2 and d_3 particle size fractions, defined earlier, were studied.

5.3 Results and Discussion

5.3.1 Sorbent Characterization

5.3.1.1 Elemental Composition

The elemental composition of all four sorbents were determined by SEM-EDS and shown in Table 5.2. In addition, the SEM images of bulk V_2O_5, ZnO and SrO as well as ZnO and SrO supported on V_2O_5 are shown in Figure 5.6 and Figure 5.7. For zinc supported on V_2O_5, the content of Zn increased rather linearly with increasing with loading during the wetness impregnation. For zinc and strontium supported on V_2O_5, the elemental composition of Sr, as measured by SEM-EDS, was slightly higher than expected based on 10 wt % loading suggesting potential localized agglomeration of SrO on the support and poorer dispersion relative to ZnO supported catalysts. The poor dispersion for SrO is likely due to its poor solubility in the aqueous incipient wetness solvent which might have resulted in uneven deposition as SrO settled down.

Table 5.2. Elemental composition of catalysts by SEM-EDS

	Elements, wt %			
Mean	V	O	Zn	Sr
V_2O_5	53.47 ± 2.30	46.53 ± 2.30	--	--
5.0 wt% Zn/V_2O_5	51.33 ± 2.44	43.9 ± 2.28	4.76 ± 0.51	--
10.0 wt% Zn/V_2O_5	51.90 ± 2.45	38.69 ± 2.61	9.41 ± 0.41	--
10 wt% ZnO-10 wt% SrO/V_2O_5	31.48 ± 2.01	44.03 ± 4.43	13.78 ± 1.58	10.71 ± 1.23

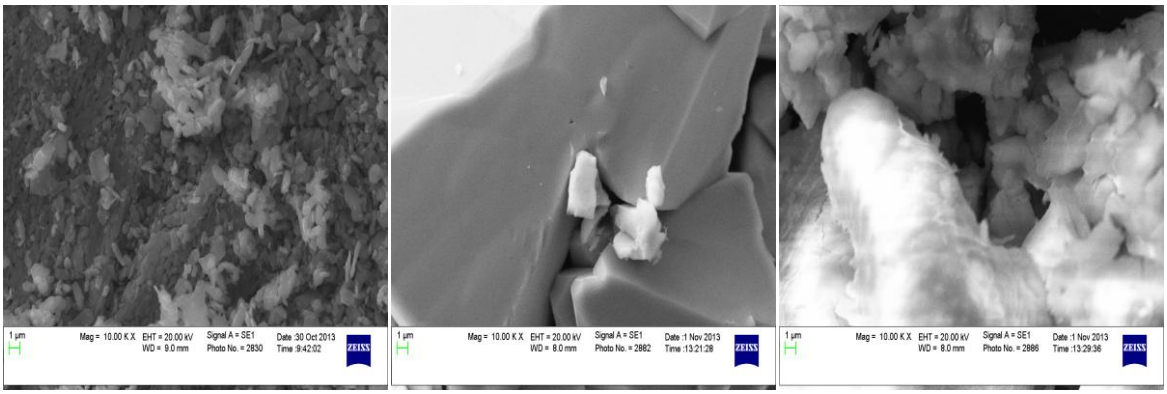

V_2O_5 ZnO SrO

Figure 5.6. SEM images of V2O5, ZnO and SrO at 10,000 magnification

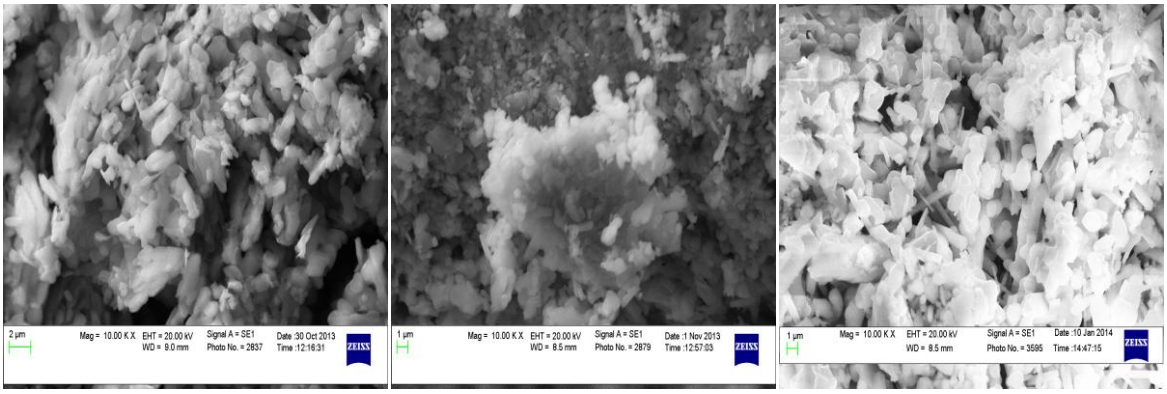

5 wt % ZnO/V_2O_5 10 wt % ZnO/V_2O_5 10 wt% ZnO-10 wt% SrO/V_2O_5

Figure 5.7. SEM images of 5 wt% ZnO/V_2O_5, 10 wt% ZnO/V_2O_5 and 10 wt% ZnO-10 wt% SrO/ V_2O_5 at 10,000 magnification

5.3.1.2 Sorbent Surface Area

The BET surface area and pore volume of V_2O_5, ZnO as well as ZnO and SrO supported on V_2O_5 are presented in Table 5.3. Bulk V_2O_5 had a surface area of 3.3 m^2/g whereas ZnO had a surface area of 3.1 m^2/g. The surface areas of bulk V_2O_5 and ZnO are similar to other values

reported where surface areas were 6 m^2/g[6] and 4.8 m^2/g[7] for V_2O_5, 2.5 m^2/g for ZnO[8]. In addition, the total pore volume of bulk V_2O_5 and ZnO were 2.50 10^{-2} and 1.1 10^{-2} cm^3/g, respectively. Sorbents of ZnO supported on V_2O_5 had lower surface areas when compared to bulk V_2O_5 with BET surface areas of 1.4 and 1.9 m^2/g and for 5 and 10 wt % loading. The total pore volume of ZnO supported V_2O_5 sorbents were respectively 2.18 10^{-2} and 2.97 10^{-2} cm^3/g, higher than ZnO but noticeably lower than V_2O_5. 10 wt% SrO-10 wt% ZnO/V_2O_5 had lower surface area (1.3 m^2/g) and total pore volume (1.50 10^{-2} cm^3/g) than all V_2O_5 supported ZnO sorbents.

Table 5.3. Physical properties of sulfidation catalysts

	BET surface area m^2/g	***Pore volume 10^2 cm^3/g***
V_2O_5	3.3	2.50
ZnO	3.1	1.10
5.0 Zn/V_2O_5	1.4	2.18
10.0 Zn/V_2O_5	1.9	2.97
10ZnO-10SrO/V_2O_5	1.3	1.50

5.3.1.3 X-ray Diffraction Analysis

In order to ascertain the presence or absence of vanadium sulfides, the fresh V_2O_5 sorbent was analyzed and its diffraction pattern is shown in Figure 5.8. As expected, the database search of the diffraction pattern of V_2O_5 did not show the presence of any other forms of vanadium besides

V_2O_5. Li and Yan[9] reported a similar diffraction pattern with sharp diffraction peaks observed between 10 and 35 2θ angles. Figure 5.9 shows the diffraction patterns of ZnO supported catalysts as well the patterns of pure ZnO and V_2O_5. XRD patterns of 2.5 and 5.0 wt% ZnO/V_2O_5 showed very similar pattern as those of V_2O_5. Although the presence of ZnO was confirmed by SEM-EDS earlier, ZnO was not detected in the XRD analysis on these catalysts in SEM-EDS elemental analysis. It has been suggested in another study that lower loading of CuO on Al_2O_3 did not yield any diffraction pattern for CuO presumably due to high dispersion on the support.[10] It is therefore likely that a similar phenomenon occurred in this study.

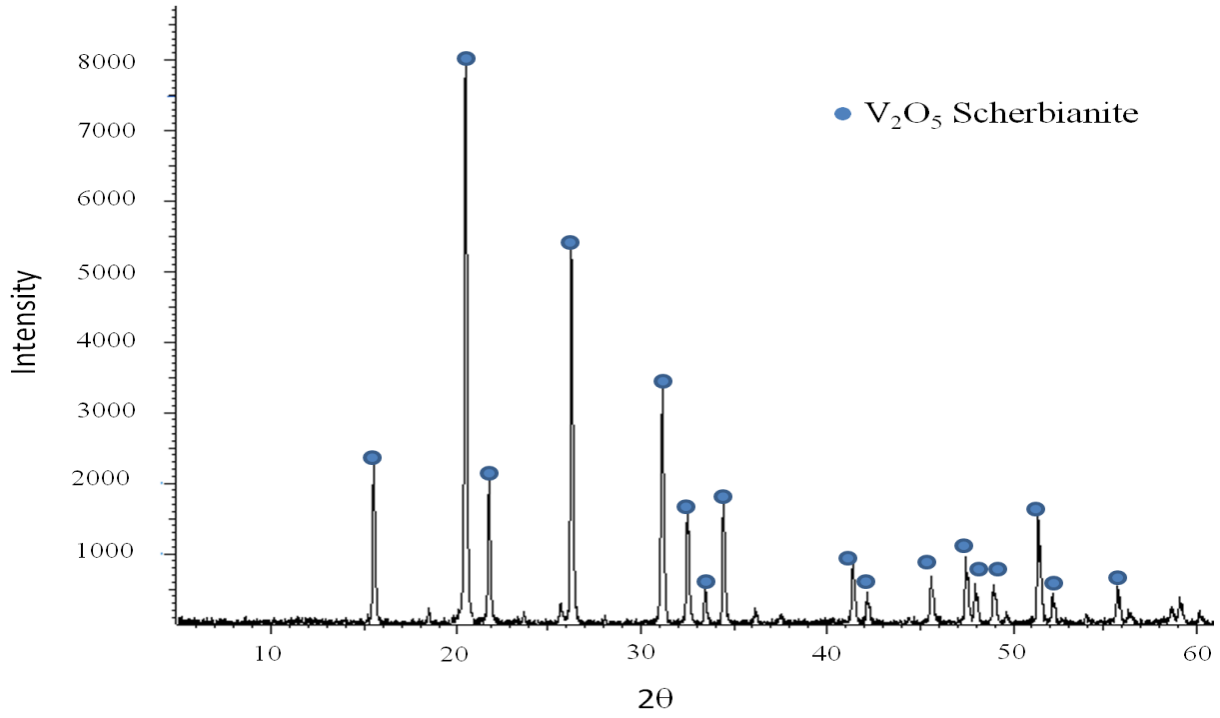

Figure 5.8. XRD diffraction pattern of V_2O_5

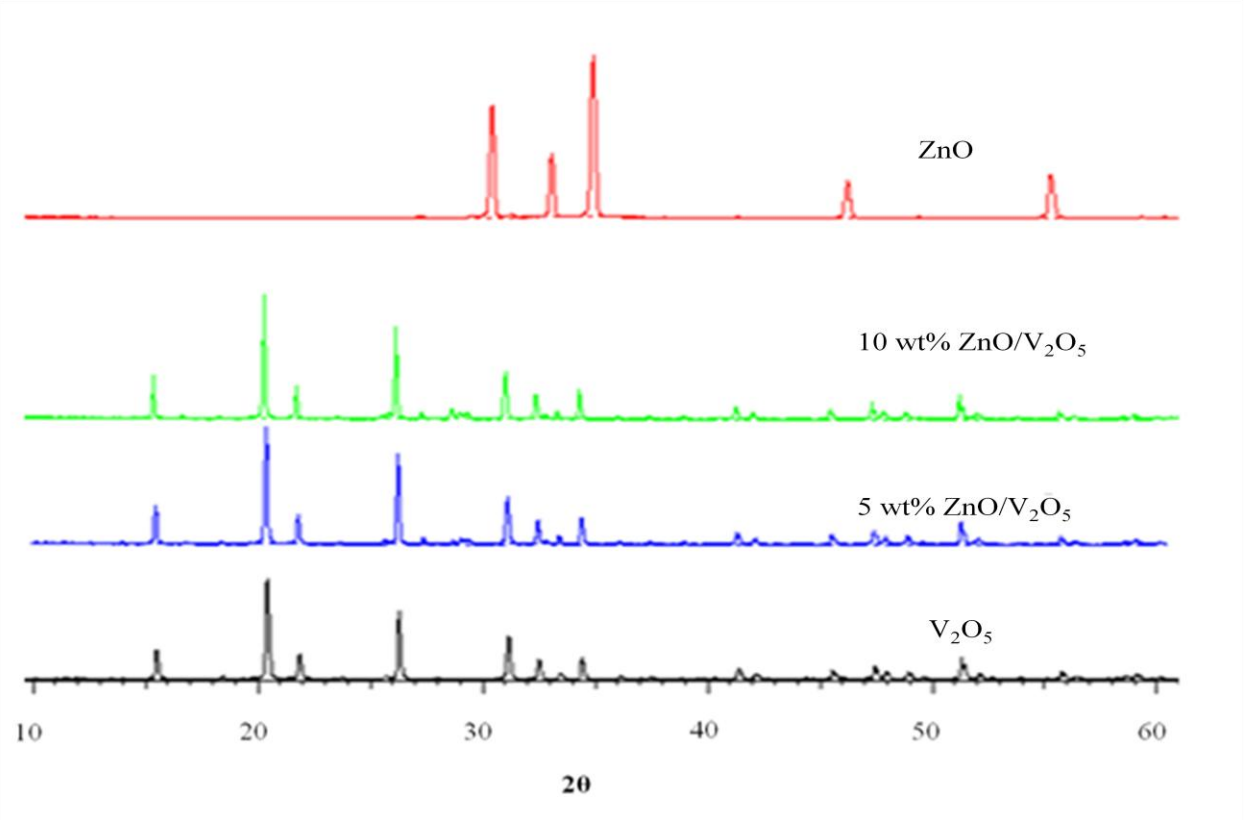

Figure 5.9. XRD pattern for fresh ZnO and ZnO supported V_2O_5 sorbents

5.3.3 H_2S Sorption

Mass transfer limitation was assessed on V_2O_5 as a reference and the suitable particle size fraction and flow rate was used in all subsequent sorption experiments.

0.18 mm < d_1 < 0.30 mm 50-80 mesh	0.30 mm < d_2 < 0.42 mm 40-50 mesh	0.42 mm < d_3 <- 0.85 mm 20-40 mesh

Figure 5.10. Particle sizes for V_2O_5 used for internal mass transfer limitation investigation

Figure 5.10 shows the representation of the different particle size fractions used in internal mass transfer assessment. External mass transfer experiments indicated that the three flow rates resulted in similar breakthrough time as shown in Figure 5.11. While the breakthrough curves had a similar trend at 75 ml/min and 100 ml/min, a higher H_2S removal was observed at a lower flow rate (50 ml/min) and sorbent bed mass (0.25 g). As there were significant differences between the three flow rates and mass of catalysts chosen, the middle conditions (F = 75 ml/min, 0.375 g of sorbent) was selected for the next set of experiments to minimize sorbent usage while avoiding a shallow bed that might lead to bypassing. It was visually observed when sorbent mass of less than 0.25 g was used in a 2 inch OD quartz reactor, there exist gaps in the bed which will cause the sorbate bypass.

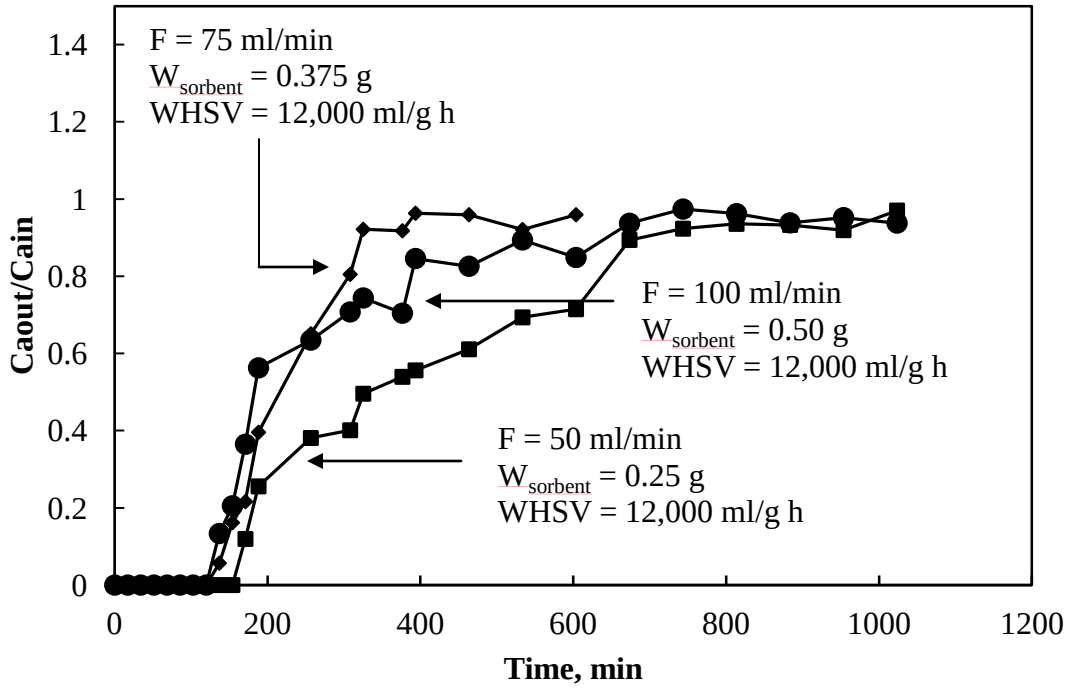

Figure 5.11. External mass transfer limitation for V_2O_5 at 250°C, WHSV = 12,000 ml/h g and particle size fraction between 0.18 mm and 0.30 mm.

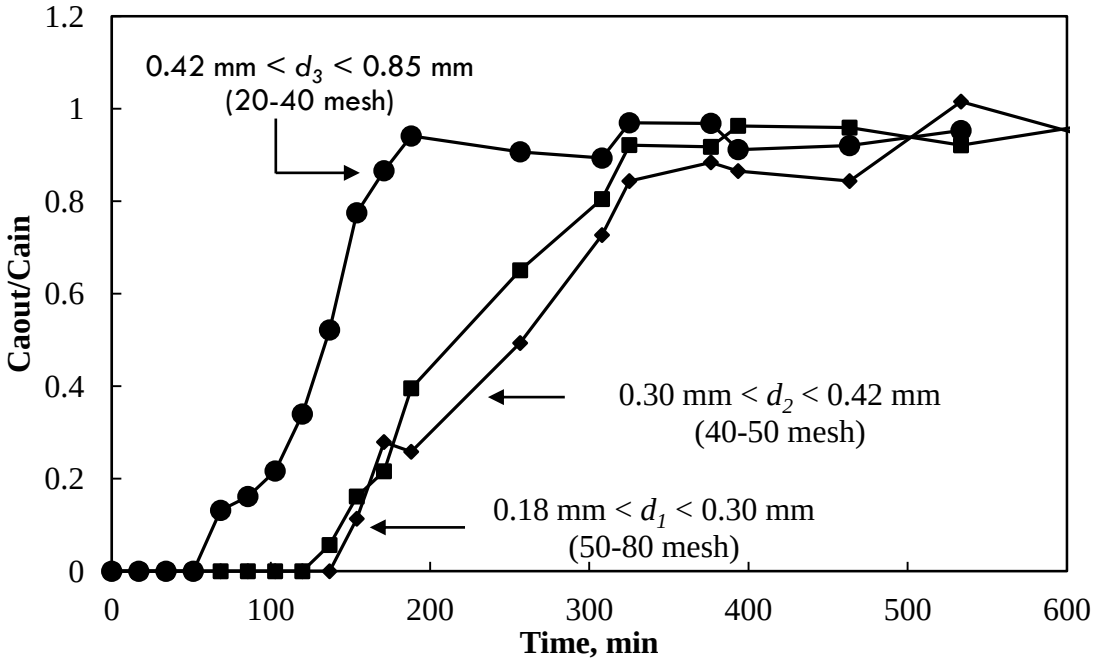

Figure 5.12. Internal mass transfer limitation for V_2O_5 at 250°C and WHSV = 12,000 ml/h g

The particle size and thus the internal diffusion had a great impact on the sorption capacity as illustrated in Figure 5.12. Particle sizes between 0.42 and 0.85 mm resulted in lower breakthrough time than d_1 and d_2 fractions. The difference between d_1 and d_2 is minimal. Nonetheless, the d_1 particle size fraction was chosen for the subsequent sorption experiments.

5.3.3.1 H_2S Sorption in the Absence of Syngas Constituents

The sulfur removal capacity of V_2O_5 catalysts were tested and compared to that of ZnO which is one of the most effective sorbent for sulfur removal. In several preliminary screening tests, it was observed that H_2S removal below breakthrough concentration can be carried on V_2O_5 for more

than 5 days at lower space velocity before experiment was terminated (WHSV = 1500 ml/g h, 1.0 g catalyst and 25 ml/min H_2S/Ar flow rate) at 50°C. As it is not practical, from the point of view of time, to carry out such long experiments, the space velocity was increased and temperature dependent experiments were carried out to determine the maximum temperature at which a breakthrough concentration of less than 1 ppmv can be obtained.

Figure 5.13 shows the breakthrough times of V_2O_5 at 50, 150, 250 and 350°C as well as the breakthrough times of ZnO at 350 and 500°C. The breakthrough times of V_2O_5 were 36, 95 and 140 min at 50, 150 and 250°C at 12,000 ml/h g WHSV, respectively. However, at 350°C, the minimal H_2S exit concentration that can be achieved was 8.52 ppmv with a breakthrough time of 171 min. As this outlet H_2S concentration exceeds the breakthrough concentration of 1 ppmv, subsequent sorption experiments were carried out at 250°C.

In contrast, ZnO achieved H_2S exit concentration below 1 ppmv with a breakthrough time of 162 min at 350°C. Further increase in temperature to 500°C resulted in an increase in the breakthrough time from 162 to 198 min. The most comparable study to the present work was carried by Rosso and coworkers[11] who carried out desulfurization experiments with 100 ppmv of H_2S on ZnO activated at different temperatures, from 300 to 600°C. Breakthrough times of 20 min or less were reported at 250°C for ZnO catalysts activated at 500°C in air. Other low temperature sulfidation studies with higher H_2S concentration were also reported.[12, 13] A mixed oxide sorbent of copper and vanadium was investigated for desulfurization using a mixture

containing 1 vol % H_2S and helium at 300˚C and a breakthrough times of 35 and 45 min were reported.[12, 13]

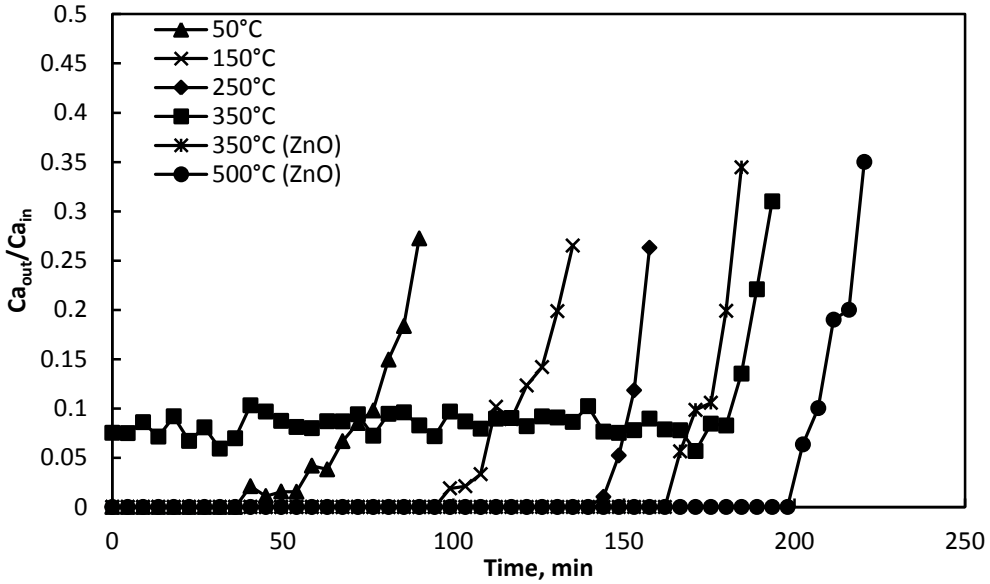

Figure 5.13. Effect of temperature on H_2S removal on ZnO and V_2O_5 at temperature ranging from 50˚C to 500˚C and WHSV = 12,000 ml/h g

5.3.3.2 H_2S Sorption in the Presence of Syngas Constituents

As it is desired to carry out gas cleanup at high temperature, the highest effective temperature from the previous section was chosen for H_2S removal in the presence of syngas. The typical sigmoid breakthrough curve for sulfur removal was not observed for V_2O_5 in the presence of syngas as seen in Figure 5.14. Nonetheless, H_2S removal was observed for V_2O_5 until saturation at 10 min resulting in a sorbent saturation capacity of 0.84 mg S/g sorbent. The decrease in H_2S adsorption, when syngas was used as a carrier, was attributed to competitive adsorption of

syngas constituents such as CO, CO_2 and CH_4 on the sorbent. At the same condition, ZnO achieved a breakthrough time of 2.4 min and sorbent saturation capacity of 9.01 mg/g sorbent. In order to improve the effectiveness of V_2O_5 in the presence of syngas, V_2O_5 was loaded with ZnO. ZnO loading of 5 and 10 wt% on V_2O_5 resulted in increasing saturation sorbent saturation capacities from to 0.84 mg S/g sorbent for V_2O_5 to 6.09 and 5.50 mg S/g sorbent, respectively. In contrast to V_2O_5 and 5 wt% ZnO/V_2O_5, ZnO, 10 wt% ZnO/V_2O_5 and 10 wt% SrO-10 wt% ZnO/V_2O_5 all exhibited typical sulfur removal sigmoid breakthrough curves with the breakthrough time increasing in the following order: ZnO < 10 wt% ZnO/V_2O_5 < 10 wt% ZnO-10 wt% SrO/V_2O_5. In coal derived syngas sulfidation experiments, ZnO based sorbents were reported to achieve higher sorption capacity when higher H_2S concentrations.[14, 15] For 10 wt% ZnO-10 wt% SrO/V_2O_5, the sorbent capacity is 8.12 mg S/g sorbent which is higher than the saturation capacity of 10 wt% ZnO/V_2O_5 indicating that SrO contributed to H_2S adsorption.

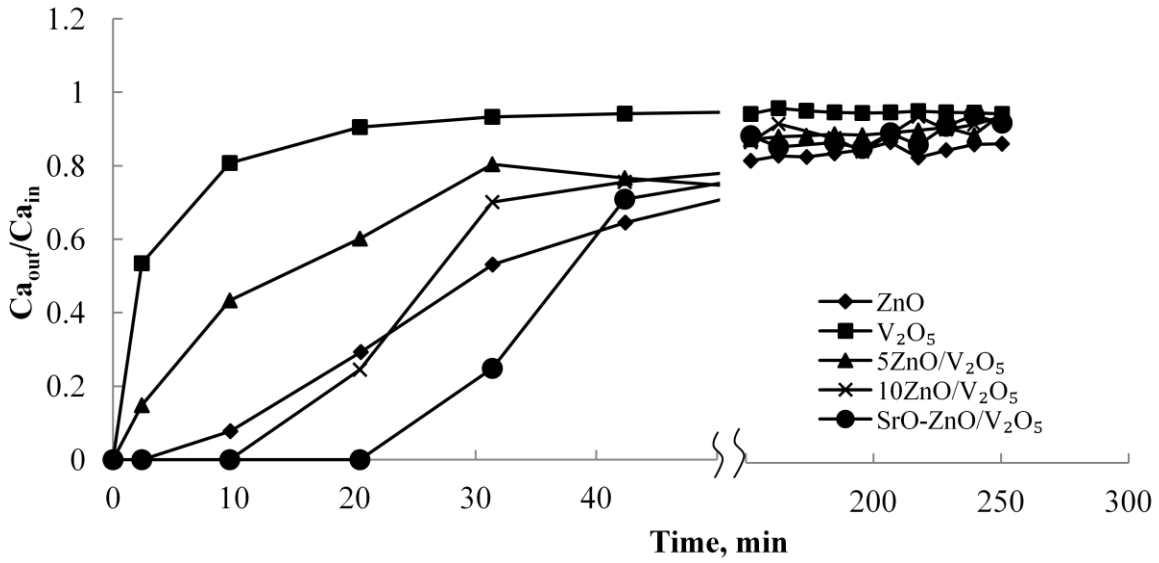

Figure 5.14. Effect of temperature on H_2S removal in the presence of syngas constituents for V_2O_5, ZnO and ZnO supported on V_2O_5 at 250^oC and WHSV = 12,000 ml/h g

At present, no study was found focusing on the removal of H_2S in the presence of syngas constituents at concentrations and temperatures of interest in this study for comparison (< 100ppmv H_2S and < 250°C). However, several studies have been carried out with higher H_2S concentrations (> 1 vol % H_2S) in hot gas cleanup temperature ranges. Desulfurization of a syngas mixture containing 1 vol% was carried out on Ni-Zn/Al_2O_3, Fe-Zn/Al_2O_3 and Co-Zn/Al_2O_3 sorbents at 650°C and GHSV of 5000 h^{-1}.[14] The authors reported breakthrough times ranging between 250 and 450 min and the occurrence of metal oxide sulfidation. Zheng and coworkers reported a breakthrough time of 75 min on CeO_2 at 800°C in for a mixture containing H_2S (1 vol %) and H_2 (10 vol%).[16] The breakthrough times reported in these studies are higher

than values observed in this study. This difference is attributed to favorable kinetics at higher temperature.

5.3.4 Spent Sorbent Characterization

X-ray diffraction (Figure 5.15) and SEM-EDS analyses were carried out on fresh and spent V_2O_5 catalysts to verify the formation or lack thereof of vanadium sulfides.

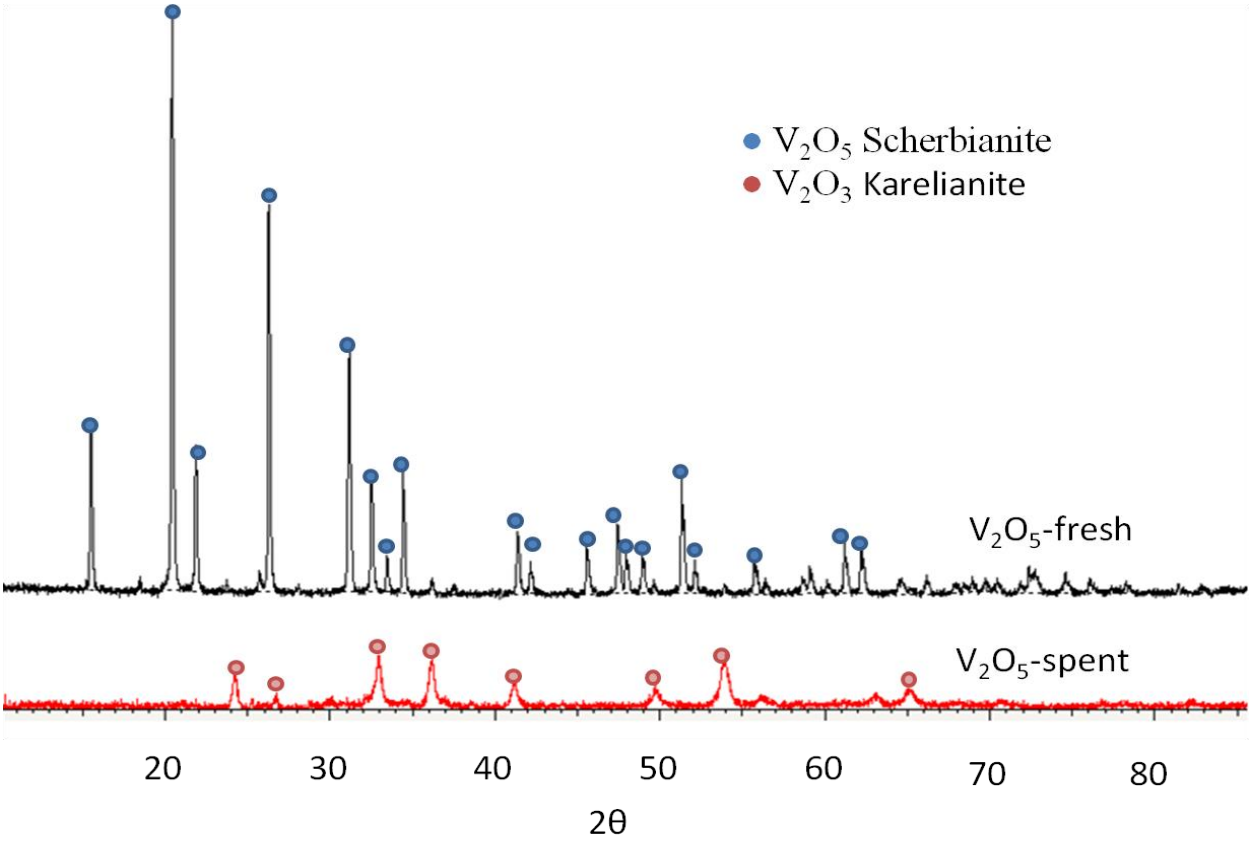

Figure 5.15. XRD patterns of spent V_2O_5 from H_2S removal from syngas

It was observed that V_2O_5 was reduced to V_2O_3 in the presence of syngas. However, forms of vanadium sulfide were not detected. However, SEM-EDS analysis indicates that 0.20 wt% S was

present in spent V_2O_5, it suggesting that H_2S removal occurred by absorption rather sulfidation. Akyurtlu *et al.* [17] also observed that bulk vanadium oxide did not form any bulk vanadium sulfide. In comparison, chemisorption capacity of TiO_2 is 0.25 mgS/g TiO_2, lower than the saturation sorption capacity of 0.84 mgS/gV_2O_5 achieved in this study.[18]

5.4 Conclusions

This chapter investigated hydrogen sulfide removal using vanadium oxide based sorbents. Five sorbents (V_2O_5, 5 wt% ZnO/V_2O_5, 10 wt% ZnO/V_2O_5 and 10 wt% ZnO-10 wt% SrO/V_2O_5) were investigated for H_2S removal. In the absence of syngas, V_2O_5 was an effective H_2S sorbent in temperature ranges of 50 to 250˚C achieving breakthrough concentrations of less than 1 ppm. At 50˚C, H_2S was removed below detection limit by V_2O_5 for more than 5 days at 1500 ml/g h WHSV. As temperature increased and gas space velocity was increased to 12,000 ml/h g, the breakthrough time increased to 36, 95 and 140 min at 50, 150 and 250˚C, respectively for V_2O_5. Bulk V_2O_5 was less effective in H_2S removal when syngas constituents were introduced along with H_2S due to competitive adsorption of other syngas constituents as H_2S adsorption was not observed. However, subsequent ZnO and SrO impregnation to produce 10 wt% ZnO/V_2O_5 and 10 wt% ZnO-10 wt% SrO/V_2O_5 improved the performance and increased the breakthrough time from 0 to 20 min in the presence of syngas constituents. This sorbent formula outperformed ZnO, commonly considered one of the best H_2S sorbent, at the same temperature. The following order was observed for sorbents: V_2O_5 < ZnO < 10 wt% ZnO/V_2O_5 < 10 wt% ZnO-10 wt%

SrO/V_2O_5. XRD characterization of spent V_2O_5 sorbent interestingly revealed that adsorption rather than sulfidation is the mode of H_2S removal. This mechanism of removal can be potentially advantageous for sorbent regeneration as H_2S is merely adsorbed on the sorbent.

References

(1) U.S Occupational Safety and Health Administration (OSHA). Health Hazards: Hydrogen Sulfide. https://www.osha.gov/SLTC/hydrogensulfide/hazards.html (accessed April 9th, 2014).

(2) Alonso, L.; Palacios, J.; Garcıa, E.;Moliner, R. Characterization of Mn and Cu oxides as regenerable sorbents for hot coal gas desulfurization. *Fuel Process. Technol.* 2000, 62, 31-44.

(3) Liu, B.; Wan, Z.; Zhan, Y.;Au, C. Desulfurization of hot coal gas over high-surface-area LaMeOx/MCM-41 sorbents. *Fuel* 2012, 98, 95-102.

(4) Westmoreland, P. R.;Harrison, D. P. Evaluation of candidate solids for high-temperature desulfurization of low-Btu gases. *Environ. Sci. Technol.* 1976, 10, 659-661.

(5) Perego, C.;Peratello, S. Experimental methods in catalytic kinetics. *Catal. Today* 1999, 52, 133-145.

(6) Tada, M. Selective oxidation catalysis on rhenium-oxide catalysts. In *Catalysis*, James J. Spivey, K. M. D., Ed. Royal Society of Chemistry: London, United Kingdom, 2011; Vol. 23, p 331.

(7) Gazzolia, D.; De Rossib, S.; Ferrarisb, G.;Valigia, M. Characterization of VO_x/ZrO_2 catalysts and their activity in the oxidation of carbon monoxide. *The Journal of the Argentine Chemical Society* 2009, 97, 39-50.

(8) Rosso, I.; Galletti, C.; Bizzi, M.; Saracco, G.;Specchia, V. Zinc oxide sorbents for the removal of hydrogen sulfide from syngas. *Ind. Eng. Chem. Res* 2003, 42, 1688-1697.

(9) Li, L.;Yan, Z. Synthesis and characterization of self-assembled V2O5 mesostructures intercalated by polyaniline. *Journal of Natural Gas Chemistry* 2005, 14, 35-39.

(10) Buelna, G.;Lin, Y. Characteristics and desulfurization-regeneration properties of sol–gel-derived copper oxide on alumina sorbents. *Sep. Purif. Technol.* 2004, 39, 167-179.

(11) Rosso, I.; Galletti, C.; Bizzi, M.; Saracco, G.;Specchia, V. Zinc oxide sorbents for the removal of hydrogen sulfide from syngas. *Industrial & Engineering Chemistry Research* 2003, 42, 1688-1697.

(12) Yasyerli, S.; Dogu, G.; Ar, I.;Dogu, T. Dynamic analysis of removal and selective oxidation of H2S to elemental sulfur over Cu–V and Cu–V–Mo mixed oxides in a fixed bed reactor. *Chemical Engineering Science* 2004, 59, 4001-4009.

(13) Yasyerli, S.; Dogu, G.; Ar, I.;Dogu, T. Activities of Copper Oxide and Cu−V and Cu−Mo Mixed Oxides for H2S Removal in the Presence and Absence of Hydrogen and Predictions of a Deactivation Model. *Industrial & Engineering Chemistry Research* 2001, 40, 5206-5214.

(14) Jung, S. Y.; Lee, S. J.; Park, J. J.; Lee, S. C.; Jun, H. K.; Lee, T. J.; Ryu, C. K.;Kim, J. C. The simultaneous removal of hydrogen sulfide and ammonia over zinc-based dry sorbent supported on alumina. *Sep. Purif. Technol.* 2008, 63, 297-302.

(15) Park, J. J.; Park, C. G.; Jung, S. Y.; Lee, S. C.; Ragupathy, D.;Kim, J. C. A study on Zn-based catalysts-sorbents for the simultaneous removal of hydrogen sulfide and ammonia at high temperature. *Res. Chem. Intermed.* 2011, 37, 1193-1202.

(16) Zeng, Y.; Zhang, S.; Groves, F.;Harrison, D. High temperature gas desulfurization with elemental sulfur production. *Chemical Engineering Science* 1999, 54, 3007-3017.

(17) Akyurtlu, J. F.;Akyurtlu, A. Hot gas desulfurization with vanadium-promoted zinc ferrite sorbents. *Gas Sep. Purif.* 1995, 9, 17-25.

(18) Flytzani-Stephanopoulos, M.; Gavalas, G. R.; Tamhankar, S. S.;Sharma, P. K. *Novel sorbents for high-temperature regenerative H_2S removal*; DOE/MC/20417-I898; Department of Energy Morgantown Energy Technology Center: Morgantown, WV, 1985.

Chapter 6
Naphthalene Removal as Tar Model Compound on Strontium Oxide

Abstract

Tar is one of the most cumbersome and abundant impurities associated with biomass gasification product gas. Tar buildup leads to blockages, plugging, corrosion, and catalyst deactivation, resulting in serious operational and maintenance problems. Consequently, its removal is essential to ensure economic and effective fuel gas utilization.

This study investigates the catalytic removal of naphthalene, as model tar compound, on strontium oxide (SrO) at high temperature (300-900°C). SrO is very effective in naphthalene decomposition. Naphthalene concentration was reduced from 6628.47 to 6392.70, 4787.97, 1562.43 and 43.68 mg/m^3 at 300, 500, 700 and 900°C, respectively corresponding to 3.56, 27.77, 76.43 and 99.34 % conversion at the same temperature in the presence of syngas.

It was observed that in the presence of syngas, SrO was more active in naphthalene decomposition suggesting the occurrence of dry reforming with lower activation energy. When helium was used as a carrier gas, the concentration of naphthalene was reduced from 6628.47 to 6512.29, 5383.03 and 3677.51 mg/m^3 at 500, 700 and 900°C corresponding to 1.75, 18.79 and 44.52 % conversion.

The activation energies were 45.24 kJ/mol when syngas was used as a carrier gas and 61.23 kJ/mol when helium was used. At 900°C, SrO was equally as active as the best commercial nickel based catalyst tested in this study.

6.1 Introduction

Biomass gasification has generated significant interest due to the potential use of producer gas in multiple applications such as power generation, fuel and chemical synthesis. However, prior to usage, producer gas must be conditioned to adjust the concentration of primary gas constituents (CO, H_2, CO_2, CH_4 and N_2 in the case air or air/steam gasification) and cleaned to remove contaminants (tar, H_2S, NH_3, halides and trace metals).

Tar is the most abundant contaminant by weight as shown in Figure 6.1 and causes technical challenges due to its tendency to condense in conduits, filters and heat exchangers and deactivate catalysts making it one of the most important technical barrier to commercialization.[1, 2]

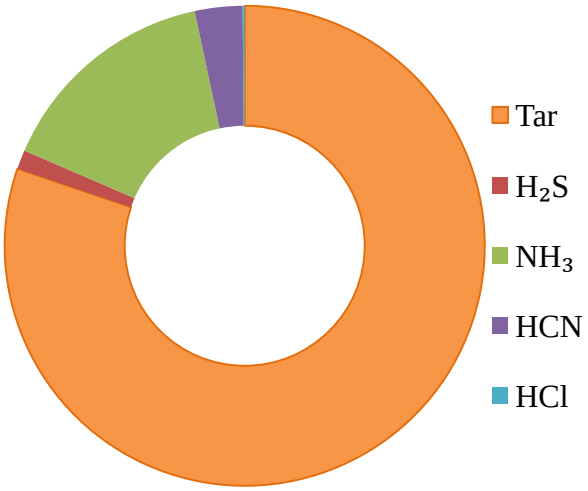

Figure 6.1. Distribution of producer gas contaminants per unit biomass
Air gasification of pine sawdust at 790°C and 0.25 ER.[1]

Catalytic tar removal studies are often carried out with model compounds such as phenol, toluene and naphthalene, the latter being particularly important as it is recalcitrant to remove by

thermal cracking. In addition to nickel and zeolites based catalysts, alkali and alkaline earth basic catalysts are known to be active in tar reforming reactions. Over the past years, several alkali and alkaline earth metal based catalysts have been investigated for tar removal such as dolomite[3, 4], olivine[5-9] and others[3, 10-15]. Among other elements of these two groups, strontium oxide has received little to no attention. The goal is to investigate the kinetics of tar removal on strontium oxide in inert gas as well as in a syngas mixture over a wide range of temperature of interest during hot gas cleanup (300-900˚C). It is hypothesized that its basic nature will enhance naphthalene decomposition.

6.2 Materials and Methods

6.2.1 Experimental Setup

The experiments were performed in a tubular reactor depicted in Figure 6.2 at 300, 500 700 and 900˚C. The reactor system consists of naphthalene evaporator maintained at 85˚C, an ½ inch stainless steel reactor maintained at the reaction temperature, the transfer line above the reactor maintained at 115˚C and the isopropanol impinger bottle to scrub naphthalene from the gas stream.

The purge and carrier gas were either helium or syngas with the following composition in vol %: 15 CO, 25 H_2, 15 CO_2, 5 CH_4 and N_2 balance with a flow rate of 100 ml/min (WHSV of 17143 ml/g h). The gas flow rate was split equally between the purge gas stream and the carrier gas stream. For each experiment, 0.35g of catalyst was loaded in the reactor and calcined at 500˚C for 60 minutes under a 100 ml/min purge stream of air. After calcination, the catalyst bed was

purged with helium for about 30 minutes prior of starting the experiment. Previously, in Chapter 5, it was determined that d_1 particle size fraction (50-80 mesh, 0.18-0.30 mm) minimizes internal diffusion limitation and thus this particle size fraction was selected for this study. It must be noted that, due to the low melting point of naphthalene and its tendency to readily crystallize, all lines were naphthalene is expected are heated and insulated.

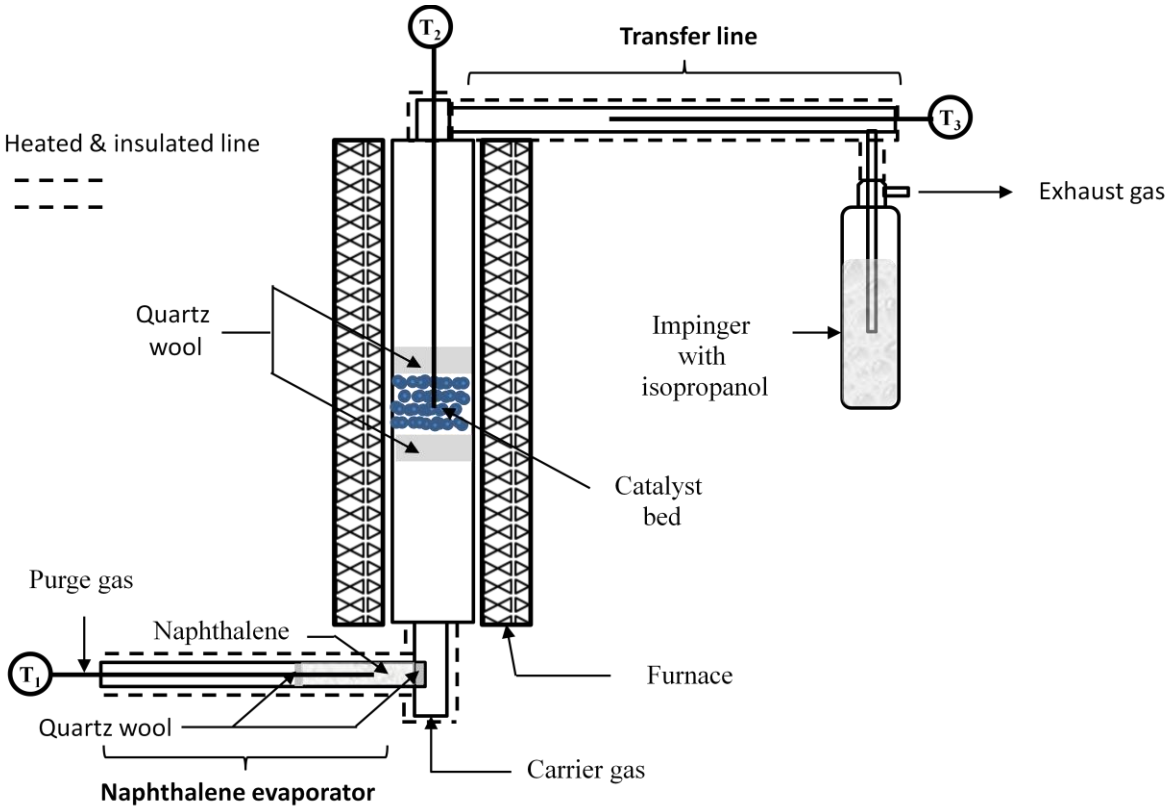

Figure 6.2. Experimental setup. T_1 = 85°C, T_2 = variable, T_3 = 115°C

6.2.2 Catalyst Characterization

Strontium oxide was characterized for BET surface area by physisorption using an Autosorb-iQ gas sorption instrument (Quantachrome Instruments, Boynton Beach, FL). The sorbent samples

were heated to 80°C at 5°C/min to 350°C and outgassed at 350°C for 6 h prior to initiating the physorption experiments using a 20 points adsorption and desorption profile. Elemental analysis and microscopic imaging was also carried out using a Zeiss EVO 50 SEM-EDS (Carl Zeiss AG, Oberkochen, Germany). The sample preparation consists of evenly dispersing the sorbent on a double sided carbon tape glued to a sample holder. The sample dispersion was carried so as to achieve monolayer coverage. SEM imaging was performed at a working distance between 8.5 and 9 mm and an electron gun voltage of 20 kV. For EDS analysis, the sample was divided in four quadrants with four runs for each sorbent. In addition, the coke formation on the spent catalysts was characterized using a thermogravimetric analyzer (Model TGA-50/50H, Shimadzu Scientific Instruments Inc., Columbia, MD). Air was used as carrier gas at a flow rate of 20 ml/min and temperature was increased at 15°C/min from room temperature to 900°C.

6.2.3 Naphthalene Sampling and Analysis

The naphthalene concentration was determined by scrubbing the exit gas into 50 ml of isopropyl alcohol. During an experiment, aliquots of scrubbing solvent were collected every 15 minutes for the first 30 minutes and every 30 minutes thereafter using a pipette. At the end of each time interval, approximately 1 ml of scrubbing solvent was withdrawn and all the aliquots thus collected were analyzed with an Agilent GC (Agilent, Santa Clara, CA) equipped with an flame photometric detector, DB-1701 capillary column (30m, 0.25mm, 0.25um, Agilent, Santa Clara, CA) to determine the concentration of naphthalene in scrubbing solvent which was in turn used

to determine the gas phase concentration of naphthalene. The GC inlet and FID detector temperature were both maintained at 250^{o}C and the oven held at 55°C for 2 min then ramped at 15^{o}C/min to 250^{o}C.

Figure 6.3 presents the underlying basis used to determine the gas phase concentration of naphthalene. The concentration of naphthalene in the scrubbing solvent and in the gas phase are linked according to eq. 6.1

$$C_{a,i} = \frac{V_{i-1} \times \Delta C_{a,i}}{\upsilon_0 \times \Delta t_i} \quad (6.1)$$

where V_{i-1} (ml) is the volume scrubbing solvent minus the volume of the previous aliquot, $\Delta C_{a,i}$ (mg/ml solvent) is the naphthalene concentration in the solvent for a given time interval Δt_i (min) and υ_0 is the total (purge and carrier) gas flow rate (ml/min).

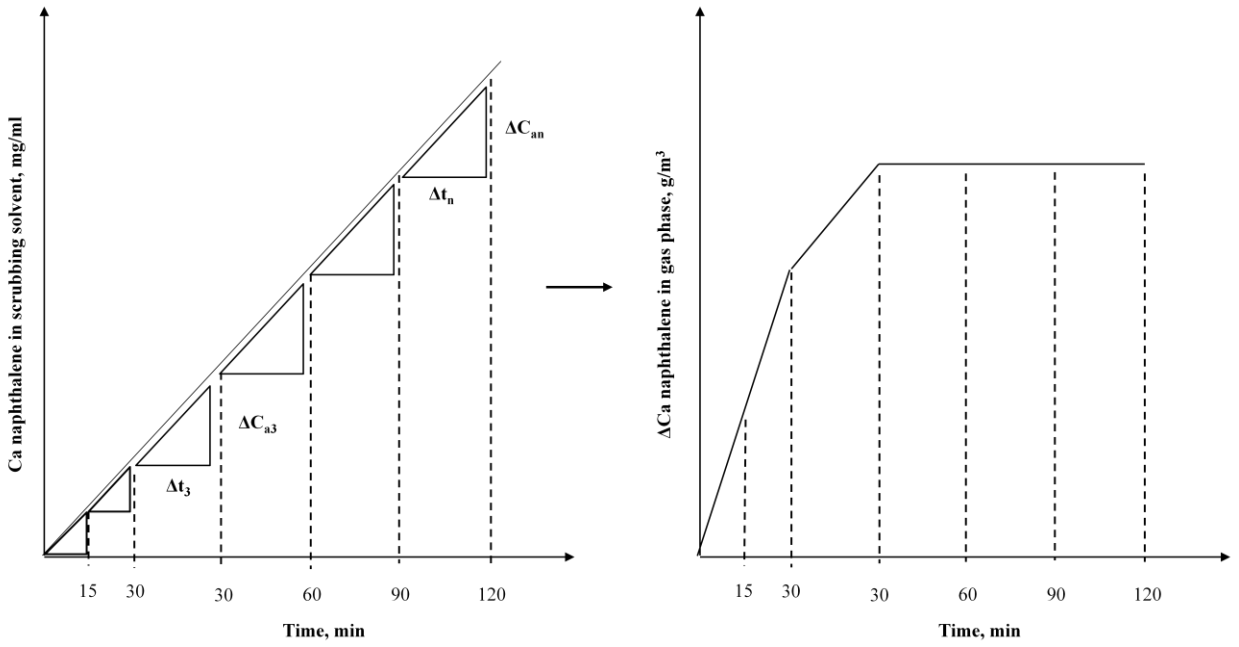

Figure 6.3. Determination of gas phase naphthalene concentration from naphthalene concentration from scrubbing solvent

Prior to catalytic experiments, several blank runs were carried without any catalyst in the reactor which was maintained at 100˚C to determine the mean inlet concentration of naphthalene in the gas phase. Using this mean inlet concentration and the final steady state concentration, the conversion was calculated as shown below in eq. 6.2.

$$X_{naphthalene} = \frac{C_{a,in} - C_{a,out}}{C_{a,in}} \quad (6.2)$$

6.2.3 Kinetic of Naphthalene Reforming in Syngas

It has been shown that naphthalene decomposition is a first order reaction.[16, 17] As such, for plug flow reactors, the rate law and the differential form of the design equation are shown below:

$$r'_A = kC_{A0}(1 - X) \tag{6.3}$$

$$\frac{dX}{dW} = \frac{kC_{A0}(1-X)}{F_{A0}} \tag{6.4}$$

where $F_{A0} = C_{A0}\upsilon_0$. The integral form of the design equation above can be expressed as

$$\int \frac{dX}{(1-X)} = \int \frac{k}{\upsilon_0} dW \tag{6.5}$$

$$K' = \frac{-ln(1-X)}{W/\upsilon_0} \tag{6.6}$$

Using the density of the catalyst, eq. 6.6 was further converted and reduced to eq. 6.7

$$K = \frac{-ln(1-X)}{\tau} \tag{6.7}$$

The temperature dependence of rate constant is expressed in eq. 6.8 and can further be rearranged to determine the activation energy in eq. 6.9.

$$K = A_0 e^{-E_a/RT} \tag{6.8}$$

$$lnK = lnA_0 - \frac{E_a}{RT} \tag{6.9}$$

where R is 8.314 J mol^{-1} K^{-1}, *Ea* is the activation energy in kJ mol^{-1} and A_0 is pre-exponential factor.

6.3 Results and Discussion

6.3.1 Effect of Temperature on Naphthalene Removal

The inlet concentration of naphthalene was determined by conducting blank runs and the inlet concentration was 6628.47 mg/m^3. Figure 6.4 shows the effect of temperature on naphthalene removal.

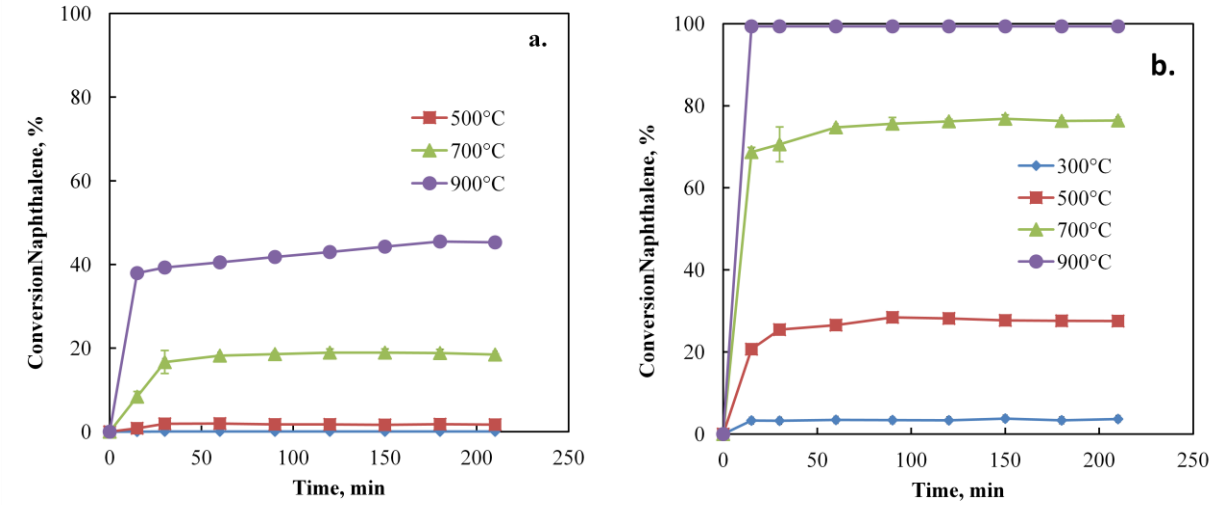

Figure 6.4. Effect of temperature on naphthalene conversion profiles without (a.) and with (b.) syngas

At steady state, the outlet concentrations were 6392.70, 4787.97, 1562.43 and 43.68 mg/m^3 corresponding to conversions of 3.56, 27.77, 76.43 and 99.34 % for 300, 500, 700 and 900°C in the presence of syngas. In the absence of syngas, the conversions were much lower for the same temperature. At 300°C in the absence of syngas, naphthalene conversion was nearly zero (0.09 ± 0.12 %). However, as temperature increased, the conversion increased to 1.75, 18.79 and 44.52 for 500, 700 and 900°C, respectively. It is expected that, in the absence of syngas, naphthalene decomposition occurs predominantly by catalytic thermal cracking as shown in the reaction below.

$$C_nH_m \rightarrow nC + \frac{m}{2}H_2 \qquad [6.1]$$

In the absence of a catalyst, high conversion by thermal cracking is only favored at very high temperature (> 1100°C)[18] due to the refractory nature of naphthalene[19]. However, in the presence of CO, naphthalene decomposition by dry reforming is possible as illustrated in the reaction below.

$$C_nH_m + nCO_2 \rightarrow 2nCO + \frac{m}{2}H_2 \qquad [6.2]$$

It is likely that the higher conversion of naphthalene in the presence of syngas as shown in Figure 6.5 is due to the dry reforming reaction depicted above.

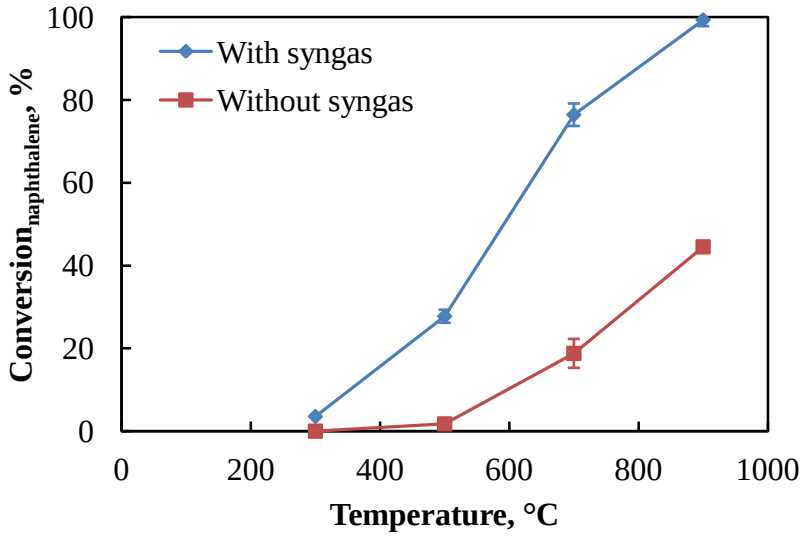

Figure 6.5. Effect of temperature on naphthalene steady state concentration under different carrier gas

The performance of SrO was compared against that of a commercial nickel based catalyst, Res-N-003 in Figure 6.6. The activity of the commercial nickel based catalyst was higher at lower temperature but similar in performance to SrO at 900°C. While detailed information on the commercial catalyst is unknown due to intellectual properties rights, it is suspected that this

catalyst is supported on a high surface material like Al_2O_3. If this true, it will likely have a higher surface area which could in turn enhance its activity. It is expected that as surface area is increased for SrO by deposition on a high surface area support, its performance will be improved to enhance activity at lower gas cleanup temperature.

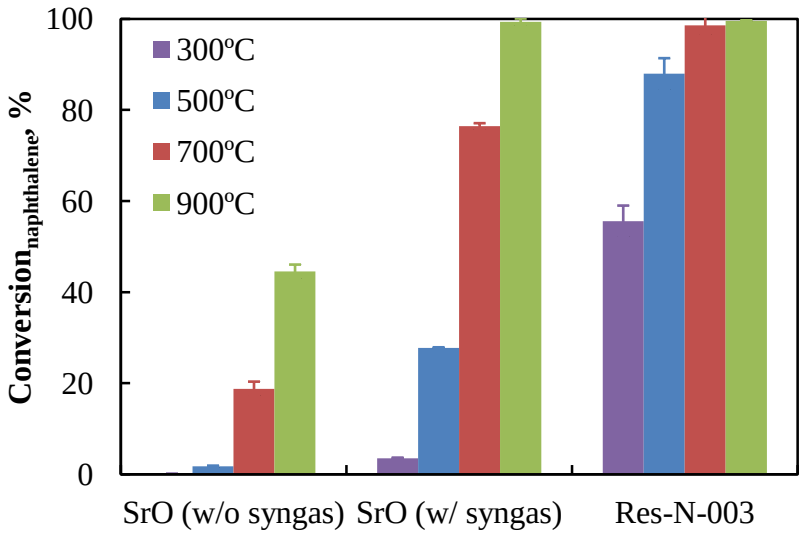

Figure 6.6. Comparison of SrO with a commercial Ni-based catalyst

6.3.2 Catalyst Characterization

The elemental analysis of strontium oxide, after calcination, by SEM-EDS confirmed the high purity of the catalyst with 85.40 wt % of Sr and 14.63 wt % of oxygen. SEM image of SrO, shown in Figure 6.7, revealed a smooth surface and an irregular particle shape with not noteworthy surface features.

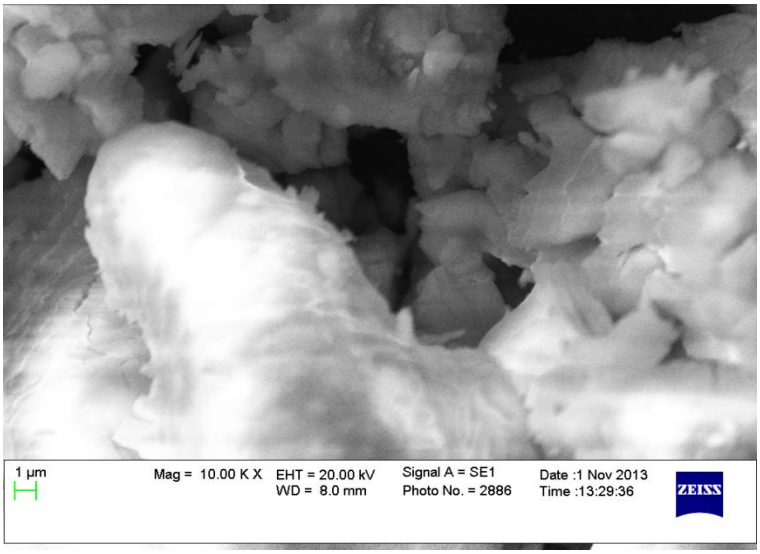

6.7. Scanning electron microscopic image of SrO

The BET surface area of SrO was 1.04 m^2/g. Due to limited sample and contamination by the quartz wool used as bed support, spent catalysts were not analyzed for surface area. Strontium oxide was characterized after the experiments by TGA to determine coke formation. As temperature increased, so did the coke content on the spent catalyst, without or without syngas. However, the presence of syngas during the reaction resulted in less coke formation at all temperatures as illustrated in Figure . At 300°C, in the absence of syngas, coke formation was minimal suggesting poor naphthalene conversion and consistent with our observations. While lower coke formation was also observed at the same temperature in the presence of syngas, the conversion of naphthalene was higher. As coke formation is primarily due to the cracking reactions, it suggests, as hypothesized earlier, that the enhanced conversion is due to the dry reforming reaction.

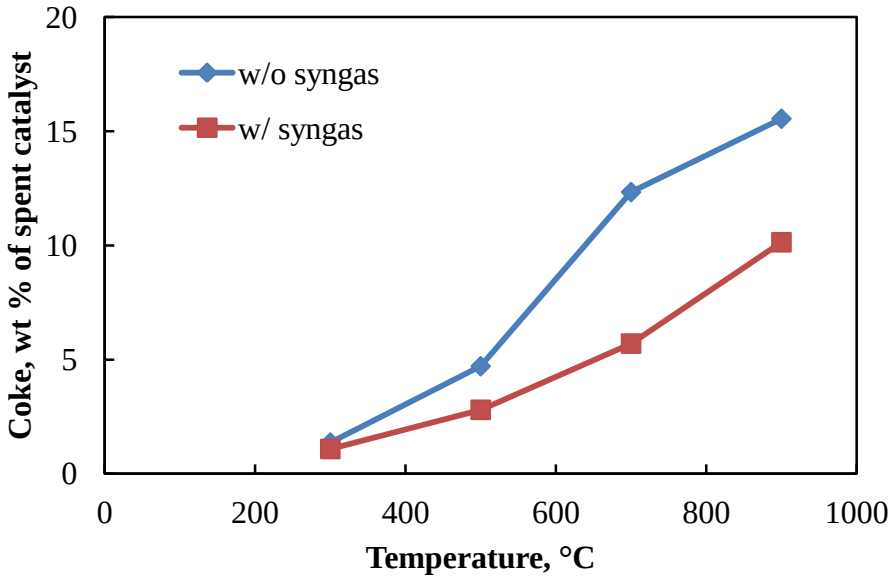

Figure 6.8. Coke formation on spent SrO

6.3.3 Kinetics of Naphthalene Removal on Strontium Oxide

The activation energy of naphthalene decomposition on strontium oxide was determined assuming first order reactions and the Arrhenius plot is shown in Figure 6.9. The activation energies are 45.24 and 61.23 kJ/mol with and without syngas as the carrier gas.

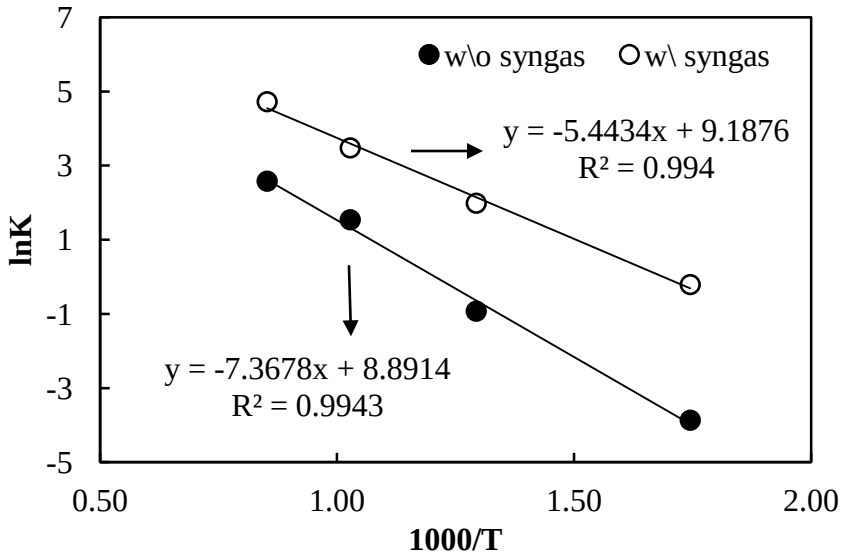

Figure 6.9. Activation energy plot of naphthalene on SrO

The activation energies calculated in this study are comparable results reported by some authors.[4, 20, 21] These values are however lower and thus better than activation energies reported for tar decomposition.[5, 22]

6.4 Conclusions

Tar is a significant problem in biomass gasification due to its tendency to condense on surface and to induce coke formation in chemical and fuel synthesis processes downstream. In this study, naphthalene was used as a model tar compound because it is one of the most difficult tar compounds to eliminate from syngas. Catalytic naphthalene decomposition was investigated in study on SrO with and without syngas constituents from 300 to 900˚C. As temperature increased, naphthalene conversion was improved from 3.56 to 99.34 % and from 0.09 to 44.52 % with and without syngas, respectively.

It was observed that in the presence of syngas, SrO was more active in naphthalene decomposition suggesting the occurrence of dry reforming. The activation energies were 45.24 kJ/mol when syngas was used as a carrier gas and 61.23 kJ/mol when helium was used. At higher temperature, SrO was equally as active as the best commercial nickel based catalyst tested in this study.

References

(1) Abdoulmoumine, N.; Kulkarni, A.;Adhikari, S. Effects of Temperature and Equivalence Ratio on Pine Syngas Primary Gases and Contaminants in a Bench-Scale Fluidized Bed Gasifier. *Ind. Eng. Chem. Res.* 2014, 53, 5767-5777.

(2) Stefan Heyne, T. L., Magnus Marklund. *Biomass gasification - A synthesis of technical barriers and current research issues for deployment at large scale*; The Swedish Knowledge Centre for Renewable Transportation Fuels: Göteborg, Sweden, 2013.

(3) Simell, P.; Kurkela, E.; Ståhlberg, P.;Hepola, J. Catalytic hot gas cleaning of gasification gas. *Catal. Today* 1996, 27, 55-62.

(4) Sun, Y.; Jiang, J.; Kantarelis, E.; Xu, J.; Li, L.; Zhao, S.;Yang, W. Development of a bimetallic dolomite based tar cracking catalyst. *Catal. Commun.* 2012, 20, 36-40.

(5) Devi, L.; Ptasinski, K.;Janssen, F. Pretreated olivine as tar removal catalyst for biomass gasifiers: investigation using naphthalene as model biomass tar. *Fuel Process. Technol.* 2005, 86, 707-730.

(6) Hurley, S.; Xu, C.; Preto, F.; Shao, Y.; Li, H.; Wang, J.;Tourigny, G. Catalytic gasification of woody biomass in an air-blown fluidized-bed reactor using Canadian limonite iron ore as the bed material. *Fuel* 2012, 91, 170-176.

(7) Kuhn, J.; Zhao, Z.; Felix, L.; Slimane, R.; Choi, C.;Ozkan, U. Olivine catalysts for methane-and tar-steam reforming. *Appl. Catal., B* 2008, 81, 14-26.

(8) Link, S.; Arvelakis, S.; Paist, A.; Martin, A.; Liliedahl, T.;Sjöström, K. Atmospheric fluidized bed gasification of untreated and leached olive residue, and co-gasification of olive residue, reed, pine pellets and Douglas fir wood chips. *Appl. Energy* 2012, 94, 89-97.

(9) Michel, R.; Łamacz, A.; Krzton, A.; Djéga-Mariadassou, G.; Burg, P.; Courson, C.;Gruber, R. Steam reforming of α-methylnaphthalene as a model tar compound over olivine and olivine supported nickel. *Fuel* 2013, 109, 653-660.

(10) D'Orazio, A.; Di Carlo, A.; Dionisi, N.; Dell'Era, A.;Orecchini, F. Toluene steam reforming properties of CaO based synthetic sorbents for biomass gasification process. *Int. J. Hydrogen Energy* 2013, 38, 13282-13292.

(11) Guan, G.; Chen, G.; Kasai, Y.; Lim, E. W. C.; Hao, X.; Kaewpanha, M.; Abuliti, A.; Fushimi, C.;Tsutsumi, A. Catalytic steam reforming of biomass tar over iron- or nickel-based catalyst supported on calcined scallop shell. *Appl. Catal., B* 2012, 115–116, 159-168.

(12) Guan, G.; Kaewpanha, M.; Hao, X.; Wang, Z.; Cheng, Y.; Kasai, Y.;Abudula, A. Promoting effect of potassium addition to calcined scallop shell supported catalysts for the decomposition of tar derived from different biomass resources. *Fuel* 2013, 109, 241-247.

(13) Jordan, C. A.;Akay, G. Effect of CaO on tar production and dew point depression during gasification of fuel cane bagasse in a novel downdraft gasifier. *Fuel Process. Technol.* 2013, 106, 654-660.

(14) Wang, T.; Chang, J.; Lv, P.;Zhu, J. Novel catalyst for cracking of biomass tar. *Energy Fuels* 2005, 19, 22-27.

(15) Kim, Y.-K.; Park, J.-I.; Jung, D.; Miyawaki, J.; Yoon, S.-H.;Mochida, I. Low-temperature catalytic conversion of lignite: 1. Steam gasification using potassium carbonate supported on perovskite oxide. *J. Ind. Eng. Chem.* 2014, 20, 216-221.

(16) Devi, L. Catalytic Removal of Biomass Tars; Olivine as Prospective in-Bed Catalyst for Fluidized-Bed Biomass Gasifiers,. PhD thesis, Technical University of Eindhoven, Eindhoven, The Netherlands, 2005.

(17) Dou, B.; Gao, J.; Sha, X.;Baek, S. W. Catalytic cracking of tar component from high-temperature fuel gas. *Appl. Therm. Eng.* 2003, 23, 2229-2239.

(18) Sutton, D.; Kelleher, B.;Ross, J. R. H. Review of literature on catalysts for biomass gasification. *Fuel Process. Technol.* 2001, 73, 155-173.

(19) Bridgwater, A. Catalysis in thermal biomass conversion. *Appl. Catal., A* 1994, 116, 5-47.

(20) Ferella, F.; Stoehr, J.; Michelis, I. D.;Hornung, A. Zirconia and alumina based catalysts for steam reforming of naphthalene. *Fuel* 2013, 105, 614-629.

(21) Buchireddy, P. R.; Bricka, R. M.; Rodriguez, J.;Holmes, W. Biomass Gasification: Catalytic Removal of Tars over Zeolites and Nickel Supported Zeolites. *Energy Fuels* 2010, 24, 2707-2715.

(22) Orio, A.; Corella, J.;Narvaez, I. Performance of different dolomites on hot raw gas cleaning from biomass gasification with air. *Ind. Eng. Chem. Res* 1997, 36, 3800-3808.

Chapter 7
Recommendations

This section contains recommendations for biomass gasification in the bench scale gasifier and gas cleanup for future studies.

7.1 Biomass Gasification

7.1.1 Fluidized Bed Gasifier: Lessons Learned and Suggestions

While the present setup fluidized bed gasifier setup was effective in carrying out the experiments for this project, it has also provided me with valuable insights on practical operating procedures and design. In the next sections, I will provide tips and suggestions for future students on operation, design modifications and potential research projects.

7.1.1.1 Operating Procedure

From the standpoint of operations, the biggest problem we have faced with the current setup is clogging at (i) the biomass inlet of the gasifier, (ii) in sand bed and (iii) the condensers. Clogging at the biomass inlet occurs due to either loss of fluidization in sand bed due to pressure buildup and biomass feeding issues. If higher than normal biomass feeding rate is used (> 300 rpm), it could result in feeding issues as sufficient time would not be provided for biomass

decomposition. The consequence of this situation is packing of biomass and sand at the entrance of gasifier and manifested through unusually high CO and H_2, with concentrations near or higher than 20 vol % for 16.5 l/min of nitrogen fluidization flow. In this scenario, the experiment behaves more like a pyrolysis experiment: as biomass accumulates at the bottom of the gasifier, the oxygen supplied per unit biomass gasified will increasingly reduced resulting in an oxygen starved region. As biomass is feed with an injection screw auger in the current setup, biomass packing will increase as the run progresses until a point when very limited biomass can be pushed by the auger into the gasifier. At this moment, the high CO and H_2 will continuously decrease while CO_2 increases in the opposite direction. Also, beyond this point, the operator might damage this motor if the run is continued by overloading the motor that powers the auger. When this situation occurred in the past, a rock like solid plug has been observed at the biomass entrance of the gasifier. It appears that the tendency to form a plug at the bottom of the gasifier is somewhat related to biomass particle size: finer particle size accentuates this tendency and tends to pack and plug at the bottom of the reactor due to, in my opinion, the ease of biomass compressibility. This aspect is not well understood as we have not focused on it much. For this reason, a minimal particle size of 500 μm is suggested although experiments can be conducted to further clarify this phenomenon.

As far as operation procedure is concerned, two approaches can be used to minimize the issue of biomass clogging. The first approach consists of improving the reliably and consistency of feeding by using a narrow particle size distribution and using the appropriate feeding rate.

Presently, when sawdust is sieved through 850 um sieve, smooth operation can be achieved. The current procedure can be improved by limiting the lower particle size to particles larger 500 um as suggested above. This can be achieved by using two sieve sizes (850 and 500 um). The hopper should always be kept at least 1/3 full or higher. It has been observed on this setup and another larger scale fluidized bed unit that the volumetric feeding rate is not constant when the biomass volume in the hopper is below a certain height. As constant feeding rate is assumed in the equivalence ratio calculation to determine the oxygen flow rate, this seemingly minor action could affect the success of the experiment and reduce variability in gas composition as biomass feeding rate is more constant. The occurrence of inconstant (decreasing) feeding rate can be reasonably assumed, in the absence of other feeding issues, whenever CO and H_2 concentrations continuously decrease while CO_2 increases beyond the typical the time required to achieve steady state for the particularly biomass. The time required to achieve steady state varies between biomass feedstocks. However, for the case of air gasification of pine, the steady state typically occurs 15 to 30 min into the run depending on the temperature and equivalence ratio. The remedy to this issue is simple: fill up the hopper.

The second approach consists of selecting the right feeding rate. In previous experiments, the feeding of the biomass was controlled by setting the speed of the twin augers on the hopper to 100 rpm. For a 100 g of sand loaded into the gasifier, 16.5 l/min of nitrogen fluidization flow rate, this hopper auger speed worked well among many conditions tested. However, this is no longer the case when the speed and the sand loading are increased as we have observed. It is

therefore recommended to conduct a parametric study to clearly elucidate the combinatory set of parameters to avoid feeding issues in the future.

Besides feeding issues, clogging in the gasifier can also occur as a result of loss of fluidization. Fluidization loss could be due to char clogging throughout the system, particularly in the condensers but also at the one inch connecting lines between the gasifier and the high temperature filter, the high temperature filter and the first condenser, and the first condenser and the second condenser. It has been observed in this system that a thorough cleanup in between each run can significantly improve operations and has the largest impact on the positive or negative outcome of the experiment. Therefore, I will recommend thoroughly cleaning the gasifier and high temperature filter with compressed air after every run. Until a cyclone or a suitable sintered metal filter is installed in the high temperature filter, it is also recommended to open and clean the first condenser adjacent to the high temperature filter and the second condenser as needed. If the shell and tube condenser is packed with char, the metal brush should be used to clean the tube. The shell should be wiped with paper and isopropanol or alternatively brushed (with a metal brush) with soap until the visible tar layer is removed.

7.1.1.2 Design Modification

The first design modification on this current setup is the installation of a cyclone before the sintered metal filter. In the early stages of this project, we experimented with sintered metal filter which was ultimately clogged due tar and char deposition causing pressure buildup problems. For gasification purposes, the sintered metal filter is probably not necessary when a cyclone

works properly. However, for pyrolysis experiments, it is likely that a metal filter will be required even if the cyclone performs well.

The second design modification suggestion will likely result in extensive redesign on the system and costly heaters. The suggestion is to adopt a more robust "inclined biomass injection" design where the injection screw is inclined rather horizontally positioned as it is presently. Furthermore, the entrance of biomass should be placed in the middle of bed rather than at the bottom, as we currently do in the setup. These suggestions are based on numerous feeding challenges encountered during early stage, limited flexibility in terms biomass feeding rate for the current design and personal experience on two bottom fed bench scale systems (bench scale at Auburn university and pilot scale at Virginia Tech) and two inclined fed units (bench scale and mobile pilot scale at Virginia Tech).

7.1.2 Biomass Contaminants Studies in Fluidized Bed Gasifier

While conducting my literature review, it was observed that studies focusing on the interactive effects of temperature, equivalence ratio and steam to biomass ratio are sparingly available. It is important to understand the interactive effect of these parameters, from a process optimization standpoint, in order to minimize contaminant emissions which can results in a reduction in gas cleanup cost. To an extent, this information is available for tar but is largely absent for hydrogen sulfide, ammonia, hydrogen halides and trace metals.

7.1.3 Biomass Contaminants Formation and Evolution Studies

Up to now, except for tar to an extent, the majority of contaminant studies have focused on the practical rather than fundamental understanding of the evolution and formation of contaminants. In the early 80's and throughout the 90's, several DOE projects have tackled the formation of tar from biomass, primarily with the goal of understanding the complex nature of pyrolysis chemistry. These studies have lead to a generalized pathway proposed by Evans and Milne[1] for the formation of tar with limited focus on the potential mechanism. For other contaminants, the availability of studies on the evolution, comprehensive characterization and mechanism of formation is even more limited than for tar. Therefore, in light of this observation, fundamental studies of the formation of contaminants in an oxidative environment would be a positive addition to the greater body on knowledge in the field of biomass gasification.

7.2 Gas Cleanup Studies

Based on my literature review, it appears that most studies dealing with contaminant cleanup, with the exception of tar cleanup studies, have focused on contaminant gas concentrations that are observed typical in coal derived syngas. This approach might be problematic as coal derived syngas has significantly higher contaminants than biomass derived syngas. In the case of hydrogen sulfide and ammonia, the two most studied contaminants after tar, typical concentration can be up to 1 or 2 vol % in coal derived syngas. However, they are rarely higher than 500 ppmv for hydrogen sulfide and 1 vol % for ammonia in biomass derived syngas.

Future hydrogen sulfide removal studies (sulfidation) focusing on biomass derived syngas can be carried out systematically as proposed in Figure 7.1 based on insights gained from my work in Chapter 5. A good model for experimental setup and various procedures for TGA based sulfidation studies can be the work of Heesink and Swaaij.[2] Furthermore, based on the findings from Chapter 5, V_2O_5 based sorbents can be further explored as absorptive sulfur removal sorbents for easy regeneration and sulfur recovery since hydrogen is merely adsorbed rather chemically reacted to form a sulfide.

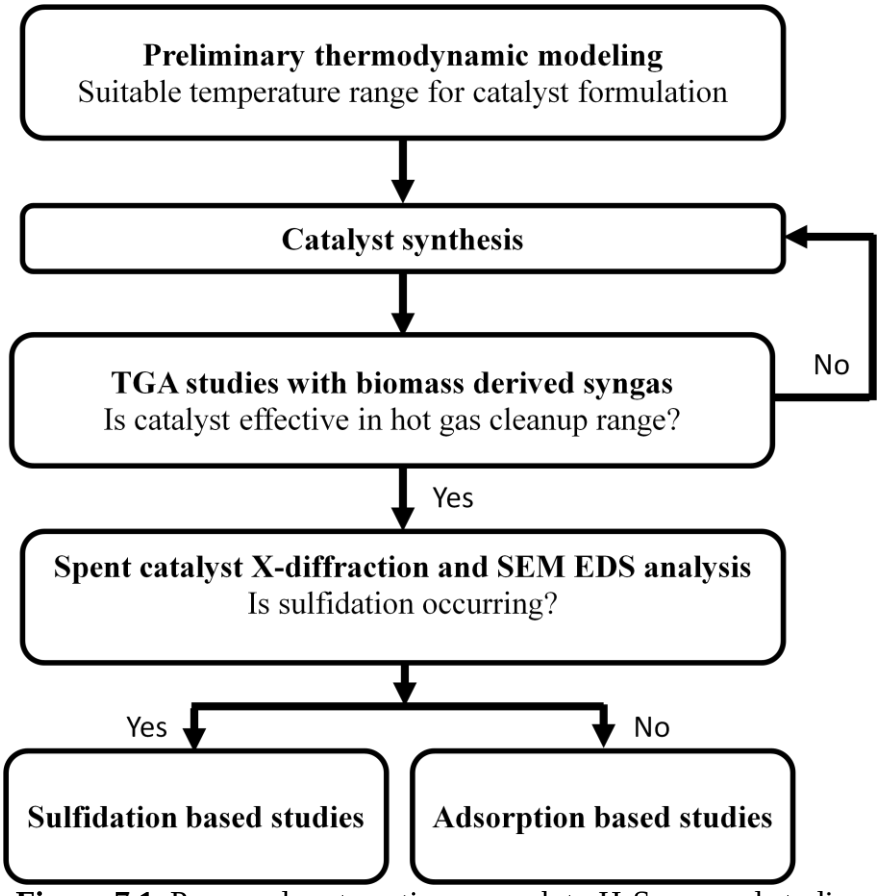

Figure 7.1. Proposed systematic approach to H_2S removal studies

As for potential future naphthalene work, studies should focus on improving catalyst formulation to achieve higher conversion at temperature below 700°C as well as on mechanistic kinetic studies. Since SrO is very effective in tar removal based on the work in Chapter 7, SrO supported catalyst formulations are suggested in the future to increase surface and catalyst utilization.

References

(1) Evans, R. J.;Milne, T. A. Molecular characterization of the pyrolysis of biomass. *Energy Fuels* **1987,** 1, 123-137.

(2) Heesink, A.;Van Swaaij, W. The sulphidation of calcined limestone with hydrogen sulphide and carbonyl sulphide. *Chem. Eng. Sci.* **1995,** 50, 2983-2996.

Appendix A1

Tar Compounds in Syngas

Table A1.1. List of primary, secondary and tertiary tar compounds

MW	Formula	Name
Primary tar compounds		
Acids		
46	$C_5H_{10}O_5$	Formic (Methanoic)
60	$C_5H_{10}O_5$	Acetic (Ethanoic)
74	$C_6H_{10}O_5$	Propanoic (Propionic)
76	$C_6H_{12}O_5$	Glycolic (Hydroxyacetic)
88	$C_6H_{12}O_5$	Butanoic (Butyric)
102	$C_{12}H_{20}O_6$	
116	CH_2O_2	Pentanoic (Valeric)
116	$C_2H_4O_2$	4-Oxopentanoic
122	$C_3H_6O_2$	Hexanoic (Caproic)
130	$C_2H_4O_3$	Benzoic
254	$C_4H_8O_2$	Heptanoic
Sugars		
150	$C_5H_{10}O_2$	D-Xylose
162	$C_5H_3O_3$	1,6 - Anhydroglucofuranose
162	$C_6H_{12}O_2$	Levoglucosan (1,6-Anhydro-β-D-Glucopyranose)
180	$C_7H_6O_2$	α-D-Glucose (α-D-Glucopyranose)
180	$C_7H_{14}O_2$	Fructose
260	$C_{16}H_{30}O_2$	Cellobiosan
Alcohols		
32	CH_4O	Methanol
46	C_2H_6O	Ethanol
Ketones		
70	C_4H_60	2-Butenone
72	C_4H_8O	2-Butanone

84	C_5H_8O	Cyclopentanone
96	C_6H_8O	2-Methyl-2-Cyclopenten-1-One
98	$C_6H_{10}O$	3-Methylcyclopentanone
98	$C_6H_{10}O$	Cyclohexanone
112	$C_7H_{12}O$	2-Ethylcyclopentanone
112	$C_7H_{12}O$	Dimethylcyclopentanone
124	$C_8H_{14}O$	Trimethylcyclopentenone
126	$C_{10}H_8O$	3-Methylindan-1-one
Aldehydes		
30	CH_2O	Methanal (Formaldehyde)
44	C_2H_4O	Ethanal (Acetaldehyde)
56	$C_3H_4O_2$	2-Propenal (Acrolein)
84	C_5H_8O	2-Methyl-2-Butenal (Crotonaldehyde-2-methyl
Phenols		
94	C_6H_6O	Phenol
108	C_7H_8O	2-Methyl Phenol o (o-Cresol) 3-Methyl Phenol m (m-Cresol) 4-Methyl Phenol p (p-Cresol)
122	$C_8H_{10}O$	2,3-Dimethylphenol (2,3-Xylenol) 3, 4-Dimethylphenol (2,3-Xylenol) 3, 5-Dimethylphenol (2,3-Xylenol) 2,4-Dimethylphenol (2,4-Xylenol) 2,5-Dimethylphenol (2,5-Xylenol) 2,6-Dimethylphenol (2,6-Xylenol)
122	$C_8H_{10}O$	2-Ethylphenol
136	$C_8H_{12}O$	2,3,5 Trimethylphenol
Guaicols		
124	$C_7H_8O_2$	Guaiacol (2-Methoxyphenol)
138	$C_8H_{10}O_2$	4-Methyl Guaiacol
152	$C_9H_{12}O_2$	4-Ethylguaiacol
164	$C_{10}H_{12}O_2$	4-Propenyl Guaiacol (Isoeugenol)
166	$C_{10}H_{14}O_2$	4-Propylguaiacol
Syringols		
154	$C_8H_{10}O_3$	Syringol (2,6-Dimethoxy Phenol)
168	$C_9H_{12}O_3$	4-Methylsyringol
182	$C_{10}H_{14}O_3$	4-Ethylsyringol
182	$C_9H_{10}O_4$	Syringaldehyde/Benzaldehyde, 4-hydroxy-3,5, dimethoxy

194	$C_{11}H_{14}O_3$	4-Propenylsyringol (4-Allylsyringol)
196	$C_{10}H_{12}O_4$	4-Hydroxy-3,5-Dimethoxyphenyl Ethanone
Furans		
68	C_4H_4O	Furan (Furfuran)
82	C_5H_6O	2-Methylfuran (furan; 2-methyl, 5-methyl furan)
84	$C_4H_4O_2$	2(5H)-Furanone
96	$C_5H_4O_2$	Furfural (2-Furaldehyde 2-furancarboaldehyde)
98	$C_5H_6O_2$	3-Methyl-2(3H) Furanone
98	$C_5H_6O_2$	Furfural Alcohol (2-Furanmethanol)
110	$C_6H_6O_2$	5-Methylfurfural (2-furaldehyde-5-methyl)
126	$C_6H_6O_3$	5-Hydroxymethyl-2-Furaldehyde
Mixed Oxygenates		
58	$C_2H_2O_2$	Glyoxal (Ethanedial, 1-2 Ethanedione)
60	$C_2H_4O_2$	Hydroxyethanal (Hydroxyacetaldehyde; Glycoaldehyde)
62	$C_2H_6O_2$	1,2-Dihyroxyethane (Ethylene Glycol)
72	$C_3H_4O_2$	Propanal-2-One (Methyl Glyoxal,2-Oxopropanal)
74	$C_3H_6O_2$	1-Hydroxy-2-Propanone (Acetol)
74	$C_3H_6O_2$	2-Hydroxypropanal (Methanolacetaldehyde)
86	$C_4H_6O_2$	Butyrolactone (gamma or beta); (2,3-Butanedione)
100	$C_5H_8O_2$	2,3-Pentenedione
110	$C_6H_6O_2$	1,2-Dihydroxybenzene (Catechol)
110	$C_6H_6O_2$	1,3-Dihydroxybenzene (Resorcinol)
110	$C_6H_6O_2$	1,4-Dihydroxybenzene (Hydroquinone)
112	$C_6H_8O_2$	2-Hydroxy-3-Methyl-2-Cyclopentene-1-One
126	$C_6H_6O_3$	2-Methyl-3-Hydroxy-2-Pyrone
152	$C_8H_8O_3$	4-Hydroxy-3-Methoxybenzaldehyde (Vanillin)
Secondary tar compounds		
16	CH_4	Methane
28	C_2H_4	Ethene
30	C_2H_6	Ethane
40	C_3H_4	Propyne
42	C_3H_6	Propene
54	C_4H_6	Butyne
54	C_4H_6	Butadienes
56	C_4H_8	1-Butene, 2-Butene
66	C_5H_6	Cyclopentadiene
67	C_4H_5N	1H-Pyrrole

78	C_6H_6	Benzene
79	C_5H_5N	Pyridine
92	C_7H_8	Toluene
93	C_6H_7N	Methylpyridine
93	C_6H_7N	2.3.4 Picoline
94	C_6H_6O	Phenol
104	C_8H_8	Styrene
102	C_8H_6	Ethynlbenzene
106	C_8H_{10}	Xylene, o, m, p
106	C_7H_6O	Benzaldehyde
107	C_7H_9N	Dimethylpyridine
107	C_7H_9N	o,m,p-Ethylpyridine
107	C_7H_9N	2,4-Lutidine
108	C_7H_8O	p-Cresol
108	C_7H_8O	o-Cresol
108	C_7H_8O	m-Cresol
110	$C_6H_6O_2$	Dihydroxybenzene
116	C_9H_8	Indene
116	C_9H_8	1-Ethynal-4-methylbenzene (indene)
118	C_9H_{10}	Methylstyrene
118	C_9H_{10}	Indan
118	C_9H_{10}	Ethylbenzene
118	C_8H_6O	Benzofuran
120	C_8H_8O	Vinylphenol
121	$C_8H_{11}N$	Trimethylpyridine
122	$C_8H_{10}O$	Dimethylphenol
124	$C_7H_8O_2$	Dihydroxytoluene
128	$C_{10}H_8$	Naphthalene
129	C_9H_7N	Isoquinoline
129	C_9H_7N	Quinoline
130	$C_8H_6N_2$	Quinazoline
132	C_9H_8O	Vinyl Benzaldehyde
132	$C_{10}H_{12}$	Methylindane
132	C_9H_8O	Methylbenzofuran
132	C_9H_8O	1-Indanone
134	$C_9H_{10}O$	Propenylphenol

135	$C_9H_{13}N$	Dimethylethylpyridine
136	$C_9H_{12}O$	Propoxybenzene
136	$C_9H_{12}O$	Methylethylphenol
142	$C_{11}H_{10}$	2-Methylnaphthalene
142	$C_{11}H_{10}$	1-Methylnaphthalene
142	$C_{11}H_{10}$	1,1-Dimethyl-1H-indene
143	$C_{10}H_7N$	Quinaldine
144	$C_{11}H_{12}$	1,2-Dihydro-3-methylnaphthalene
146	$C_{10}H_{10}O$	Methyl-1-indanone
146	$C_{12}H_{10}O$	Dimethylbenzofuran
148	$C_8H_{10}O_2$	Creosole
150	$C_{10}H_{14}O$	Dimethylethylphenol
154	$C_{12}H_{10}$	Vinylnaphthalene
154	$C_{12}H_{16}$	Biphenyl
156	$C_{12}H_{12}$	Dimethylnaphthalene
156	$C_{12}H_{12}$	2-Ethylnaphthalene
166	$C_{13}H_{12}$	Methyl acenaphthalene
168	$C_{13}H_{12}$	Methylbiphenyl
168	$C_{12}H_8O$	Dibenzofuran
168	$C_{12}H_8O$	Naphthofuran
168	$C_{13}H_{12}$	Diphenylmethane
170	$C_{13}H_{14}$	Propylnaphthalene
179	$C_{13}H_9N$	Benzoquinoline
180	$C_{14}H_{12}$	Methylflourene
182	$C_{13}H_{10}O$	Phenylbenzaldehyde ((4-Phenyl carboxaldehyde)
182	$C_{14}H_{14}$	Dimethylbiphenyl
190	$C_{15}H_{10}$	Methylenephenanthrene
192	$C_{15}H_{12}$	Methylphenanthrene
202	$C_{16}H_{10}$	Acephenathrylene
204	$C_{16}H_{12}$	Phenylnapthalene
204	$C_{15}H_{10}$	4H-Cyclopenta [def]phenanthrene
216	$C_{17}H_{12}$	Methylpyrene
216	$C_{17}H_{12}$	11H-Benzo [a,b] fluorene
226	$C_{18}H_{10}$	Benzo [ghi] flouranthene
228	$C_{18}H_{12}$	Benzo [c] phenanthrene

Tertiary tar compounds

16	CH_4	Methane
26	C_2H_2	Acetylene
66	C_5H_6	Cyclopentadiene
78	C_6H_6	Benzene
92	C_7H_8	Toluene
104	C_8H_8	Styrene
116	C_9H_8	Indene
128	$C_{10}H_8$	Naphthalene
152	$C_{12}H_8$	Acenaphthalene
154	$C_{12}H_{10}$	Acenapthene
166	$C_{13}H_{10}$	Fluorene
178	$C_{14}H_{10}$	Anthracene
178	$C_{14}H_{10}$	Phenanthrene
202	$C_{16}H_{10}$	Pyrene
202	$C_{16}H_{10}$	Fluoranthene
202	$C_{16}H_{10}$	Benzacenaphthalene
216	$C_{17}H_{12}$	Methylpyrene
216	$C_{17}H_{12}$	Benzo [a,b,c] fluorene
226	$C_{18}H_{10}$	Benzo [ghi] fluoranthene
228	$C_{18}H_{12}$	Chrysene
228	$C_{18}H_{12}$	Benz [a] anthracene
228	$C_{18}H_{12}$	Triphenylene
228	$C_{18}H_{12}$	Benzoanthracene
228	$C_{18}H_{12}$	Benzo [c] phenanthrene
230	$C_{18}H_{14}$	2H-Benzo [d] phenathrene

Appendix A2

One-way Analysis of Variance of the Effect of Temperature on Product Distribution

Table A2.1. Effect of temperature on char product yield one-way analysis of variance

Source of Variation	SS	df	MS	F	P-value	F crit
Between Groups	14.60	2	7.30	3.57	0.07	4.10
Within Groups	20.46	10	2.05			
Total	35.05	12				

Table A2.2. Effect of temperature on condensate product yield one-way analysis of variance

Source of Variation	SS	df	MS	F	P-value	F crit
Between Groups	142.43	2	71.22	13.52	0.001	4.10
Within Groups	52.67	10	5.27			
Total	195.11	12				

Table A2.3. Effect of temperature on syngas product yield one-way analysis of variance

Source of Variation	SS	df	MS	F	P-value	F crit
Between Groups	219.14	2	109.57	11.38	0.003	4.10
Within Groups	96.30	10	9.63			
Total	315.44	12				

One-way Analysis of Variance of the Effect of Equivalence ratio on Product Distribution

Table A2.4. Effect of equivalence ratio on char product yield one-way analysis of variance

Source of Variation	SS	Df	MS	F	P-value	F crit

Between Groups	33.36	2	16.68	19.75	0.00016	3.89
Within Groups	10.14	12	0.84			
Total	43.50	14				

Table A2.5. Effect of equivalence ratio on condensate product yield one-way analysis of variance

Source of Variation	SS	df	MS	F	P-value	F crit
Between Groups	201.11	2	100.56	9.53	0.003	3.89
Within Groups	126.57	12	10.55			
Total	327.68	14				

Table A2.6. Effect of equivalence ratio on gas product yield one-way analysis of variance

Source of Variation	SS	df	MS	F	P-value	F crit
Between Groups	100.00	2	50.00	3.82	0.052	3.89
Within Groups	157.02	12	13.09			
Total	257.02	14				

One-way Analysis of Variance of the Effect of Temperature on Primary Gases

Table A2.7. Effect of temperature on CO one-way analysis of variance

Source of Variation	SS	df	MS	F	P-value	F crit
Between Groups	44.40	2	22.20	60.86	0.000006	4.26
Within Groups	3.28	9	0.36			
Total	47.68	11				

Table A2.8. Effect of temperature on CO_2 one-way analysis of variance

Source of Variation	SS	df	MS	F	P-value	F crit
Between Groups	11.53	2	5.77	52.12	0.000	4.26

Within Groups	1.00	9	0.11			
Total	12.53	11				

Table A2.9. Effect of temperature on CH_4 one-way analysis of variance

Source of Variation	SS	df	MS	F	P-value	F crit
Between Groups	5.27	2	2.63	9.19	0.007	4.26
Within Groups	2.58	9	0.29			
Total	7.84	11				

Table A2.10. Effect of temperature on H_2 one-way analysis of variance

Source of Variation	SS	df	MS	F	P-value	F crit
Between Groups	51.52	2	25.76	44.68	0.00002120	4.26
Within Groups	5.19	9	0.58			
Total	56.71	11				

Table A2.11. Effect of temperature on C_2H_2 one-way analysis of variance

Source of Variation	SS	df	MS	F	P-value	F crit
Between Groups	0.00768	2	0.0038402	10.79	0.0072	4.74
Within Groups	0.002491	7	0.0003558			
Total	0.010171	9				

Table A2.12. Effect of temperature on C_2H_4 one-way analysis of variance

Source of Variation	SS	df	MS	F	P-value	F crit
Between Groups	0.84	2	0.42	6.68	0.038	5.79
Within Groups	0.32	5	0.06			
Total	1.16	7				

One-way Analysis of Variance of the Effect of Equivalence Ratio on Primary Gases

Table A2.13. Effect of equivalence ratio on CO one-way analysis of variance

Source of Variation	SS	df	MS	F	P-value	F crit
Between Groups	17.35	2.00	8.68	22.26	0.0001	3.98
Within Groups	4.29	11.00	0.39			
Total	21.64	13				

Table A2.14. Effect of equivalence ratio on CO_2 one-way analysis of variance

Source of Variation	SS	df	MS	F	P-value	F crit
Between Groups	21.13	2	10.56	67.50	0.0000007	3.98
Within Groups	1.72	11	0.16			
Total	22.85	13				

Table A2.15. Effect of equivalence ratio on CH_4 one-way analysis of variance

Source of Variation	SS	df	MS	F	P-value	F crit
Between Groups	0.34	2	0.17	7.25	0.01	3.98
Within Groups	0.26	11	0.02			
Total	0.60	13				

Table A2.16. Effect of equivalence ratio on H_2 one-way analysis of variance

Source of Variation	SS	df	MS	F	P-value	F crit
Between Groups	41.74	2	20.87	50.43	0.00000289	3.98
Within Groups	4.55	11	0.41			
Total	46.30	13				

Table A2.17. Effect of equivalence ratio on C_2H_2 one-way analysis of variance

Source of Variation	SS	df	MS	F	P-value	F crit
Between Groups	0.002964	2	0.0014821	16.90	0.002093	4.74

Within Groups	0.000614	7	8.771E-05			
Total	0.003578	9				

Table A2.18. Effect of equivalence ratio on C_2H_4 one-way analysis of variance

Source of Variation	SS	df	MS	F	P-value	F crit
Between Groups	0.79	2	0.39	3.80	0.12	6.94
Within Groups	0.42	4	0.10			
Total	1.20	6				

One-way Analysis of Variance of the Effect of Temperature on Contaminants

Table A2.19. Effect of temperature on H_2S one-way analysis of variance

Source of Variation	SS	df	MS	F	P-value	F crit
Between Groups	23.28	2	11.64	1.25	0.35	5.14
Within Groups	55.79	6	9.30			
Total	79.07	8				

Table A2.20. Effect of temperature on NH_3 one-way analysis of variance

Source of Variation	SS	df	MS	F	P-value	F crit
Between Groups	150037.5	2	75018.76	8.211724	0.01459	4.737414
Within Groups	63948.98	7	9135.568			
Total	213986.5	9				

Table A2.21. Effect of temperature on HCN one-way analysis of variance

Source of Variation	SS	df	MS	F	P-value	F crit
Between Groups	59.22443	2	29.61221	1.87346	0.233266	5.143253
Within Groups	94.83698	6	15.80616			

Total	154.0614	8

Table A2.22. Effect of temperature on HCl one-way analysis of variance

Source of Variation	SS	df	MS	F	P-value	F crit
Between Groups	7.4468056	2	3.723403	15.14369	0.002867	4.737414
Within Groups	1.7211013	7	0.245872			
Total	9.1679069	9				

One-way Analysis of Variance of the Effect of Equivalence Ratio on Contaminants

Table A2.23. Effect of equivalence ratio on H_2S one-way analysis of variance

Source of Variation	SS	df	MS	F	P-value	F crit
Between Groups	59.187703	2	29.59385	2.041098	0.21076	5.143253
Within Groups	86.993931	6	14.49899			
Total	146.18163	8				

Table A2.24. Effect of equivalence ratio on NH_3 one-way analysis of variance

Source of Variation	SS	df	MS	F	P-value	F crit
Between Groups	46974.02	2	23487.01	3.827843	0.075305	4.737414
Within Groups	42950.84	7	6135.834			
Total	89924.86	9				

Table A2.25. Effect of equivalence ratio on HCN one-way analysis of variance

Source of Variation	SS	Df	MS	F	P-value	F crit
Between Groups	1767.779	2	883.8893	9.072548	0.015345	5.143253
Within Groups	584.5476	6	97.42459			
Total	2352.326	8				

Table A2.26. Effect of equivalence ratio on HCl one-way analysis of variance

Source of Variation	SS	Df	MS	F	P-value	F crit
Between Groups	7.4468056	2	3.723403	15.14369	0.002867	4.737414
Within Groups	1.7211013	7	0.245872			
Total	9.1679069	9				

Appendix A3

Table A3.1. Higher heating value and Shomate heat capacity coefficients for gas components

Gases	Cp, J/mol k^{-1} [(a)] $Cp_{,i}$ = A + B*T' + C*T'^{2}+ D*T'^{3} + E/T'^{2}, T' = Tgasifier/1000					Validity Range
	A	B	C	D	E	T (K)
CO	25.568	6.0961	4.0547	-2.67	0.131	298-1300
	35.151	1.3001	-0.206	0.014	-3.283	1300-6000
CH_4	-0.703	108.48	-42.52	5.863	0.6786	298-1300
	85.812	11.265	-2.114	0.138	-26.42	1300-6000
H_2	33.066	-11.36	11.433	-2.773	-0.16	298- 1000
	18.563	12.257	-2.86	0.2682	1.978	1000- 2500
	43.414	-4.293	1.2724	-0.097	-20.5	2500 – 6000
C_2H_2	40.687	40.73279	-16.1784	3.669741	-0.66	298- 1100
	67.472	11.7511	-2.02147	0.136195	-9.8064	1100- 6000
C_2H_4	-6.388	184.4	-113	28.496	0.316	298. – 1200
	106.51	13.733	-2.628	0.1746	-26.1	1200-6000
N_2	28.98641	1.853978	-9.647459	16.64	0.000117	100-500
	19.50583	19.88705	-8.598535	1.37	0.527601	500-2000
	35.51872	1.128728	-0.196103	0.015	-4.55376	2000-6000

[(a)]Burgess, D. R.; Afeefy, H. Y.; Liebman, J. F.;Stein, S. E. *Gas Phase Thermochemistry Data*. *In* NIST Chemistry WebBook; Mallard, W. G.; Linstrom, P. J. eds. NIST Standard Reference Database Number 69; National Institute of Standards and Technology: Gaithersburg, MD, 2005 (http://webbook.nist.gov).

Table A3.2 Densities of primary gas constituents at 25˚C and 1 atm

Gases	**Density, g/dm$^{3(a)}$**	**HHV, kJ/g[(b)]**
CO	1.1453	10.1
CO_2	1.8080	0
CH_4	0.6569	36.4
H_2	0.0823	142.2

C_2H_2	1.0893	50.2
C_2H_4	1.1533	57.7
N_2	1.1452	0
O_2	1.3088	0

[(a)] Lemmon, E. W.; McLinden, M. O.;Friend, D. G. *Thermophysical Properties of Fluid Systems*. *In* NIST Chemistry WebBook; Linstrom, P. J.; Mallard, W. G. eds. NIST Standard Reference Database Number 69; National Institute of Standards and Technology: Gaithersburg, MD, 2011 (http://webbook.nist.gov).

[(b)] Borman, G. L.;Ragland, K. W. *Combustion engineering*. 2nd ed.; McGraw-Hill New York, New York, 1998.

Sample Mass and Carbon Balance Calculations

Gasification conditions: 934°C and ER = 0.25
Mass balance basis = 100 g of pine

Input calculations

Run information

Pine feeding rate = F_{pine} = 5.43 g/min

$C^{in}_{pine,c} =$ 46.99 wt %

Total runtime = t_{run} = 60 min

Oxygen flow rate = F_{oxygen} = 1.5 l/min

Density of oxygen = ρ_{oxygen} = 1.3088 g/l

The mass of gasifying agent for 100 g of biomass gasified supplied is

Mass of oxygen supplied

$$m^{in}_{O_2} = (Mass\ balance\ basis) \times \frac{F_{O_2} \times t_{run} \times \rho_{O_2}}{F_{pine} \times t_{run}}$$

$$m^{in}_{oxygen} = 100g\ biomass \times \frac{1.5\ l\ O_2/min \times 60\ min \times 1.3088\ g/l}{5.43\ g\ biomass/min \times 60\ min} = 36.15\ \text{g } O_2$$

Mass of nitrogen (for air equivalent nitrogen supply) supplied

$$m^{in}_{nitrogen} = \frac{m^{in}_{oxygen}}{0.232} - m^{in}_{oxygen} = \frac{36.15\ g\ oxygen}{0.232} - 36.15\ g\ oxygen$$

$$m^{in}_{nitrogen} = 119.02\ g\ nitrogen$$

Total mass of gasifying agent is

$$m^{in}_{gasifying\ agent} = m^{in}_{O_2} + m^{in}_{N_2} = 36.15g + 119.02g$$

$m^{in}_{gasifying\ agent}$*=155.17 g*

The total mass input to the system is

$$m^{in}_{total} = m^{in}_{pine} + m^{in}_{gasifying\ agent}$$

$$m^{in}_{total} = 100\ g\ biomass + 155.17\ g\ gasifying\ agent = 255.17g$$

The total mass of carbon input to the system is

$$m^{in}_{c} = C^{in}_{pine,c} \times m^{in}_{pine} = 0.4699 \times 100\ g\ pine$$

$$m^{in}_{c} = 46.99\ g$$

Output calculations

Mass of gas output

$m^{out}_{CO} = 45.56\ g$ $m^{out}_{CO_2} = 50.52\ g$ $m^{out}_{CH_4} = 5.07\ g$

$m^{out}_{H_2} = 2.61\ g$ $m^{out}_{C_2H_2} = 0.70\ g$ $m^{out}_{C_2H_4} = 5.48\ g$

$m^{out}_{N_2} = 119.02\ g$ $m^{out}_{contaminants} = 1.08\ g$

$m^{out}_{gas} = 228.96\ g$ *(includes primary gas and all contaminants)*

Mass of carbon from gas output (CO, CO_2, CH_4, C_2H_2 and C_2H_4 are considered)

Mass fraction of carbon in gas species

$$w^{out}_{CO,c} = \frac{12n}{MW_{CO}} = \frac{12}{28} = 0.43$$ *(n=1 for CO)*

Similarly, mass fractions of carbon for all other gas species are

$w_{CO_2,c}^{out} = 0.27$, $w_{CH_4,c}^{out} = 0.75$, $w_{C_2H_2,c}^{out} = 0.92$, $w_{C_2H_4,c}^{out} = 0.82$

Mass of carbon output in gas species

$$m_{CO,c}^{out} = w_{CO,c}^{out} \times m_{CO}^{out} = 0.43 \times 45.56\ g = 19.59\ g$$

Similarly, the mass of carbon for all other gas species are

$m_{CO_2,c}^{out} = 13.64\ g$ $\quad$ $m_{CH_4,c}^{out} = 3.80\ g$

$m_{C_2H_2,c}^{out} = 0.64\ g$ $\quad$ $m_{C_2H_4,c}^{out} = 4.49\ g$

Mass of carbon in gas output

$$m_{gas_c}^{out} = \sum_s m_{s,c}^{out} = 19.59g + 13.64g + 3.80g + 0.64g + 4.49g$$

$$m_{gas_c}^{out} = 42.16\ g$$

Mass of liquid condensate output

$m_{liquid}^{out} = 22.85g$

$C_{liquid,c}^{out} = 0.49\ {}^{mg\ C}/_{g\ liquid\ condensate}$

$m_{liquid_c}^{out} = 11.20\ 10^{-3}g$

Mass of char output

$m_{char}^{out} = 4.91g$

$C_{char,c}^{out} = 0.84g\ C/g\ char$

$m_{char_c}^{out} = 4.12\ g$

The total mass output of the system is

$$m^{out} = m^{out}_{gas} + m^{out}_{liquid\ condensate} + m^{out}_{char}$$

$$m^{out} = 228.96\ g + 22.85g + 4.91g = 256.72\ g$$

The total mass of carbon output of the system is

$$m^{out}_{c} = m^{out}_{gas_c} + m^{out}_{liquid_c} + m^{out}_{char_c}$$

$$m^{out}_{c} = 42.16\ g + 11.20\ 10^{-3} g + 4.12g = 46.29g$$

Mass and carbon balances

$$m^{in} = 255.17g \qquad m^{out} = 256.72g$$

$$\emptyset_{mass} = \frac{100 \times m^{out}}{m^{in}} = \frac{100 \times 256.72g}{255.17g} = 100.61\ \%$$

$$....m^{in}_{c} = 46.99g \qquad m^{out}_{c} = 46.29g \qquad \emptyset_{c} = \frac{100 \times m^{out}_{c}}{m^{in}_{c}} = \frac{100 \times 46.29g}{46.99g} = 95.51\ \%$$

Carbon conversion efficiency

$$\eta_{carbon} = \frac{100 \times m^{out}_{gas_c}}{m^{in}_{c}} = \frac{100 \times 42.16g}{46.99g} = 84.49\ \%$$

Sample Energy Analysis and Gas Heating Value Calculations

Gasification conditions: 934°C and ER = 0.25
Energy balance basis = 100 g of pine

Input calculations

Using the heating value of pine, the energy value input to the system can be determined as follows

$$(E_{HHV})_{pine}^{in} = m_{pine}^{in} \times HHV_{pine}$$

$$(E_{HHV})_{pine}^{in} = 100\ g \times 20.18 kJ/g = 2018\ kJ$$

Output calculations

Gas heating value outputs

Using the heating value of each gas constituents in Table A3.1, the heating value of CO can be determined as follows

$$E_{HHV_{CO}}^{out} = m_{CO}^{out} \times HHV_{CO,primary\ gas} = 45.56g \times 10.1 kJ/g = 460.16\ kJ$$

Similarly, the heating value outputs for all other gas constituents are determined below

$E_{HHV_{CH_4}}^{out} = 281.49\ kJ$ $E_{HHV_{H_2}}^{out} = 370.76\ kJ$

$E_{HHV_{C_2H_2}}^{out} = 35.46\ kJ$ $E_{HHV_{C_2H_4}}^{out} = 316.14\ kJ$

The total gas heating value outputs is

$$(E_{HHV})_{primary\ gas}^{out} = E_{HHV_{CO}}^{out} + E_{HHV_{CH_4}}^{out} + E_{HHV_{H_2}}^{out} + E_{HHV_{C_2H_2}}^{out} + E_{HHV_{C_2H_4}}^{out}$$

$$(E_{HHV})_{primary\ gas}^{out} = 460.16kJ + 281.49kJ + 370.76kJ + 35.46kJ + 316.14kJ$$
$$(E_{HHV})_{primary\ gas}^{out} = 1464.01\ kJ$$

Char heating value

$$(E_{HHV})_{char}^{out} = m_{char}^{out} \times HHV_{char} = 4.91g \times 29.98\ kJ/g = 147.20\ kJ$$

Consequently, the heating value loss is

$$(E_{HHV})_{loss} = (E_{HHV})_{pine}^{in} - (E_{HHV})_{primary\ gas}^{out} - (E_{HHV})_{char}^{out}$$
$$(E_{HHV})_{loss} = 2018\ kJ - 1464.01kJ - 147.20\ kJ = 406.79\ kJ$$

Sensible heat outputs

Using the Shomate equation and the coefficients in Table A3.1, the specific heat capacity of CO can be determined as follows

$$T = 934℃ + 273 = 1207K \qquad T' = {}^{T}/_{1000} = 1.207$$

$$C_{p,CO} = 25.57 + 6.10(1.207) + 4.05(1.207)^2 - 2.67(1.207)^3 + \frac{0.13}{1.207^2}$$

$$C_{p,CO} = 34.23\ J/mol\ K \quad or \quad C_{p,CO} = 1.22\ 10^{-3} kJ/g\ K\ by$$

dividing by the molecular weight of CO

Similarly, the specific heat capacities for all other gas constituents are reported below

$$C_{p,CO_2} = 1.28\ 10^{-3} kJ/g\ K \quad C_{p,CH_4} = 4.94\ 10^{-3} kJ/g\ K$$

$$C_{p,H_2} = 15.51\ 10^{-3} kJ/g\ K \quad C_{p,C_2H_2} = 2.78\ 10^{-3} kJ/g\ K$$

$$C_{p,C_2H_4} = 3.63\ 10^{-3} kJ/g\ K \quad C_{p,N_2} = 1.21\ 10^{-3} kJ/g\ K$$

Using the specific heat capacities, the sensible heat of the output gas can be determined as follows

$$Q_{CO}^{out} = m_{CO}^{out} \times C_{p,CO} \times (T - 298)$$

$$Q_{CO}^{out} = 45.56g \times 1.22\ 10^{-3} kJg^{-1}K^{-1} \times (1207 - 298)K$$

$$Q_{CO}^{out} = 50.52\ kJ$$

Similarly, the sensible heat for all other gas constituents are reported below

$Q_{CO_2}^{out} = 58.83\ kJ$ $Q_{CH_4}^{out} = 22.78kJ$

$Q_{H_2}^{out} = 36.76\ kJ$ $Q_{C_2H_2}^{out} = 1.78\ kJ$

$Q_{C_2H_4}^{out} = 18.08\ kJ$ $Q_{N_2}^{out} = 130.42\ kJ$

The total sensible heat of the gas output is

$$Q_{primary\ gas}^{out} = Q_{CO}^{out} + Q_{CO_2}^{out} + Q_{CH_4}^{out} + Q_{H_2}^{out} + Q_{C_2H_2}^{out} + Q_{C_2H_4}^{out} + Q_{N_2}^{out}$$

$$Q_{primary\ gas}^{out} = 50.52\ kJ + 58.83kJ + 22.78kJ + 36.76kJ + 1.78kJ + 18.08kJ + 130.42kJ$$

$$Q_{primary\ gas}^{out} = 319.17\ kJ$$

Cold and hot gas efficiency

$$\eta_{cold\ gas} = 100 \times \frac{(E_{HHV})_{primary\ gas}^{out}}{(E_{HHV})_{pine}^{in}}$$

$$\eta_{cold\ gas} = 100 \times \frac{1464018\text{kJ}}{2018\ \text{kJ}} = 72.55\%$$

$$\eta_{hot\ gas} = 100 \times \frac{(E_{HHV})_{primary\ gas}^{out} + Q_{primary\ gas}^{out}}{(E_{HHV})_{pine}^{in}}$$

$$\eta_{hot\ gas} = 100 \times \frac{1464.01\text{kJ} + 319.17\text{kJ}}{2018\ \text{kJ}} = 88.36\ \%$$

Volumetric gas heating value

Using densities from Table A3.2, the gas volume for each species was determined

$$v_{CO}^{out} = \frac{m_{CO}^{out}}{\rho_{CO}} = \frac{45.56g}{1.1453g\ /dm3} = 39.78\ dm^3$$

Similarly

$v_{CO_2}^{out} = 27.94\ dm^3$ $v_{CH_4}^{out} = 7.72\ dm^3$

$v_{H_2}^{out} = 31.68\ dm^3$ $v_{C_2H_2}^{out} = 0.65\ dm^3$

$v_{C_2H_4}^{out} = 4.75\ dm^3$ $v_{N_2}^{out} = 103.93\ dm^3$

$v_{gas}^{out} = 216.45\ dm^3$

$$Q_v^{out} = \frac{(E_{HHV})_{gas}^{out}}{v_{gas}^{out}} = \frac{1464.01kj}{216.45\ dm^3} = 6.76\ kJ/dm^3 = 6.76MJ/m^3$$

Carbon balance	Mean	SD
In, g	46.99	0.00
Out, g	41.02	0.60
Discrepency, g	5.97	0.60
Closure, %	87.29	1.29

Carbon flow	Mean	SD
C_{gas}, %	35.74	1.26
C_{char}, %	4.82	0.91
Cl_{liquid}, %	0.04	0.00
$C_{unaccounted}$, %	6.39	0.60

Energy efficiency	Mean	SD
η_{cold}, %	56.12	2.04
η_{hot}, %	67.51	2.76

Energy flow	Mean	SD
E_{gas}, kJ	1132.57	41.12
E_{char}, kJ	170.44	32.27
E_{loss}, kJ	714.99	44.62

Heating value, MJ/m^3	4.93	0.06

Basis

Biomass, g	100
C, g	46.99

	Mean	SD
$HHV_{biomass}$, kJ	2018	21

Mass balance	Mean	SD
In, g	221.33	4.97
Out, g	215.75	6.21
Discrepency, g	5.58	1.51
Closure, %	97.47	0.72

	Mean	SD
Gasifying agent, g	121.33	4.97

Tar, g	0.83

	Mean	SD
Char, g	5.90	1.12
C, g	4.82	0.91

	Mean	SD
HHV_{char}, kJ	170.44	170.44

	Mean	SD
Liquid condensate, g	20.74	1.14
C, g	0.022	0.001

Primary gas components	Mean	SD
CO, g	37.96	3.25
CO_2, g	46.39	2.52
CH_4, g	8.58	1.67
H_2, g	1.75	0.34
C_2H_2, g	0.06	0.01
C_2H_4, g	0.52	0.12
N_2, g	93.06	3.81
Total primary gases, g	188.18	8.39
X_{carbon}	76.06	2.68
C, g	35.74	1.26

Contaminants	Mean	SD
H_2S, g	0.01	0.00
NH_3, g	0.16	0.02
HCN, g	0.02	0.00
HCl, g	0.00	0.00
Total contaminants, g	0.11	0.10

Figure A3.1. Process mass and energy balance diagram at 790˚C and 0.25 ER

Carbon balance	Mean	SD
In, g	46.99	0.00
Out, g	43.37	2.90
Discrepency, g	3.62	2.90
Closure, %	92.29	6.17

Mass balance	Mean	SD
In, g	223.00	1.58
Out, g	214.63	8.98
Discrepency, g	8.37	7.73
Closure, %	96.24	3.48

Tar, g	0.96

Carbon flow	Mean	SD
C_{gas}, %	39.62	1.30
C_{char}, %	3.26	1.61
Cl_{iquid}, %	0.00	0.00
$C_{unaccounted}$, %	4.10	2.90

Energy efficiency	Mean	SD
η_{cold}, %	67.45	1.60
η_{hot}, %	83.83	1.75

Energy flow	Mean	SD
E_{gas}, kJ	1439.81	138.22
E_{char}, kJ	117.95	58.17
E_{loss}, kJ	460.24	97.39

Heating value, MJ/m^3	5.73	0.02

Basis

Biomass, g	100
C, g	46.99

	Mean	SD
$HHV_{biomass}$, kJ	2018	21

	Mean	SD
Char, g	4.09	2.02
C, g	3.34	1.65

	Mean	SD
HHV_{char}, kJ	117.95	58.17

	Mean	SD
Liquid condensate, g	11.75	0.67
C, g	0.013	0.001

	Mean	SD
Gasifying agent, g	123.00	1.58

Primary gas components	Mean	SD
CO, g	64.70	11.92
CO_2, g	31.18	2.81
CH_4, g	2.92	0.40
H_2, g	4.27	0.11
C_2H_2, g	0.18	0.23
C_2H_4, g	0.14	0.05
N_2, g	94.34	1.21
Total primary gases, g	197.69	10.43
X_{carbon}	84.32	2.77
C, g	39.62	1.30

Contaminants	Mean	SD
H_2S, g	0.02	0.00
NH_3, g	0.10	0.01
HCN, g	0.03	0.00
HCl, g	0.00	0.00
Total contaminants, g	0.14	0.01

Figure A3.2. Process mass and energy balance diagram at 1078˚C and 0.25 ER

Carbon balance	Mean	SD
In, g	46.99	0.00
Out, g	39.62	4.72
Discrepency, g	7.37	4.72
Closure, %	**79.09**	**6.13**

Carbon flow	Mean	SD
C_{gas}, g	34.82	4.67
C_{char}, g	4.14	0.78
Cl_{iquid}, g	0.00	0.00
$C_{unaccounted}$, g	8.02	4.72

Energy efficiency	Mean	SD
η_{cold}, %	63.85	5.60
η_{hot}, %	78.06	6.43

Energy flow	Mean	SD
E_{gas}, kJ	1288.59	112.91
E_{char}, kJ	146.62	35.96
E_{loss}, kJ	582.80	148.88

Heating value, MJ/m^3	7.11	0.42

Basis

Biomass, g	100
C, g	46.99

	Mean	SD
$HHV_{biomass}$, kJ	2018	21

Mass balance	Mean	SD
In, g	175.93	3.56
Out, g	162.10	10.21
Discrepency, g	13.83	7.32
Closure, %	**89.82**	**2.44**

	Mean	SD
Gasifying agent, g	75.93	3.56

Tar, g	1.31

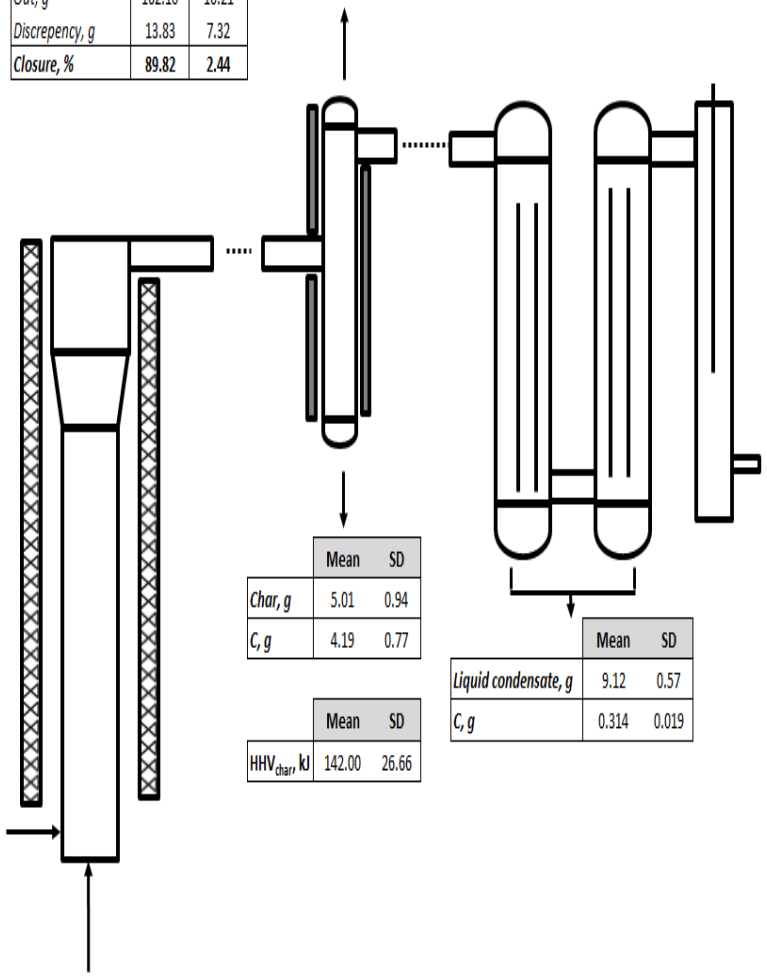

	Mean	SD
Char, g	5.01	0.94
C, g	4.19	0.77

	Mean	SD
HHV_{char}, kJ	142.00	26.66

	Mean	SD
Liquid condensate, g	9.12	0.57
C, g	0.314	0.019

Primary gas components	Mean	SD
CO, g	51.84	5.43
CO_2, g	27.57	2.92
CH_4, g	4.75	0.16
H_2, g	3.52	0.41
C_2H_2, g	0.08	0.00
C_2H_4, g	0.74	0.21
N_2, g	58.29	2.78
Total primary gases, g	146.51	9.40
X_{carbon}	74.10	9.94
C, g	34.82	4.67

Contaminants	Mean	SD
H_2S, g	0.02	0.003
NH_3, g	0.18	0.013
HCN, g	0.02	0.002
HCl, g	0.00	0.000
Total contaminants, g	0.22	0.02

Figure A3.3. Process mass and energy balance diagram at 934˚C and 0.15 ER

Carbon balance	Mean	SD
In, g	46.99	0.00
Out, g	40.94	4.08
Discrepency, g	6.05	4.08
Closure, %	**87.13**	**8.69**

Mass balance	Mean	SD
In, g	278.57	2.87
Out, g	270.06	12.67
Discrepency, g	8.51	10.64
Closure, %	**96.93**	**3.80**

Tar, g	0.28

Carbon flow	Mean	SD
C_{gas}, g	39.78	4.10
C_{char}, g	1.00	0.24
Cl_{liquid}, g	0.02	0.00
$C_{unaccounted}$, g	6.19	4.08

Energy efficiency	Mean	SD
η_{cold}, %	52.84	4.24
η_{hot}, %	73.52	4.79

Energy flow	Mean	SD
E_{gas}, kJ	1121.47	143.81
E_{char}, kJ	34.51	8.14
E_{loss}, kJ	862.01	142.98

Heating value, MJ/m^3	*3.28*	0.21

Basis

Biomass, g	100
C, g	46.99

	Mean	SD
$HHV_{biomass}$, kJ	2018	21

	Mean	SD
Char, g	1.26	0.30
C, g	1.06	0.24

	Mean	SD
HHV_{char}	34.51	8.14

	Mean	SD
Gasifying agent, g	178.57	2.87

	Mean	SD
Liquid condensate, g	18.17	4.42
C, g	0.625	0.152

Primary gas components	Mean	SD
CO, g	46.06	6.09
CO_2, g	59.19	4.48
CH_4, g	4.93	0.85
H_2, g	2.49	0.38
C_2H_2, g	0.07	0.01
C_2H_4, g	0.04	0.16
N_2, g	136.96	2.20
Total primary gases, g	249.86	11.64
X_{carbon}	84.66	8.74
C, g	39.78	4.10

Contaminants	Mean	SD
H_2S, g	0.05	0.06
NH_3, g	0.65	0.86
HCN, g	0.10	0.13
HCl, g	0.00	0.00
Total contaminants, g	0.80	1.06

Figure A3.4. Process mass and energy balance diagram at 934˚C and 0.35 ER